FINAL REPORT

ASSESSMENT OF LIQUEFACTION POTENTIAL FOR THE 1995 KOBE, JAPAN EARTHQUAKE INCLUDING FINITE-SOURCE EFFECTS

Prepared for
U.S. Army Engineer Waterways Experiment Station
Corps of Engineers

February 15, 1999

Pacific Engineering and Analysis
311 Pomona Avenue
El Cerrito, CA 97530

February 15, 1999
FINAL REPORT

ASSESSMENT OF LIQUEFACTION POTENTIAL FOR THE 1995 KOBE, JAPAN EARTHQUAKE INCLUDING FINITE-SOURCE EFFECTS

Prepared for

U.S Army Engineer Waterways Experiment Station

Corps of Engineers

Contract #DACW39-97-K-0015

by

Walter Silva
Carl Costantino

of

Pacific Engineering and Analysis
311 Pomona Avenue

El Cerrito, CA 94530

and

Yoshinori Iwasaki
Geo-Research Institute
Utsubo-Honmachi,
Nishi-Ku, Osaka,550 Japan

ACKNOWLEDGEMENTS

This project has been jointly sponsored by the U.S. Department of Energy (DOE) and the U.S. Nuclear Regulatory Commission (NRC). The project managers for DOE were Mr. Jeffrey Kimball of DOE Headquarters and Mr. Brent Gutierrez of the Savannah river Operations Office. The project managers for NRC were Mr. Rober Kornasicwicz and Mr. Roger Kenneally of RES/SSEB. They were supported by Mr. Donald Yule at the Waterways Experiment Station. The authors wish to thank these gentlemen for their encouragement and support during the conduct of this study. A special thanks to the invaluable support provided to the project by the staff at the Geo-Research Institute. Without their kind assistance, this study would not have been possible.

CONTENTS

CONTENTS

LIST OF TABLES

LIST OF FIGURES

LIST OF FIGURES

LIST OF FIGURES

LIST OF FIGURES

LIST OF FIGURES

LIST OF FIGURES

LIST OF FIGURES

ASSESSMENT OF LIQUEFACTION POTENTIAL FOR THE KOBE EARTHQUAKE INCLUDING FINITE-SOURCE EFFECTS

1.0 INTRODUCTION

Recent recordings in the near-source regions of large earthquakes have shown differences in strong ground motion characteristics compared to more distant motions which are of significance to engineering design. Near-source motions (≤ 10 - 15 km) for large (**M** ≥ 6 ¼) earthquakes are typified in the time domain by short durations and, at intermediate-to-long periods, by rupture directivity. The effects of rupture directivity are to reduce durations and increase low-frequency spectral content for sites situated with significantly more rupture toward them than away. These effects are significant at close distances, particularly for vertical strike slip ruptures, and their influence on structures, slope stability, and liquefaction potential needs to be assessed. The recent occurrence of the Kobe earthquake, a large (**M** 6.9) predominately vertical strike slip earthquake, with both close-in and more distant firm and soft soil conditions and with mapped liquefaction zones, presents a unique opportunity to evaluate the combination of current approaches to assess liquefaction susceptibility with a finite-fault simulation procedure. The finite-fault simulation naturally accommodates the effects of rupture directivity and short durations for close-in sites, resulting in estimates of liquefaction parameters (cyclic stress ratios and strain energies) appropriate for specific source-site geometries. The approach used in this evaluation is to compare regions of mapped liquefaction (or no liquefaction) to regions where liquefaction is predicted to be extensive, moderate, or not to occur. Average soil column information was developed from detailed boring log data at a large number of profiles available in the region. This approach has the advantage of statistical stability by evaluating several hundred sites subjected to varying levels of control motions but is limited by not considering detailed site specific information at each site location. The level of site information available for this study is not unlike the data generally available in the generation of liquefaction hazard maps.

1.1 Description of Event

The Hyogoken-Nanbu (Kobe) earthquake occurred at 5:47 am on January 17, 1995, approximately one year after the Northridge earthquake of southern California. Much information is available in the open literature on the earthquake and its consequences and much work is continuing to be developed since it is such an important event with much information available from documentation and recordings. Two large summary documents are available describing much of this information, the first being the report (Hamada, et al., 1995) describing soil conditions, surface manifestation of liquefaction and ground displacements resulting from the event and the second being the "Special Issue on Geotechnical Aspects" published on the first anniversary of the event. This section of the report presents a brief summary of the earthquake and its consequences from these and other references.

As described by Comartin, et al., (1995), the epicenter of the event was located in the vicinity of the northern tip of Awaji Island which lies between Shikoku and Honshu Islands (34.6°N, 135°E, Figure 1.1). The epicentral region is located on Awaji Island about 20 km

southwest of Kobe City (Figure 1.2) in Osaka Bay. The rupture was a shallow bilateral strike-slip fracture with a focal depth of 10km and a length of about 60 km. The earthquake was assigned a moment magnitude of 6.9 and a local magnitude of 7.2 by the Japanese Meteorological Agency (JMA). Aftershocks recorded during the first week following the event indicate that the fault extends from Awaji Island through the Kobe City area and into the Itami region northeast of Kobe. Although the event was of a size similar to the Northridge event, its impact on the inhabitants and infrastructure in the area was an order ofmagnitude greater than occurred at Northridge since it passed directly below this highly populated area.

Although Japan is known as a highly active seismic region, the occurrence of this large event in the Kobe area was apparently a surprise to the seismological community. Many of the larger events that have occurred in the past have been subduction events with epicentral regions generally off-shore. Shallower strike-slip events, similar to the California experience, have occurred on land. These are generated from the complex movement and interaction of the four major plates which interface in the region: the Eurasian, the North American, the Pacific and the Philippine Sea plates. Inthe Kobe City vicinity, the shallow crustal structure is highly complex and the rocks are highly fractured, with many faults having been mapped in the immediate vicinity of Kobe City. The epicentral locations of some of the major seismic events that have occurred in the Kobe region are indicated in Figure 1.3, generally supporting the view that the region is a relatively active seismic zone.

The slip was initiated on the Nojima fault, which is labeled as Fault No. 1 in Figure 1.4, and is located on the northern tip of Awaji Island. The fault runs along the northwest side of the island. It was reported that the main shock consisted of three subevents with a total rupture time of 11 seconds. The surface manifestation of the fracture was clear and easily identifiable on Awaji Island since the relatively soft rock is exposed at the ground surface over much of the island. Indications of the surface displacement run to the waters edge on the northern tip of Awaji Island. Fault movement has also been confirmed along Faults 63, 64, 65 and 66 in Kobe City, and suspected along Fault 35 (the Suma Fault) as well as along Faults 39, 79 and 80. The indicators, however, were not as clear as those noted along Awaji Island since this area is a soil site, with fill placed atop the insitu soil and bedrock. This anecdotal information agrees well with the aftershock evidence that the total fault length extends from Awaji Island under Kobe City to the Itami area, a length of approximately 50 km.

Along the Nojima Fault, the magnitude of horizontal slip was indicated (Ito, 1995) to be as much as 1.5m (59 inches). Vertical movement along this fault varied both in magnitude and direction, with the surface rupture indicated to be about 0.4m (16 inches). Between Awaji Island and Kobe City, the tower foundation of the Akashi-Kaikyo Bridge, being constructed at the time of the event and now essentially completed, was indicated to have displaced over 1m horizontally and 0.25m vertically (Matsuo, 1995).

1.2 Strong Motion Information

Intensity estimates in the region affected by the event refer to the JMA intensity scale. A comparison of this intensity scale, consisting of eight levels of damage, with the Modified Mercalli system used in the United States is shown in Table 1.1 (Reiter, 1990). In the immediate vicinity

of the epicenter at Awaji Island and downtown Kobe City, the intensity was indicated to reach levels 6 and 7, the most severe on the JMA scale. Strong motions caused by the earthquake were recorded at many locations, some of which are shown in Figure 1.5, in the Kansai area. Some of the recorded horizontal PGA's are shown on Figure 1.6. As may be noted, the largest recorded horizontal acceleration for which we have information is 833 gals (0.85g) and occurred at the Fukai station, a shallow soil site in Kobe City (Hamada et al., 1995).

The ratios of vertical to horizontal peak accelerations recorded (V/H ratios) at these various sites are shown in Figures 1.7 and the distribution of the magnitudes of these ratios in Figure 1.8. The average value of this ratio is 0.87, which is higher than the value of 2/3 typically assumed in seismic evaluations. In addition, it may be noted thatthe ratios are relatively low in the vicinity of Kobe City closer to the fault, while in the Osaka area across the bay, a greater portion of the readings exceed unity. A typical cross-section of the geologic configuration from the Kobe area to Osaka is presented in Figure 1.9 (Osaka Soil Foundation Map, 1987). The bedrock forms a "saucer" between Mount Rokko west of Kobe City to Mount Ikoma east of Osaka City, with relatively soft soils deposited in the valley between the two hills. The soils underlying Osaka being significantly deeper (softer) than at Kobe may explain this distribution of V/H ratios (Silva, 1998).

1.3 Damage Summary

The vast majority of structural damage occurred in the immediate vicinity of the fault zone from Awaji Island to downtown Kobe, Ashiya, Nishinomiya and Takarazuka cities. Away from the immediate fault region, the intensity levels decreased rapidly as did the damage. The outline of the JMA Intensity 7 zone is shown in Figure 1.10 (Kimura, 1996) which corresponds approximately to MMI IX. It is indicated that more than 30% of the residential damage occurred in this vicinity. Interestingly this high intensity zone roughly corresponds to the zone of soft soils which lies between rock and hard soils to the northand reclaimed land to the south (Figure 2.1) forming the edge of the Osaka basin. Depth to basement increases sharply from north to south and is rather uniform along the soft soil high damage zone (Kagawa et al., 1993). The confined high intensity zone may be attributed to shallow soil conditions (Suetomi and Yoshida,1998) and/or deep basin edge effects (Kawase, 1996).

A number of failures occurred which are primarily related to the generation of failure conditions in soil. Some of these failures are well known, would be expected tooccur in such a large event and their effects are calculable using current analysis techniques. On the other hand, other soil related failures occurred which have not typically been noted to occur during other relatively large seismic events in the past.

As an example of the former case, soil liquefaction occurred in a large area along the coastline from Kobe to Osaka as well as at several inland locations. Aerial surveys (Hamada, et al., 1995) as well as ground inspection were used to map the zones in which surface expressions of liquefaction (sand boils, fissures, movement of seawalls, damage to embankments, etc.) could be determined. An approximate plot of the areas in which widespread liquefaction occurred as determined from the aerial photos is shown in Figure 1.11. These zones were generally restricted to the reclaimed lands and man-made islands of the Osaka Bay. Other more restricted areas in

which sand boils were noted by field inspections occurred in the coastal zone further east of this area to sites well south of Osaka. Some liquefaction also was noted in inland sites at Nishinomiya and Takarazuka cities northeast of Kobe as well as along the Yodo River in Osaka.

As an example of this latter situation, failures at four subway stations were reported. Such failures are highly unusual as it is normally considered that damage from transient motions would not occur in near surface buried tunnels, except possibly at locations of section discontinuities (portals, rock/soil interfaces, etc.). As noted by Matsuo (1995), the failures occurred at the center columns of these structures, which are concrete box structures constructed by the normal cut-and-cover techniques. Total load on the box is relatively small since the thickness of soil cover is typically small. In fact, such structures usually have an effective weight less than the soil they displace.

At the artificial island called Port Island, major damage occurred in the northern half of the island which is generally associated with the widespread zones of liquefaction and dynamic settlements induced by the seismic motions. Port Island is a typical off-shore man-made island which was created by placing relatively uncompacted clean sands (weathered granite, Section 2) atop the existing soft silts and clays of the alluvial soils in the harbor.It was constructed in two stages, with the northern half being first constructed. The southern half of Port Island incorporated more effort to preconsolidate the dumped soils by a variety of soil improvement methods. Damage to the island corresponded to these zones, except for wharf areas where damage occurred along the entire island.

Failures also were reported at the site of small earth embankments in the Nishinomiya vicinity and descriptions of these failures are reported by Krinitzsky, et al. (1995). These small dams, known as the Koyoen dams, are part of a reservoir system a few kilometers from the edge of the epicentral region. They are reported to be 8m to 10m high and are approximately 75m long. They suffered extensive damage from the earthquake and the reservoir was empty at the time of inspection. No indications were provided of any additional damage from breaches in the retaining system. This inspection team also reported some damage to the portal structure and the lining of the Rokko Mountain tunnel of the Japan Rail's Shinkansen line. In the Nigawa area of Nishinomiya, a major slide failure occurred in a residential community causing the death of a number of people. Some additional slide areas were encountered near the fault zone on Awaji

Table 1.1 Comparison of Intensity Scales (from Reiter, 1990)	
Modified Mercalli (MM) 1931	Japanese Scale 1960
I	0
II	1
III	2
IV	2.3
V	3
VI	4
VII	4.5
VIII	5
IX	6
X	6
XI	7
XII	7

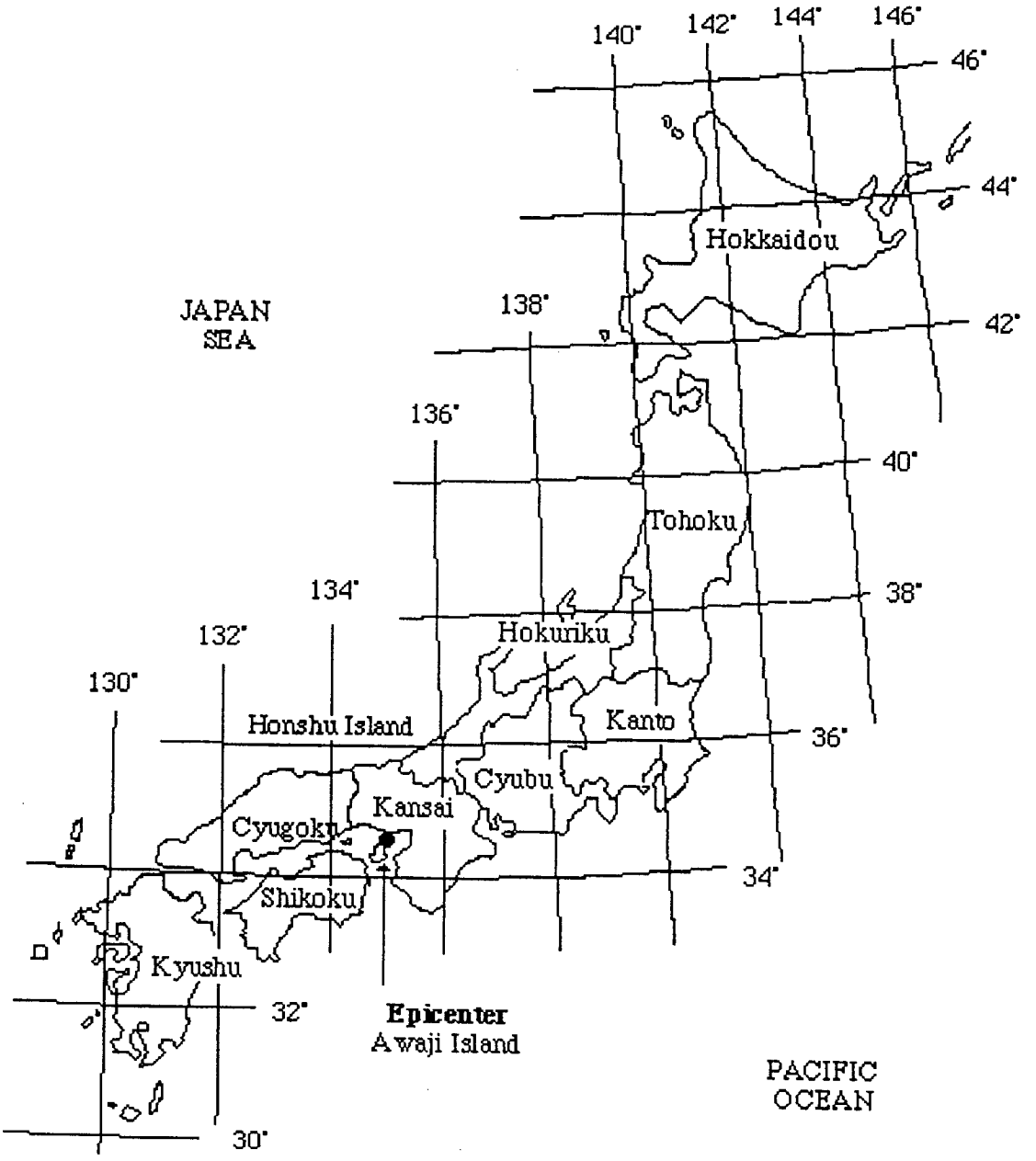

Figure 1.1. Map of Japan

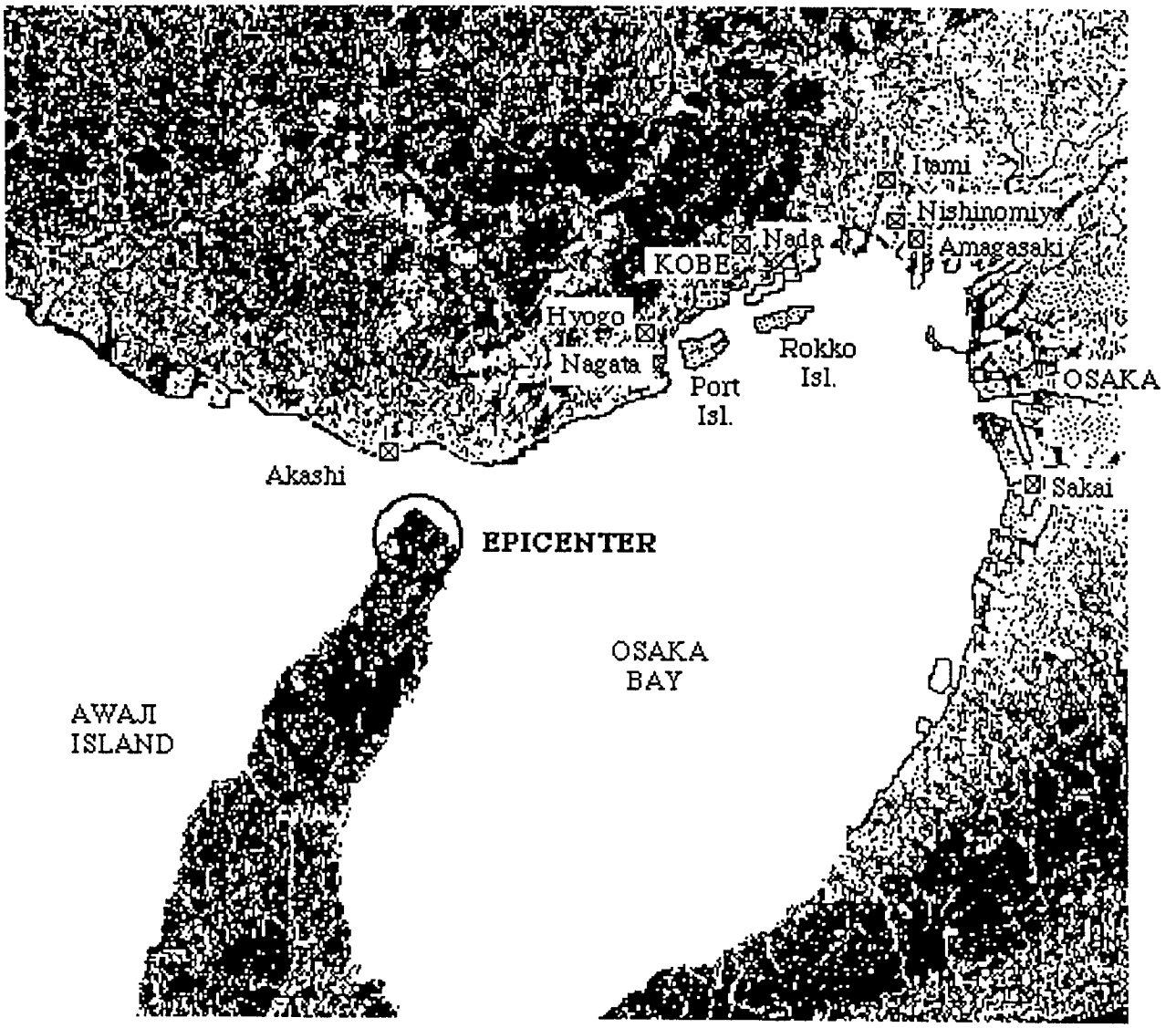

Figure 1.2 Osaka Bay Region

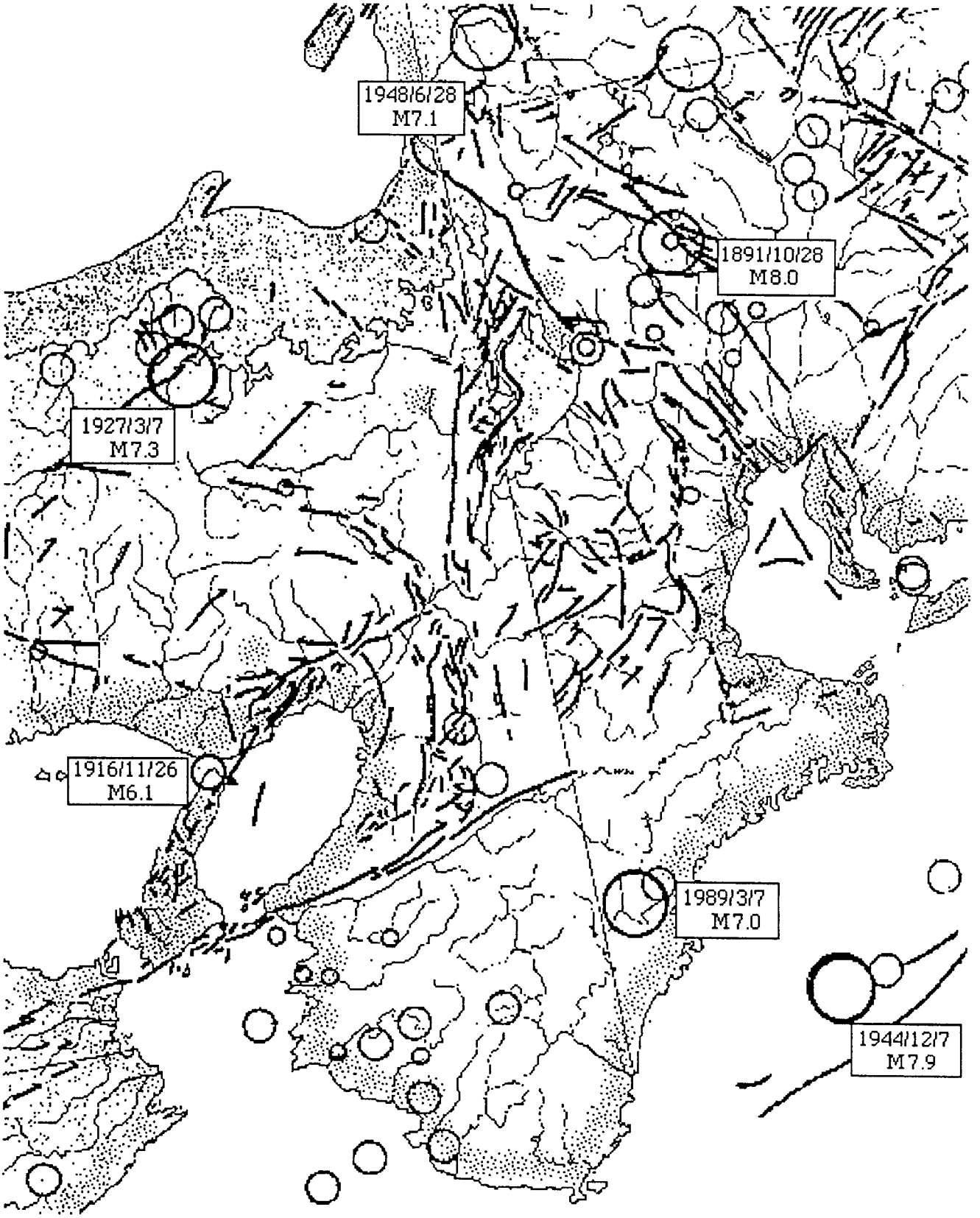

Figure 1.3. Epicentral locations of some large earthquakes.

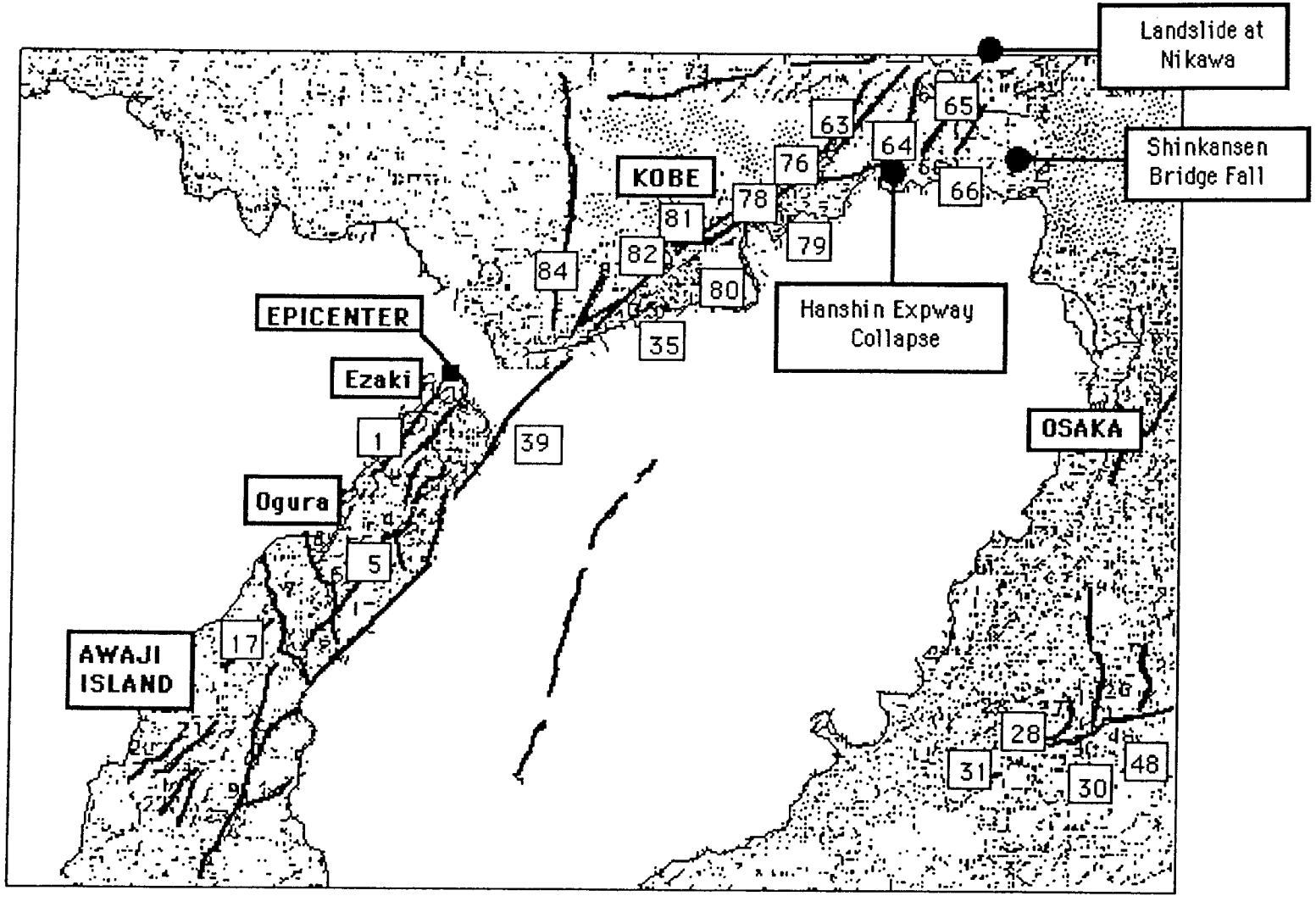

Figure 1.4. Active faults identified in Kobe region.

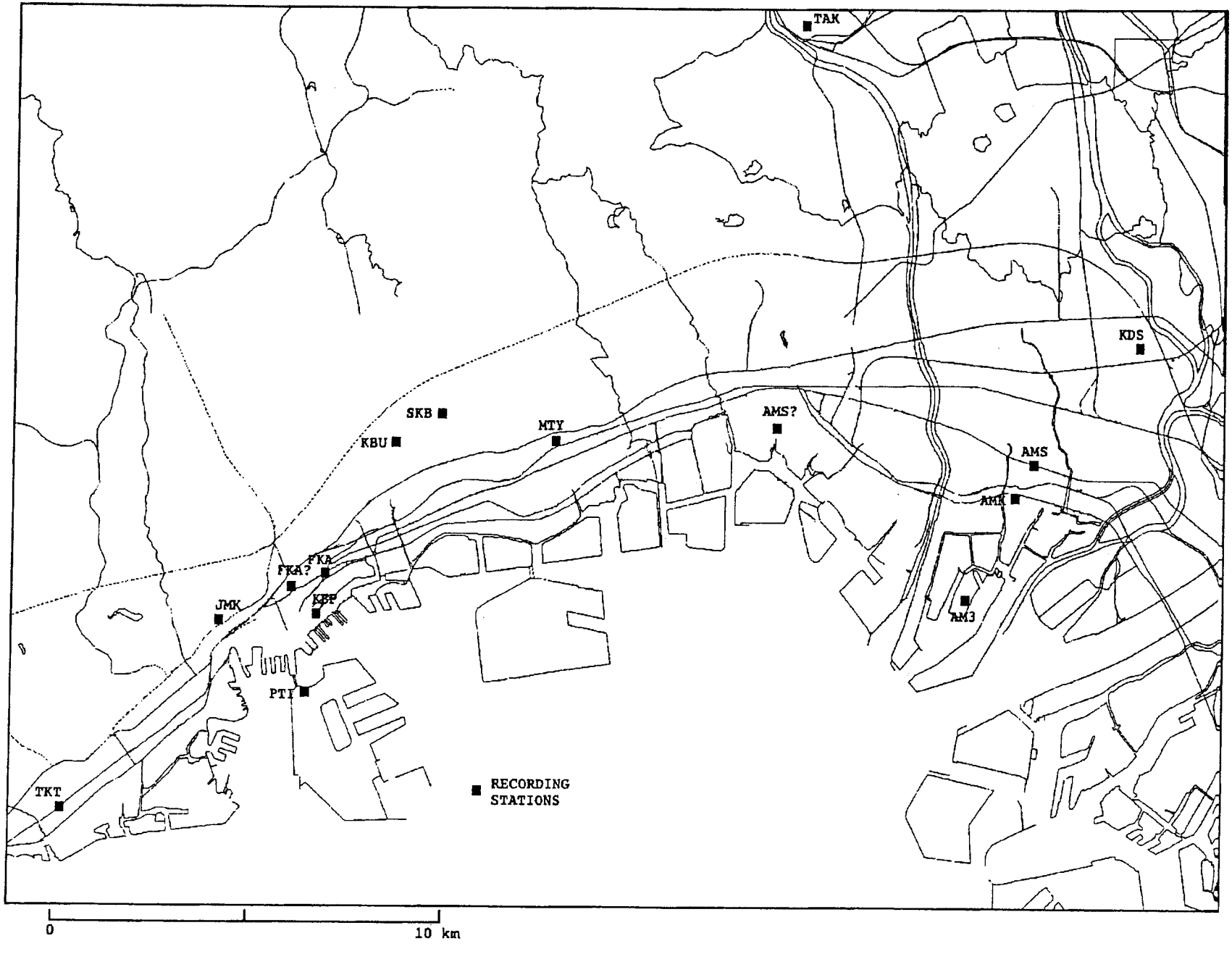

Figure 1.5. Recording station locations.

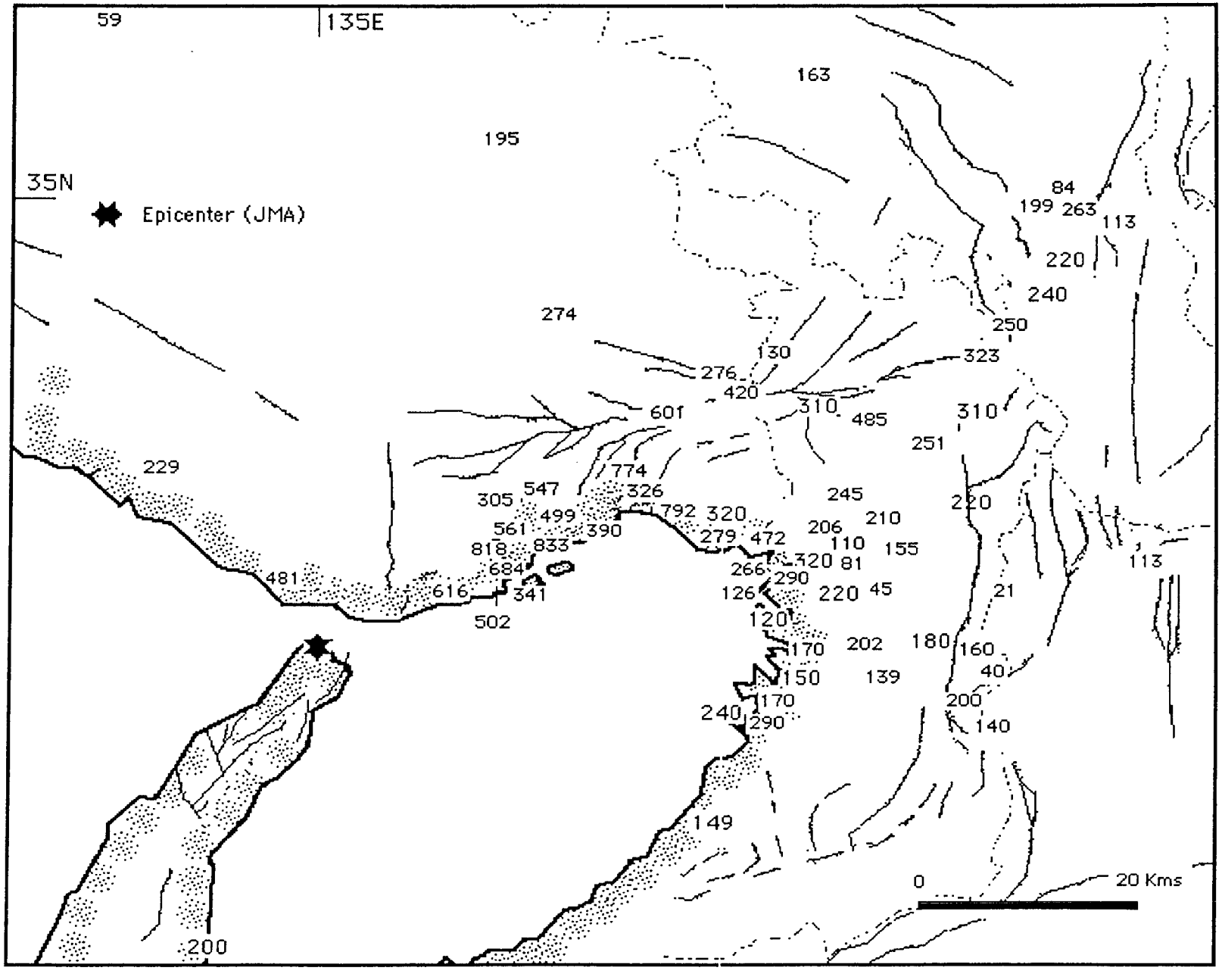

Figure 1.6. Recorded horizontal PGA's (in gals).

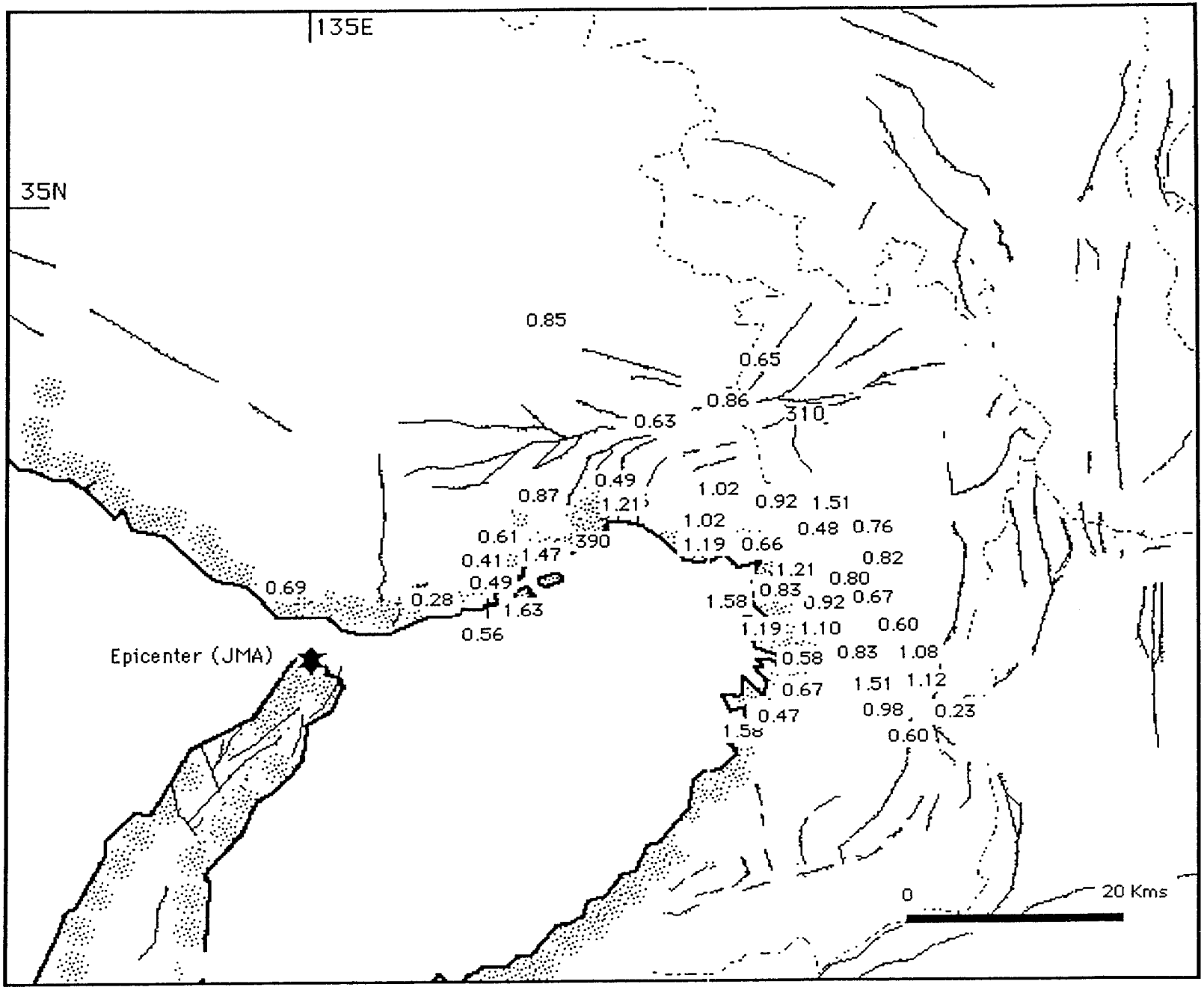

Figure 1.7. Ratios of peak vertical to horizontal PGA's.

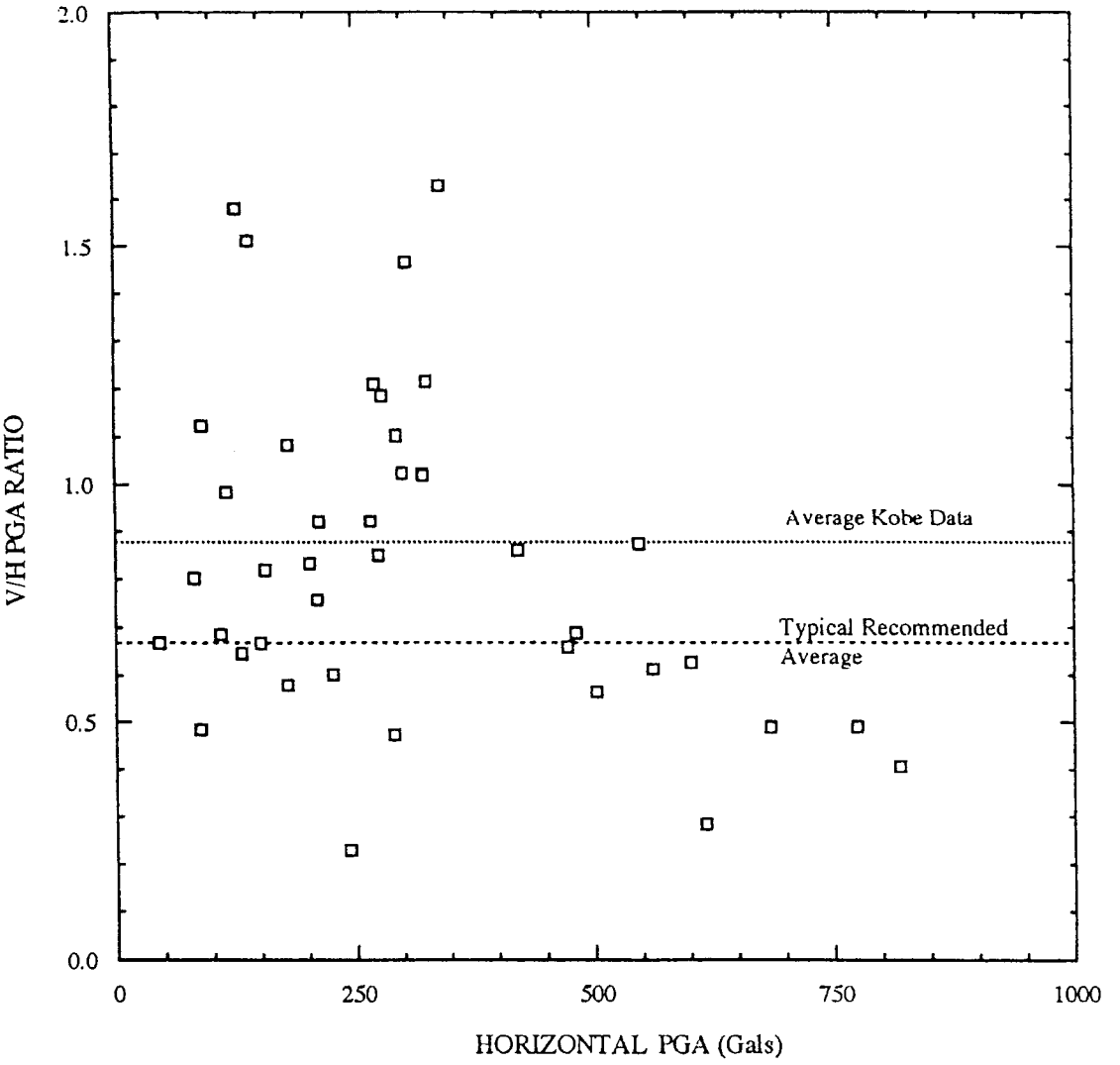

Figure 1.8. Ratios of peak vertical to horizontal accelerations.

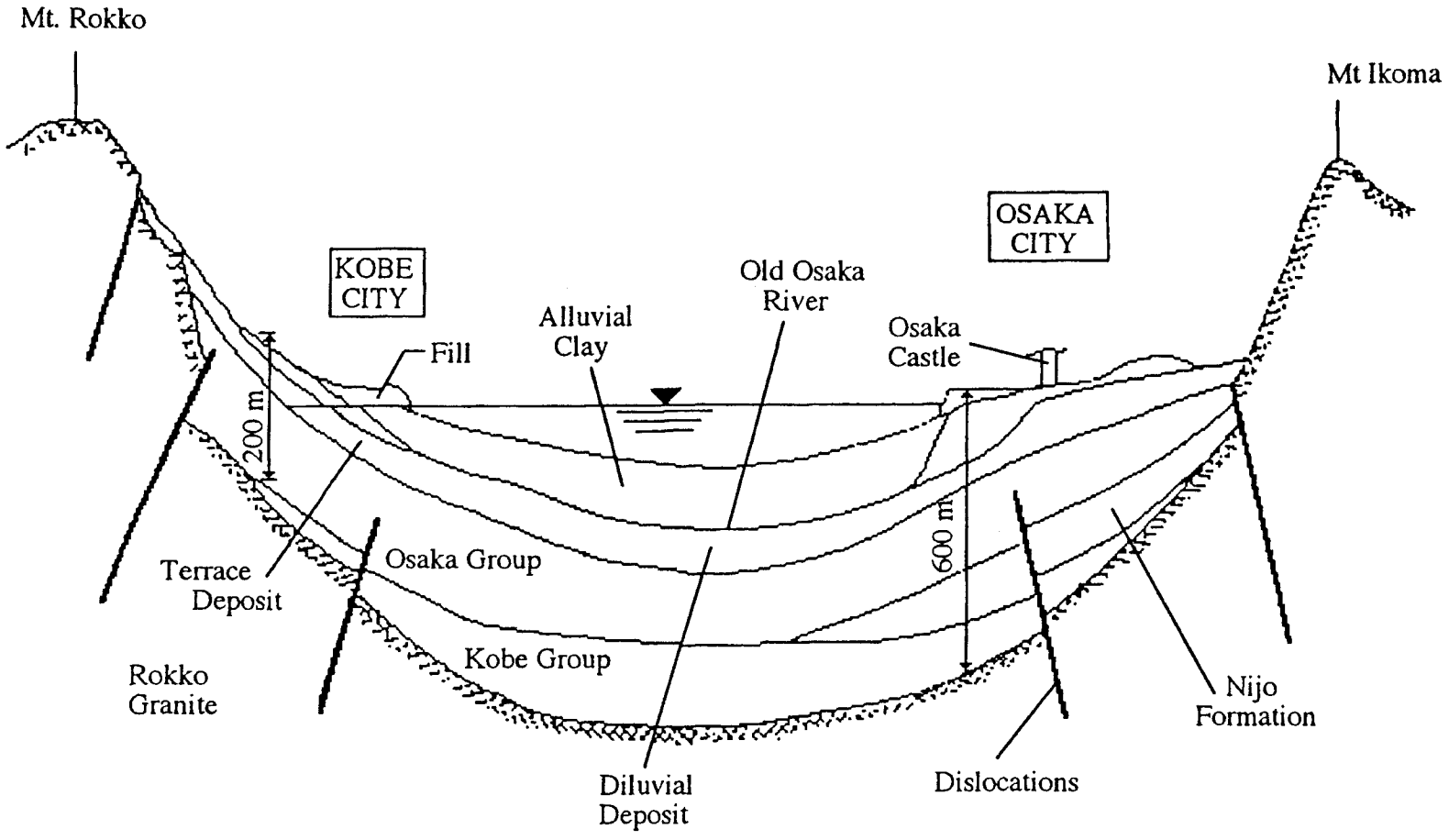

Figure 1.9. Schematic description of rock/soil profile beneath Kobe and Osaka cities.

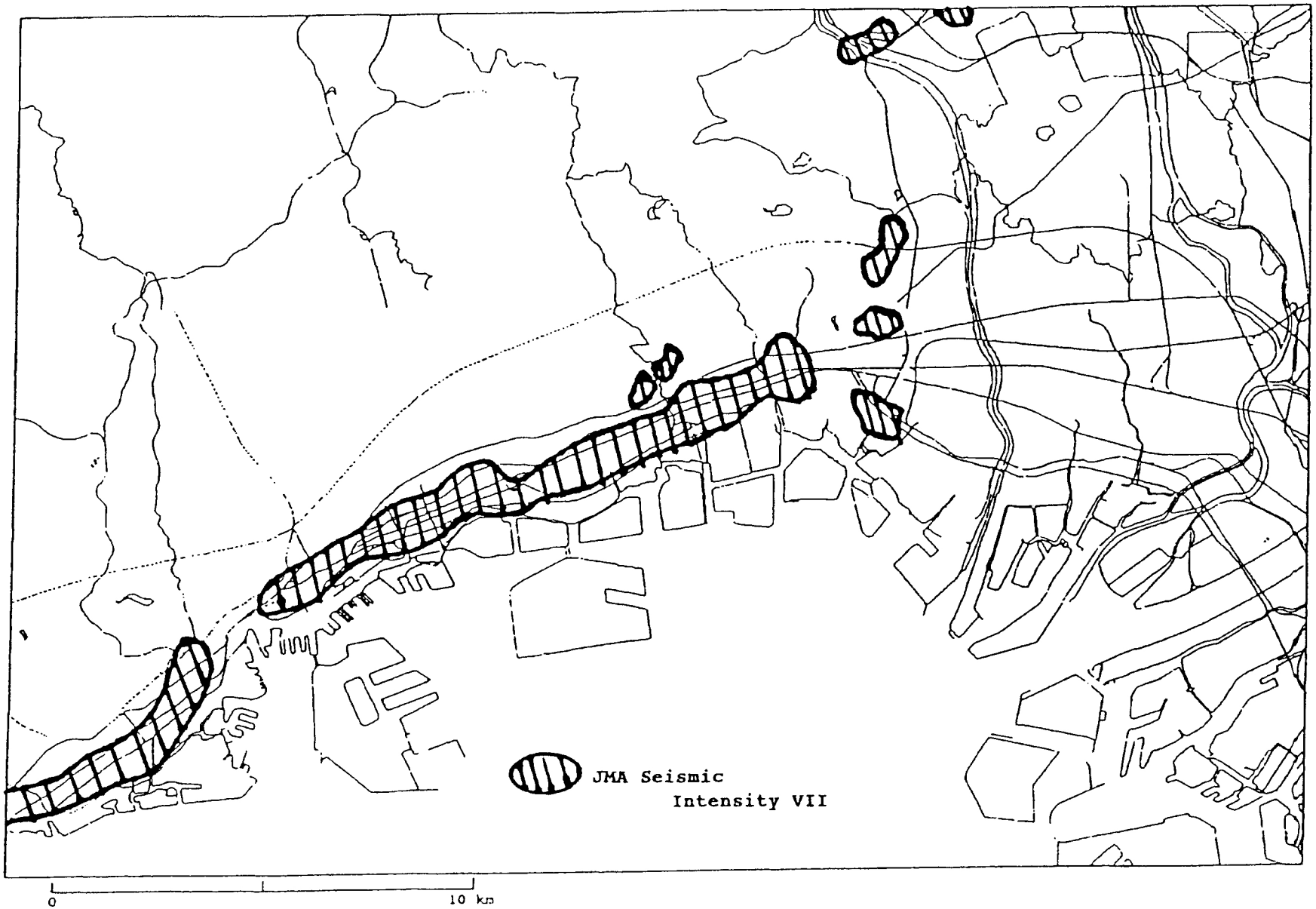

Figure 1.10. Approximate zones of JMA intensity VII (from Kimura, 1996).

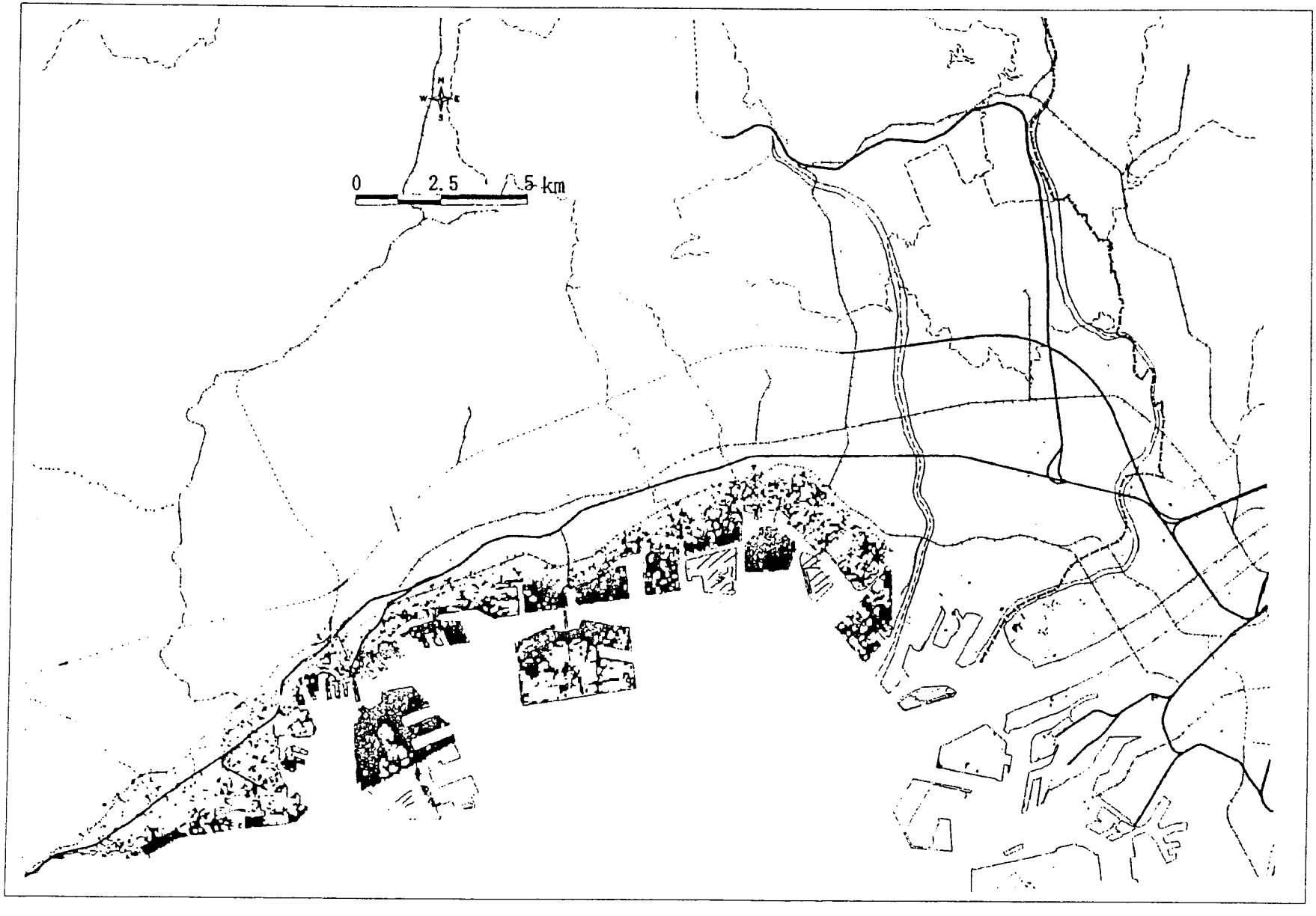

Figure 1.11. Zones of surface expression of ground failure (from Iwasaki, 1997),

2.0 GENERAL GEOTECHNICAL CONDITIONS

The Osaka/Kobe region consists of a complex grouping of soils which varies significantly across the valley and has been significantly altered by the fault dislocations which have occurred over the centuries (Osaka Soil Foundation Map, 1987). The simplified saucer configuration shown in Figure 1.9 indicates that the area is essentially founded on an alluvial and diluvial plateau consisting of soils of variable density and stiffness overlying bedrock. Since the 1930's, it has been recognized that long term settlement and subsidence is a problem for the softer silt and clay soils in the region. This subsidence has been related to consolidation effects induced by extraction of ground water, which has been exacerbated by the industrialization which has occurred since WWII. Depending upon location, the soil profile consists of alternating layers of softer silt/clay and sands/gravels forming the typical delta formation. The bottom of the softer alluvial soils in the center of Osaka Bay is approximately 100m below average sea level at Osaka Port (O.P.) and occurs at the location of the old Osaka River basin.

The site of Kobe City is located at the southern foot of the Rokko Mountains and is approximately 3 km wide in the NS direction and about 20 km long in the EW direction. It consists of a coastal plain and lands reclaimed from the sea. The Rokko Mountains, with elevations of about 3,000 ft in the east and about 1,500 ft in the west, is composed of a relatively soft granite rock with many faults running generally in the EW direction. The various fault movement occurring over the centuries results in the sharp changes in elevation from the mountains to the bay. The granite easily weathers and decomposes into the silty soil known as "Masado". It is characterized (Hamada, et al., 1995) by properties of low plasticity, low cohesion, high permeability and ease of erosion. These characteristics are different from those of Masado found in other regions around Osaka. Many alluvial fans have developed along the southern foot of the Rokko Mountains composed of coarse granite materials including sand, gravel and boulders which were transported by rivers heading to the bay.

Significant filling and creation of reclaimed lands of Osaka Bay began in the 1880's with construction of wharves and factories. As described by Hamada et al. (1995), a new reclamation project of cut and fill was conducted from 1953 to 1970, in which the fill material was excavated from the Rokko Mountains and dumped into the sea along the shoreline. The follow-on stage of the project, including reclamation of both Port Island and Rokko Island, was initiated in 1966 to expand the port facilities. Similar filling operations have been carried out in the adjacent cities of Ashiya and Nishinomiya. In the filled operation, various methods of soil improvements were applied where major structures were built to accelerate consolidation of the marine clays as well as compaction of the newly dumped fills.

Based on the descriptions provided by Shibata et al. (1996), the effects of the earthquake revealed that the loosely placed weathered Masado granite soil containing gravel sizes can liquefy. This soil was used heavily in the first phase of construction of Port Island as well as at parts of Rokko Island to the east. The results of cyclic triaxial tests indicate that the Masado gravelly soils can liquefy even at relatively high relative densities since the soil possesses contractive behavior during shear straining. Along the coastline to the east towards Osaka, at the mouth of rivers to the bay, the fine grained alluvial surface soils are relatively uniform grained and show tendency to easily liquefy in laboratory cyclic experiments.

2.1 Available Borehole Data and Soil Profiles

A substantial number of borings and standard penetration tests (SPT) have been performed for various projects in the region to clarify foundation conditions beneath structures in the survey area. A number of these are reprinted in Hamada et al. (1995) which were in turn compiled from other sources. On the basis of this information, a number of profiles were developed with sections drawn to help define generic subsurface conditions in this area. For this study, a number of additional profiles were provided by the Geo-Research Institute with soil descriptions and corresponding SPT N-values for locations from the Kobe City area eastward toward Osaka City.

On the basis of this data, the soil sites were divided in three relatively broad categories as shown in Figure 2.1. The harder sites (termed diluvium) occur at the higher elevations along the mountain side with the softer sites (alluvium) occurring at the base of the mountain along the original coastal plain. The relatively recently reclaimed lands occur adjacent to the coastline and comprise sites with the softest condition of the upper soils. The profiles used in this study are shown schematically in Figures 2.2 and 2.3, together with the locations (soil zones) of the specific borings comprising the profiles.

The available boring data were orgainzed by location in the EW direction from the Kobe City area (Zone A), the Nishinomiya area (Zone B) and the Osaka area (Zone C). The distribution of the sample blow count data in each area, for each generic soil type and for specific depth ranges is shown in Tables 2.1 through 2.3. The distribution of the SPT data indicates the usual stiffening of the soil with depth, but no major difference between the zones.

The generic description of the soil profiles in the reclaimed areas is essentially fill overlying soft Holocene marine clay. These, in turn, rest on a series of Pleistocene deposits which consist of alternate layers of dense sand and gravels, and stiff silty clays and clays. The fill is primarily composed of decomposed granite and Pliocene deposits of mudstone, sandstone and conglomerate, some Pleistocene marine clay, gravels and dredged sands. The fill also contains rubble and refuse from construction sites (Hamada et al., 1995). The thickness of the fill in the survey area varies from 5 m to 25 m generally increasing in thickness toward the bay. On the whole, the SPT N-value ranges between 5 to 20 bpf through the fill with some counts exceeding 50 bpf.

2.2 Profile Descriptions

The specific boring sections for each profile considered in this study is shown in Figures 2.4a through 2.4m. The boring is given a profile letter/number combination (H for hard area, S for soft area and R for reclaimed area). Each boring cross-section indicates the soil type and SPT blow counts available for that boring. Based on this information, a generic soil column was developed which consists of the following soil layers from the ground surface down:

surface fill layer (alluvium)
upper sand layer (alluvium)
upper clay layer 1 (alluvium)
upper gravel layer 1 (alluvium)

lower clay layer 2 (diluvium)
lower gravel layer 2 (diluvium)

Not all borings contained all these layers, in which case the specific thicknesses were set to zero in the computations.

2.3 Estimates of Soil Column Shear Wave Velocities

After each soil boring profile was developed for the specific soil layering description mentioned above, the next step in the process was to convert the sample SPT blow count data to estimates of low strain shear wave velocity for use in the site response calculations. This was done by using the correlation model generated by Iwasaki, et al. (1987). The correlation data were developed for borings taken in the Osaka region, a typical profile line being shown in Figure 2.5. The profiles were for similar soils as encountered in the Kobe region and are considered appropriate for the softer soils in the upper parts of the soil columns, namely the upper sands, clays and gravels. The borings used in the correlation development extended to depths of about 40m (about 120 ft). The specific correlation model is shown in Figure 2.6 together with a comparison between shear-wave velocities inferred from low-strain ground motion data and those predicted from blow counts. The hard, soft, and fill shear-wave velocity profiles are described in Section 4.0 (Finite-Fault Simulations).

Table 2.1

PERCENTILE DISTRIBUTION OF SPT'S FOR SANDY SOILS

Zone	Site Category	Depth Range (m)	SPT Blow Count Range N60						Sum
			0-5	5-10	10-20	20-30	30-50	>50	
A	Hard Ground	0-5	14	14	54	14	4	0	100
		5-10	0	0	19	38	43	0	100
		10-15	0	0	10	25	65	0	100
		15-20	0	0	5	15	80	0	100
	Soft Ground	0-5	0	10	44	23	23	0	100
		5-10	0	0	11	41	48	0	100
		10-15	0	2	4	12	82	0	100
		15-20	0	0	2	6	73	19	100
	Reclaimed Land	0-5	0	45	55	0	0	0	100
		5-10	0	0	50	50	0	0	100
		10-15	0	0	0	60	40	0	100
		15-20	0	0	28	28	44	0	100
B	Hard Ground	0-5	9	4	41	19	24	3	100
		5-10	0	4	22	27	40	7	100
		10-15	0	0	0	10	75	15	100
		15-20	0	0	0	3	75	22	100
	Soft Ground	0-5	0	21	67	8	4	0	100
		5-10	0	3	55	30	12	0	100
		10-15	0	4	24	33	33	6	100
		15-20	0	4	26	31	31	8	100
	Reclaimed Land	0-5	0	10	90	0	0	0	100
		5-10	0	0	78	22	0	0	100
		10-15	0	0	50	30	20	0	100
		15-20	0	0	37	19	44	0	100

Table 2.2

PERCENTILE DISTRIBUTION OF SPT'S FOR CLAY SOILS

Zone	Site Category	Depth Range (m)	SPT Blow Count Range N60							Sum
			0-2	2-4	4-8	8-12	12-20	20-30	>30	
A	Hard Ground	0-5	0	10	70	10	10	0	0	100
		5-10	0	2	30	40	22	0	6	100
		10-15	0	0	22	35	33	5	5	100
		15-20	0	0	0	10	60	25	5	100
	Soft Ground	0-5	0	37	24	23	9	3	4	100
		5-10	0	5	46	14	22	3	10	100
		10-15	0	2	25	23	24	11	15	100
		15-20	0	0	7	25	25	23	20	100
	Reclaimed Land	0-5	0	0	0	0	0	0	0	0
		5-10	0	0	40	60	0	0	0	100
		10-15	0	0	40	60	0	0	0	100
		15-20	0	0	100	0	0	0	0	100
B	Hard Ground	0-5	0	10	27	22	31	5	5	100
		5-10	0	4	0	16	45	10	25	100
		10-15	0	0	0	8	42	50	0	100
		15-20	0	0	0	15	45	0	40	100
	Soft Ground		(0-2)	(2-5)	(5-10)	(10-20)	(20-30)	(>30)		
		0-5	2	49	43	4	2	0		100
		5-10	0	49	41	10	0	0		100
		10-15	0	45	45	10	0	0		100
		15-20	0	17	44	23	8	8		100
	Reclaimed Land	0-5	23	67	10	0	0	0	0	100
		5-10	5	45	50	0	0	0	0	100
		10-15	0	39	44	13	4	0	0	100
		15-20	0	5	50	45	0	0	0	100

Table 2.3

PERCENTILE DISTRIBUTION OF SPT'S FOR GRAVELLY SOILS

Zone	Site Category	Depth Range (m)	SPT Blow Count Range N60						Sum
			0-5	5-10	10-20	20-30	30-50	>50	
A	Hard Ground	0-5	0	6	27	31	29	7	100
		5-10	0	0	2	9	80	9	100
		10-15	0	0	0	2	97	1	100
		15-20	0	0	0	4	73	23	100
	Soft Ground	0-5	0	5	27	34	34	0	100
		5-10	0	0	0	4	75	21	100
		10-15	0	0	0	0	55	45	100
		15-20	0	0	0	0	55	45	100
	Reclaimed Land	0-5	0	31	50	12	0	7	100
		5-10	0	20	0	0	80	0	100
		10-15	20	0	0	0	75	5	100
		15-20	0	0	0	0	100	0	100
B	Hard Ground	0-5	12	10	21	38	19	0	100
		5-10	0	0	0	25	50	25	100
		10-15	0	0	0	30	70	0	100
		15-20	0	0	0	0	48	52	100
	Soft Ground	0-5	9	21	33	31	4	2	100
		5-10	2	2	4	26	50	16	100
		10-15	0	0	0	15	50	35	100
		15-20	0	0	0	0	49	51	100
	Reclaimed Land	0-5	20	30	50	40	0	0	100
		5-10	3	0	0	76	21	0	100
		10-15	0	3	0	2	95	0	100
		15-20	0	0	0	7	54	39	100

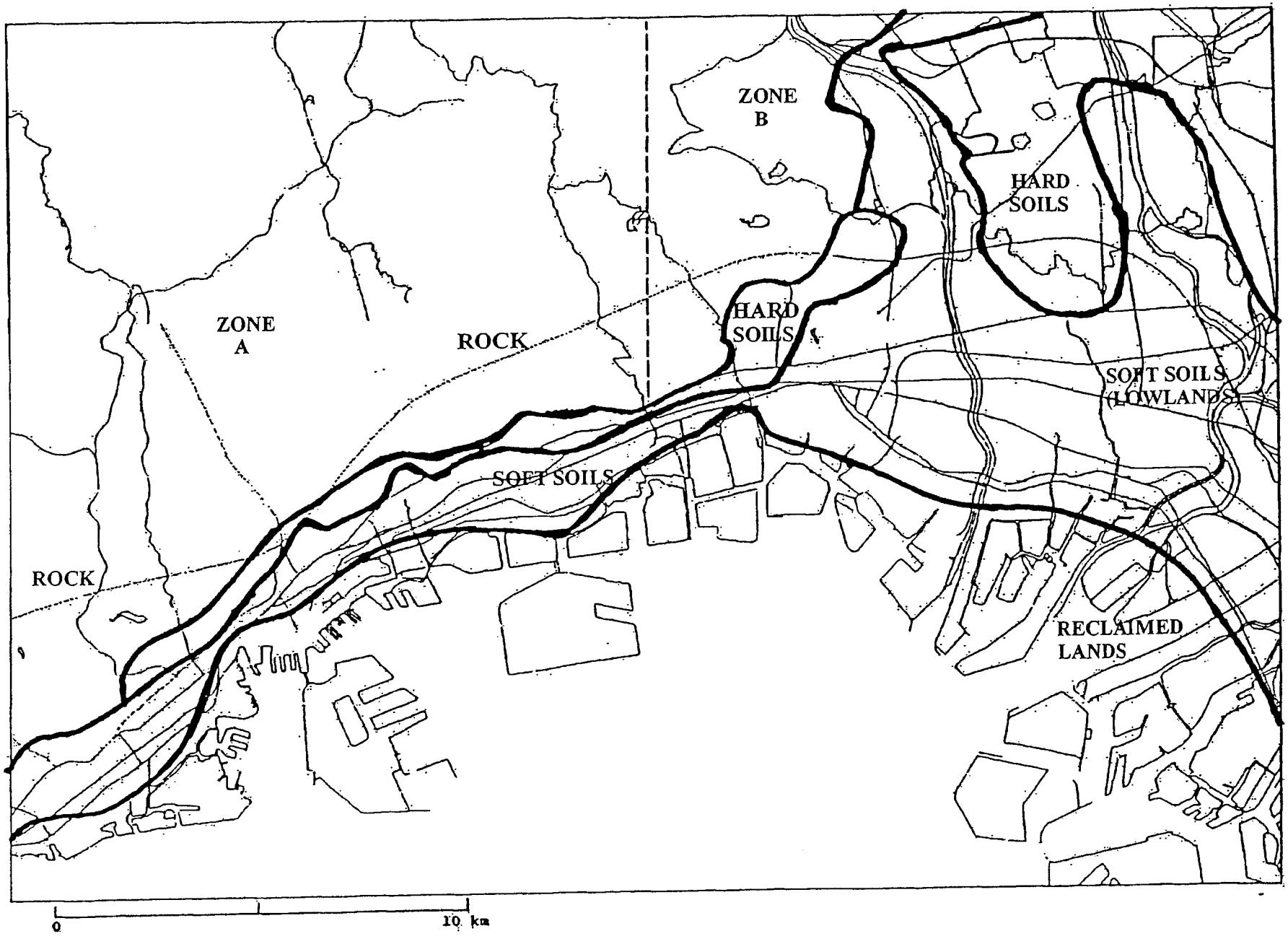

Figure 2.1. General site categories (rock, hard, soft, and fill soils).

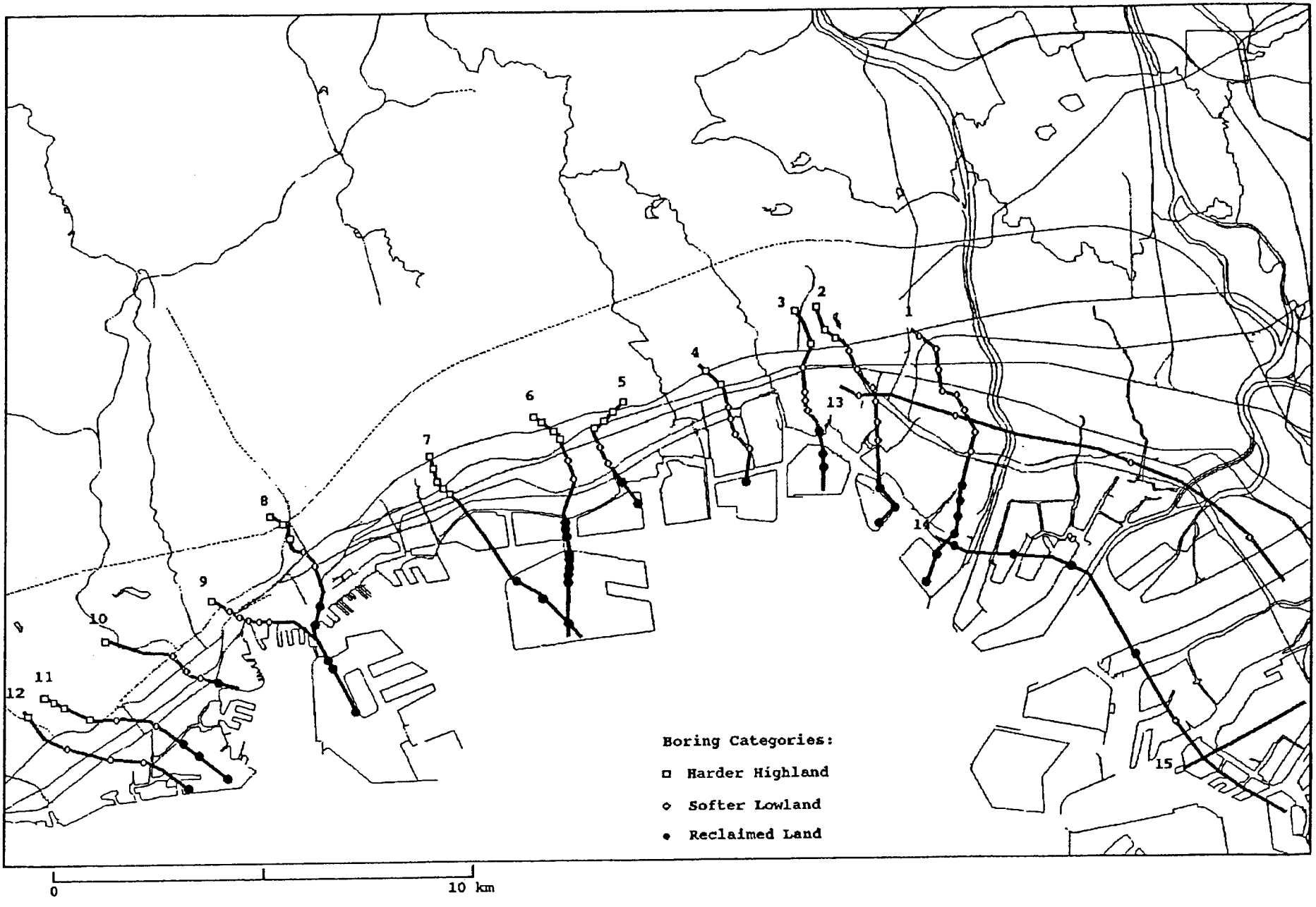

Figure 2.2. Soil profiles evaluated (from Iwasaki, 1997).

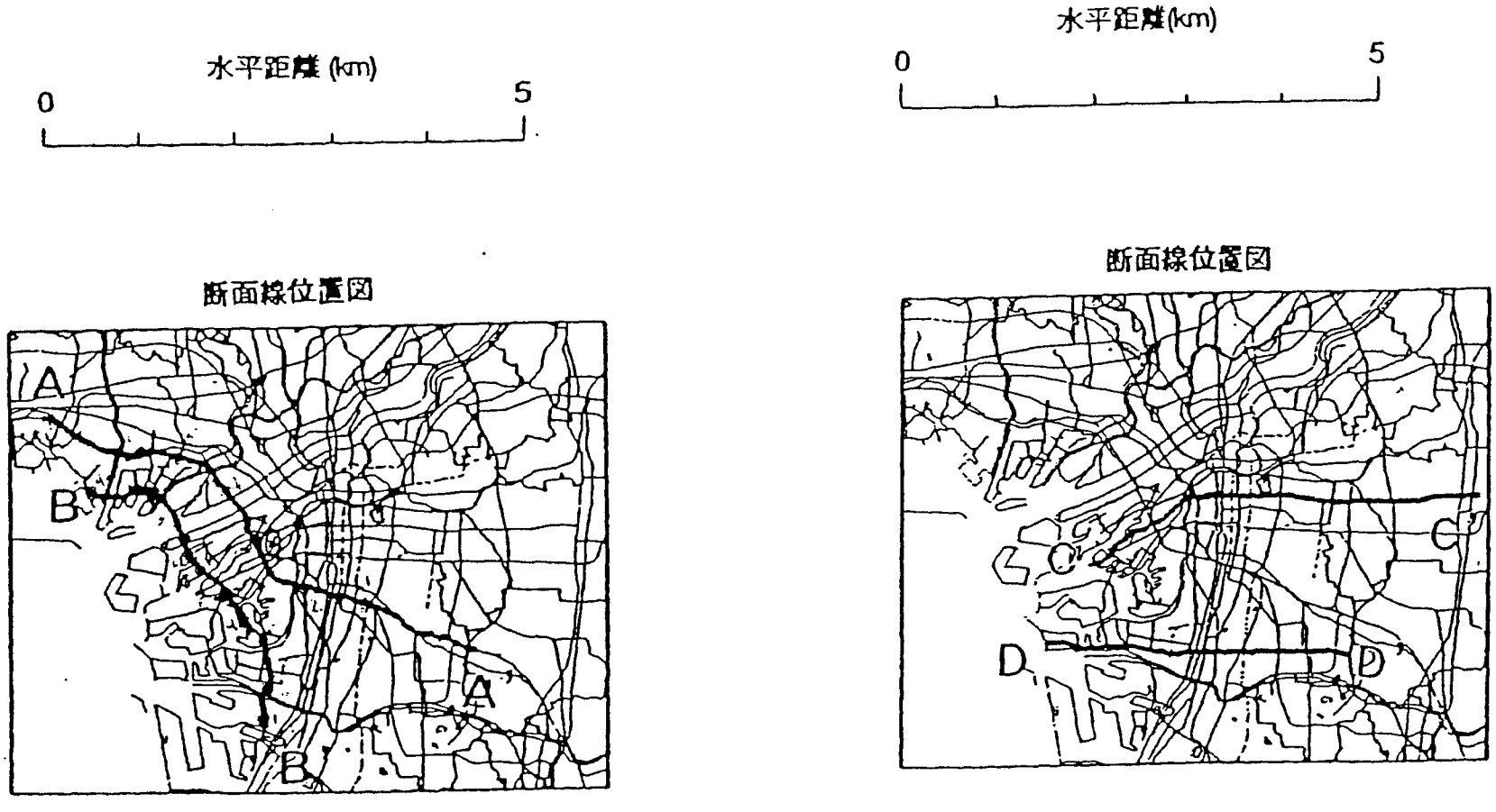

Figure 2.3. Additional soil profiles evaluated (from Iwasaki, 1995).

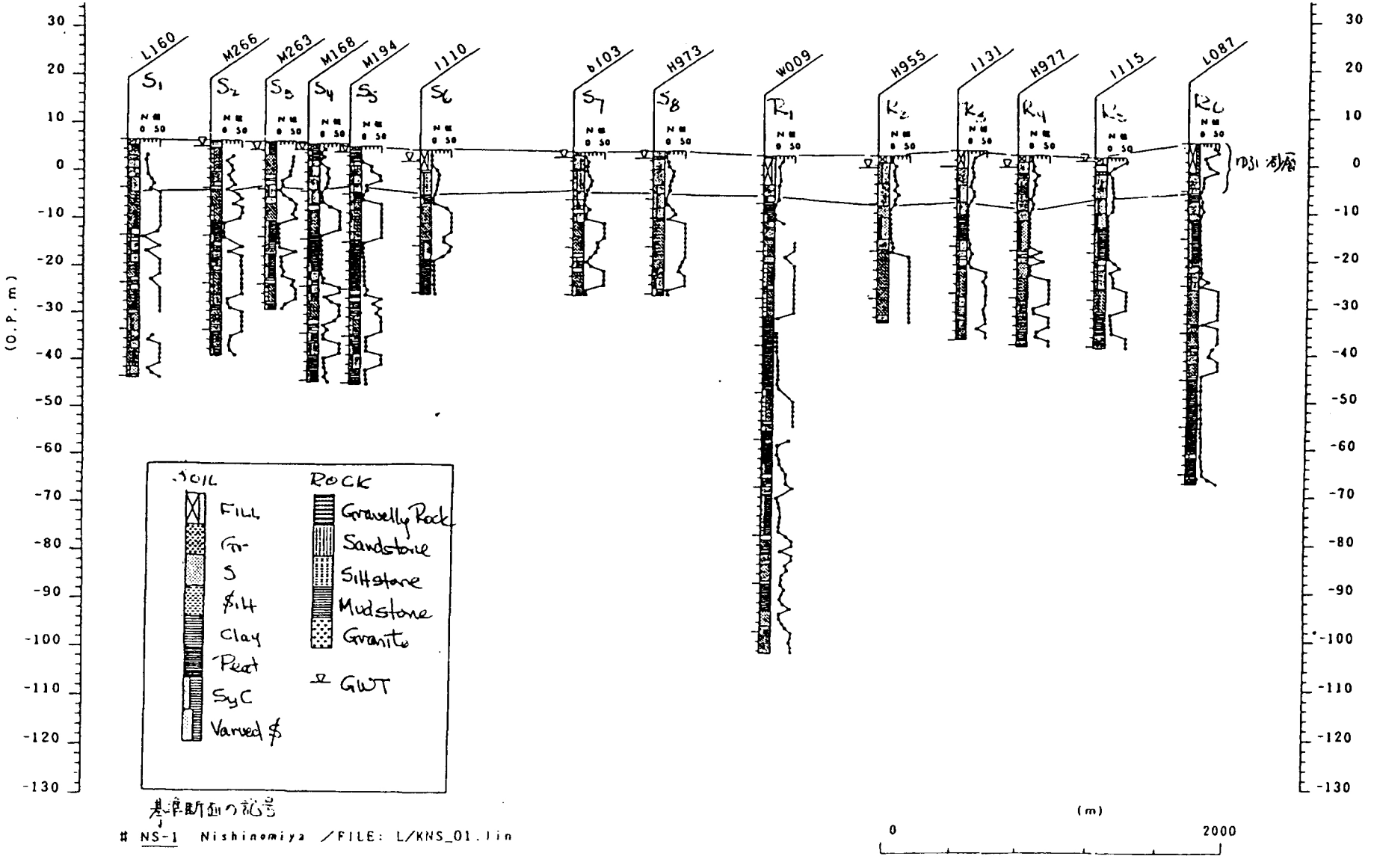

Figure 2.4a. Soil profile boring logs and blow counts.

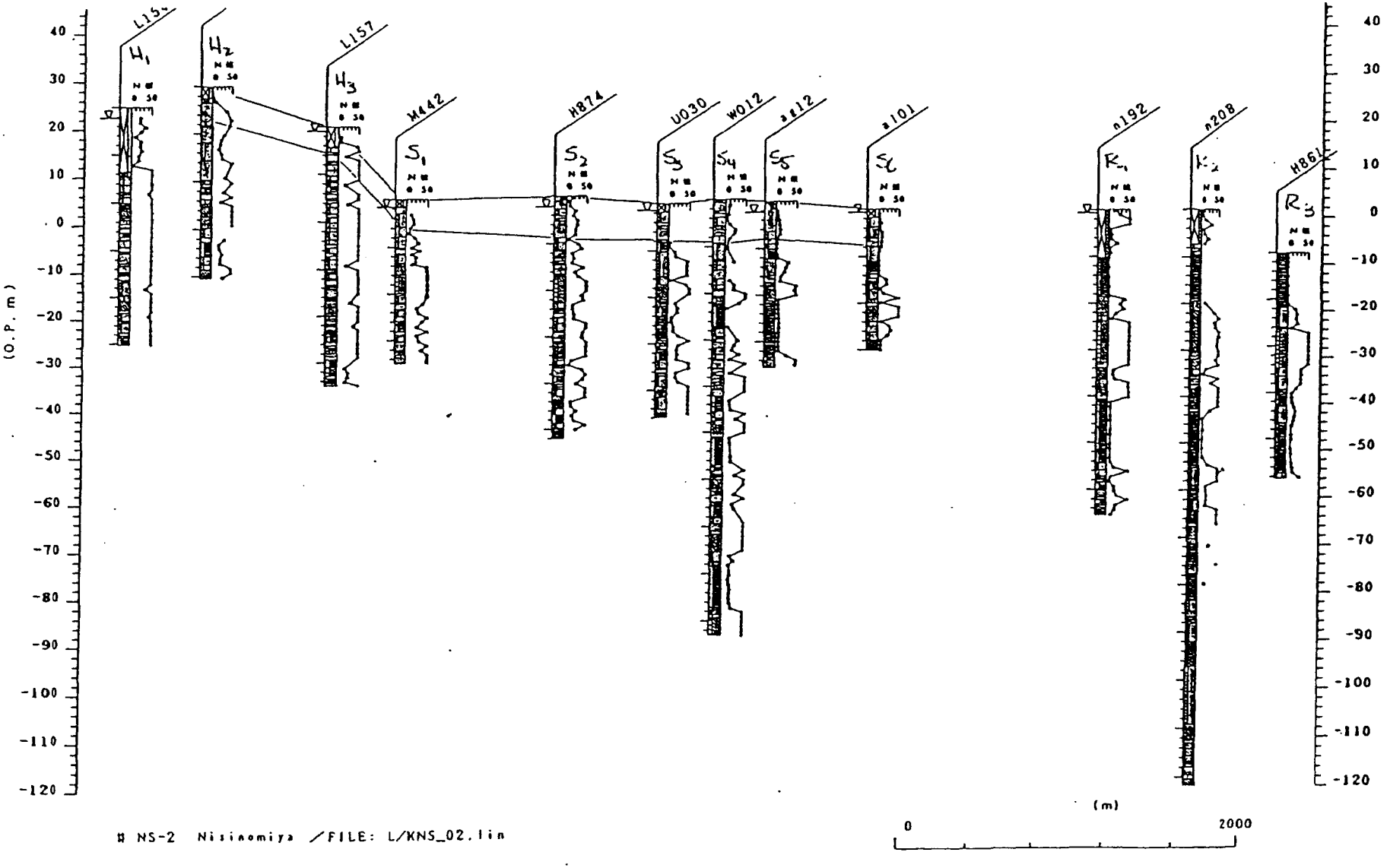
(O.P.m)
40
30
20
10
0
-10
-20
-30
-40
-50
-60
-70
-80
-90
-100
-110
-120
L152
L157
M442
H874
U030
W012
n192
n208
H861
(m)
0
2000
NS-2 Nishinomiya /FILE: L/KNS_02.lin

Figure 2.4b.

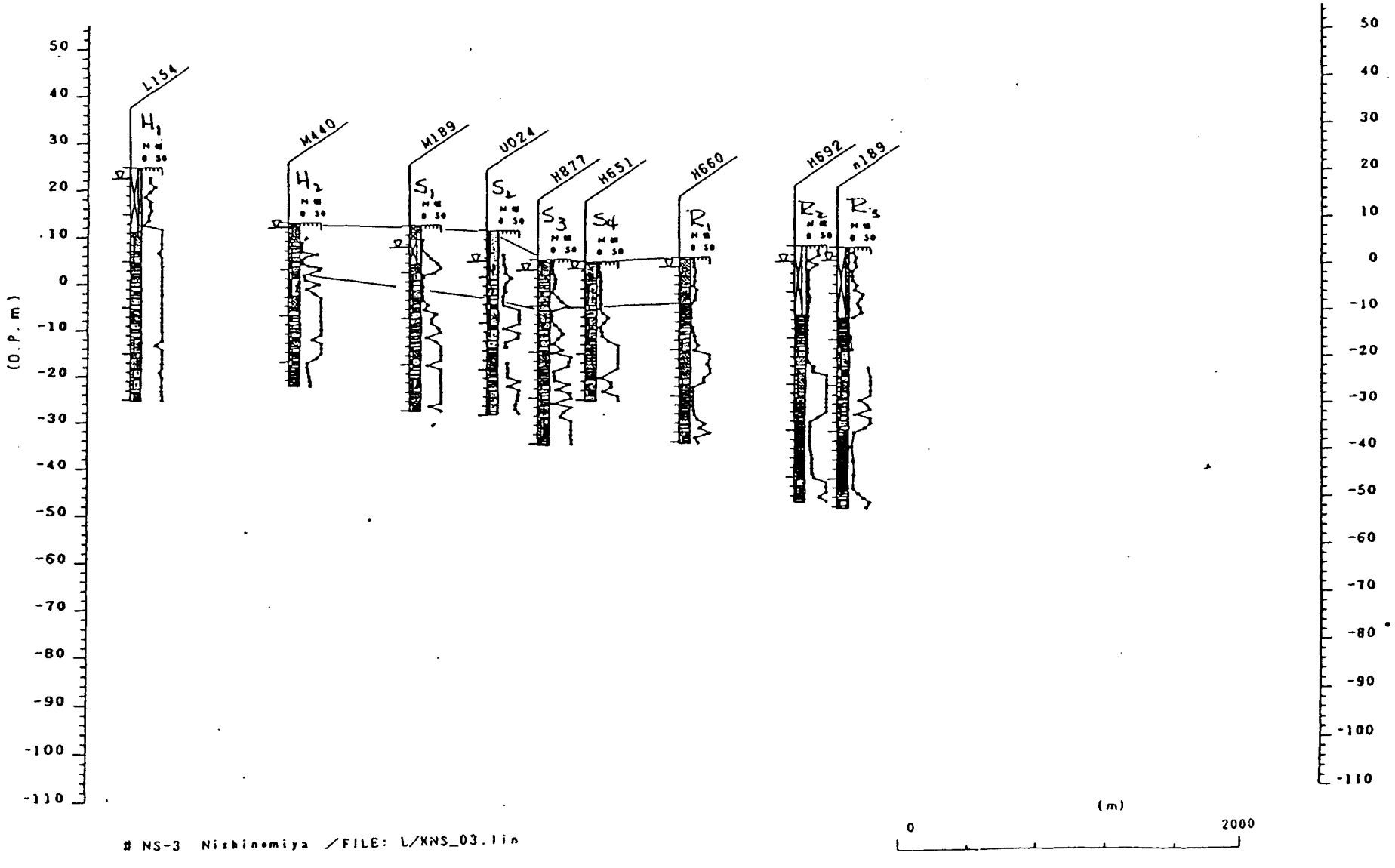
L154
M440
M189
U024
H877
H651
H660
H692
n189
(O.P.m)
50
40
30
20
10
0
-10
-20
-30
-40
-50
-60
-70
-80
-90
-100
-110
(m)
0
2000
NS-3 Nishinomiya /FILE: L/KNS_03.lin

Figure 2.4c.

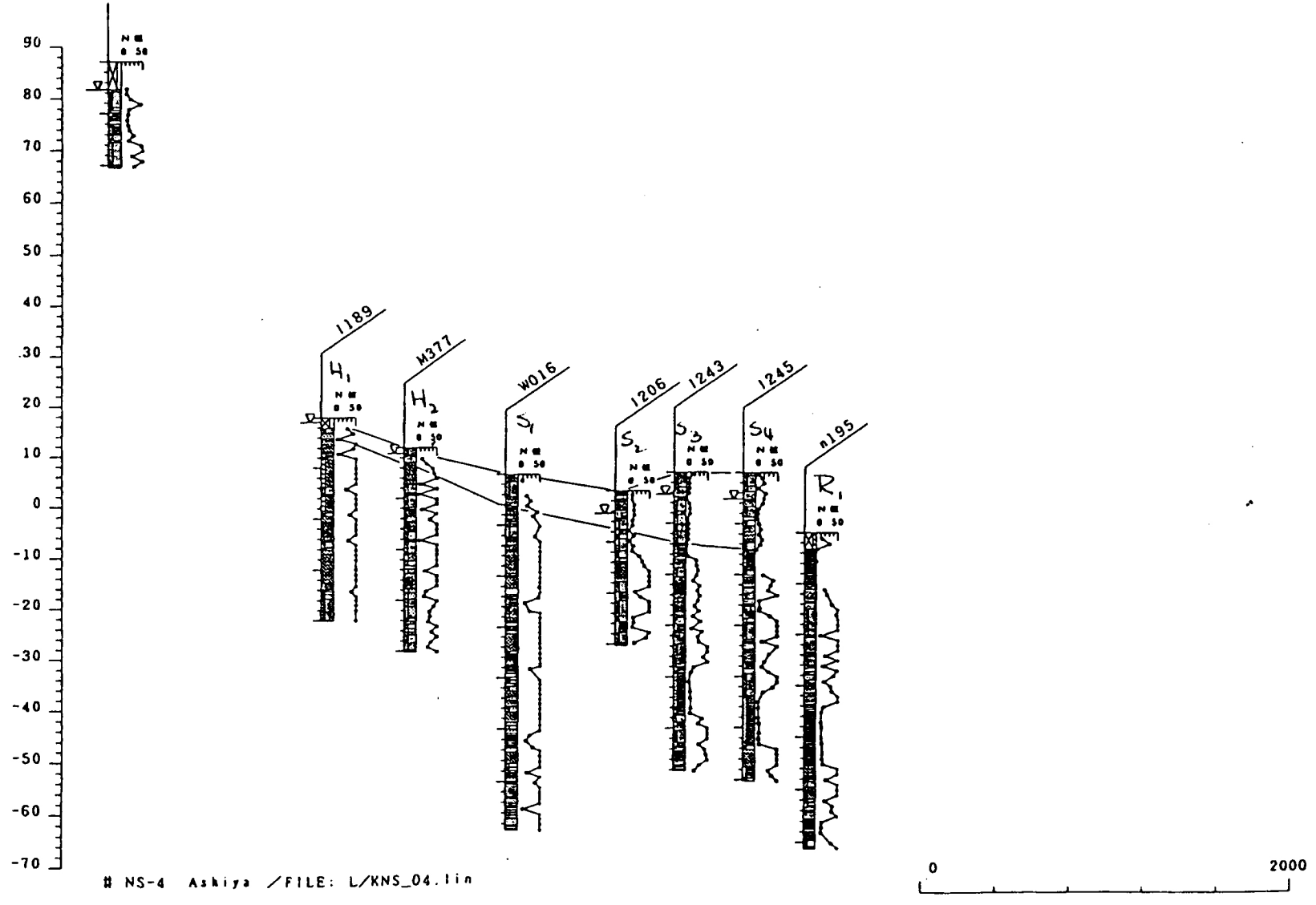
1189
M377
W016
1206
1243
1245
n195
90
80
70
60
50
40
30
20
10
0
-10
-20
-30
-40
-50
-60
-70
(O.P.m)
NS-4 Ashiya /FILE: L/KNS_04.lin
0
2000

Figure 2.4d.

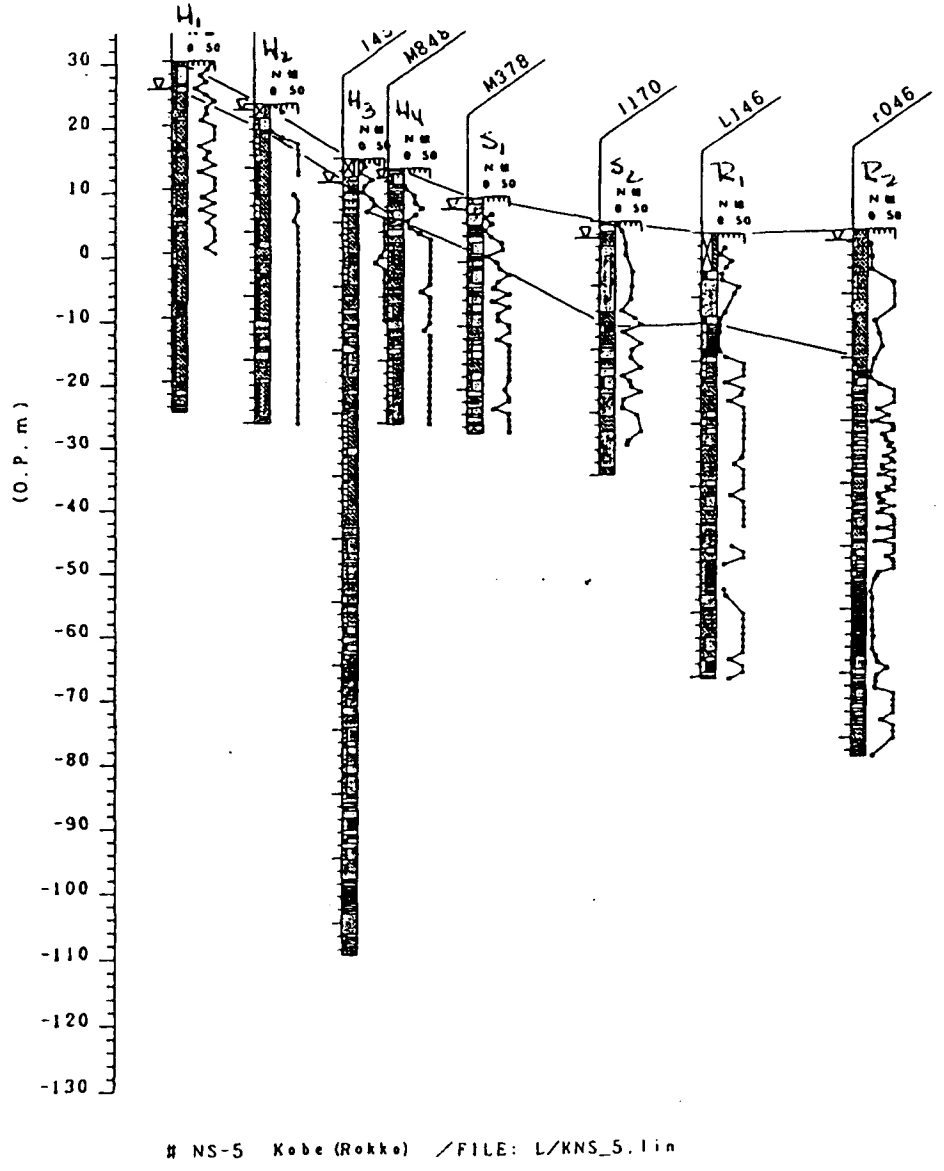
M84b
M378
1170
L146
r046
(O.P.m)
30
20
10
0
-10
-20
-30
-40
-50
-60
-70
-80
-90
-100
-110
-120
-130
NS-5 Kobe (Rokko) /FILE: L/KNS_5.lin


(m)
0
2000

Figure 2.4e.

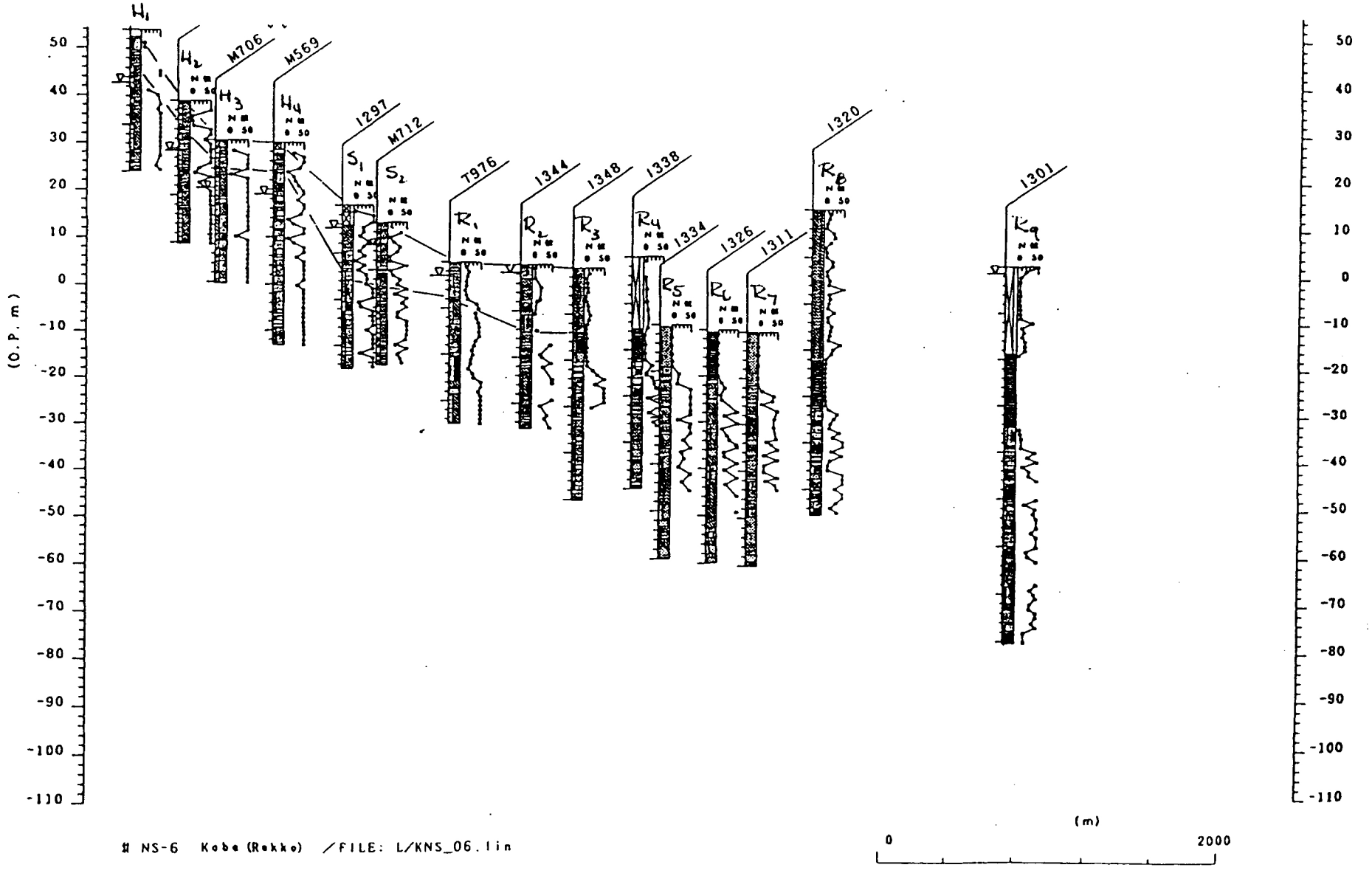
H1
H2
M706
H3
M569
H4
1297
S1
M712
S2
7976
R1
1344
R2
1348
R3
1338
R4
1334
R5
1326
R6
1311
R7
1320
R8
1301
R9
50
40
30
20
10
0
-10
-20
-30
-40
-50
-60
-70
-80
-90
-100
-110
(O.P.m)
NS-6 Kobe (Rokko) /FILE: L/KNS_06.lin
(m)
0
2000

Figure 2.4f.

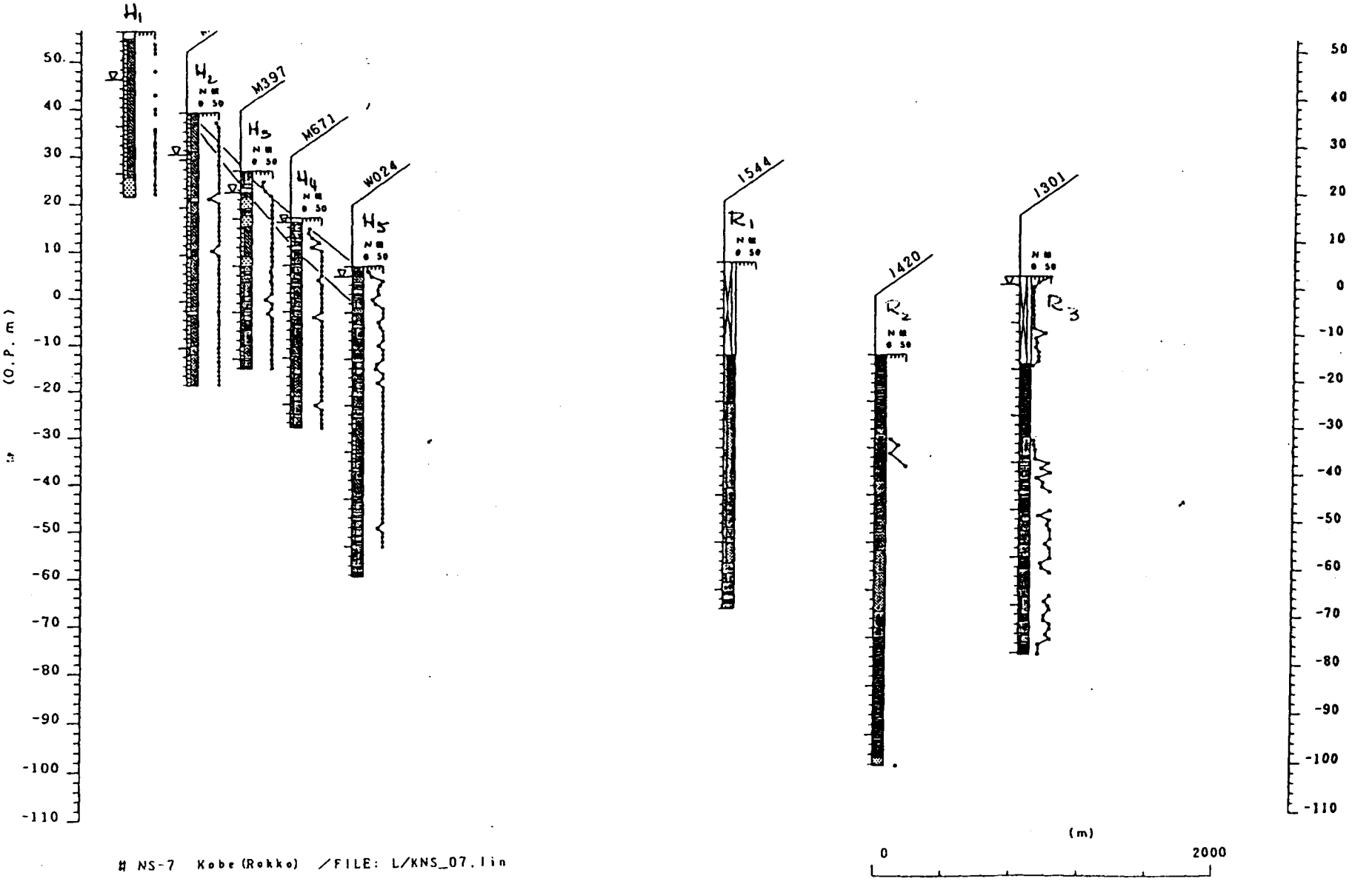
H1
H2
H3
H4
H5
M397
M671
W024
1544
1420
1301
R1
R2
R3
(O.P.m)
50
40
30
20
10
0
-10
-20
-30
-40
-50
-60
-70
-80
-90
-100
-110
(m)
0
2000
NS-7 Kobe (Rokko) /FILE: L/KNS_07.lin

Figure 2.4g.

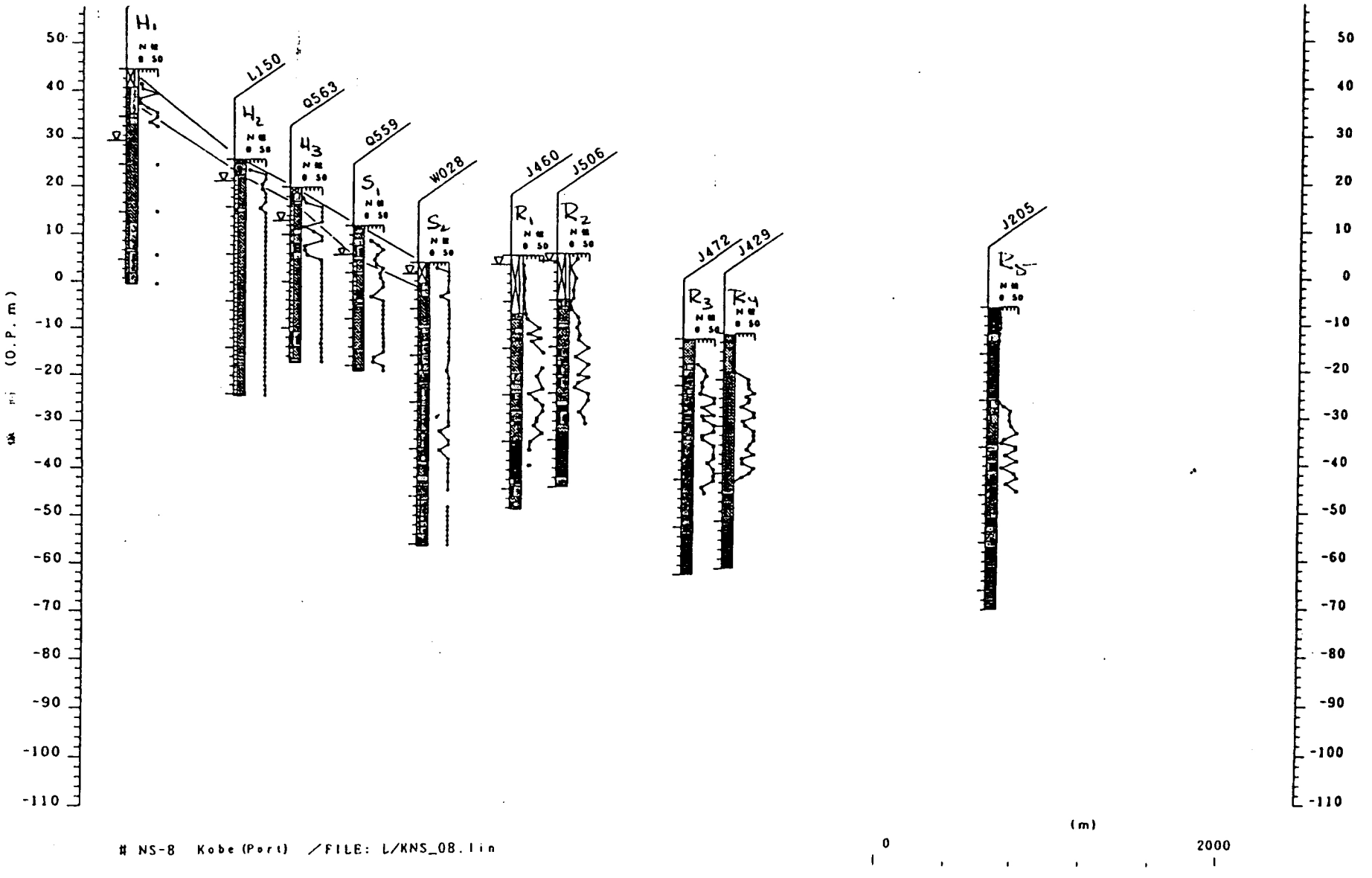
H1
L150
H2
Q563
H3
Q559
S1
W028
S2
J460
J506
R1
R2
J472
J429
R3
R4
J205
J3
50
40
30
20
10
0
-10
-20
-30
-40
-50
-60
-70
-80
-90
-100
-110
(O.P.m)
NS-8 Kobe (Port) /FILE: L/KNS_08.lin
0
2000
(m)

Figure 2.4h.

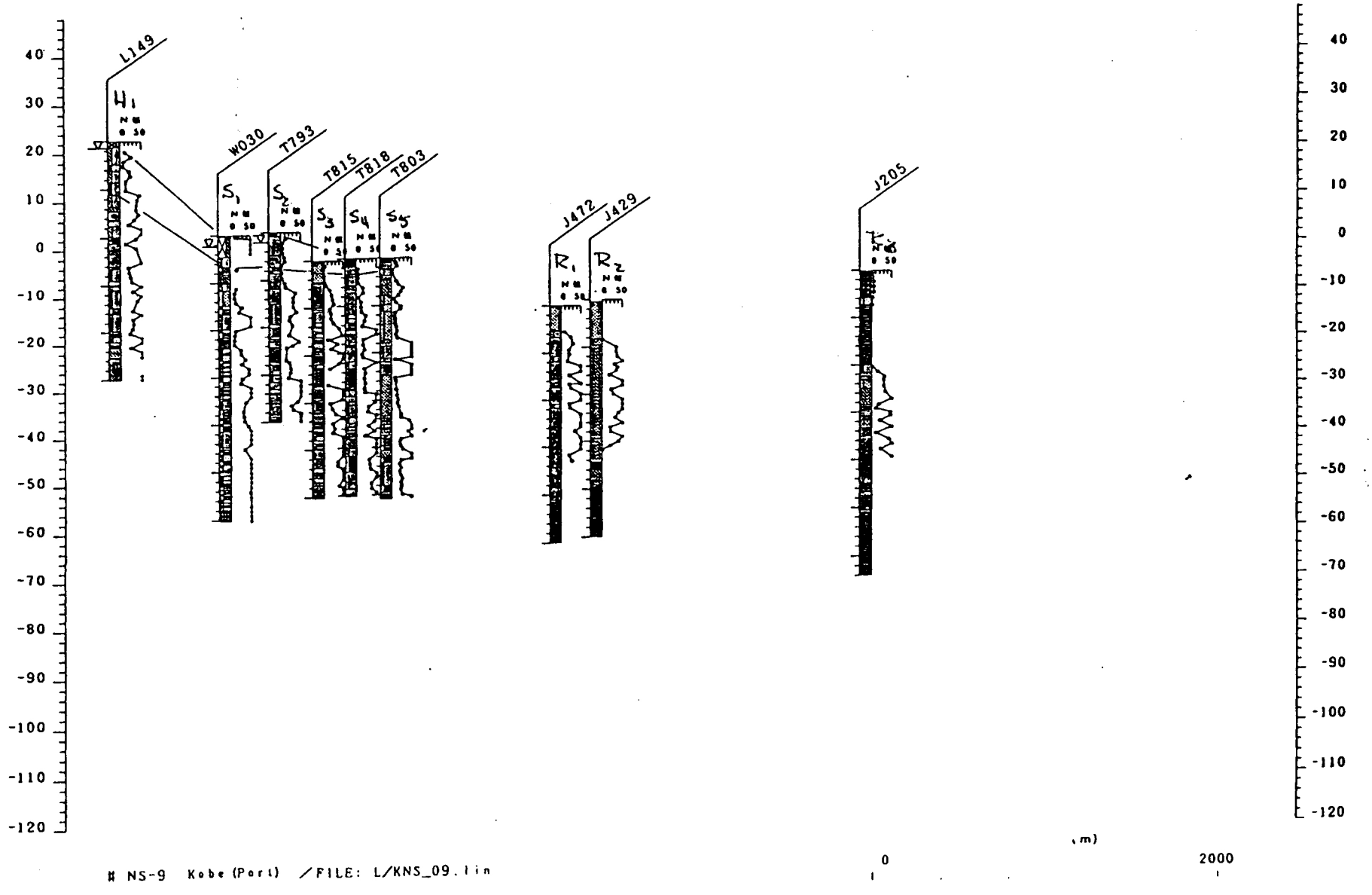
L149
W030
T793
T815
T818
T803
J472
J429
J205
(O.P.m)
0
2000
(m)
NS-9 Kobe (Port) /FILE: L/KNS_09.lin

Figure 2.4i.

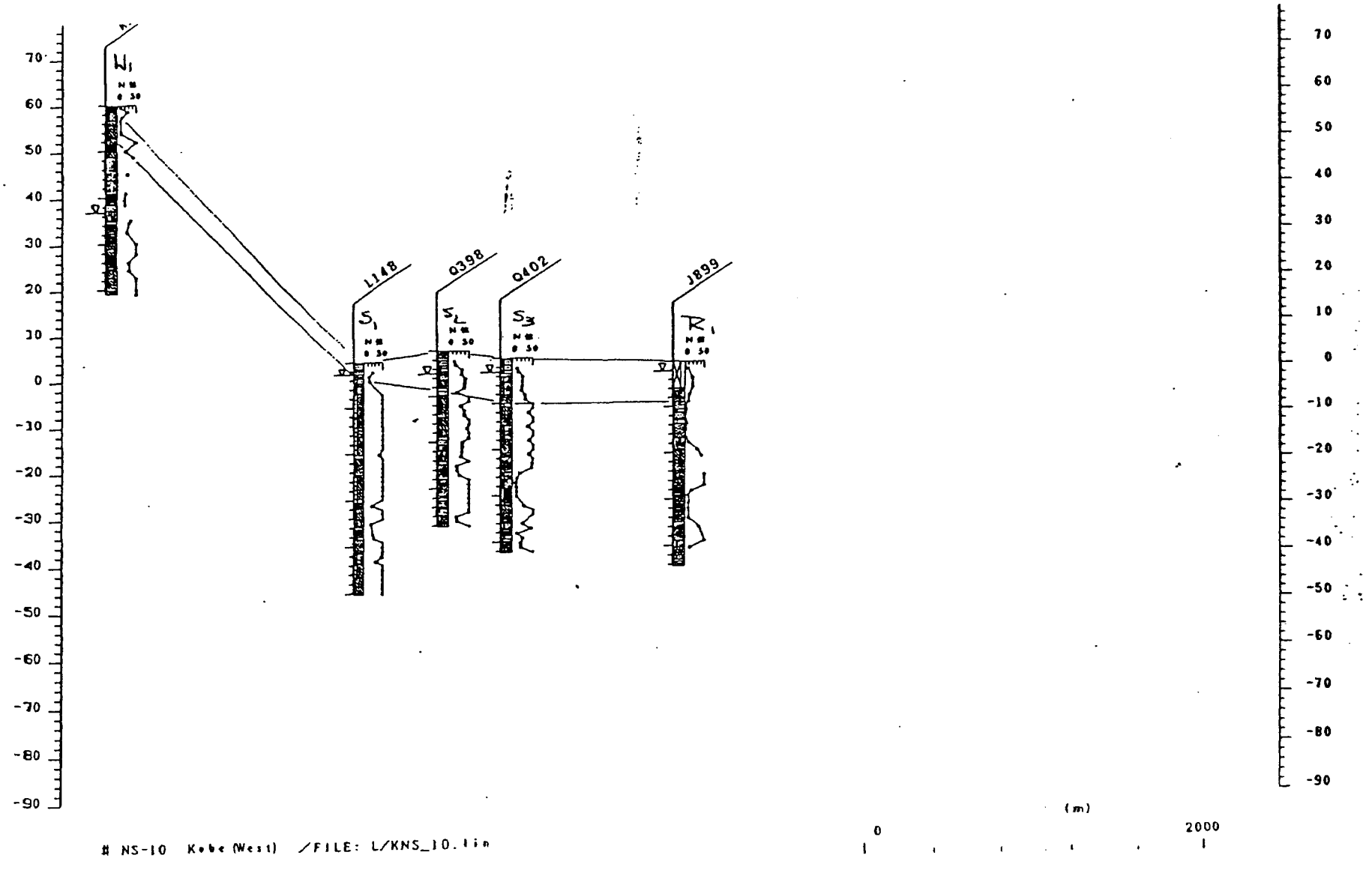
(O.P.m)
70
60
50
40
30
20
10
0
-10
-20
-30
-40
-50
-60
-70
-80
-90
L148
Q398
Q402
J899
(m)
0
2000
NS-10 Kobe (West) /FILE: L/KNS_10.lin

Figure 2.4j.

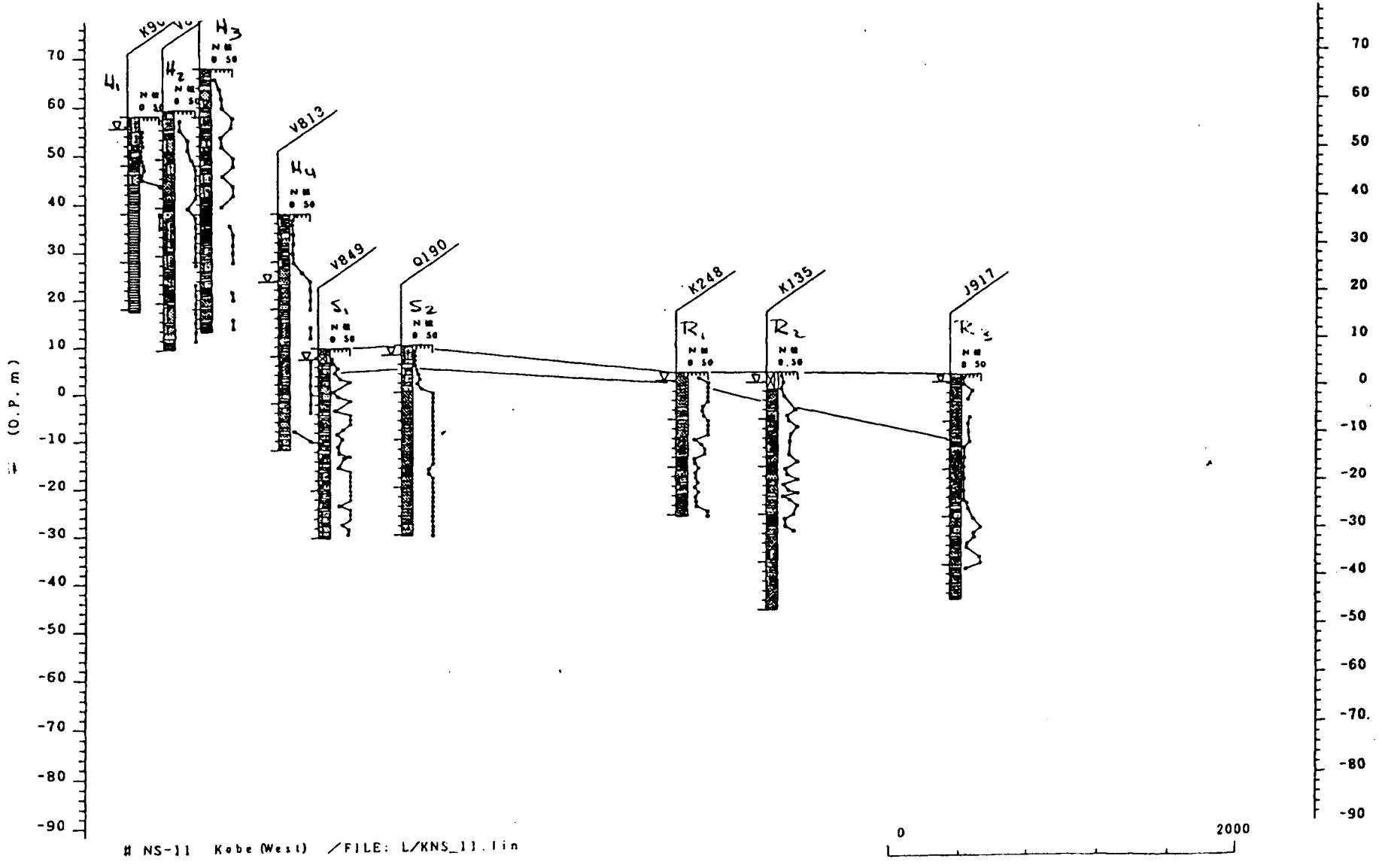
K94
H3
H2
H1
V813
H4
V849
Q190
S1
S2
K248
K135
J917
R1
R2
R3
(O.P.m)
70
60
50
40
30
20
10
0
-10
-20
-30
-40
-50
-60
-70
-80
-90
NS-11 Kobe (West) /FILE: L/KNS_11.lin
0
2000

Figure 2.4k.

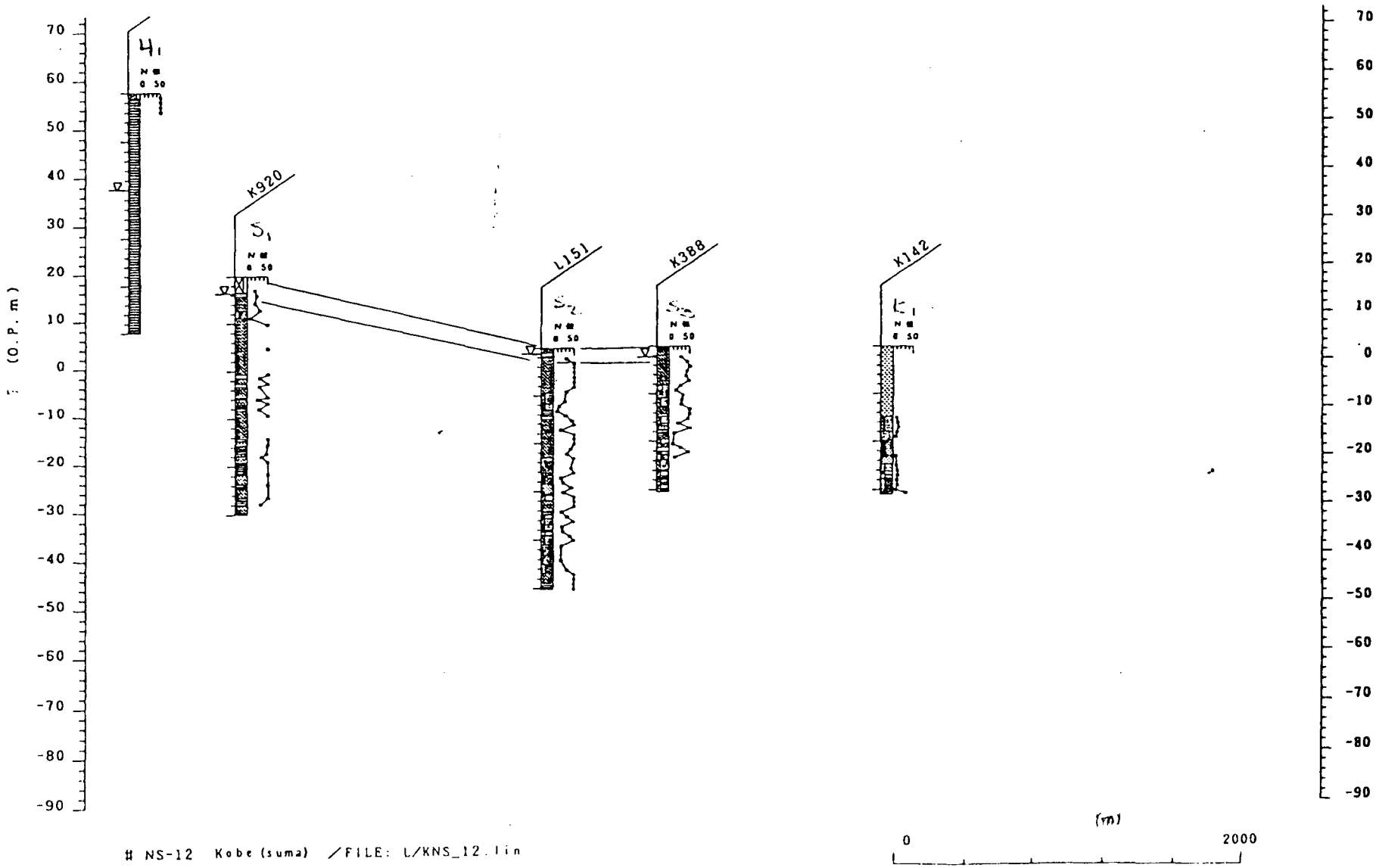
K920
L151
K388
K142
(O.P.m)
(m)
0
2000
NS-12 Kobe (suma) /FILE: L/KNS_12.lin

Figure 2.41.

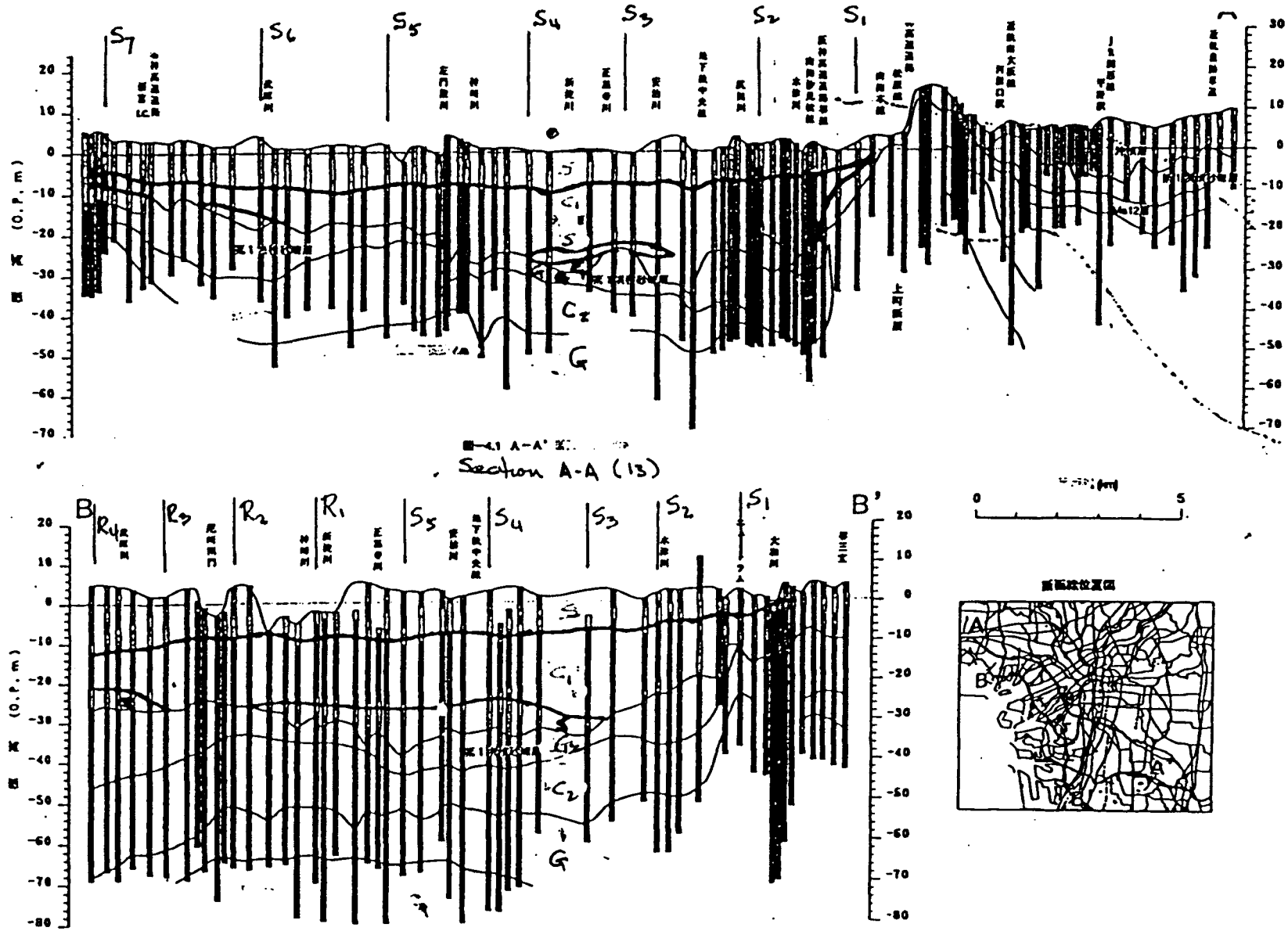

Figure 2.4m. Section B-B (14).

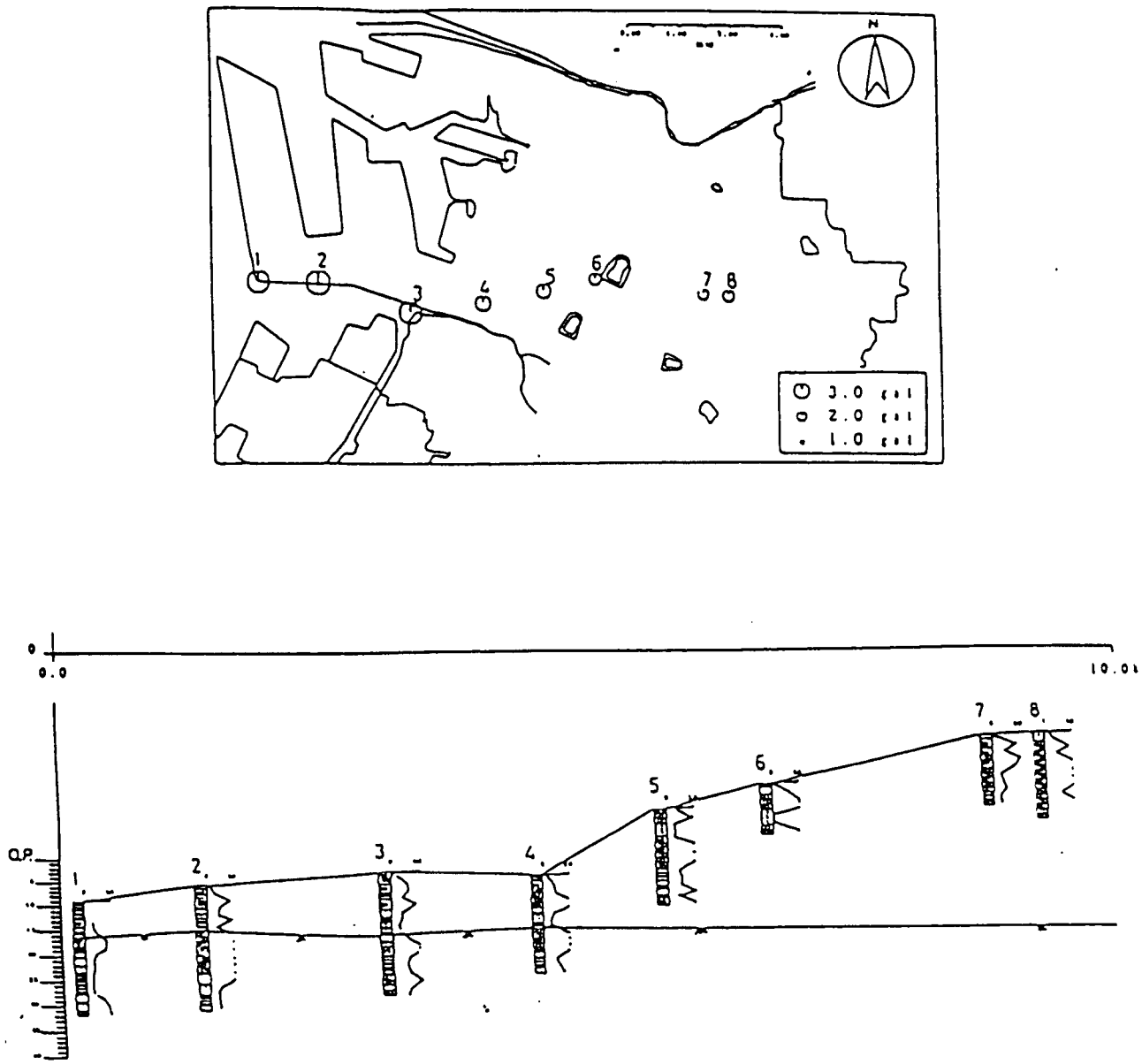

Figure 2.5. Features of profile at Sakai City (south of Osaka) (Iwasaki et al., 1987).

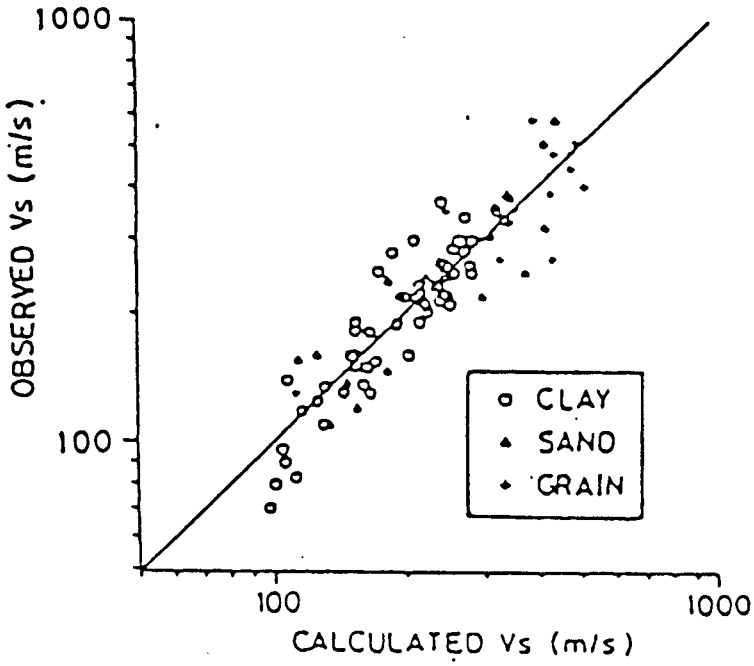

$$V_S = 34.824 \cdot F \cdot (N + 1)^{0.244} P^{0.175}$$

F = 1.000 Clay

= 0.922 Sand

= 0.851 Gravel

N = SPT Blow Count

P = Mean Interguanular Pressure

$$= \frac{2}{3} (\gamma D - u)$$

Figure 2.6. (From Iwasaki et al., 1987).

3.0 LIQUEFACTION ASSESSMENTS

A number of approaches to evaluating liquefaction susceptibility are in use and under continuing improvement in their ability to predict the onset of liquefaction. Following the occurrence of major earthquakes, the details of each method are reinvestigated and modifications proposed to improve the accuracy of the predictions. This investigation is following along the same path to try to develop improved prediction methods with lower uncertainty.

3.1 Deterministic Stress-Based Method

The primary method currently used to predict the triggering or onset of liquefaction is the stress-based method developed by Seed and Idriss (1967). In this approach, an equivalent uniform cyclic shear stress ratio induced by the seismic event is compared to a corresponding estimate of the resistance of the soil required to initiate liquefaction. This latter parameter is typically estimated from Standard Penetration Test (SPT) or Cone Penetrometer Test (CPT) data measured insitu at the site. The most widely used curves are those shown in Figure 3.1 and are based on correlations of field performance with evidence of liquefaction. A number of empirical correction factors must also be applied in any assessment to account for the effects of earthquake magnitude (duration or cycles of shaking), evaluation of equivalent stress cycles in a given event, fines content, soil confinement, sample disturbance and aging. Recent modifications to some of these parameters (Arango, 1994, Idriss, 1997) have been proposed by a number of researchers in an attempt to improve prediction capability.

This deterministic "go/nogo" approach to liquefaction evaluation must by its very nature provide a conservative estimate of site response since it is based on the minimum strengths estimated from field performance data. Also, the case history database is biased toward sites that have liquified: sites that have liquified are studied preferentially to those that did not. Since the method was developed when only more distant (> 10 to 15 km) ground motion data were available, the generally short duration and impulsive nature of near-source time histories as evidenced by the Loma Prieta, Landers, and Kobe earthquakes was not generally known. Recorded ground motions from these events indicated very high accelerations (and corresponding high shear-stress ratios) with very few equivalent cycles of motion. As will be discussed in the following paragraphs, the simplified deterministic stress-ratio approach would predict much more extensive zones of liquefaction when applied to these sites than were in fact recorded. An alternate deterministic strain-based method for predicting the onset of liquefaction is described by Dobry et al. (1982) in which effective shear-strains determined from ground response analyses are compared with the results of laboratory data. The strain-based method does not currently enjoy the wide range of applicability as does the stress-based approach although it shares many features in common with the stress-based method.

To incorporate the effects of earthquake magnitude into the analysis, a "magnitude correction factor" was introduced to represent the experimentally observed behavior of reduced liquefaction capacity (DeAlba et al., 1976) as the number of cycles imposed on the samples is increased. The effective number of cycles associated with a given magnitude event recommended (Seed et al., 1975) to account for this behavior is

Earthquake Magnitude	No. of Cycles
5.25	2-3
6.00	5
6.75	10
7.50	15
8.50	26

The normalized soil strength parameter associated with this behavior (Figure 3.2) indicates the loss of strength as a function of effective cycles (or magnitude). This factor has recently been modified (Idriss, 1997) to account for the effects of improved sampling and testing methods. In either case, the data indicates that if liquefaction occurs at a much lower number of effective applied cycles, the capacity of the soil increases by a significant amount. For example, based on the later test data, the strength at 1 cycle is about 2.4 times the corresponding strength at 15 cycles to liquefaction.

A comparison of the effect of number of cycles to liquefaction on the basic capacity estimate for clean sands is shown in Figure 3.3 for cases of 1 cycle, 4 cycles and 15 cycles. The impact of this parameter on the evaluation of liquefaction at Kobe is extremely important. For this magnitude 6.9 event, one would expected the effective number of cycles to liquefaction to be between 10 and 15, based on the recommended procedures from Seed and Idriss (1967) At close-in locations, however, the effective number of cycles imposed on the soil was very low. Reviewing some of the recorded motions indicates effective cycles of between 1 and 4.

3.2 Probabilistic Stress-Based Method

The deterministic approach recommended by Seed and his coworkers, although highly empirical, is founded on a solid base of field and laboratory observations. The site strength, as measured by the SPT measurements (suitably corrected for confinement), defines the horizontal coordinate while the induced shear stress ratio defines the vertical coordinate of Figure 3.1. If in a particular site evaluation a point falls below the curve, it is concluded that liquefaction will not occur while if the point falls above, liquefaction is considered likely. However, no information is provided on the margin of safety incorporated into the analysis. In addition, the data points used to define the line of demarcation between liquefaction/no liquefaction is clouded with uncertainty due to a lack of information available from the sites considered in the evaluation. For example, peak ground accelerations were not measured at all sites but were inferred based on magnitude/distance estimates. In addition, the definition of an appropriate SPT value to attach to a given site incorporates significant uncertainty in the recommendation.

To overcome some of these shortcomings and incorporate an evaluation of uncertainty into the liquefaction evaluation, Liao (1986) presented the results of a reinvestigation of the available catalog of liquefaction case studies to incorporate the effects of limitations and biases in the data base on estimating the risk of liquefaction. A comparison of the results of predicted shear strength estimates for mean and one-sigma estimates with the Seed deterministic model is shown in Figure 3.4a for clean sand sites. A similar plot is shown for the case of silty sand sites (greater than 12% fines) in Figure 3.4b. The results also confirm the recommendation previously considered in the deterministic evaluation that as median

grain size decreases (soils get finer), strength against liquefaction increases. By comparing Figures 3.4a and 3.4b, it is noted, however, that the prediction of liquefaction at "dirtier" sites is less certain; that is, the differences in the one-sigma values from the mean is much greater for the silty sand sites than for the clean sand sites.

3.3 Modifications Due to Distance or Imposed Cycles

This probabilistic approach, however, is still based on the data base from distant events and therefore still suffers from the problem of estimating the variability in strength of the soil to the number of imposed cycles of loading. The data of Figures 3.4a and 3.4b are therefore estimates of probability of liquefaction assuming 15 cycles to failure, typically associated with a magnitude 7.5 event. To try to include the effect of a reduced number of cycles to failure on the probability estimates, the same factors used in Figure 3.3 were applied to the probabilistic curves for the magnitude 7.5 event. The results for 4 cycles and 1 cycle to failure for the two cases of clean and silty sands are shown in Figures 3.4c through 3.4f. The results indicate the significant increase in strength against liquefaction as the induced cycles of loading decrease.

To capture this distance effect within the standard analysis procedure, an evaluation was developed by Kavazanjian et al. (1984) incorporating the probable development of excess pore pressure during a given earthquake as a function of number of equivalent uniform cycles of loading. The work was applied to a hypothetical soil site composed of clean sand (Monterey #0 sand) for which laboratory cyclic stress data were available. The results shown in Figure 3.5 indicate that the equivalent number of cycles applied by a given event is highly nonlinear and is strongly dependent on epicentral distance. As distance increases, the probability of developing pore pressure, or causing the onset of liquefaction, significantly decreases. Thus, from a design perspective, site evaluations must incorporate estimates for distances to the event as well as magnitude. The curves of Figure 3.5 would have to be modified for fines content, which would reduce the probabilities of liquefaction even further, and generated for intermediate magnitude events to be appropriate for use in site evaluations.

A fundamentally different approach has been proposed by a number of researchers in recent years (for example, Ostadan et al., 1996) to try to overcome this deficiency in the standard liquefaction evaluations discussed above. In this method, the strain energy required to initiate liquefaction, or lead to a pore pressure ratio of unity, is estimated based on the results of a large number of laboratory cyclic stress tests. These data are then compared with the strain energy developed in the site soils to determine whether or not liquefaction will be initiated from a given imparted ground motion, irrespective of its distance from the site, magnitude of event, etc. In principal, the approach can be evaluated for a number of different configurations which are not easily captured by the standard stress-based method. Issues of local site effects, soil-structure interaction, nonuniform site conditions, etc. can be treated, provided of course that these issues can be appropriately treated in the analysis.

The data base used in the development is a series of 150 cyclic stress tests for a number of different soil types and test conditions. The soils tested included clean sand samples reconstituted in the laboratory as well as a number of controlled samples of silty sands. The computed strain energy to failure from all these tests was computed and these are plotted in Figure 3.6. The scatter in the figure can be reduced, of course, by separating the data by both soil type and test conditions. The strain energy to liquefaction

determined experimentally was found to be a function of relative density for clean sands and of confining pressure for silty sands. The results of the study were compared with recorded behavior at several sites and found to provide a robust estimate of liquefaction potential. The evaluation can be easily incorporated into a probabilistic framework to liquefaction predictions by considering scatter in the strain energy from the data as well as uncertainty in the predictions of site response.

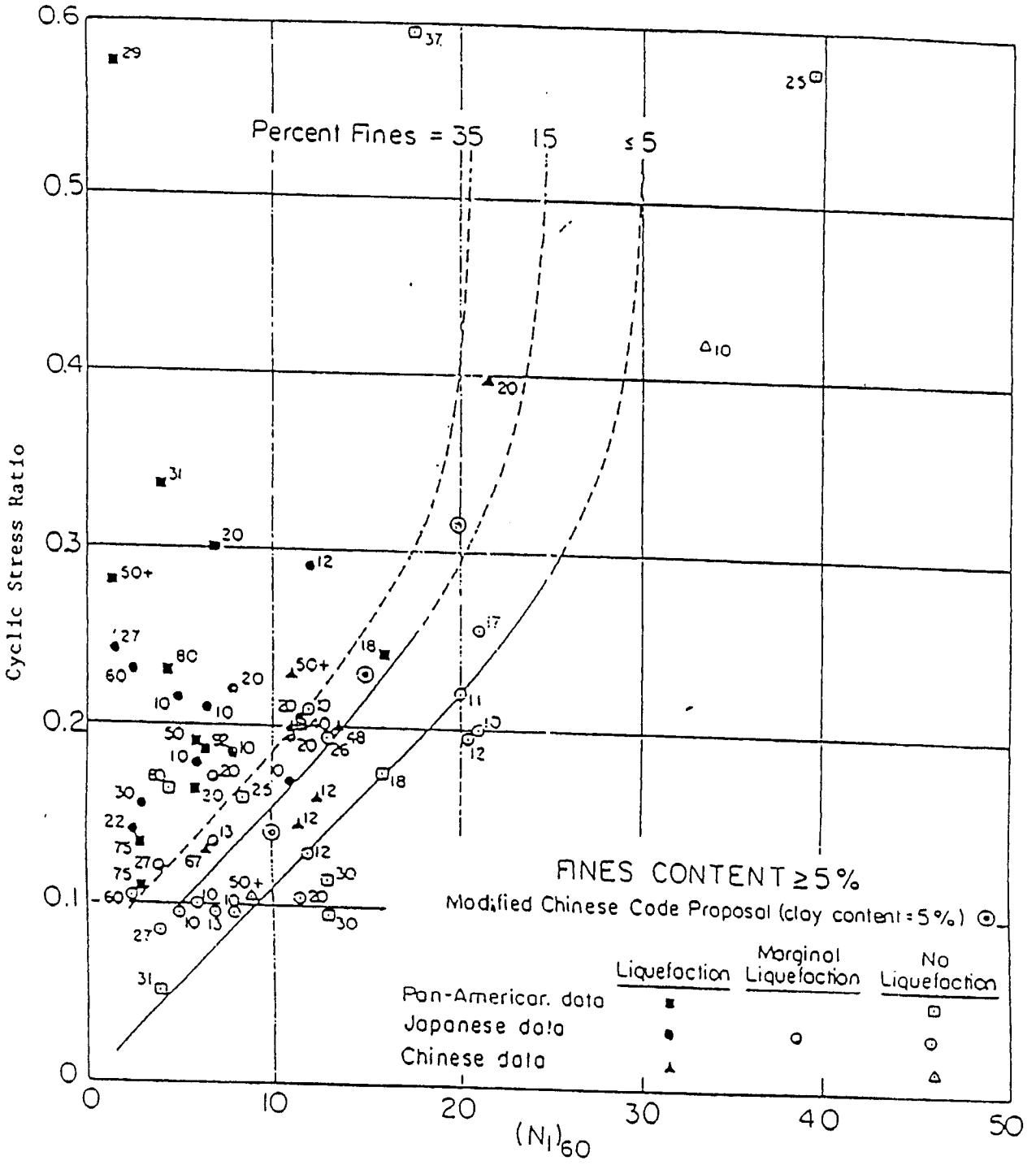

Figure 3.1. Deterministic estimate of resistance to liquefaction for M = 7.5 earthquakes (Seed et al., 1984).

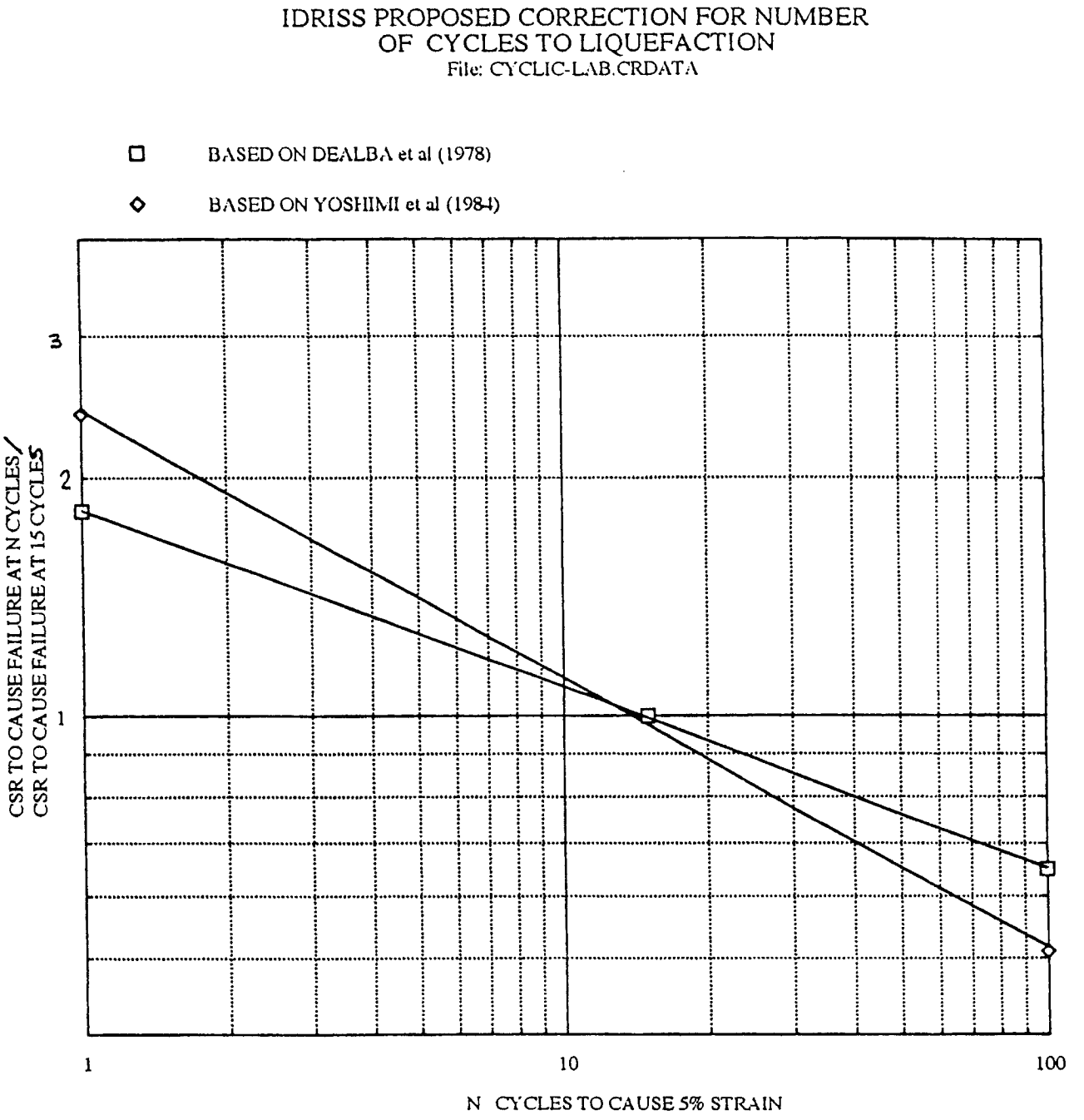

Figure 3.2. Normalized cyclic stress ratios to trigger liquefaction (Idriss, 1997).

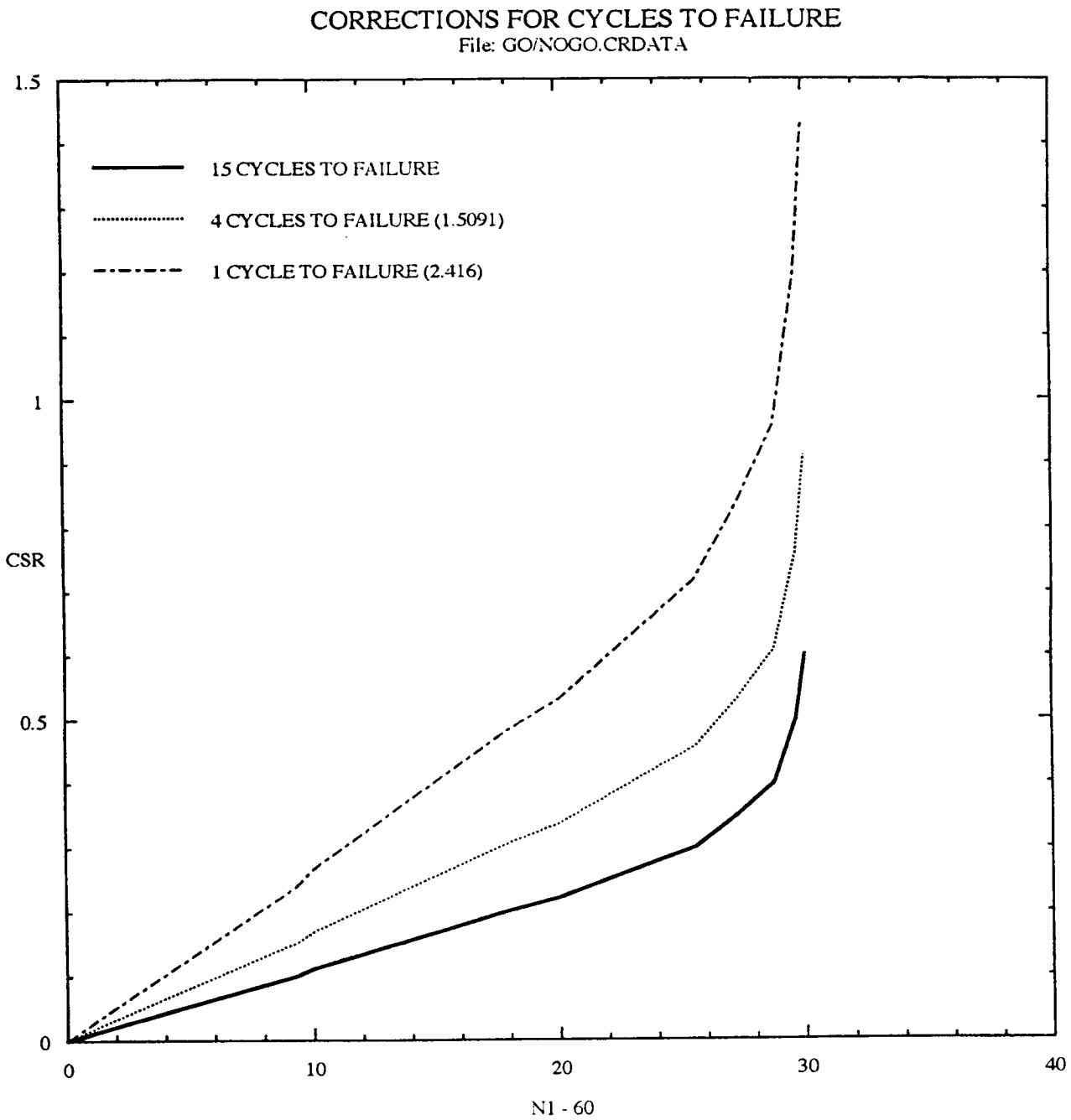

Figure 3.3. Increase in soil liquefaction capacity with fewer cycles to liquefaction (Idriss, 1997).

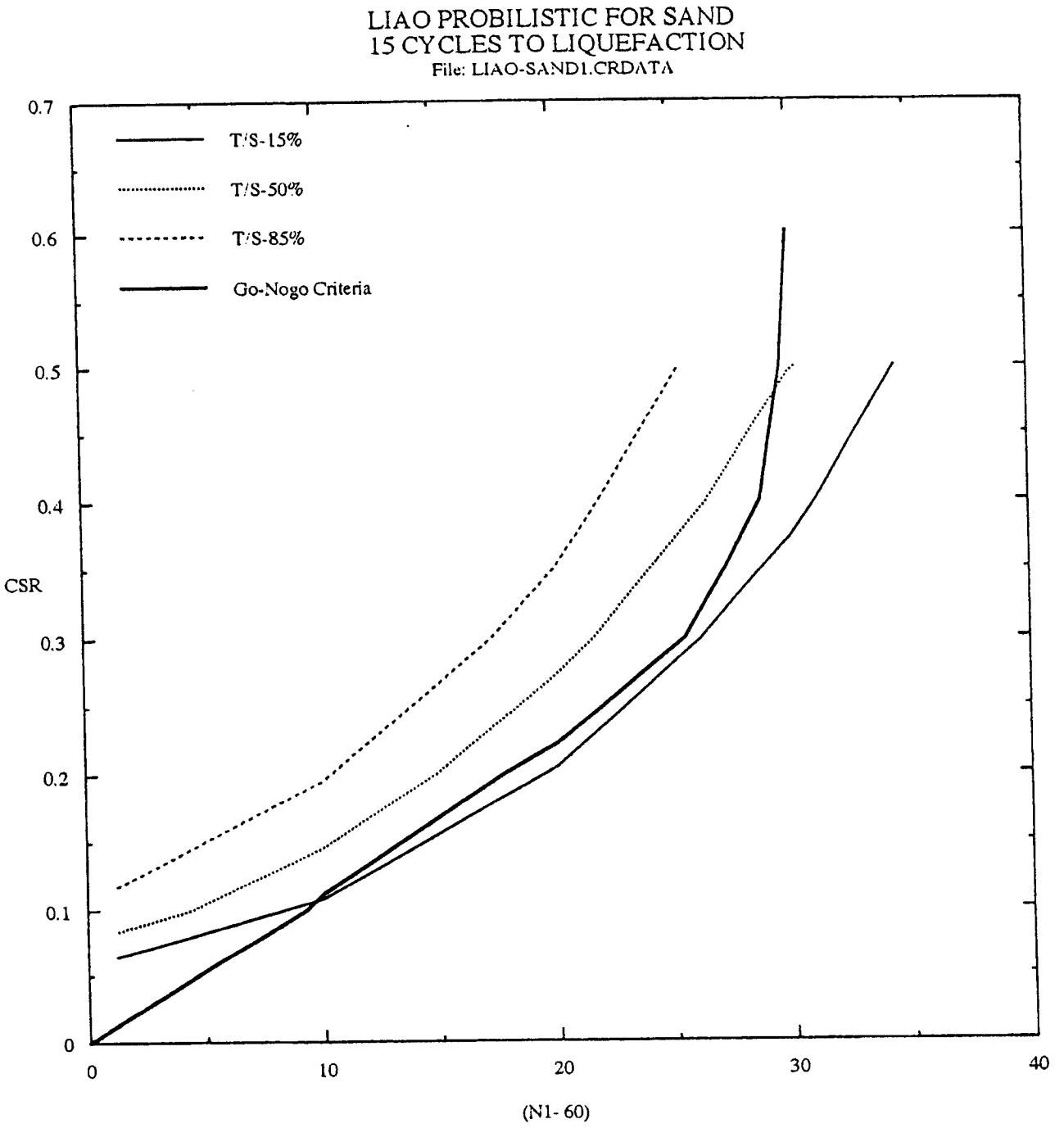

Figure 3.4a. Comparison of deterministic and probabilistic estimates of liquefaction for sand sites (Liao, 1986).

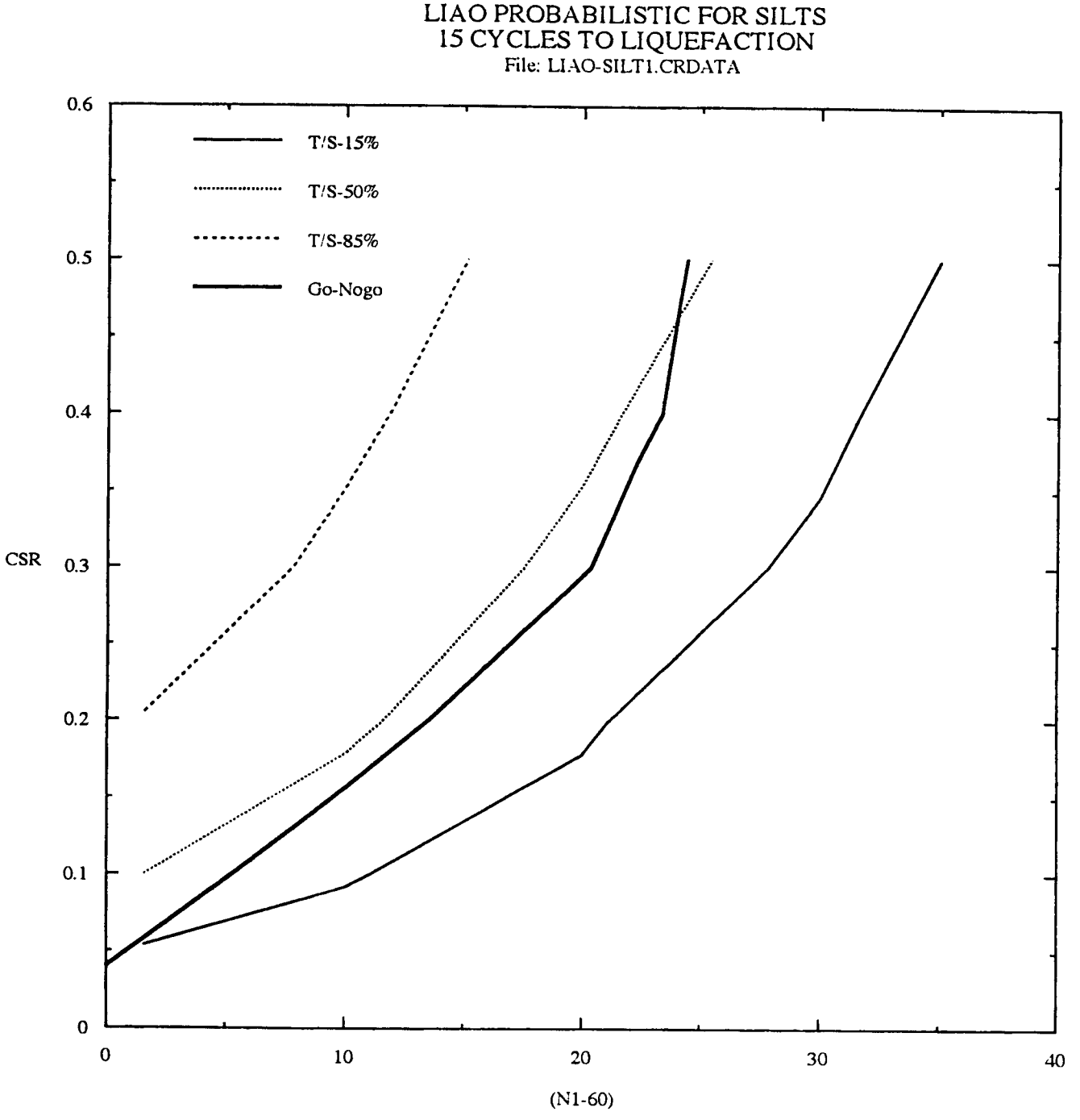

Figure 3.4b. Comparison of deterministic and probabilistic estimates of liquefaction for silty sites (Liao, 1986).

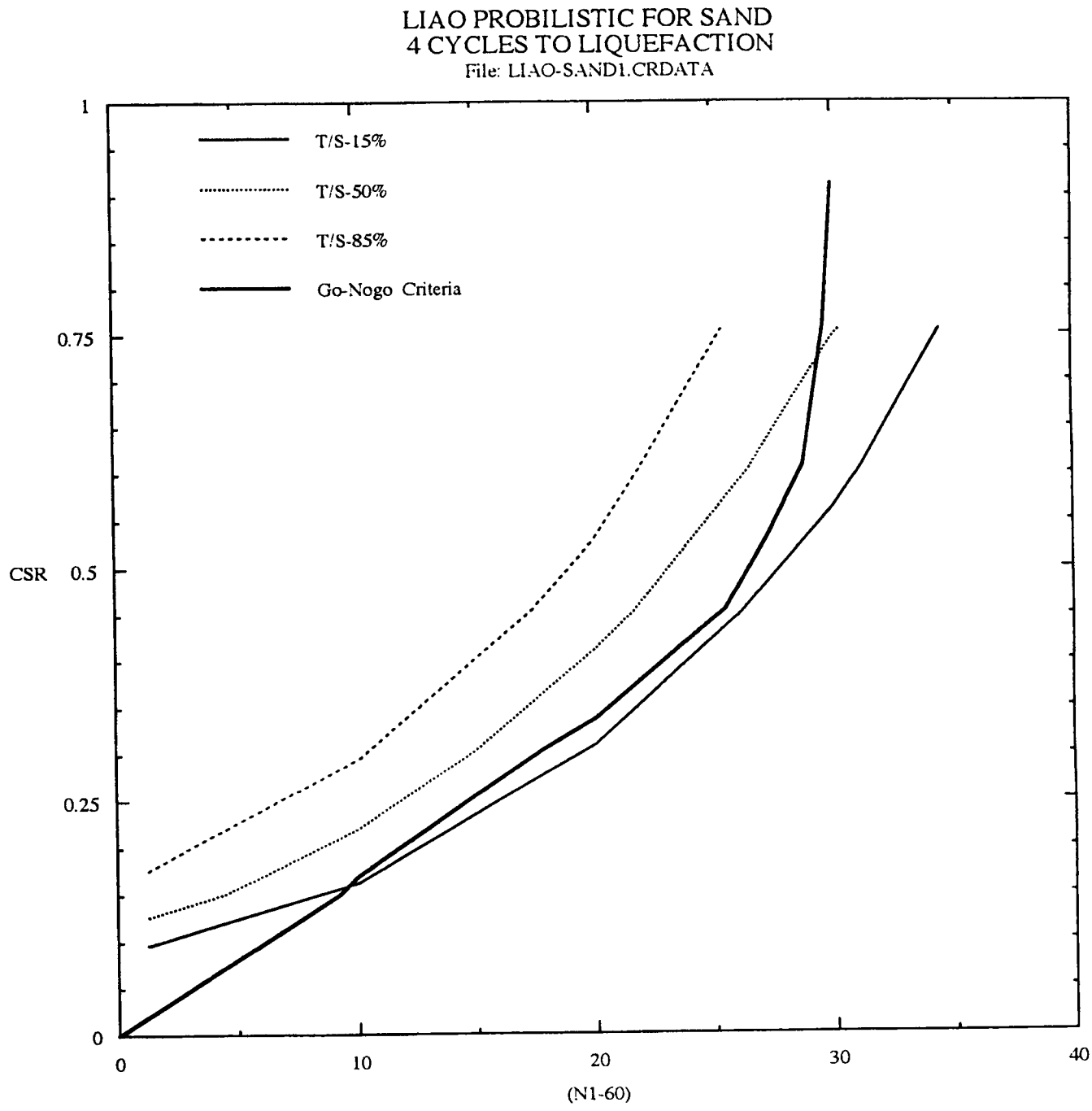

Figure 3.4c. Comparison of deterministic and probabilistic estimates of liquefaction for sand sites modified for 4 cycles of loading.

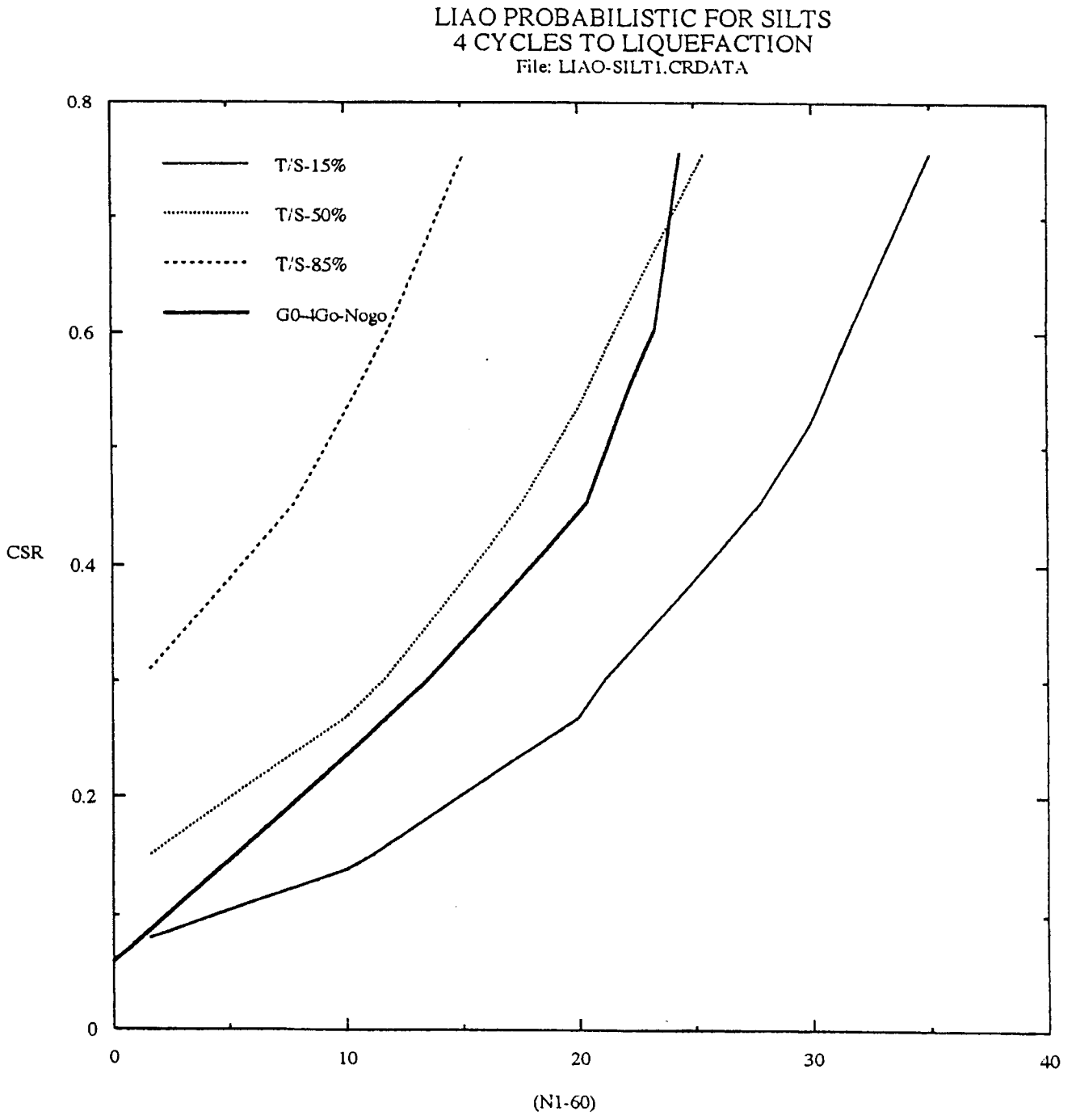

Figure 3.4d. Comparison of deterministic and probabilistic estimates of liquefaction for silty sites modified for 4 cycles of liquefaction.

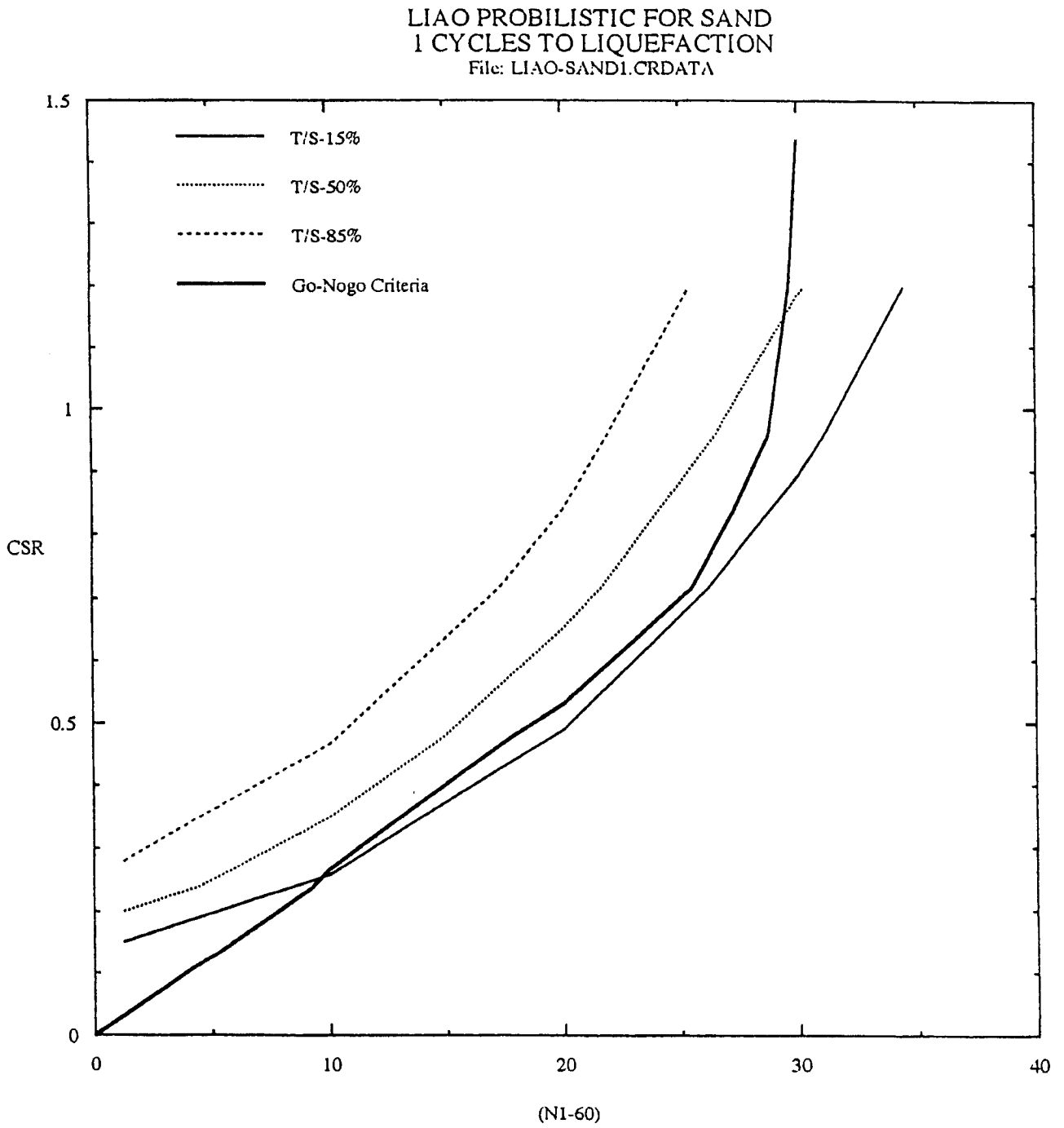

Figure 3.4e. Comparison of deterministic and probabilistic estimates of liquefaction for sand sites modified for 1 cycle of loading.

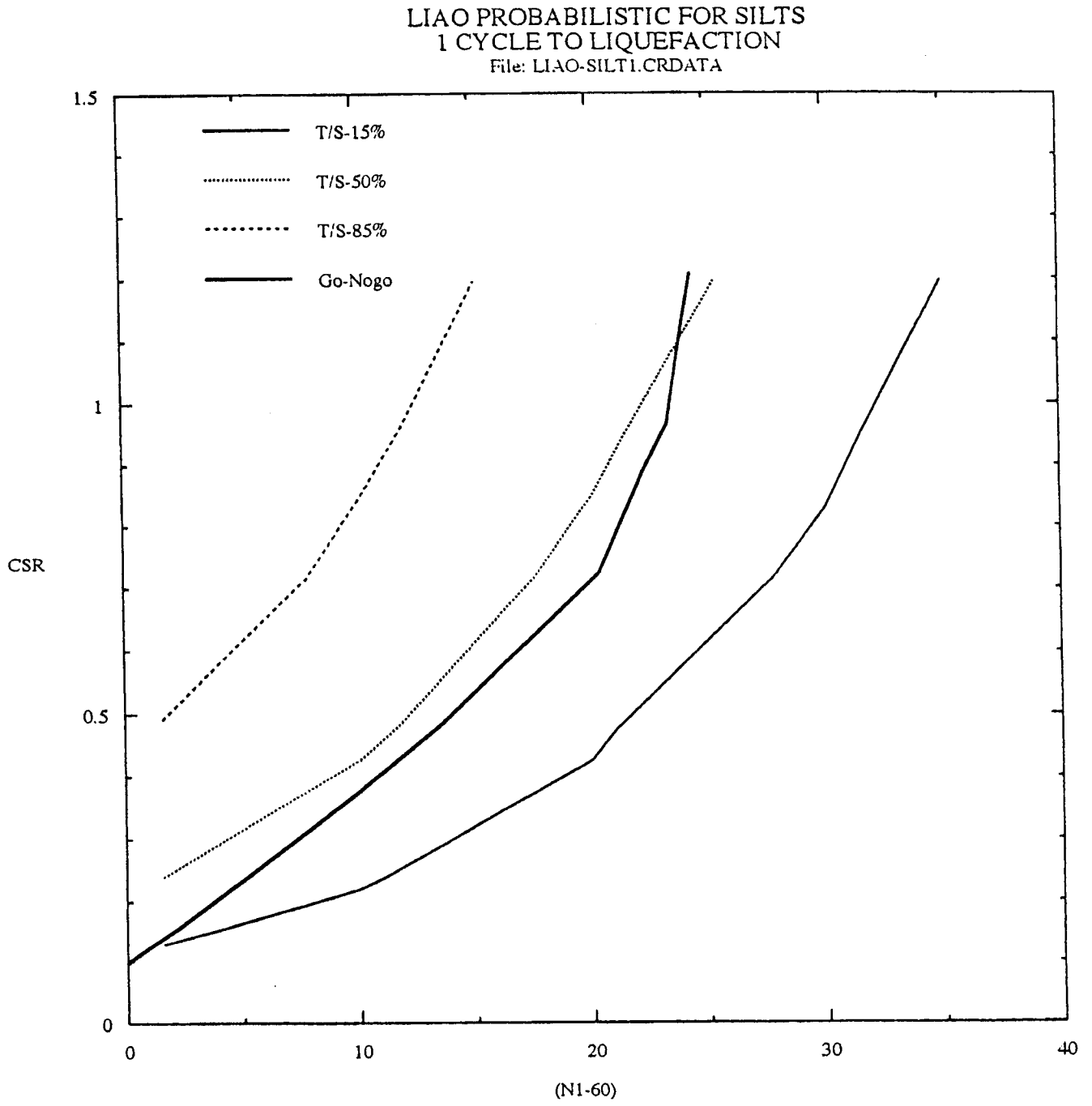

Figure 3.4f. Comparison of deterministic and probabilistic estimates of liquefaction for silty sites modified for 1 cycle of loading.

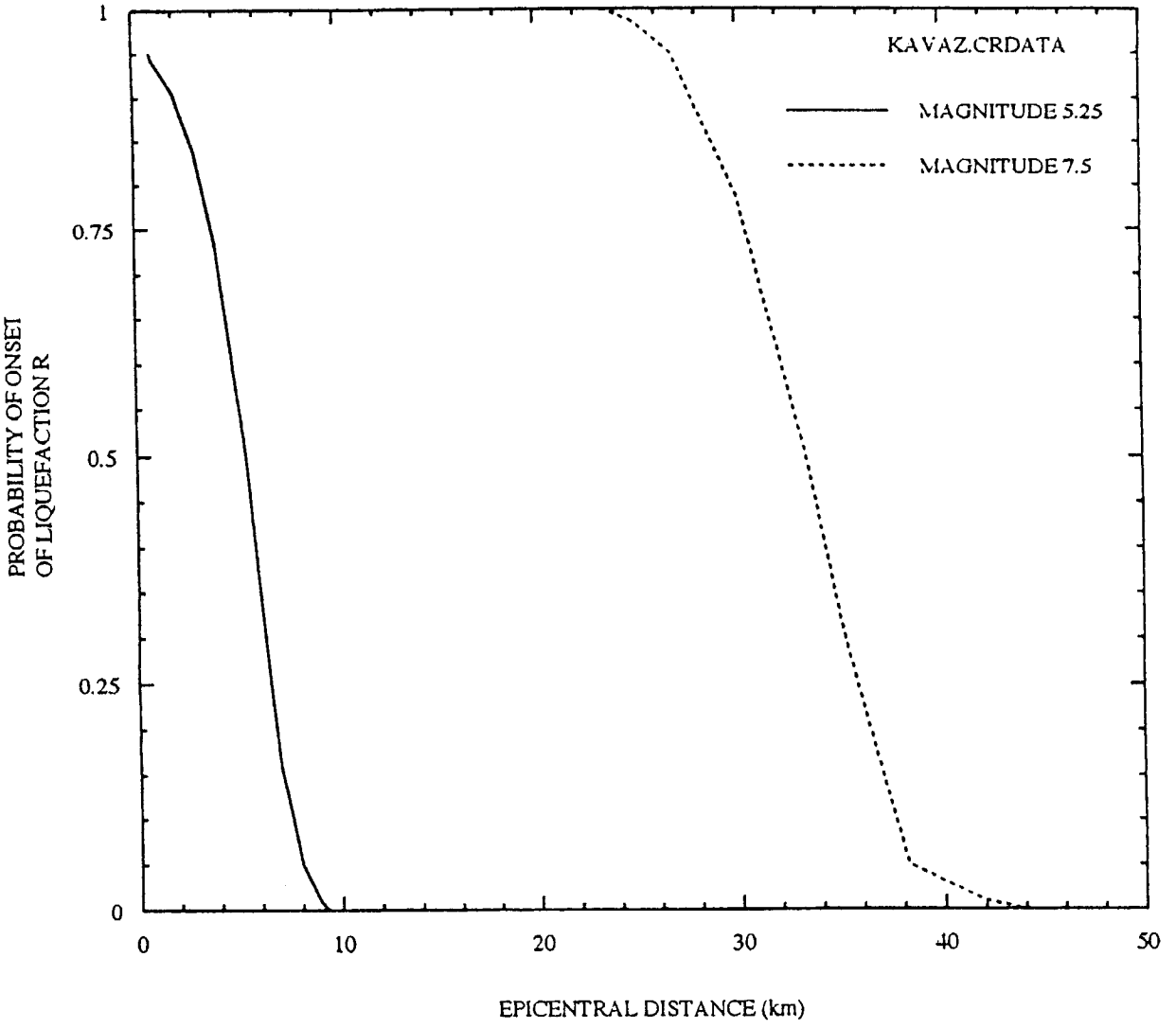

Figure 3.5. Probabilistic estimate of pore pressure generation for different magnitude events as a function of epicentral distance (Kavazanjian, 1984).

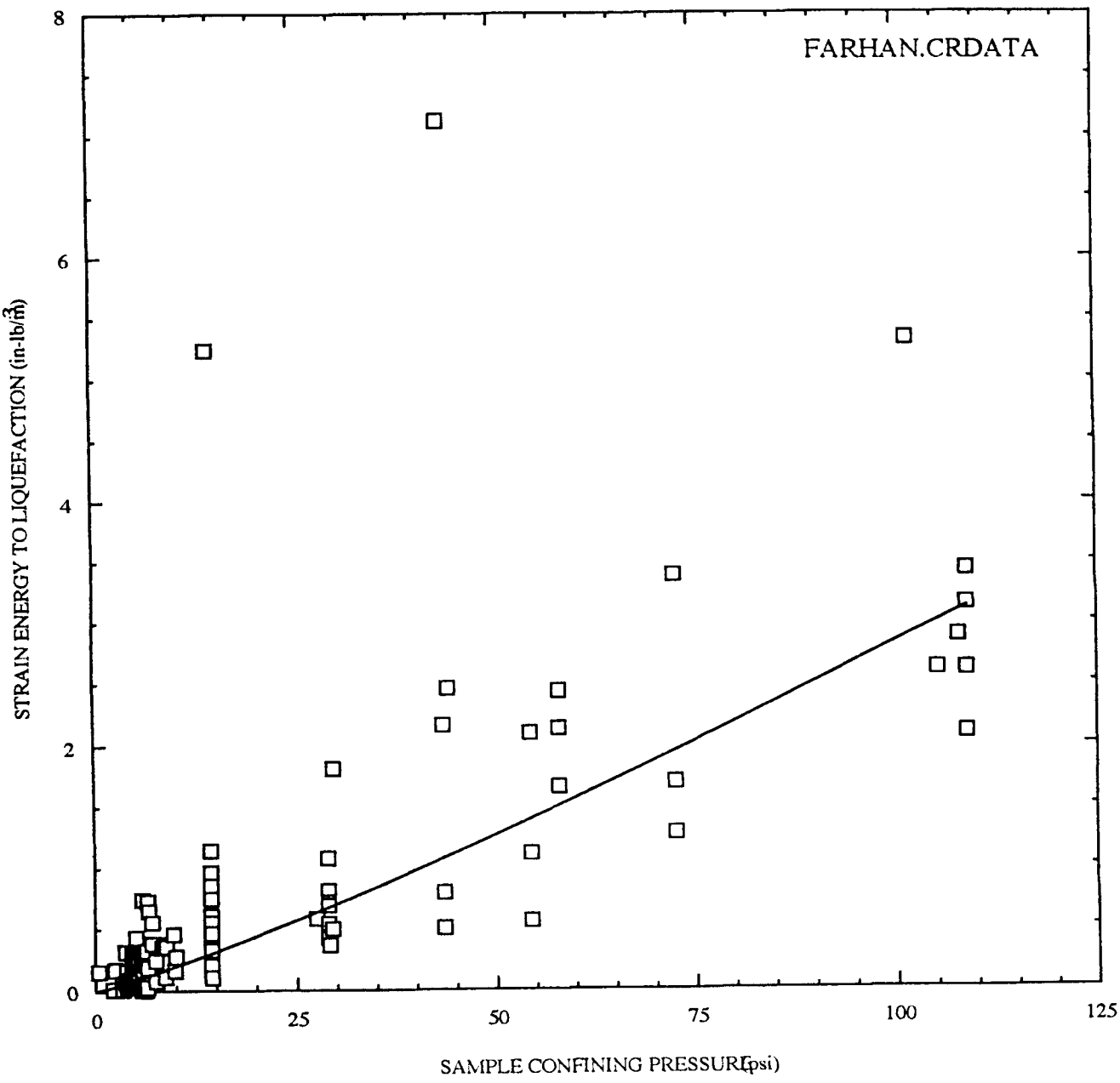

Figure 3.6. Laboratory determination of strain energy to initial liquefaction (Ostadan, 1996).

4.0 FINITE-FAULT SIMULATIONS

At close distances ($\leq$ 10 - 15 km) to extended sources (**M** $\geq$ 6.4) the character of ground motions is distinctly different than at larger distances. In general, near-fault durations are significantly shorter in acceleration, velocity, and displacements resulting in fewer stress cycles for large magnitude earthquakes compared to greater distances. Additionally, rupture directivity, particularly for predominated vertical strike-slip mechanisms, has a strong influence both in duration of shaking as well as spectral content at low frequencies ($\leq$ 2 Hz). Sites located with significantly more rupture toward them than away experience shorter duration over a wide frequency range and enhanced low frequency energy compared to an average over all near source sites. In order to assess these effects in the assessment of liquefaction susceptibility, the computation of the cyclic stress ratios was incorporated into the equivalent-linear site response component of the finite-fault simulation code. The finite-fault simulations (Appendix A) produce motions that are shorter in durations for near source sites in general and both shorter durations and elevated low frequency motions for sites subjected to forward directivity effects. The site response component of the simulations use a random vibration (RVT) equivalent-linear formulation (Appendix B). Since the methodology does not use time histories as control motions for the soil columns, control motion durations are incorporated in the estimates of peak strains (stresses for the cyclic stress ratios) from the strain (stress) power spectra. Shorter control motion durations result in larger estimates of peak time domain strains and stresses for a given control motion power spectrum. Additionally, random process theory is used to estimate the number of stress cycles over the duration (taken as the time interval between the 5% and 75% Arias intensity).

4.1 Velocity Profiles, Kappa, and Q(f)

For the finite-fault simulations the basic crustal model used is that of Wald (1996) which is listed in Table 4.1 for both rock and soil sites. These crustal models with surface velocities of about 3,000 ft/sec and 1,000 ft/sec for rock and soil sites respectively do not reflect shallow geotechnical conditions and are not appropriate for modeling short period (< 1 sec) motions (Wald, 1996). To accommodate the shallow hard, soft, and fill soil conditions (Section 2) as well as surficial (weathered) rock site conditions, shallow profiles are used to replace the top sections of the Wald (1996) crustal models. For rock sites, two profiles are used: a site-specific Kobe University (KBU) profile from Motosaka and Nagano (1997) and a generic California soft rock profile (Silva et al., 1997). The KBU profile is used only in the validation exercise for site KBU while the generic soft rock profiles is used for all other rock sites. The hard, soft, and fill soil profiles are based on blow count correlations with shear-wave velocity (Figure 2.6) applied to each of the 18 profiles shown in Figures 2.2 and 2.3. To extend the profiles below the blow count data, the 2-D basin model of Kagawa et al., (1993) was placed below the shallow geotechnical profile at each site location. To develop generic profiles for each soil category, all hard, soft, and fill profiles were averaged and the deeper Wald (1996) crustal model added. The shallow profiles are shown in Figure 4.1 down to 500 ft with the deeper sections shown in Figure 4.2. Below a depth of about 2 km (shear-wave velocity 3.2 km/sec), all the profiles reflect the deep Wald (1996) crust.

Shallow crustal damping (kappa, Appendix A) is constrained to have a small strain value of 0.04 sec for the rock, hard, soft, and fill profiles. This value is based on inversions of the rock and soil empirical attenuation relations of Abrahamson and Silva (1997) as well as Sadigh et al. (1997). In these inversions little difference was seen between rock and soil shallow damping values at low levels of loading

(expected rock peak accelerations less than about 5%g). To determine appropriate kappa values beneath the nonlinear zones, the small strain damping from the damping curves throughout the nonlinear zones is subtracted from the total kappa value of 0.04 sec. The remaining kappa, generally about 0.03 sec, is applied beneath the nonlinear zones.

The Q(f) model (Appendix A) used is $184\ f^{0.6}$ and is appropriate for northern California. It is based on inversions of the 1989 **M** 6.9 Loma Prieta, 1984 **M** 6.2 Morgan Hill, and 1979 **M** 5.7 Coyote Lake earthquakes (Silva et al., 1997). The overall similarity in crustal structures and tectonic environments between the Kobe region and northern California (Wald et al., 1991) suggests that the Q(f) models may be similar. Since most of the sites are at close fault distances, the effects of deep crustal damping are likely to be quite small resulting in little sensitivity of the motions and stress to the particular Q(f) model.

4.2 Modulus reduction and Damping Curves

To approximately account for nonlinear site response at both rock and soil sites, equivalent-linear analyses (Appendix B) are used to estimate ground motions, strain energy (PSI), and cyclic stress ratios (CSR). For the rock sites, the G/G_{max} and hysteretic damping curves shown in Figure 4.3 are used. These curves were developed by modeling the strong ground motions predicted at rock sites by the empirical attenuation relation of Abrahamson and Silva (1997) as well as motions recorded at about 200 rock sites from about 15 earthquakes (Silva et al., 1997). For the soil sites, the EPRI (1993) curves are used for the cohesionless soils (Figure 4.4) while for the clay zones (Section 2), the curves shown in Figure 4.5 are used. These cohesive soil G/G_{max} and hysteretic curves reflect depth dependency which was found to be required in modeling the motions at the Kobe Port Island (KPI) vertical array. The shallow curves are used in the Pleistocene clays and are consistent with those of Kazama et al. (1998) based on laboratory test data for the same materials. For the fill material (consisting of weathered granite (Masado)), a set of G/G_{max} and hysteretic damping curves (Figure 4.5) based on gravely soils (Seed et al., 1984) is used. The fill material G/G_{max} and damping values for strains exceeding about 1% were decreased and increased respectively to reflect the shear-wave velocity and damping values at KPI during the mainshock by Kokusho et al. (1996) and Elgamal et al. (1996). Sites are treated as nonlinear to depths of 500 ft or shear-wave velocities exceed depth 3,000 ft/sec, whichever occurs first with depth.

The appropriateness of the suite of G/G_{max} and hysteretic damping curves was assessed by modeling the motions (5% damped response spectra) at the KPI vertical array using the generic fill profile (Figure 4.1). The finite-fault model is used to simulate the motions at the deepest accelerograph (83m) as well as at levels 32m, 16m, and the surface. The recorded and computed motions one compared in Figure Set 4.10 (sites KPI, KP2, KP3, and KP4). In general the finite-source model using equivalent-linear soil response captures the motions and changes in motions with depth reasonably well.

4.3 Distribution of Sites and Surficial Soils

For the liquefaction evaluation, a total of 558 sites were simulated to cover the Kobe, Nishinamiya, and Osaka areas (Figure 1.11). Figure 4.6 shows the sites overlain on the general area map and Figure 4.7 shows the distributions of rock, hard, soft, and fill areas.

4.4 Validation of Kobe Simulations

The accuracy of the finite-fault simulations along with the equivalent-linear site responses are evaluated by comparisons to recorded motions (5% damped average horizontal component response spectra) at 25 sites. Figure 4.8 shows the recording sites in the Kobe/Osaka region and Figure 4.9 shows the slip model derived from modeling the recorded motions. In general, slip is concentrated in two large zones or asperities. One asperity is located under Awaji Island, toward the southeast portions of the rupture surface and extends to the surface. The second asperity is deep, below about 5 km, and is located beneath the city of Kobe.

The comparison of simulations to recorded motions is shown in Figure 4.10 in terms of average horizontal component response spectra (5% damping). In general, the motions are predicted reasonably well.

Figure 4.11 shows the modeling uncertainty and bias. The uncertainty averages about 0.5 (σ_{ln}) or about a ± 65% error over the entire frequency range. The bias plot show little bias below about 2 Hz with a overprediction for higher frequencies. This is largely controlled by two sites, KBU and OSA, both with anornalously low short-period motions (Figure 4.10). In general, the simulations provide a good fit to the data and indicate that the model is capturing the overall character of the motions acceptably well.

4.5 Simulated Motions for the Kobe, Nishinomiya, and Osaka Areas

To simulate motions, cyclic stress ratios, and strain energies at each site location reflecting randomness and uncertainty in material properties, fifteen random profiles are generated at each site along with equivalent-linear site response analyses. Shear-wave velocity and layer thicknesses are varied using a statistical model based on an analysis of variance of over 500 shear-wave velocity profiles (EPRI, 1993; Silva et al., 1997). Additionally, for the hard, soft, and fill profiles the depth to 1 km/sec materials (Figure 4.2) is varied ± 100m, ± 200m, and ± 300m respectively. Median and ± 1σ response spectra (112 periods from 0.1 to 100.0 Hz) as well as cyclic stress ratios and strain energies verses depth are computed at each site location. Both cyclic stress ratio and strain energy median values are averaged over the top four meters (13 ft) below the water table which averages 2.1m, 2.7m, and 7.1m at the fill, soft, and hard sites respectively.

For the rock, hard, soft, and fill areas (Figure 4.7), Figure 4.12 shows the median predicted peak acceleration values. The rock and hard soil sites (red) have the highest acceleration values which are near 1g. These are the stiffest sites and closest to the rupture surface. The yellow band, with median peak accelerations in the 0.6 to 0.8g range, generally corresponds to the soft sites (Figure 4.7). The fill and more distant soft sites (Nishinomiya area) show significantly lower peak acceleration values being in the 0.3 to 0.6g range. Finally the Osaka region (most distant) shows the lowest peak acceleration values (below 0.3g). Interestingly, the soft soils with the band of intermediate levels of peak accelerations contains the high intensity (damage) zone (Figure 1.10) suggesting that the effects of surficial soils may have been a contributing factor. Since few structures are located in the rock and hard soil hill areas, the effects of nonlinear response of the fill soils may have lowered the high frequency (> 1 Hz) motions sufficiently enough to reduce damage levels. This aspect of surficial geology was also demonstrated by Suetomi and Yoshida (1998) but attributed the reduction in motions from the soft to the fill zones to the nonlinear response of the shallow (alluvial) marine clay layer which is thin or absent in the soft soil zone. An alternative explanation is the basin edge effect (Kawase, 1996; Pitarka et al., 1996; Inoue and Miyatake,

1997; Kamae et al., 1998) where edge generated surface waves superpose with direct shear-waves from the source to form a band of enhanced motions which parallels the edge of the basin. It is likely that both effects are present to some degree and more detailed analyses are needed to more fully understand this important issue: the effects of local shallow structure verses deep and perhaps non-local structures on strong ground motions.

Table 4.1
Kobe Regional Velocity Model
Rock Sites (Wald, 1996)

V_P (km/s)	V_S (km/s)	Density (g/cm^3)	Thickness (km)	Depth (km)
2.50	1.00	2.10	0.10	0.00
3.20	1.80	2.10	0.40	0.10
5.50	3.20	2.60	4.50	0.50
6.00	3.46	2.70	22.00	5.00
6.80	3.83	2.87	5.00	27.00
7.80	4.50	3.50		32.00
Soil Sites				
V_P (km/s)	V_S (km/s)	Density (g/cm^3)	Thickness (km)	Depth (km)
0.60	0.30	1.70	0.10	0.00
1.20	0.50	1.82	0.10	0.10
2.50	1.00	2.10	1.00	0.20
3.20	1.80	2.10	0.40	1.20
5.50	3.20	2.60	4.50	1.60
6.00	3.46	2.70	20.90	6.10
6.80	3.83	2.87	5.00	27.00
7.80	4.50	3.50		32.00

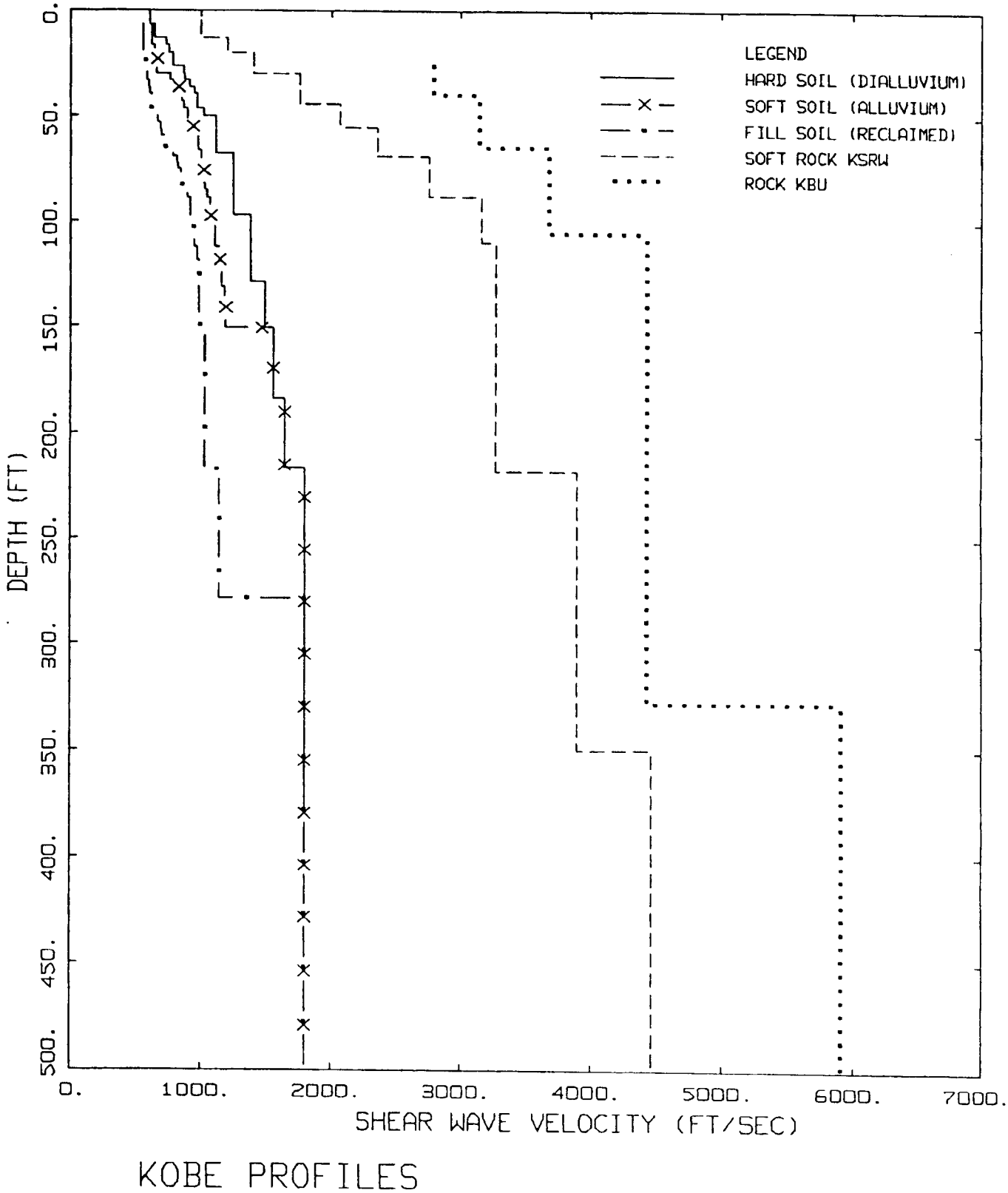

Figure 4.1. Shallow hard, soft, and fill (reclaimed) soil profiles and generic soft rock as well as site specific Kobe University rock site profile.

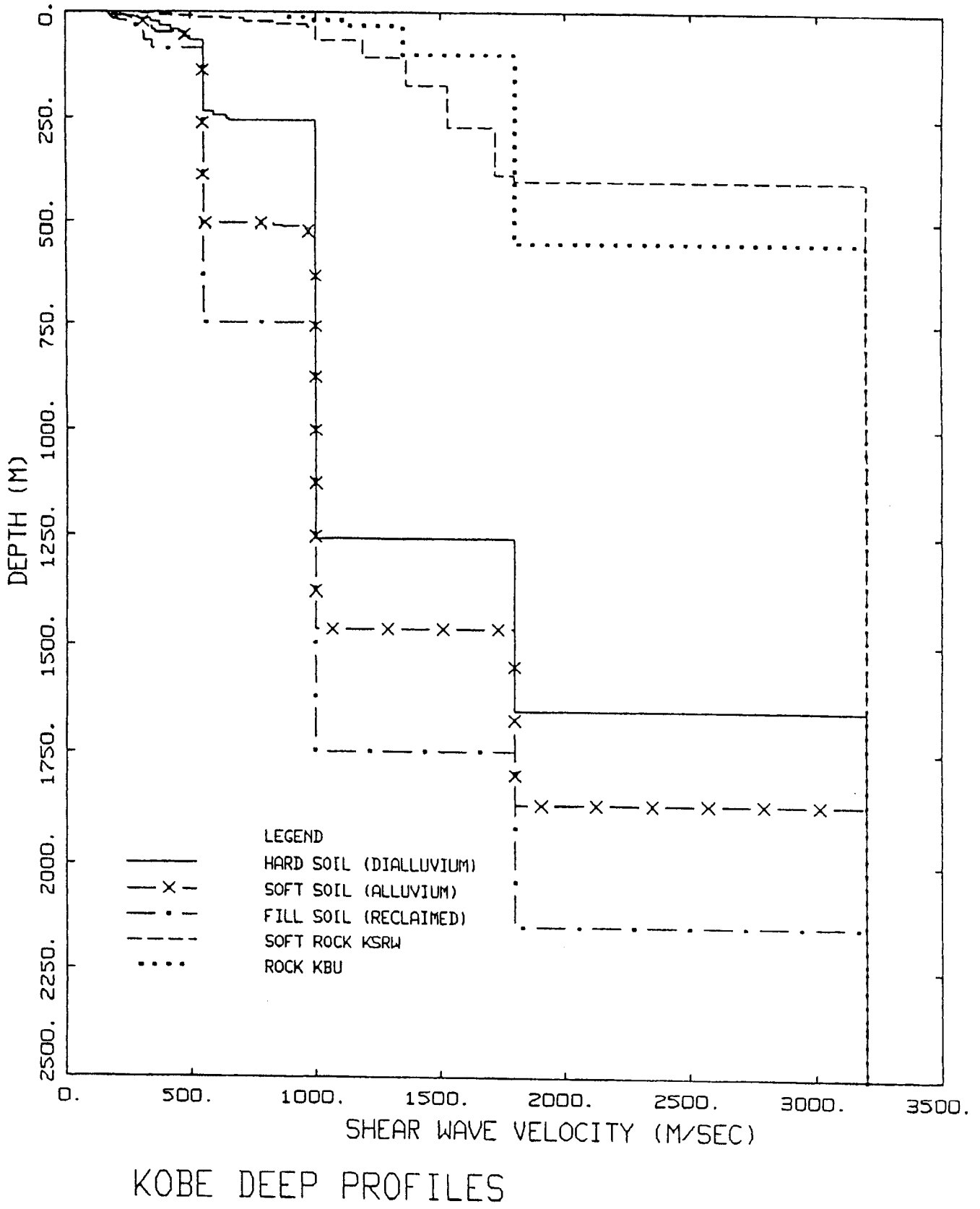

Figure 4.2. Deep hard, soft, and fill (reclaimed) soil profiles and generic soft rock as well as site specific Kobe University rock site profile.

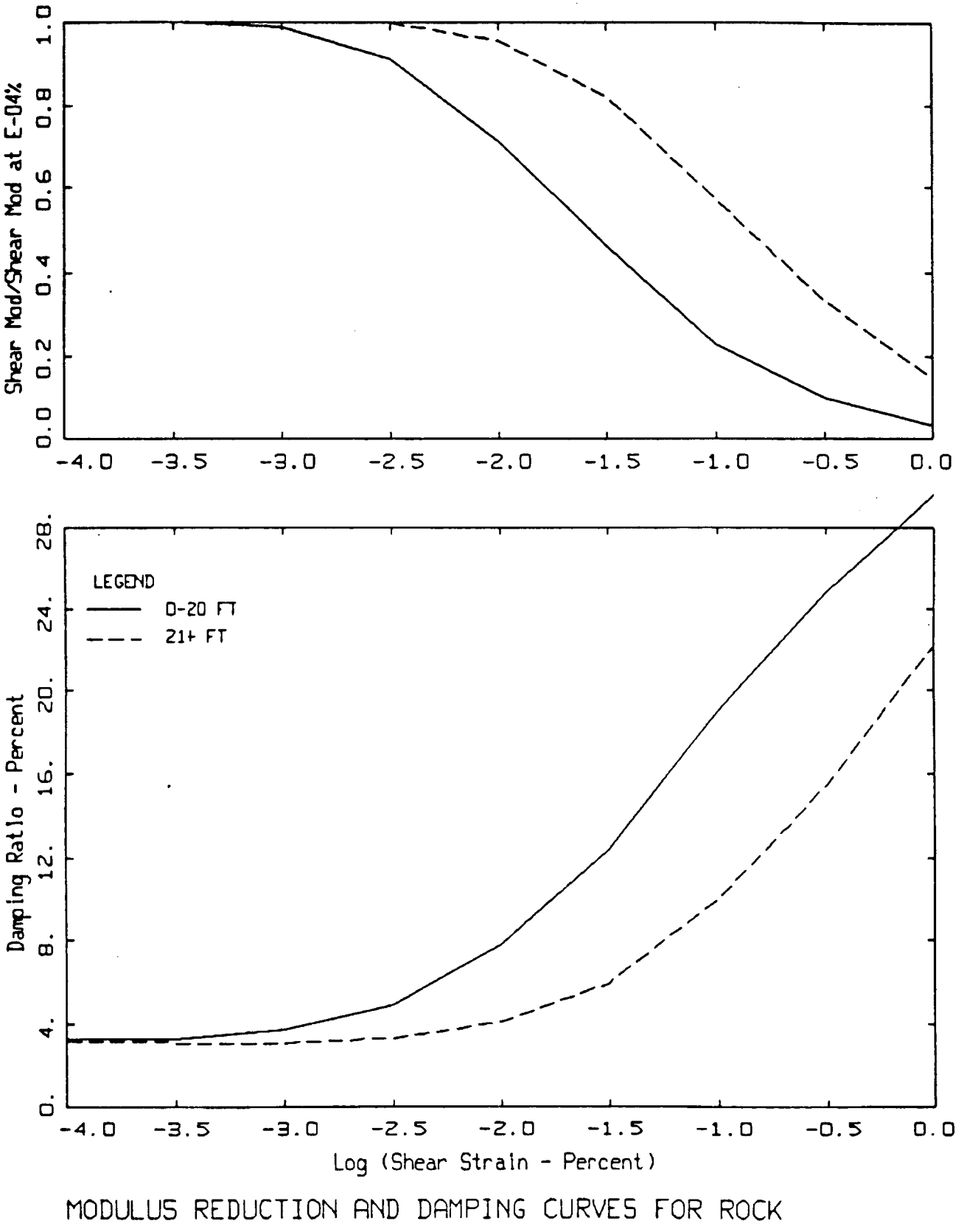

Figure 4.3. Generic G/G_{max} and hysteretic damping curves for soft rock.

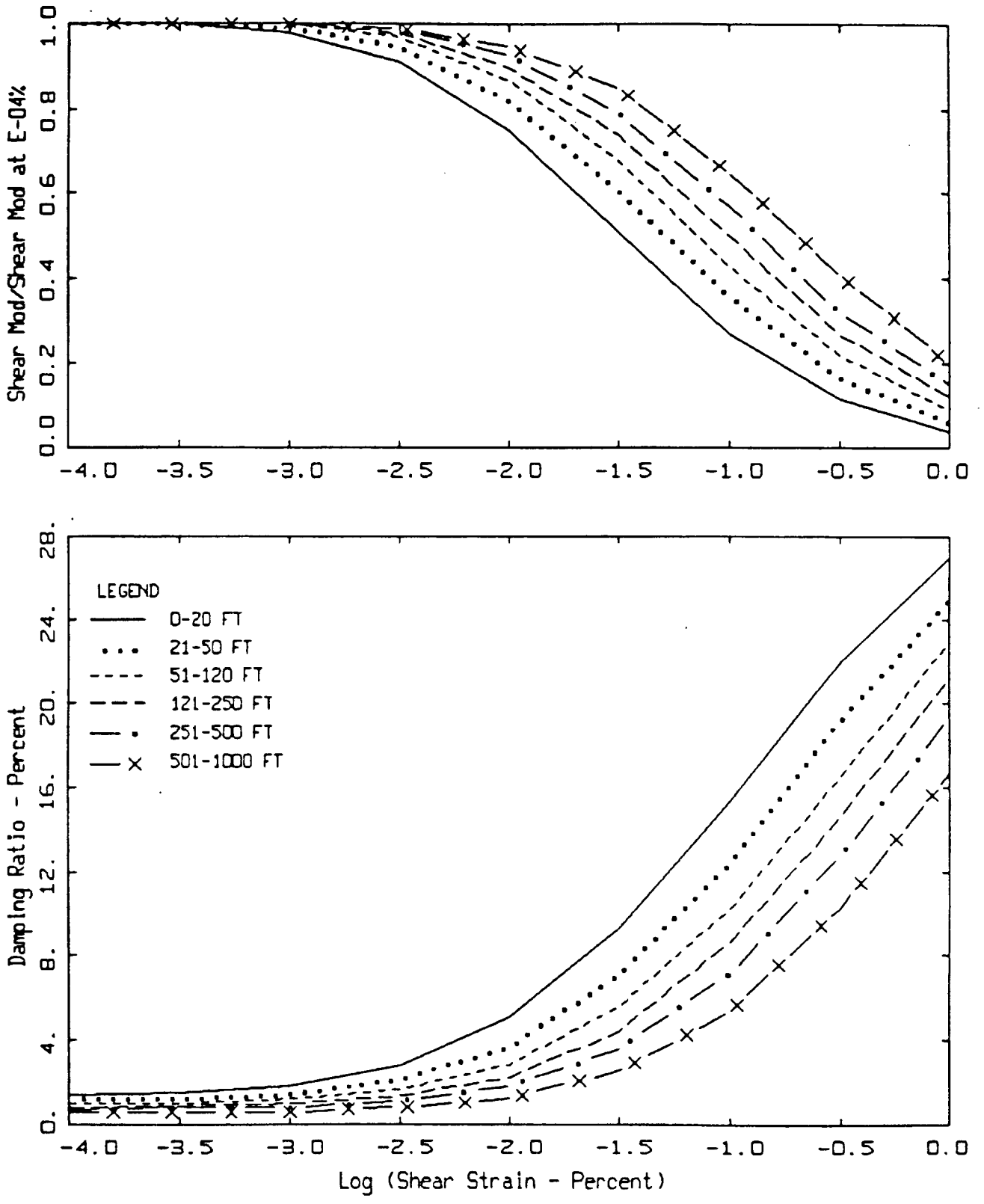

Figure 4.4. Generic G/G_{max} and hysteretic damping curves for cohesionless soils (EPRI, 1993).

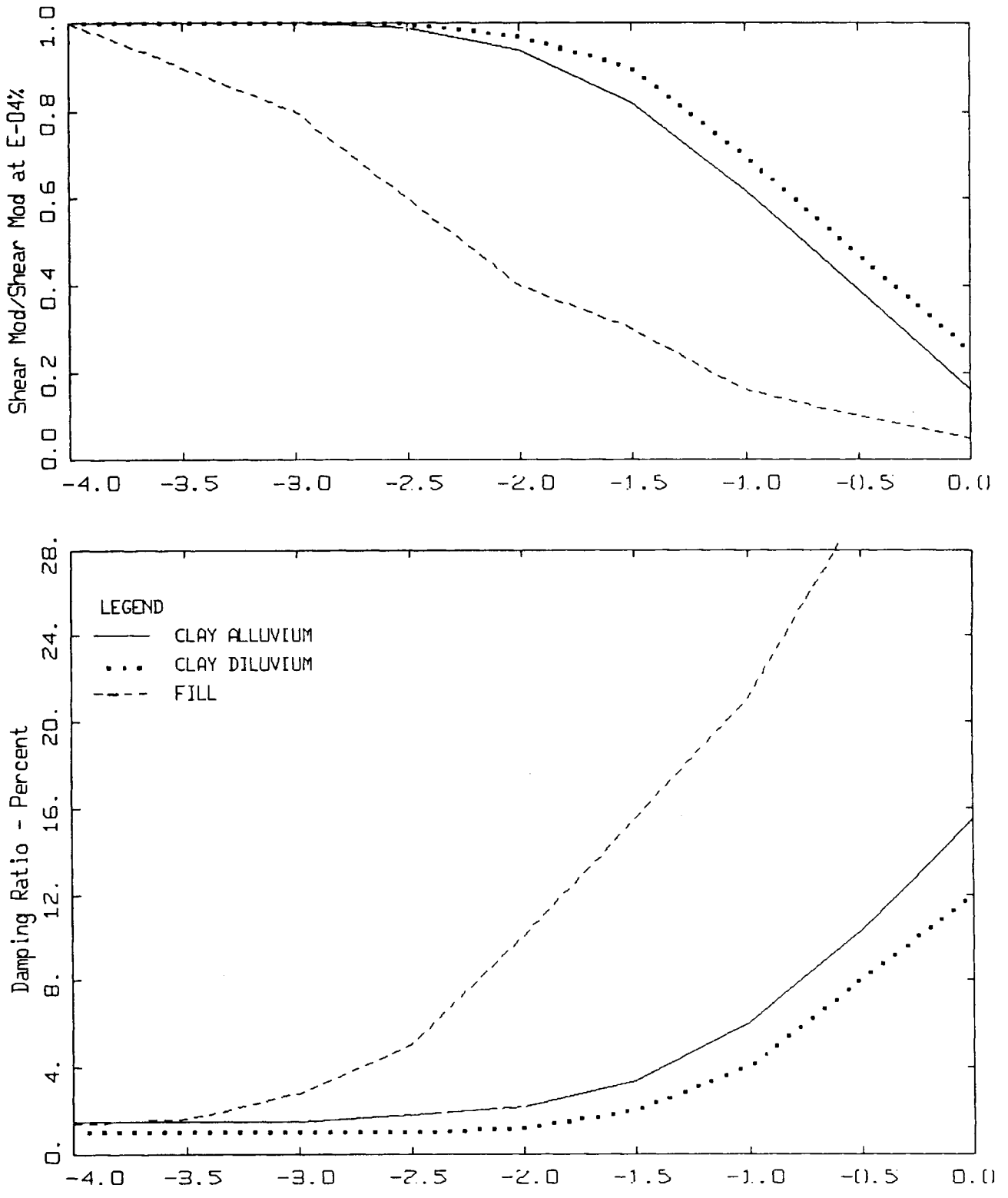

Figure 4.5. Generic G/G_{max} and hysteric damping curves for Kobe cohesive soils (alluvial and diluvial clays) and fill materials (weathered granite, Masado).

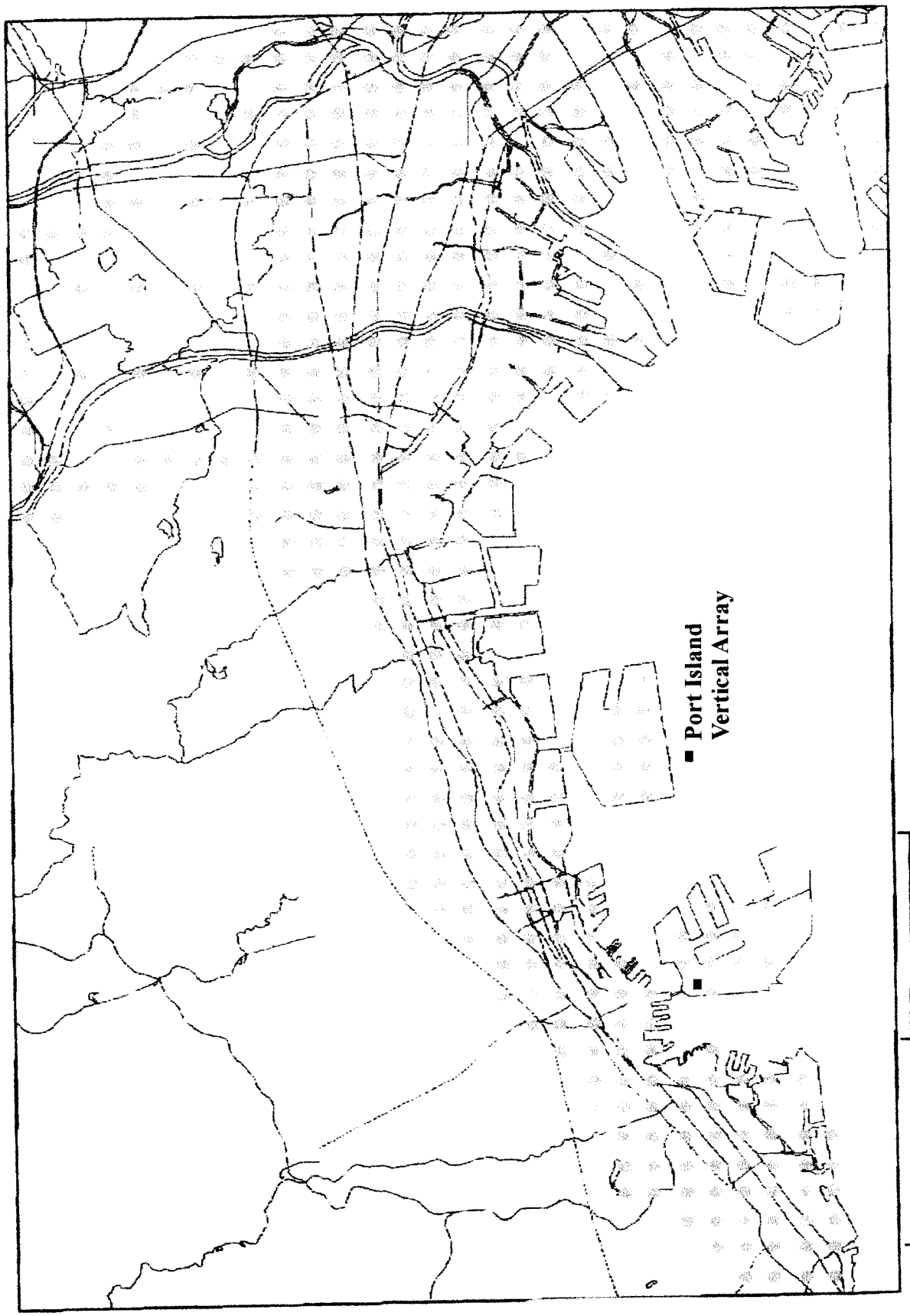

Figure 4.6. Site locations for liquefaction assessment.

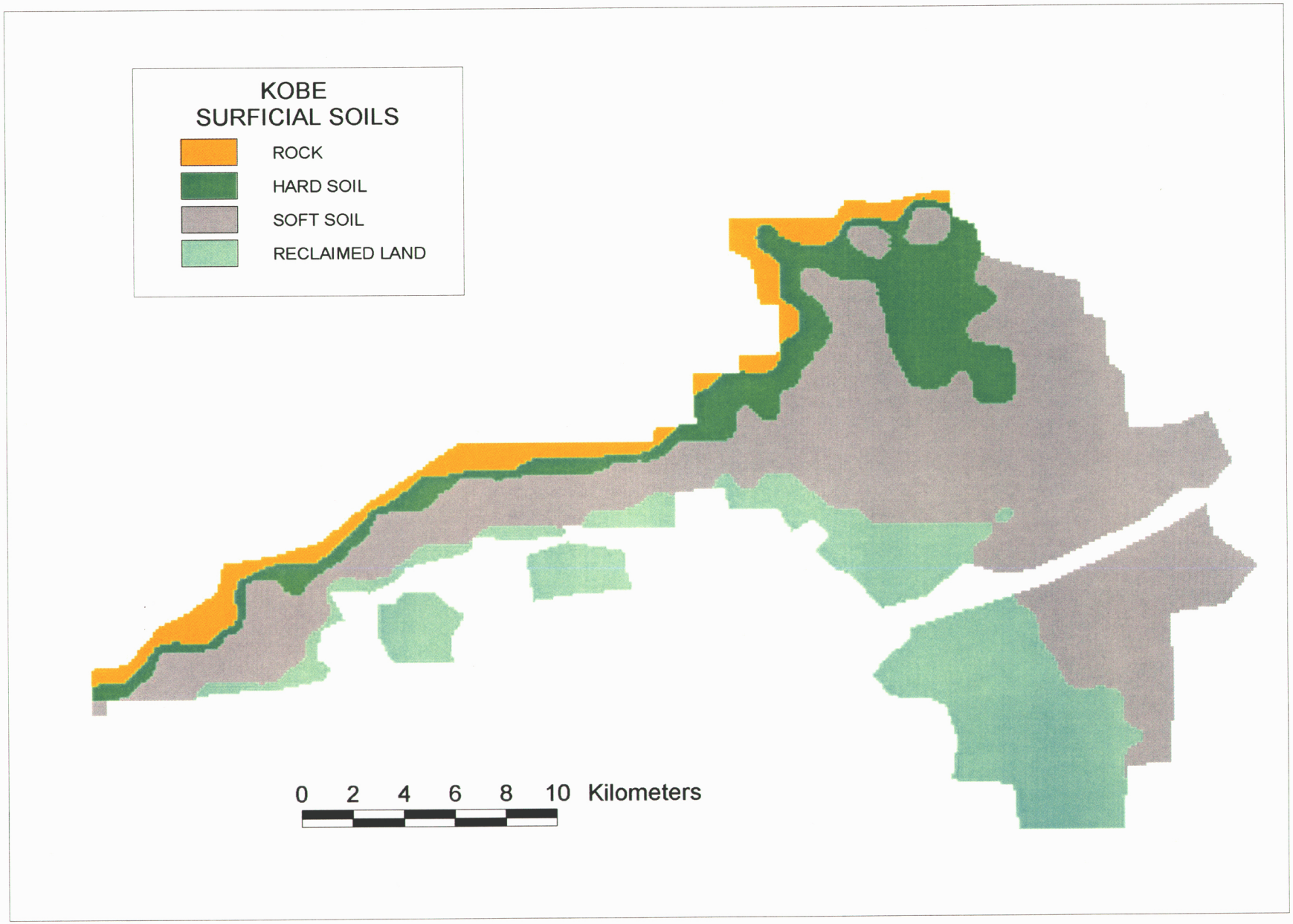

Figure 4.7. Surficial geology of the Kobe, Nishinomiya, and Osaka areas.

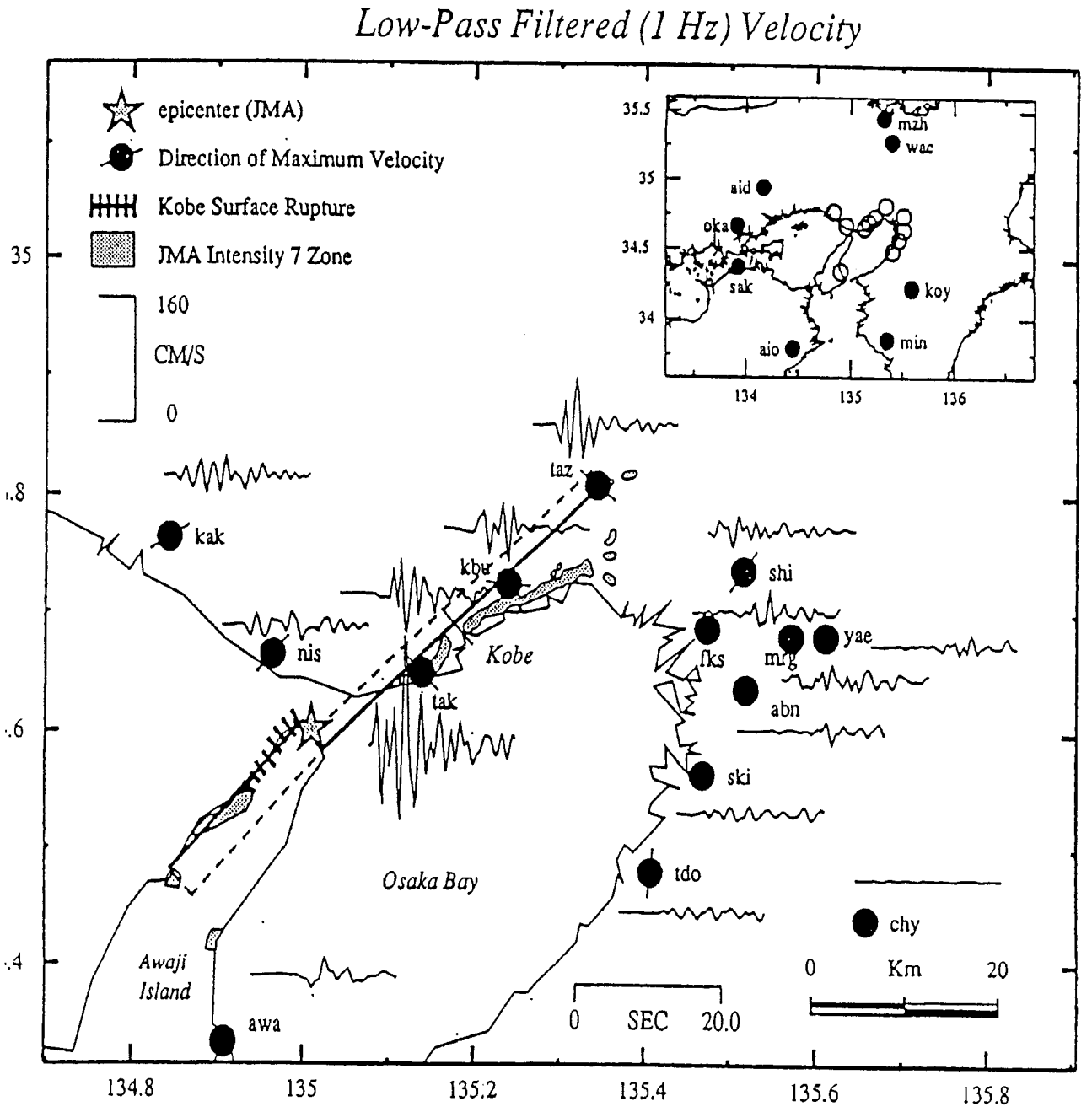

Figure 4.8. Recording station map of the Kobe, Osaka, and surrounding regions (from Wald, 1996).

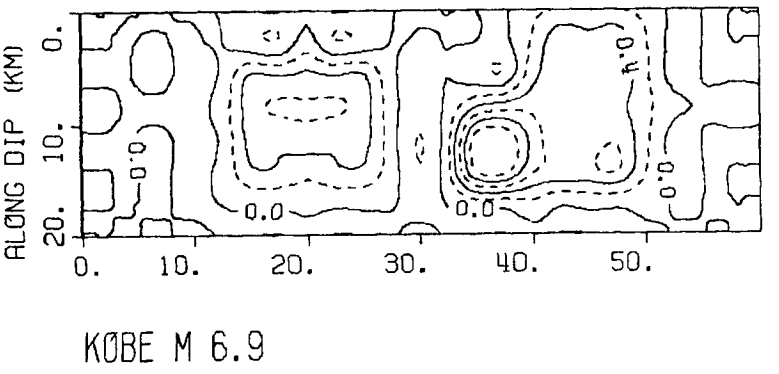

Figure 4.9. Slip model for the Kobe earthquake.

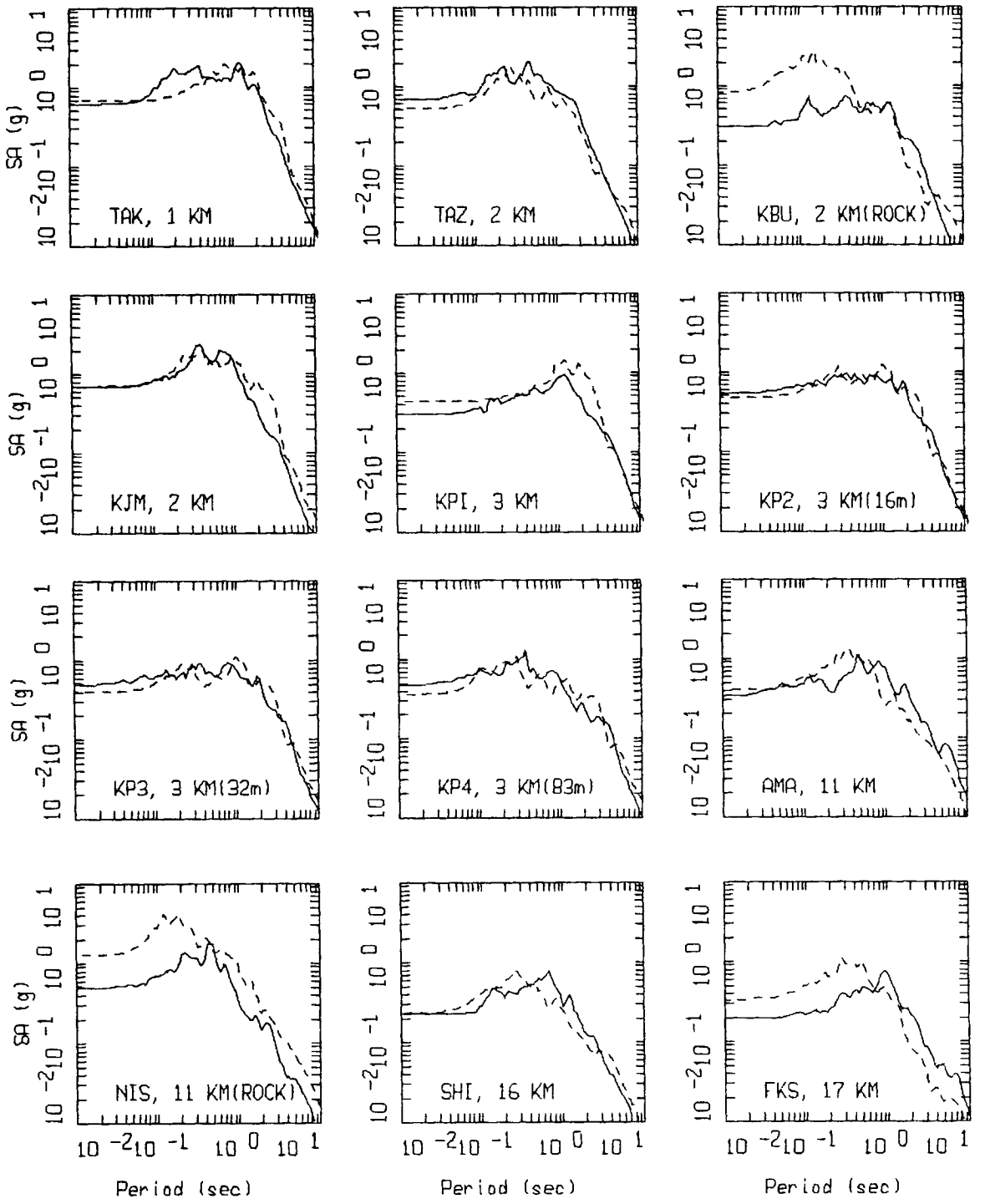

KOBE, FINITE SOURCE MODELING, PAGE 1 OF 3.

LEGEND

——— DATA

- - - - - MODEL

Figure Set 4.10. Comparison of simulations to recorded motions (5% damped response spectra).

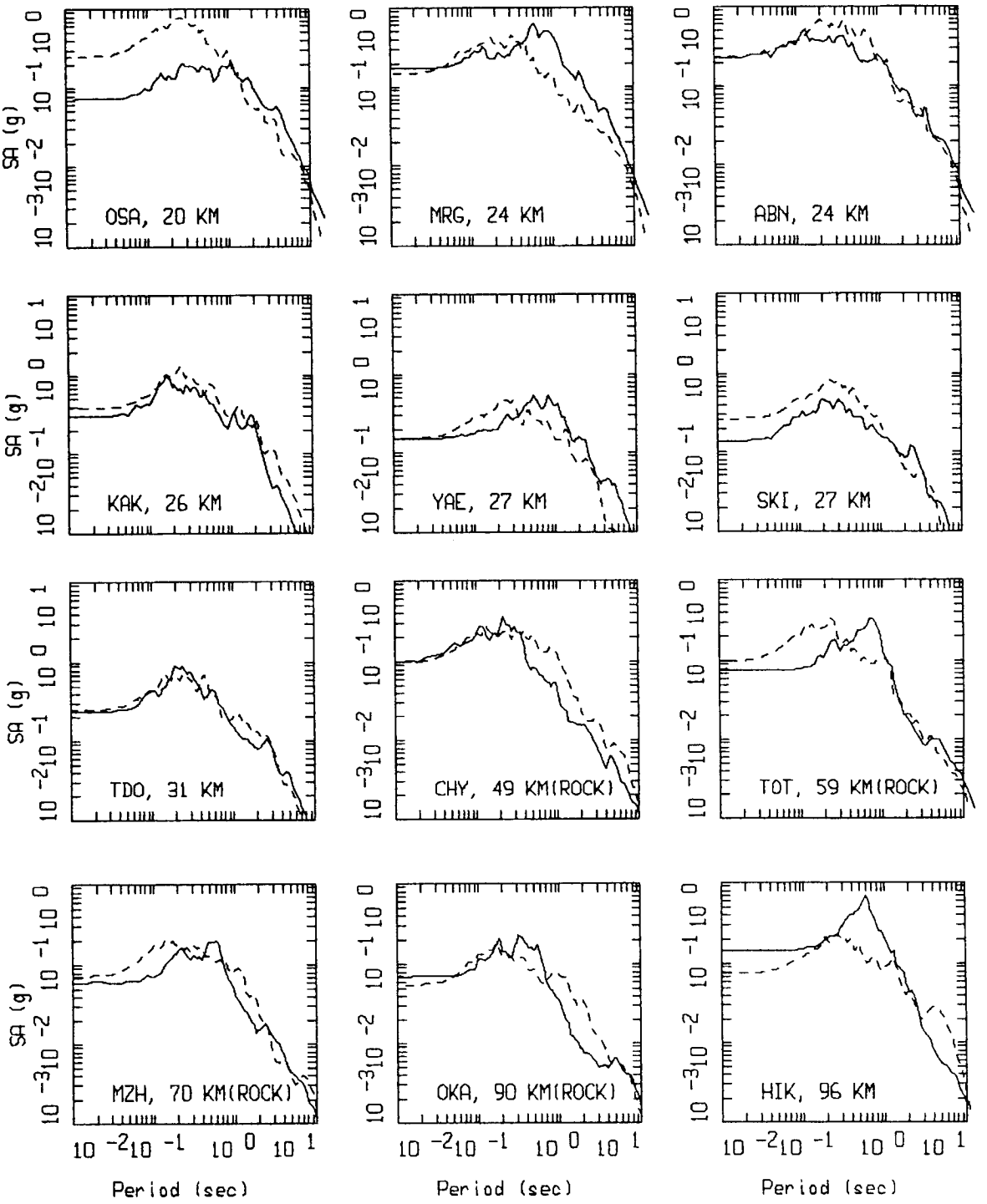

KOBE, FINITE SOURCE MODELING, PAGE 2 OF 3.

LEGEND

——— DATA

- - - - - MODEL

Figure Set 4.10. (Continued)

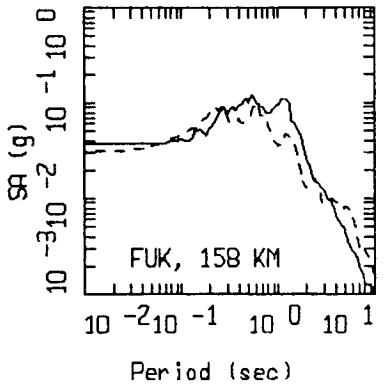

KOBE, FINITE SOURCE MODELING, PAGE 3 OF 3.

LEGEND
——— DATA
- - - - - MODEL

Figure Set 4.10. (Continued)

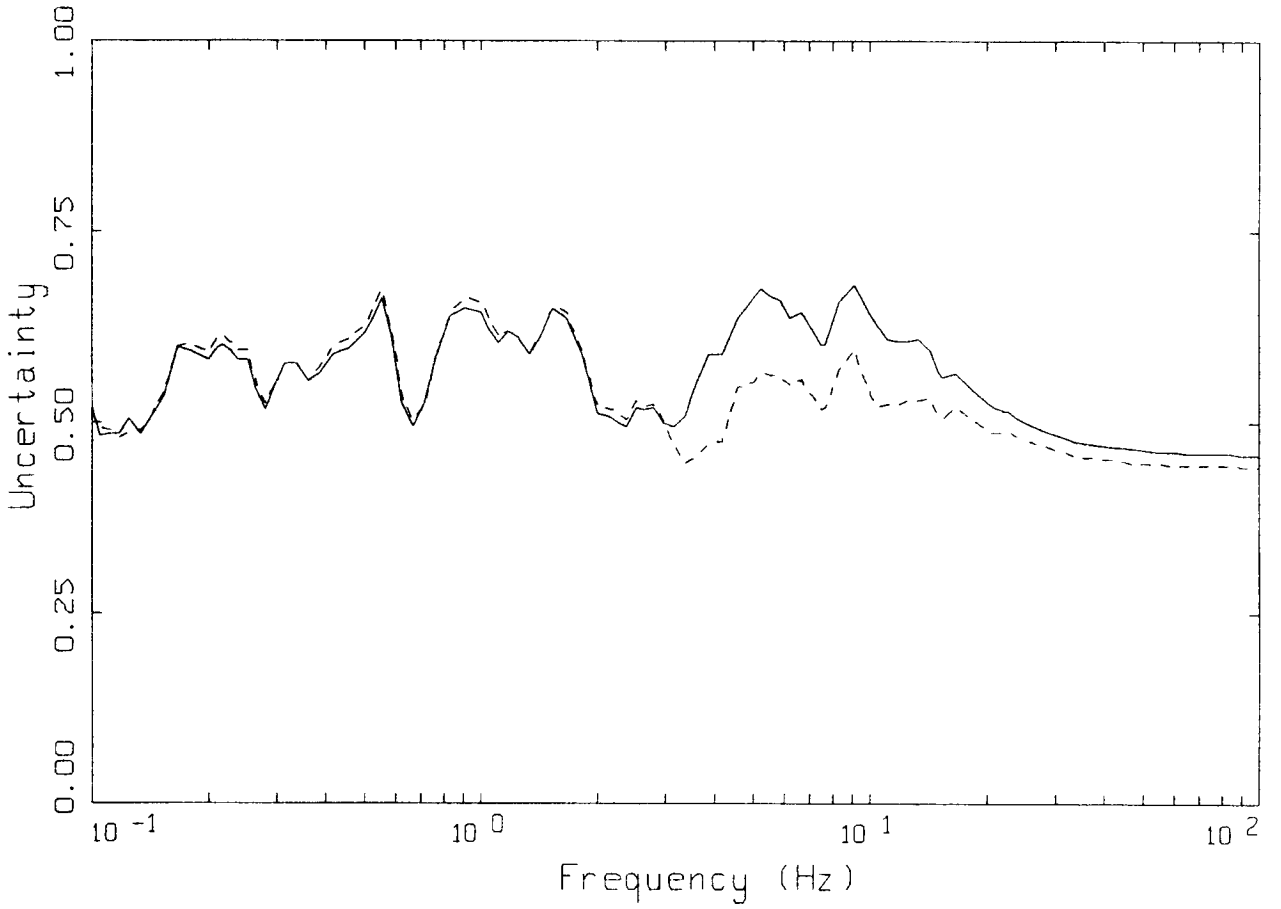

Figure Set 4.11. Model uncertainty and bias estimates computed over the 25 recording sites (fault distance range of 1 - 158 km).

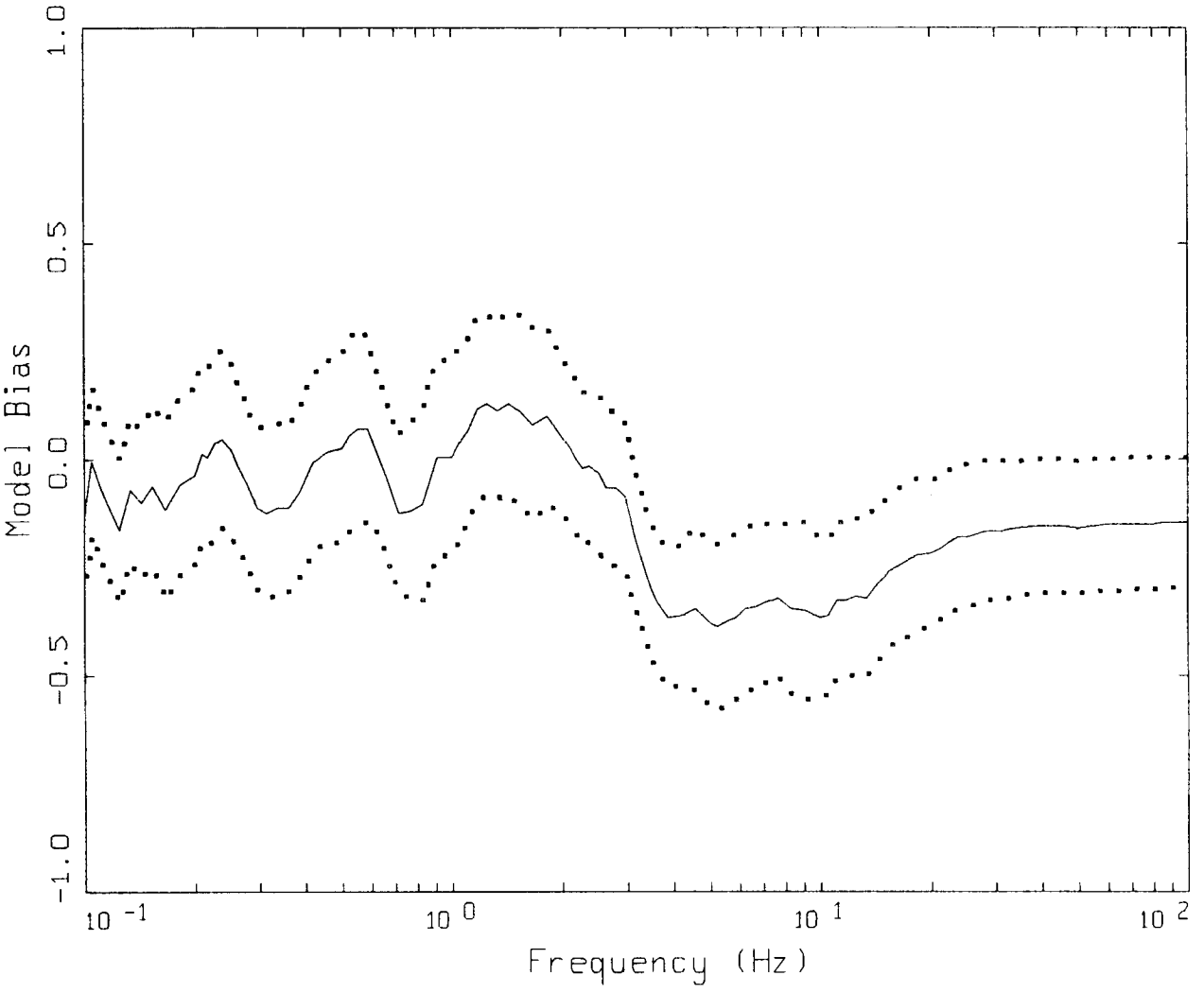

KOBE FINITE SOURCE, MODELING BIAS
NONLINEAR, ALL 25 SITES PAGE 2 OF 2.

LEGEND

——— MODELING BIAS

• • • • 90% CONFIDENCE INTERVAL OF MODELING BIAS

• • • • 90% CONFIDENCE INTERVAL OF MODELING BIAS

Figure Set 4.11. (Continued)

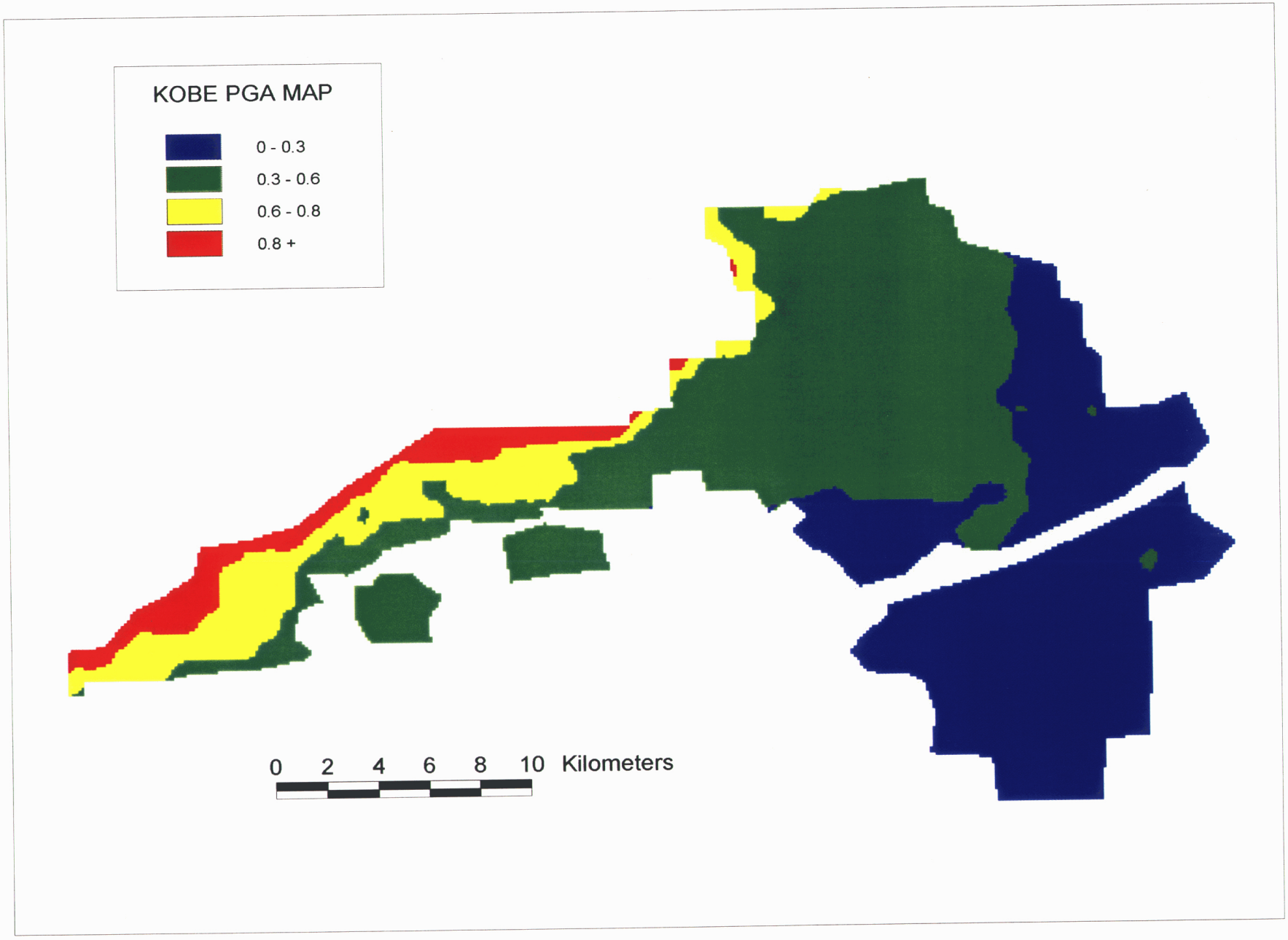

Figure 4.12. Median estimates of peak acceleration values for the rock, hard, soft, and fill areas of Kobe, Nishinomiya, and Osaka.

5.0 LIQUEFACTION ASSESSMENTS

Prior to performing detailed site-specific calculations, some preliminary assessments were undertaken to estimate the general characteristics of the site responses that could be anticipated.

5.1 Preliminary Simplified Estimates

Liquefaction capacities were first estimated based on the simplified or deterministic approach of Seed-Idriss. These estimates account in an approximate way for the influence of relative density of granular soils on liquefaction susceptibility (Ferritto, 1982) and estimate the level of peak acceleration required to cause liquefaction. The calculations assume a relatively uniform deposit of sand with the water table about 5 to 6 feet below ground surface. The critical depth for liquefaction (minimum ratio of capacity/demand) is then typically about 20 feet below grade.

The acceleration levels required to cause liquefaction for this simplified configuration is shown in Table 5.1 as a function of relative density of the granular material. As described in the following sections, the average SPT data available for the hard, soft, and fill sites were used to estimate the average relative densities of the upper soils of the three site categories. The results indicate that the relative densities of the upper soils at the hard sites is approximately 60%, those at the soft sites are about 40% and those at the reclaimed or fill sites are approximately 25%. In Section 4, the peak accelerations estimated for the hard sites were generally calculated to be above 0.8g, those at the soft or alluvial sites ranged from 0.4g to 0.8g and those at the fill or reclaimed sites were estimated to generally exceed 0.2g. By comparing these acceleration levels with the calculations of Table 5.1, the simplified approach to estimate liquefaction capacity would indicate the occurrence of extensive zones of liquefaction in all three site categories.

5.2 Average Soil Columns

For this initial assessment, the three average site columns (hard, soft, and fill; Section 4) were placed at the Kobe JMA site (Figure 5.1). This location is acturally within the area of hard soils (Figures 2.1 and 4.7) and the soft and fill soil areas lie just to the southeast. At such close fault distances, control (baserock) motions would not be expected to vary significantly in going from the hard to soft and to the coastal fill areas. The plot of shear-wave velocity profiles for the three generic KJM profiles is shown in Figure 5.2.

Using the stochastic finite-fault RVT ground motion model, site response calculations were made for these three generic soil columns, all assumed to be located at the Kobe JMA site. The calculations include source, path, and local site effects as previously described to determine motions at the ground surface as well as cyclic shear stress ratios and strain energy in each soil layer within the soil columns. A plot of the calculated cyclic shear stress ratios for these three sites is shown in Figure 5.3. It may be noted that the stress ratios reach their peak values at relatively shallow depths of between 10 and 20 feet below grade. For the fill sites (reclaimed lands), computed values of CSR reach peak values of approximately unity, the soft sites reach peak values of about 1.25, and hard sites reach peak values of about 0.7.

5.3 Cyclic Stress Ratio or Strength Comparisons

By comparing the computed CSR values for these average sites with the standard CSR plot of Figure 3.1, one would conclude that the fill and soft sites, which generally have relatively low values of SPT blow counts immediately below the ground water table, would be expected to liquefy under the applied earthquake loading. At the source distances associated with the Kobe JMA site, the fill sites did indeed generally liquefy (Figure 5.4). However, the same conclusion cannot be reached for the soft sites at the same source distances even though computed cyclic stress ratios reach such high values. These sites did not generally liquefy, indicating that the simple deterministic stress ratio liquefaction criteria do not capture the recorded behavior. A principal parameter of interest is the number of cycles to liquefaction induced by the seismic motion, which is typically not treated in the standard deterministic stress ratio method of analysis. To demonstrate the importance of this parameter, the impact of cycles to liquefaction was incorporated into the evaluation in the following manner.

From the sample blow count data presented in Section 2 for the various soil profiles considered for the Kobe region, the distribution of SPT data for the sandy soils at the hard, soft, and fill sites in the near surface region (0 to 5m) and immediately below (5 to 10m) were determined and are shown in Figure 5.5. These data were then modified to corrected N1-60 blow counts over the depth ranges of interest for comparison with the stress ratio data. The plots of the distributions of these data for each site category are shown in Figures 5.6a and 5.6b for the two depth ranges of interest.

These figures of sample blow count distributions were then placed on the probabilistic strength plots for silty soils developed by Liao and corrected for duration as described in Section 3. The base of the distribution plot in each case is then placed at about the level of the average cyclic shear stress developed over the appropriate depth range for the particular soil column of interest. Figures 5.7a, 5.7b and 5.7c, for example, present the data for the distribution of sample blow counts at hard sites at shallow depth range of 0 - 5m. The average cyclic stress ratio developed for the hard sites is about 0.55. As the number of cycles to liquefaction decreases, the strength curves move up while the computed CSR remains at the same level. In Figure 5.7a, the strength curves are based on an assumed value of 15 cycles to liquefaction and they indicate that more than 50% of the samples will have blow counts below the 50th percentile strength curve at the CSR level applied, indicating that these sites would be expected to liquefy. Figure 5.7b shows the same data but assuming that only 4 cycles occur to liquefaction. This plot indicates that the situation is somewhat improved with about 50% of the samples having blow counts at the 50th percentile strength curve.

Figure 5.7c, however, based on an assumed 1 cycle to liquefaction, indicates that well below 50% of the samples have blow counts at values associated with the 50th percentile strength curve. In this case, the hard sites would not be expected to liquefy, which in fact they didn't. Figures 5.7d through 5.7f present the same data for hard sites, but this time for samples taken at the deeper depth range of 5 to 10m. The average developed CSR in this depth range is higher than in the upper soil layers, reaching a value of about 0.7. Although the average applied loading (CSR) is higher than in the soil layers above, the same conclusions are reached, since for 1 cycle to liquefaction less than 50% of the samples in this depth range have blow counts less than those associated with the 50th percentile strength curve. That is, the soils are stiffer at the lower depths with higher N1-60 blow counts.

Figures 5.8a through 5.8f present similar information obtained for the soft sites considered in the study. These sites are located at the base of the hills surrounding Kobe and are generally termed the alluvial sites. The average cyclic stress ratio in the upper soil layers (0 to 5 m) is about 0.90. The results again indicate that if the strength data associated with 1 cycle to liquefaction is used in the assessment, about 50% of the sample blow counts are at or above the 50th percentile strength curve (Figure 5.8c). For the deeper soil layers, the average applied CSR is somewhat less at about 0.80, which indicates that less than 50% of the samples have blow counts below the 50th percentile strength levels. Thus, these sites would show more tendencies to liquefy than the hard sites, although they would not be expected to show massive zones of liquefaction. The soft site areas (Figure 4.7) did show evidence of liquefaction although not nearly as extensively as the fill areas (Figure 5.4).

Figures 5.9a through 5.9f present similar information at the fill sites associated with the reclaimed lands along the shore of Kobe. The average CSR in the upper soils is about 1.0 and in the lower soils from 5m to 10m is somewhat less with values of about 0.85. These results indicate that more than 50% of the fill soils have blow counts below the 50th percentile strength curve in the upper layers (Figure 5.9c). It would then be expected that wide zones of liquefaction would occur in this region even if only 1 cycle to onset of liquefaction occurs. At deeper depths (Figure 5.9f), about half of the samples show blow counts at the 50th percentile level indicating that liquefaction at these depths is less prevalent than would occur in the upper soil layers.

Comparisons of these CSR ranges for estimates of probabilities of liquefaction are then made with the results of the site specific computations of CSR described in Section 4 and shown in Figure 5.10. The fill or reclaimed zone in the vicinity of the water's edge in Figure 5.10 indicates values of CSR which range between 0.40 to 0.75. Comparing this computed "demand" with the capacities estimated in Table 5.2, this zone would be expected to have a high probability of liquefaction if 4 cycles of motion were generated to induce liquefaction or a moderate probability of liquefaction if 1 cycle of motion were generated. The zones of soft alluvial materials adjacent to, but further inland from, the reclaimed zone are indicated in Figure 5.10 to have seismic "demand" CSR's in the range of 0.75 to 1. This level of CSR corresponds to a very high probability for the occurrence of liquefaction according to the criteria of Table 5.2 if 4 cycles of motion were generated or a moderate probability of liquefaction if 1 cycle of strong motion were generated. Based on the observations of surface expressions of liquefaction noted in the field, the area of the soft alluvial sites would not be expected to show this high probability of liquefaction. Thus, it appears that the use of CSR does not correlate well with the recorded data and tends to be overly conservative in its estimate of zones of extensive liquefaction. The areas of hard material bordering the soft alluvial sites are also indicated to have high values of CSR, reaching levels greater than 1.0. Again, these high levels would indicate high probabilities of liquefaction, although no significant liquefaction occurred in these zones. However, it should be noted that in many cases, ground water levels in this region were relatively low (average 7.1m, Section 4.5) as compared to the other two zones, making this comparison of CSR suspect.

Thus, it is concluded from these results that when attempting to evaluate the potential for liquefaction based on CSR, it is important to account for the appropriate number of cycles to the onset of liquefaction which is a function of both earthquake magnitude and distance to the fault. The results of this comparison indicates that the use of CSR, either probabilistically or deterministically, leads to a conservative estimate of the extent of liquefaction for these close-in regions.

5.4 Strain Energy to the Onset of Liquefaction

An alternate approach to the assessment of liquefaction potential is also evaluated. This approach is based on estimating the strain energy generated at each depth in the soil column by the seismic motion and comparing this energy with similar data generated from cyclic laboratory experiments. As described in Section 3, the results from a number of cyclic triaxial experiments were reduced to determine the strain energy required to generated pore pressure ratios of unity; that is, the energy required to cause the pore pressures in the sample to reach the applied confining pressures. The data from the 150 samples (Ostadan et al., 1996) shown in Figure 3.6 are replotted in Figure 5.11a in which the strain energy to the onset of liquefaction is plotted as a function of sample confining pressures. For the clean sand samples, the same data are plotted in Figure 5.11b as a function of relative density. As may be noted, the results indicate that for the clean sand samples confining pressure and relative density are important parameters controlling the magnitude of energy to liquefaction.

Regression of the laboratory data was then performed to obtain the relationship between strain energy, confining pressure, and relative density for the sand samples. The results of the regression leads to the form:

$$\text{Log}_{10} [\, E_{liq} \,] = A + B * \text{Log}_{10} [\sigma_C \,] + C * D_R$$

where $A = -2.215$, $B = 0.8509$, $C = .01369$, D_R is the relative density in percent and E_{liq} is the strain energy to achieve a pore pressure ratio of unity in psi (or in-lbs/in^3 of soil). The results of this regression is shown in Figure 5.11c for the case of relative densities of 0%, 50% and 100%. A similar regression was performed for the available silty samples to try to estimate the influence of silt content on the strain energy to liquefaction. The results of the regression lead to

$$\text{Log}_{10} [\, E_{liq} \,] = D + E * \text{Log}_{10} [\sigma_C \,] + F * (\%\text{Fines})$$

where $D = -2.177$, $E = 1.269$ and $F = 0.005147$. The results of this regression are shown in Figure 5.11d and indicate that silt content is not a major parameter in determining strain energy to liquefaction.

To make use of these correlations in the site evaluations, estimates of relative density for the Kobe soils had to be generated. Some typical correlations of SPT blow counts with relative density (Burmister, 1962) are shown in Figure 5.12 for average soil descriptions. The results indicate that for the same SPT blow count, the finer the soil, the higher the expected value of relative density. A wider range of soil descriptions could be used from very coarse to very fine in this evaluation, but these are most likely not appropriate for the range of soils described for the Kobe region. The site descriptions presented in the Special Issue on Geotechnical Aspects prepared by Japanese Geotechnical Society following the Kobe earthquake indicate that the fill soils are generally gravelly sands while the soft and hard site areas are generally more fine grained or dirtier.

Based on the SPT data available for the hard, soft and fill sites, the relative densities were estimated for the upper soils of the three site categories to obtain an average value of relative density.

The result of this exercise indicates that the relative densities of the upper soils at the hard sites is approximately 60%, those at the soft sites are about 40% and those at the reclaimed or fill sites are approximately 25%.

From the calculations for site response using the three average soil columns located at the Kobe JMA site, the strain energy for each site soil column is shown in Figures 5.13a through 5.13c. The calculated strain energies are shown as a function of mean confining pressure (which is related directly to depth and unit weight of the site soil columns). The results for the fill site are shown in Figure 5.13a together with the mean, 1-sigma and 2-sigma energy estimates of strain energy required for liquefaction for the site soils at their appropriate relative densities. As can be noted, the fill sites indicate high probability of liquefaction for the upper soils immediately below the ground water table (energies at the 2-sigma level). Figure 5.13b shows similar results for the soft sites but indicates somewhat less likelihood to generate liquefaction conditions (pore pressure ratios of unity) as compared to the fill sites The results for the upper soils immediately below the ground water table, however, are still relatively high (slightly above the 1-sigma level). The corresponding results for the hard sites are all well below the mean energy level required for liquefaction and therefore indicate little likelihood for liquefaction.

The results for energy to the onset of liquefaction must be modified to convert the estimates to a surface expression of liquefaction. The capacity estimates for the CSR or strength approach have already accounted for this effect since the estimates, both deterministic and probabilistic, have been correlated with the empirical data base which is based on noted surface expressions of damage. To perform a similar transformation for the energy approach, the energy capacities based on laboratory data for pore pressure ratios of unity were modified to account for the layer of soil above the water table which would serve to restrict any upward flow of water and/or ejecta, leading to surface expressions of liquefaction. The data provided by Ishihara (1985) were used to perform this conversion. The estimates of average strain energy in the top 4m immediately below the ground water table required to cause surface expression of liquefaction is shown in Table 5.2 for the three soil site types.

The results of the computation of average energies computed in the upper 4m of soil located immediately below the ground water table in the site specific soil columns, described in Section 4, is shown in Figure 5.14. This plot represents the seismic energy "demand" applied to the shallow soils in the various areas studied. For the fill sites at Port and Rokko Islands, the computed strain energy is found to vary from 0.025 psi to 0.05 psi. This would correspond to a moderate probability for the onset of liquefaction for areas where significant areas of liquefaction occurred. Closer to the fault rupture in this reclaimed zone, the strain energy levels reached values of 0.05 to 0.10 which would correspond to a high probability for liquefaction. In the soft zones of alluvial materials, the calculated strain energy of the upper soils reached values of between 0.025 psi to 0.05 psi. This corresponds to a low probability of liquefaction in these zones. In the hard sites and soft zones further east of Kobe, the probability of liquefaction based on the calculated strain energy levels would be considered low.

A comparison of these results with the areas of recorded observations of liquefaction shown in Figure 1.11 would indicate that these predictions are significantly closer to the observations of liquefaction than were the very conservative predictions based on CSR. It should be noted, however,

that the calculated strain energy levels within each soil column were found to be very much more sensitive to the particular level of shear modulus and damping than were the calculated CSR's, that is, the variability in the strain energy calculations were found to be significantly greater than the variability in the CSR's. This is understandable given that strain energy is a function of both stress and strain level whereas the CSR is a function of stress level only.

For example, the sigma in the natural log of the peak strain energy computed for the randomly generated (Section 4.5) soil columns at a particular location was estimated to be approximately 1.0. The corresponding sigma in the natural log of the CSR in the same soil columns was found to be 0.2. This indicates that the uncertainty in the computation of strain energy is much higher than that of the CSR, given the same uncertainty in the primary soil column parameters controlling site response (shear-wave profile and nonlinear dynamic properties). To reduce this uncertainty in computed strain energy would require enough additional site data to reduce the uncertainty in site properties.

Table 5.1
Estimated Accelerations (g) Required
To Cause Initial Liquefaction Based on
Simplified Seed-Idriss Approach

Relative Density (%)	Cycles of Strong Ground Shaking			
	15	10	4	1
25	0.065	0.073	0.089	0.131
40	0.103	0.116	0.141	0.208
50	0.128	0.145	0.177	0.260
60	0.154	0.174	0.212	0.312
70	0.179	0.203	0.248	0.364

Table 5.2
Estimates of Average Strain Energy (psi)
for Surface Expression of Liquefaction

Depth Range (meters)	Probability of Liquefaction	Reclaimed Ground	Soft Ground	Hard Ground
0 - 4	Low	< 0.02	< 0.05	< 0.08
	Moderate	0.02 - 0.08	0.05 - 0.22	0.08 - 0.45
	High	> 0.08	> 0.22	> 0.45

Table 5.3 Estimates of Cyclic Stress Ratios (Tau/Sigma) For Surface Expression of Liquefaction				
Depth Range (meters)	Probability of Liquefaction	Reclaimed Ground	Soft Ground	Hard Ground
Estimated 4 cyclers of motion to liquefaction:				
0 - 5	Avg SPT Blows	15	20	25
	Low	< 0.3	< 0.45	< 0.60
	Moderate	0.3 - 0.55	0.45 - 0.75	0.60 - 1.00
	High	> 0.55	> 0.75	> 1.00
5 - 10	Avg SPT Blows	20	25	30
	Low	< 0.40	< 0.55	< 0.70
	Moderate	0.40 - 0.70	0.55 - 0.90	0.70 - 1.20
	High	> 0.70	> 0.90	> 1.20
Estimated 1 cycle of motion to liquefaction:				
0 - 5	Avg SPT Blows	15	20	25
	Low	< 0.45	< 0.65	< 0.75
	Moderate	0.45 - 0.70	0.65 - 1.00	0.75 - 1.10
	High	> 0.70	> 1.00	> 1.10
5 - 10	Avg SPT Blows	20	25	30
	Low	< 0.55	< 0.80	< 1.00
	Moderate	0.55 - 1.05	0.80 - 1.30	1.00 - 1.30
	High	1.05	> 1.30	> 1.30

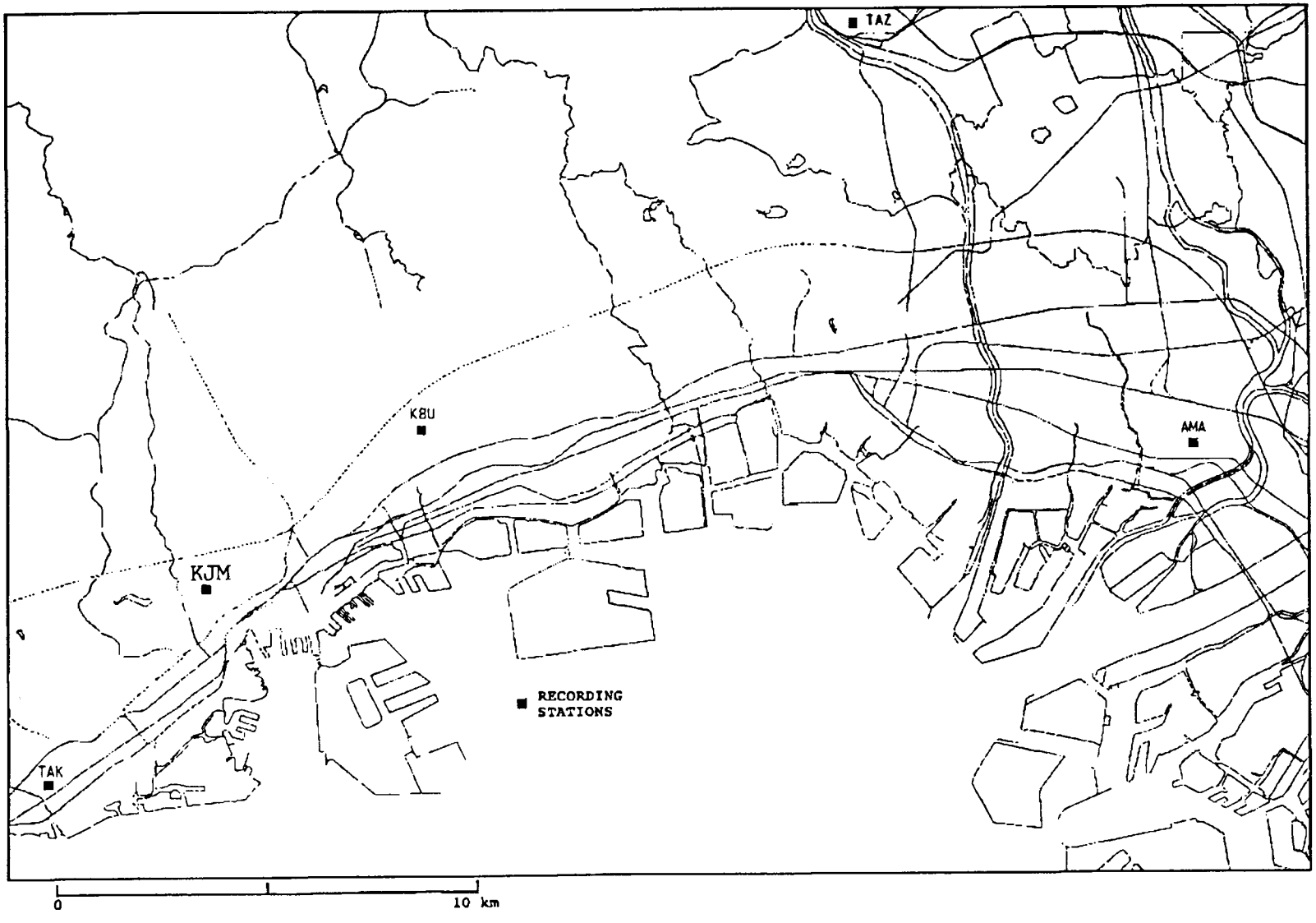

Figure 5.1. Location of Site KJM used in this evaluation.

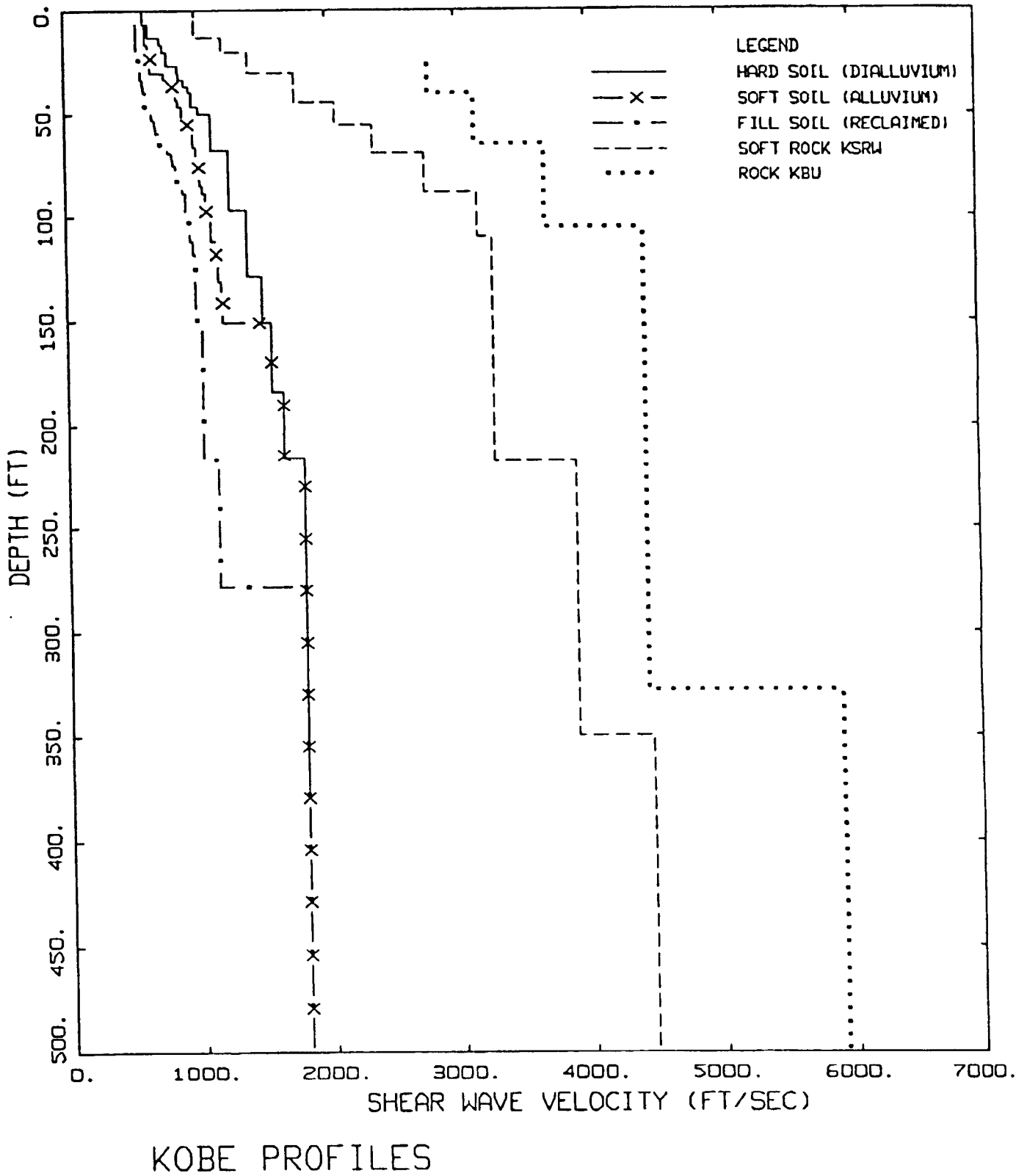

Figure 5.2. Shallow hard, soft, and fill (reclaimed) soil profiles and generic soft rock as well as site specific Kobe University rock site profile.

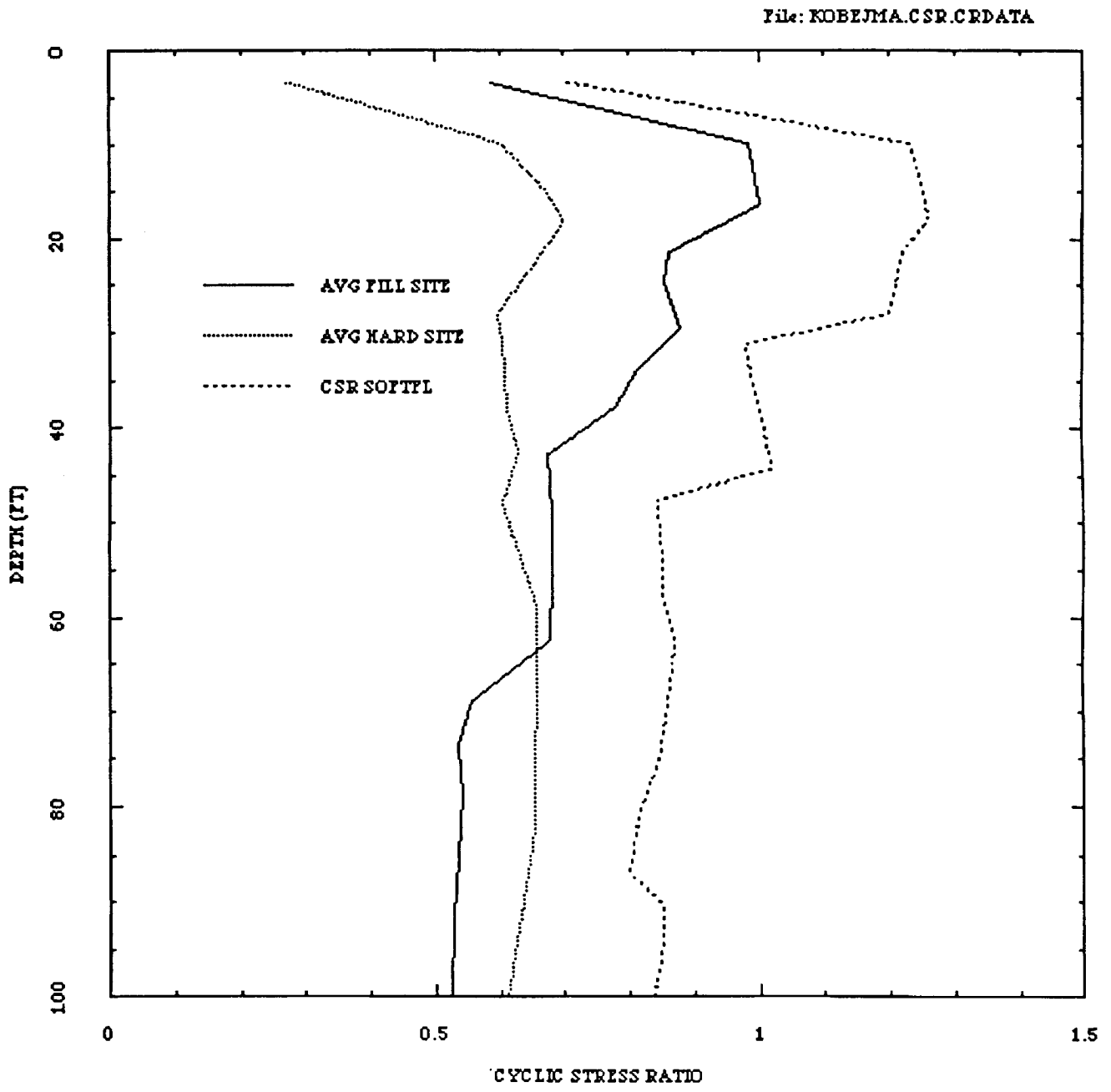

Figure 5.3. Computed cyclic stress ratios for the generic soil columns at the Kobe JMA site.

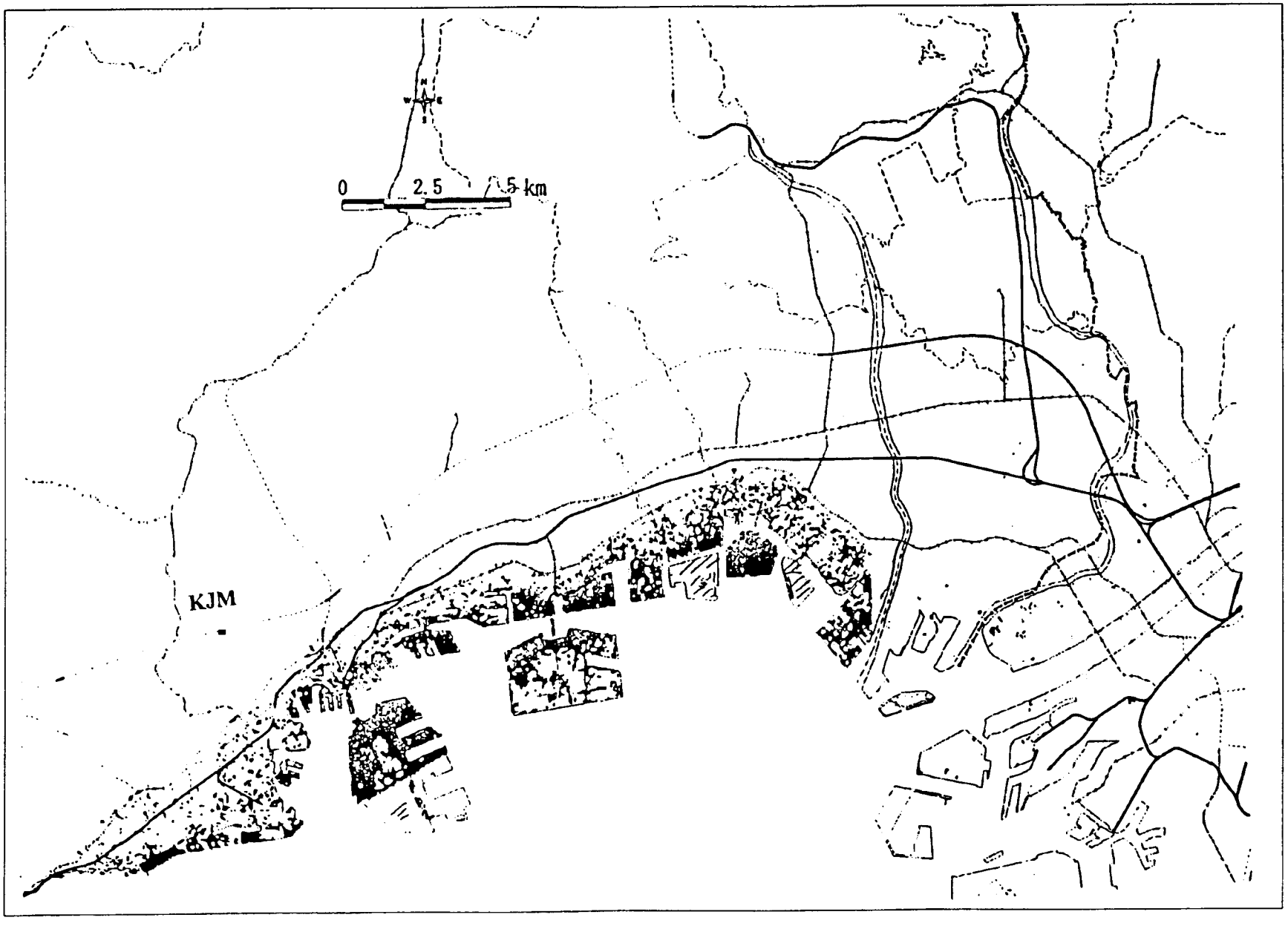

Figure 5.4. Zones of surface expression of ground failure (from Iwasaki, 1997).

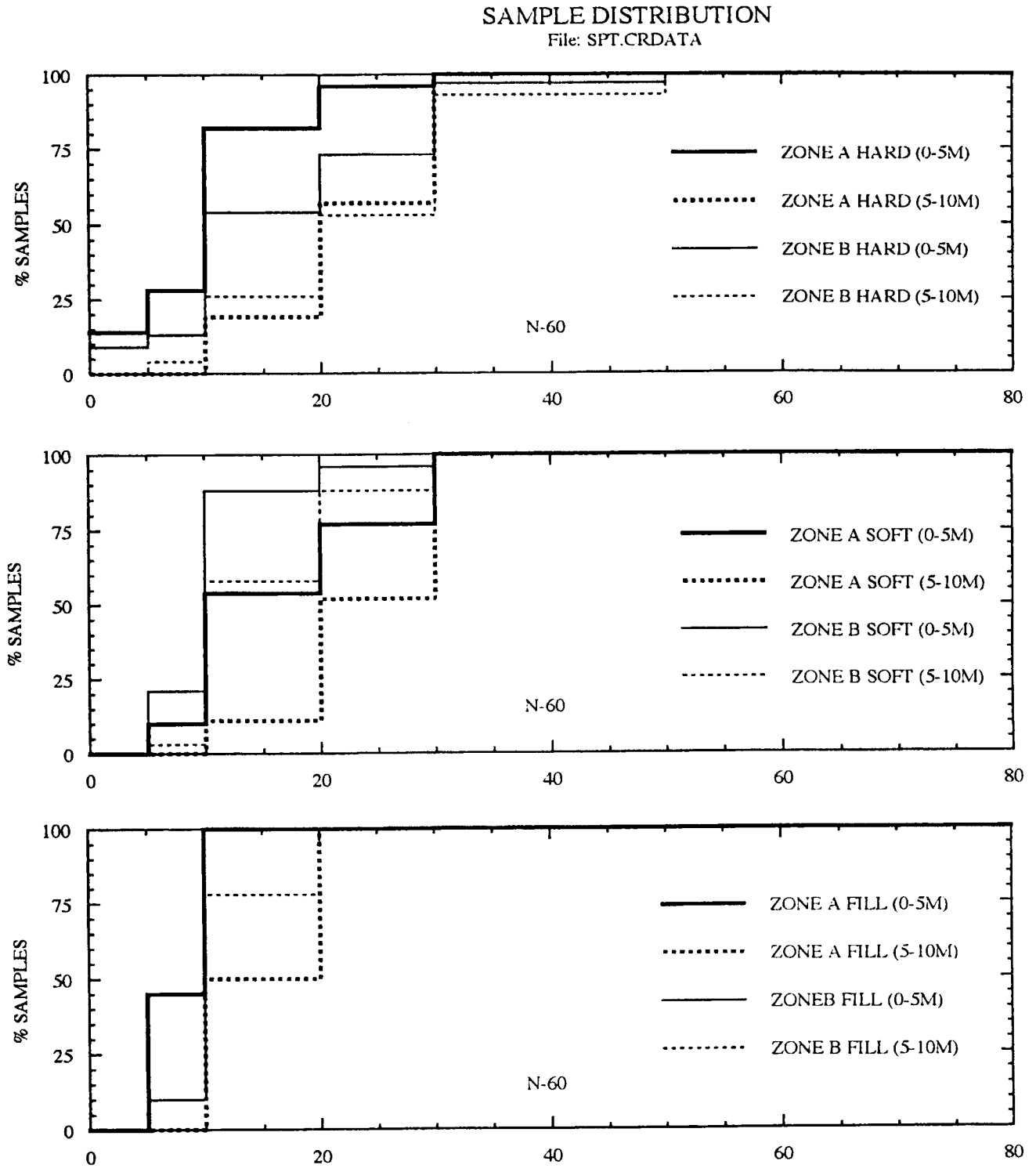

Figure 5.5. Distribution of sandy sample SPT blow counts in upper portion of soil profiles.

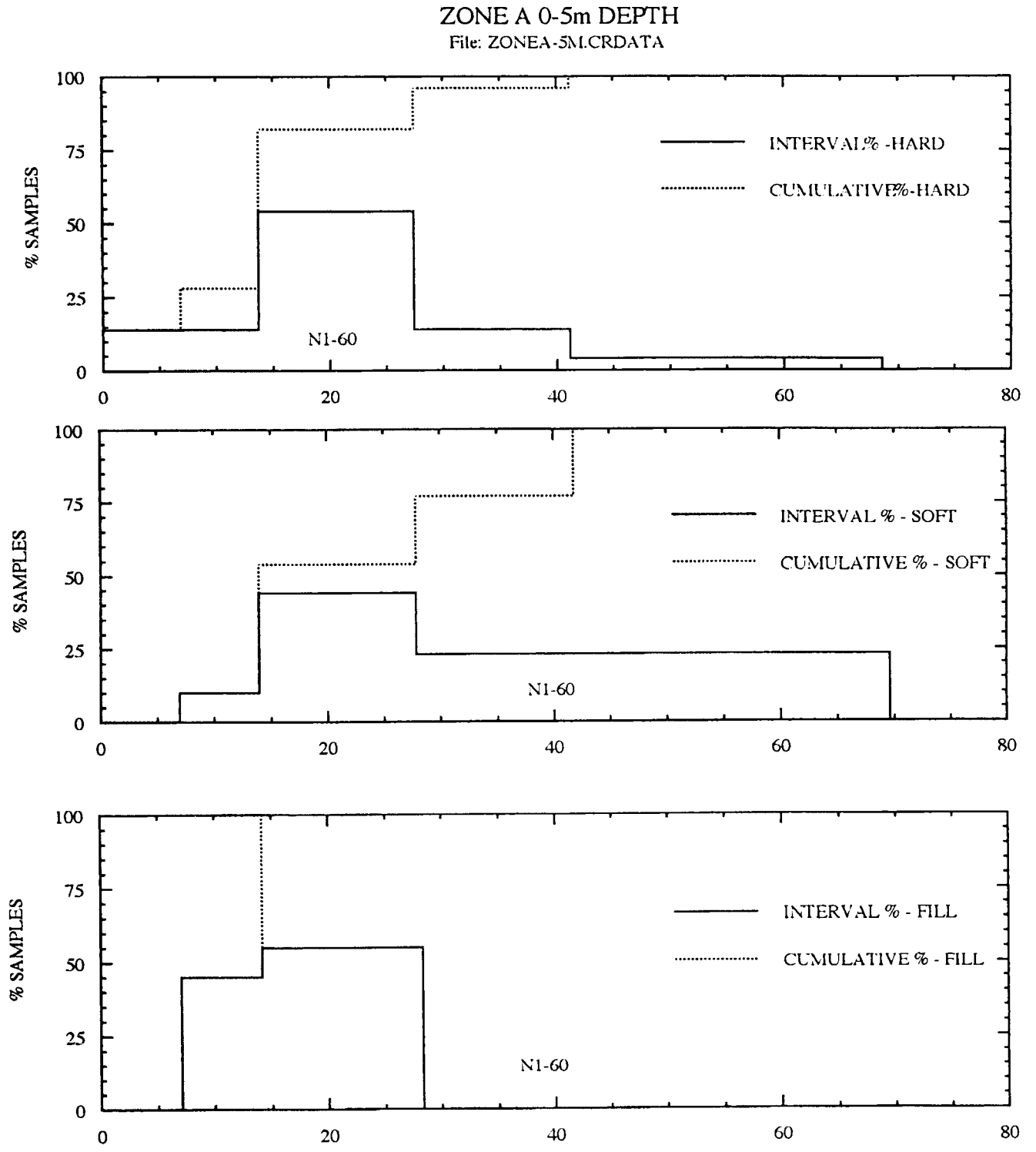

Figure 5.6a. Distribution of N_{1-60} blow count data for sandy soils at the tree site profiles from 0 - 5m depth.

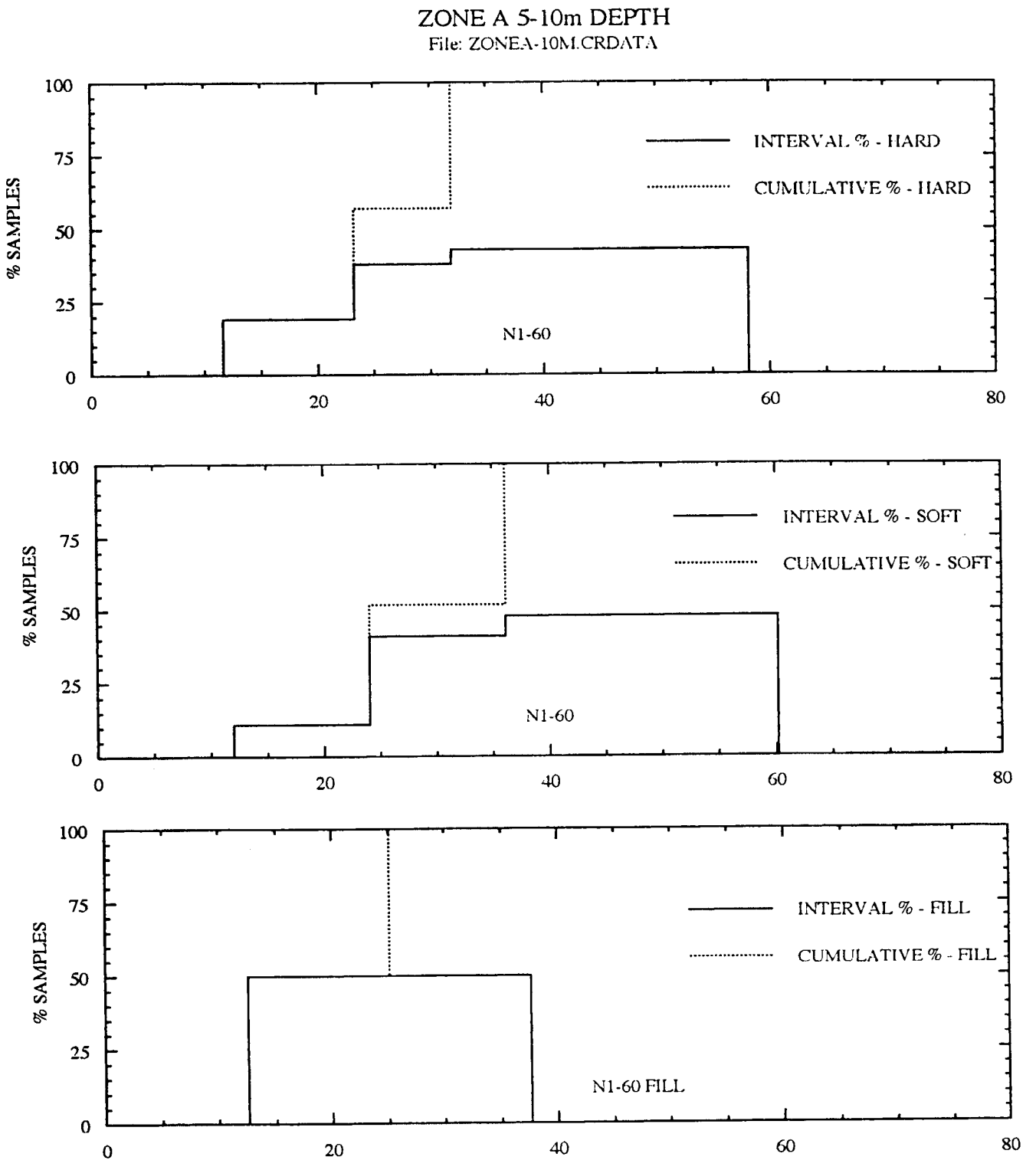

Figure 5.6b. Distribution of $N_{1\text{-}60}$ blow count data for sandy soils at the three site profiles from 5 - 10m depth.

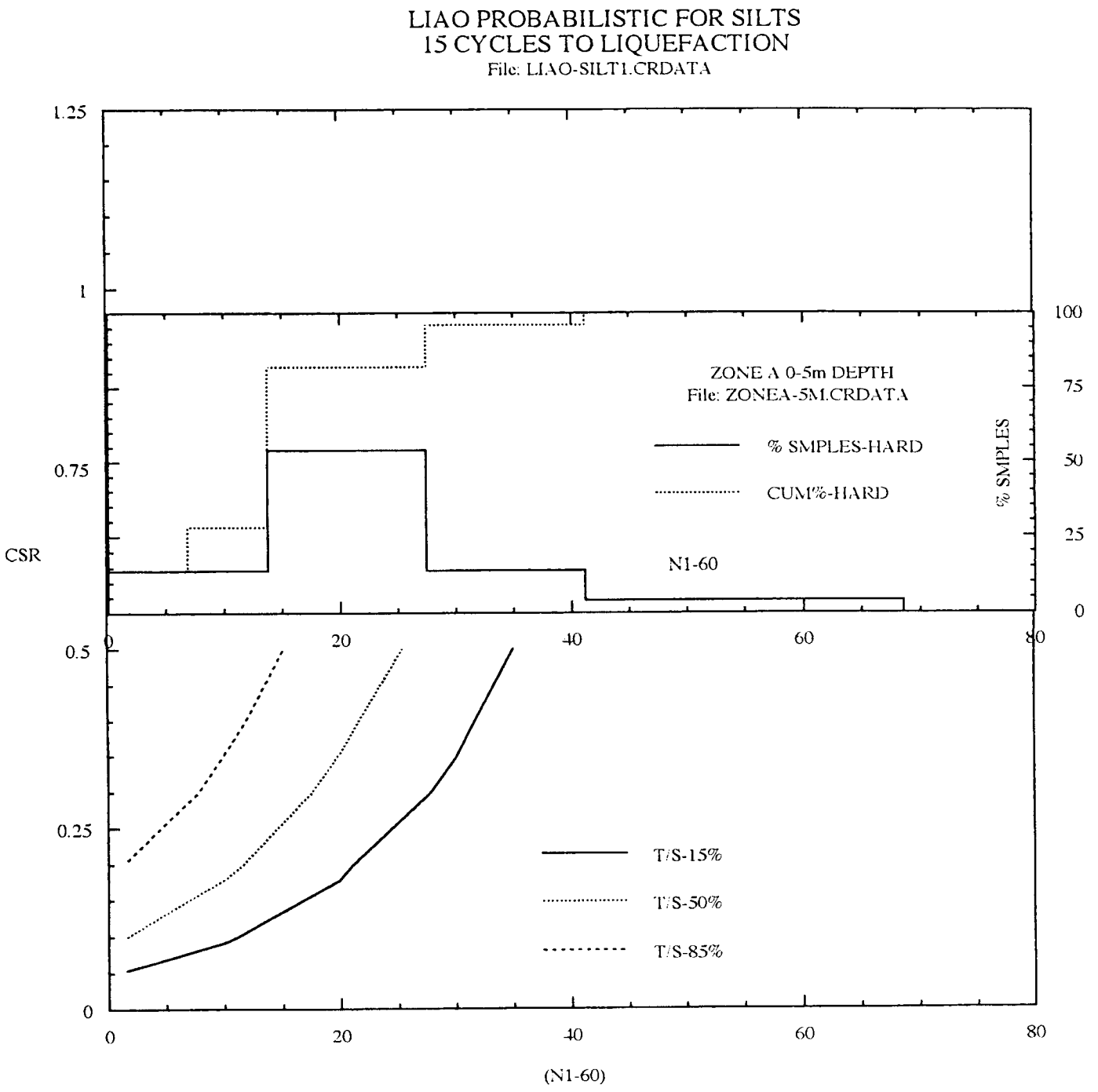

Figure 5.7a. Comparison of $N_{1\text{-}60}$ sample data at hard site with strength criteria associated with 4 cycles to liquefaction (0 - 5m depth).

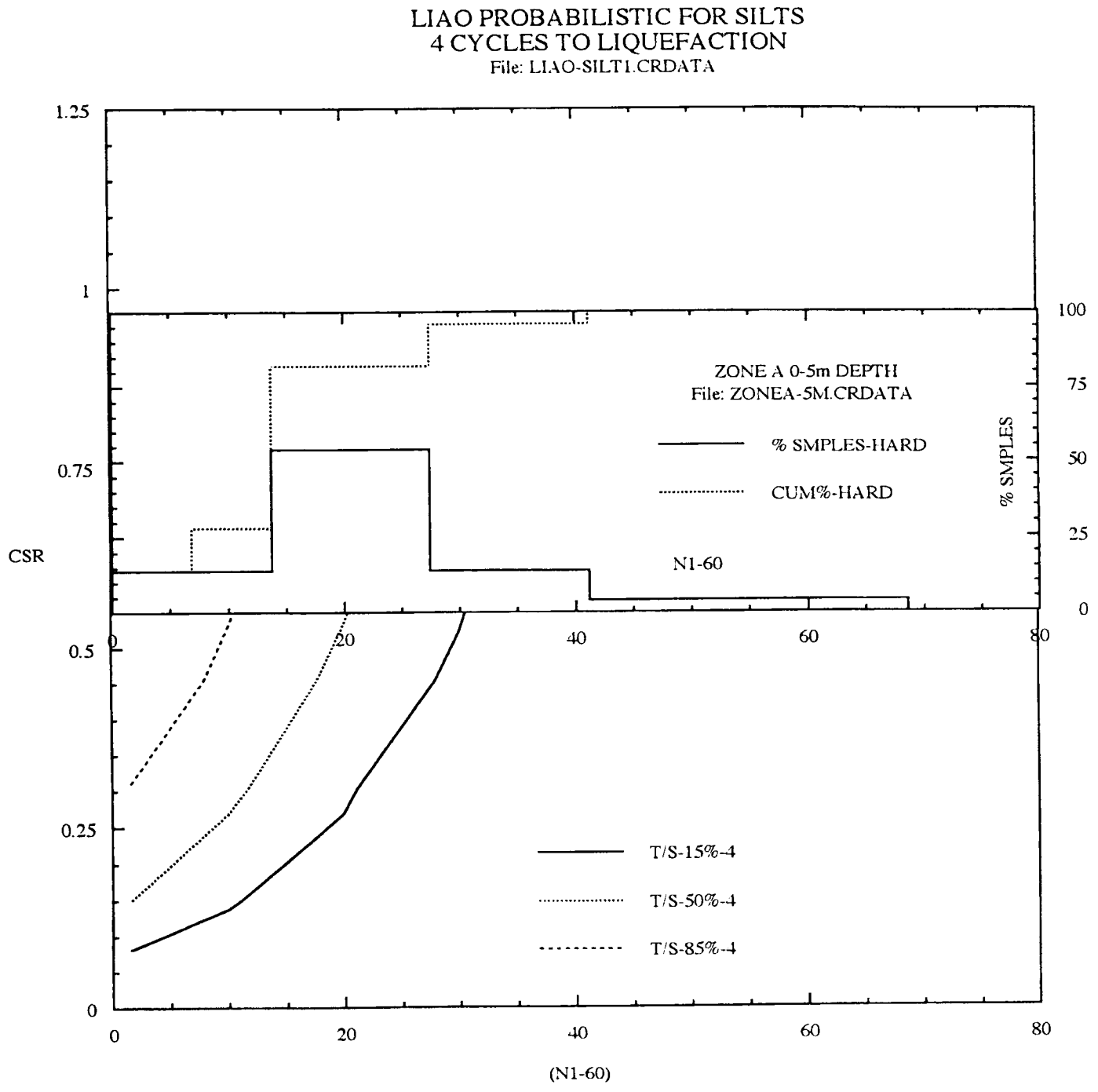

Figure 5.7b. Comparison of $N_{1\text{-}60}$ sample data at hard sites with strength criteria associated with 4 cycles to liquefaction (0 - 5m depth).

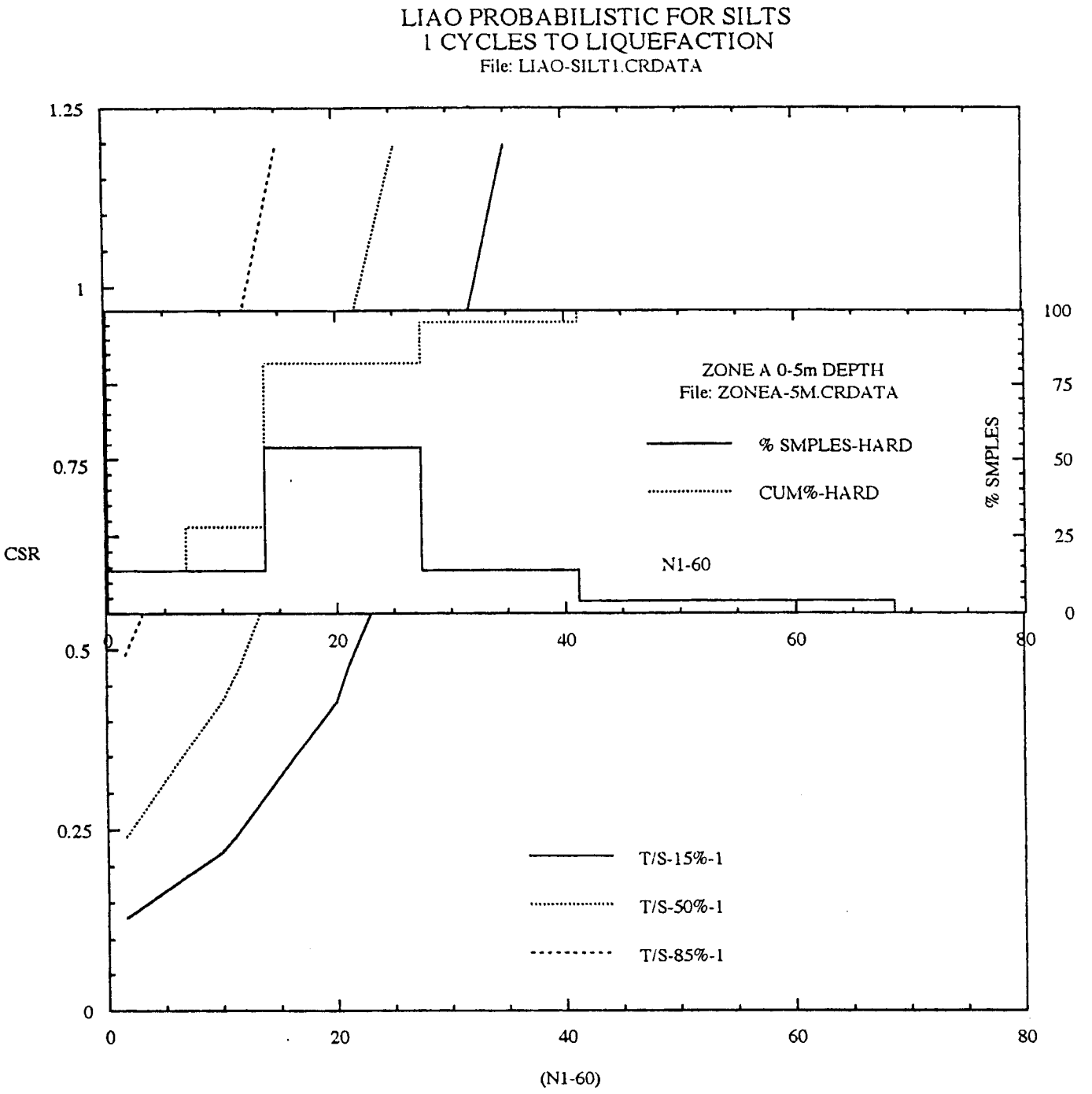

Figure 5.7c. Comparison of $N_{1\text{-}60}$ sample data at hard sites with strength characteristics associated with 1 cycle to liquefaction (0 - 5m depth).

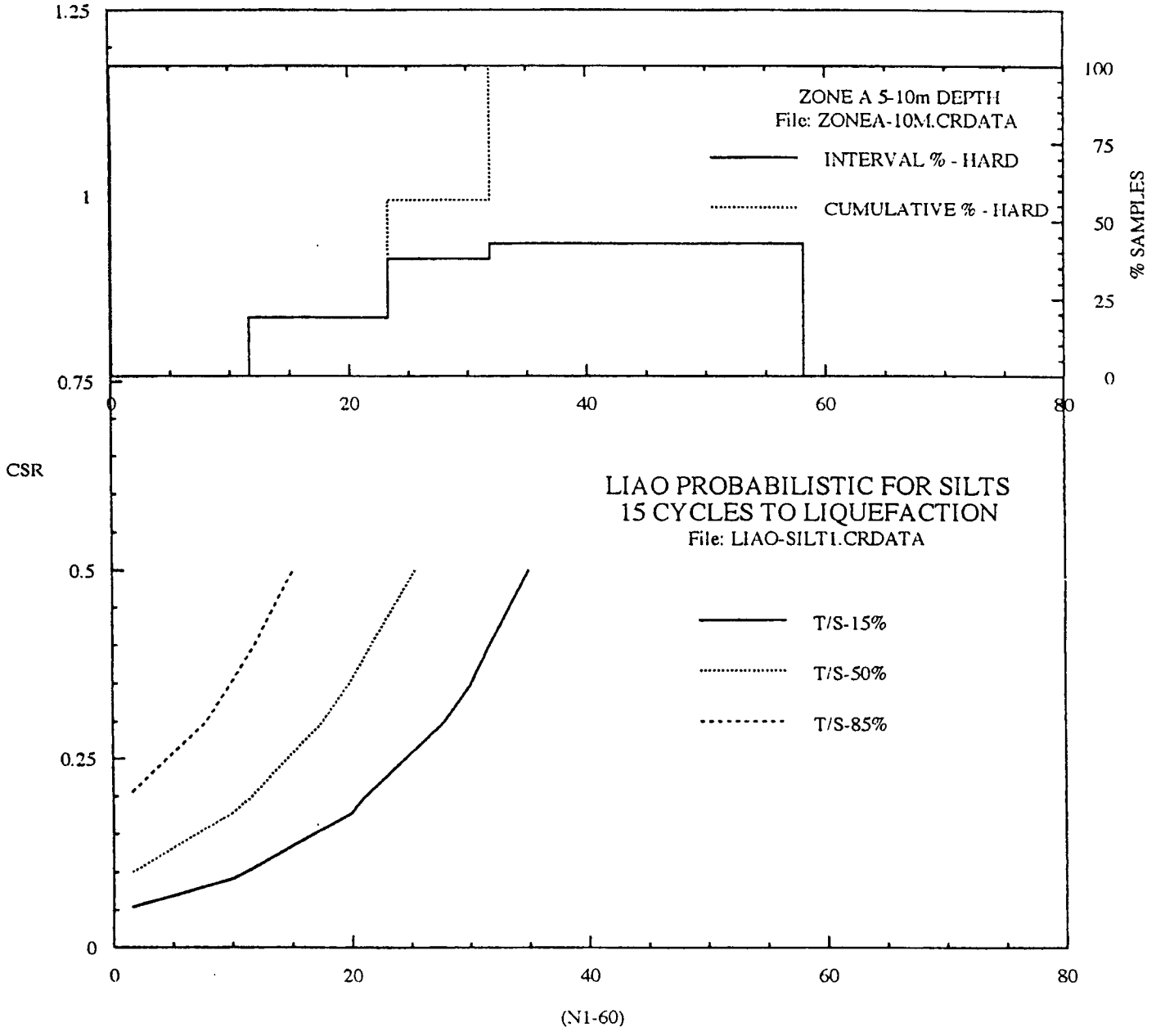

Figure 5.7d. Comparison of $N_{1\text{-}60}$ sample data at hard sites with strength characteristics associated with 15 cycles to liquefaction (5 - 10m depth).

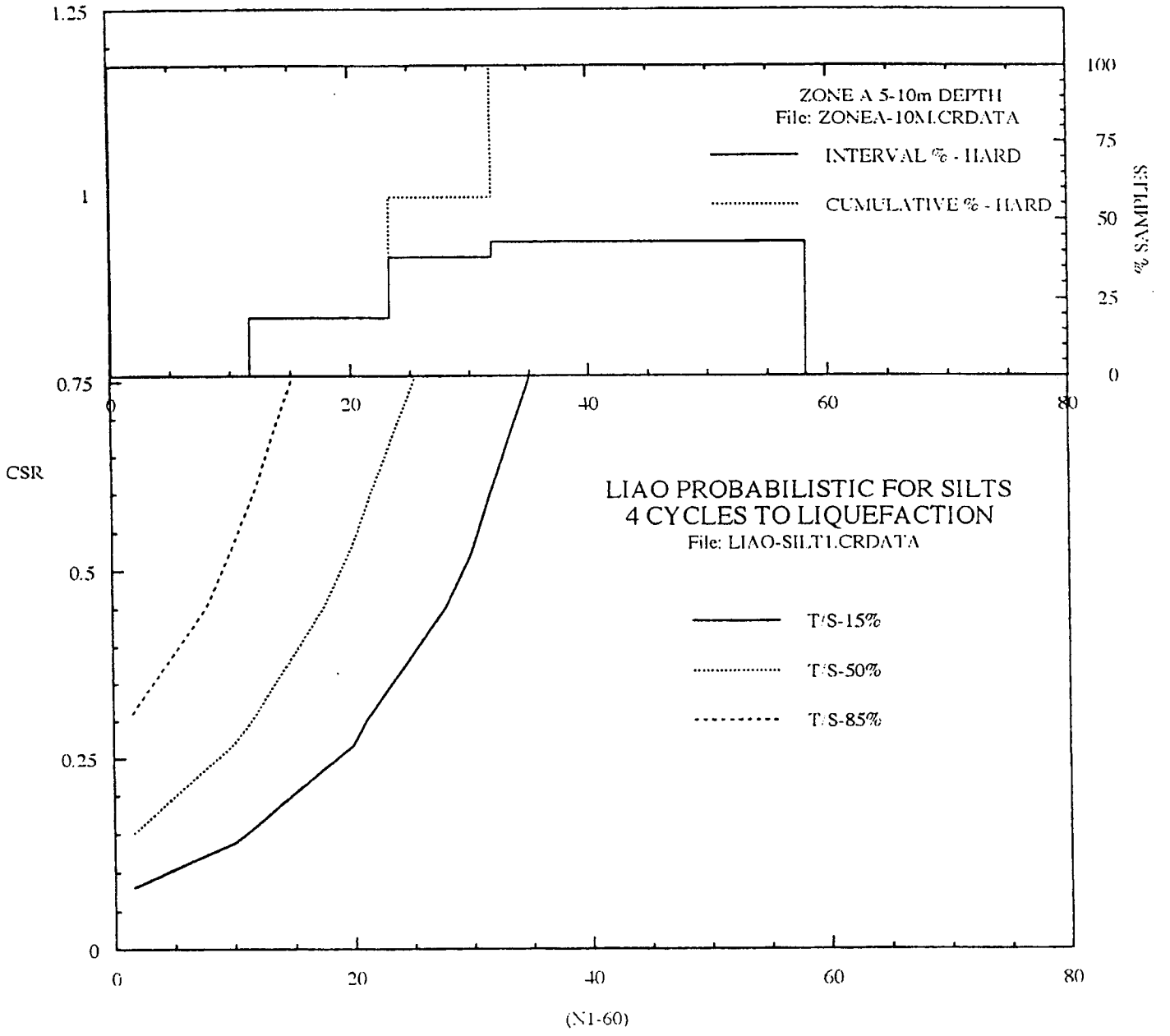

Figure 5.7e. Comparison of $N_{1\text{-}60}$ sample data at hard sites with strength characteristics associated with 4 cycles to liquefaction (5 - 10m depth).

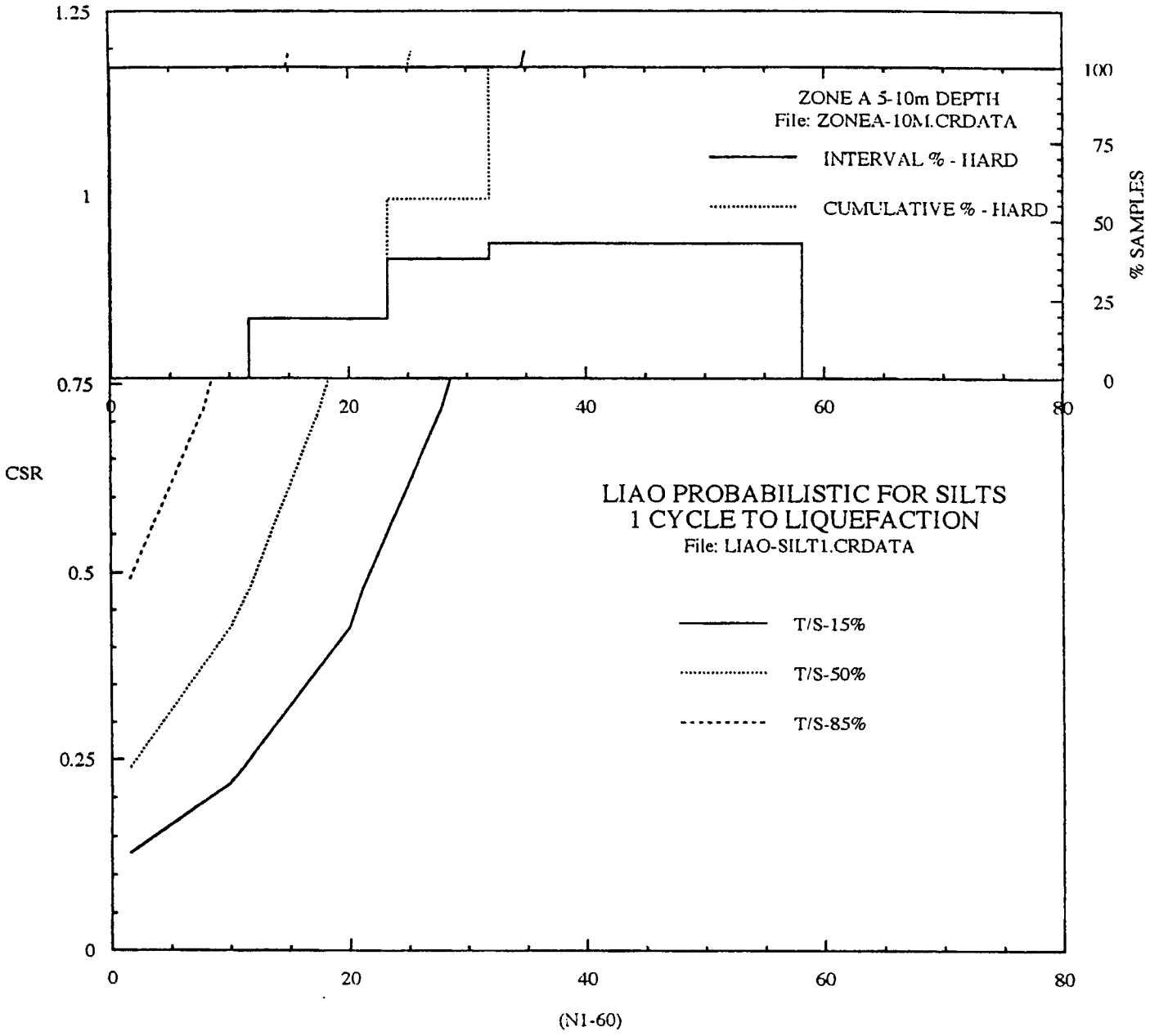

Figure 5.7f. Comparison of N_{1-60} sample data at hard sites with strength characteristics associated with 1 cycle to liquefaction (5 - 10m depth).

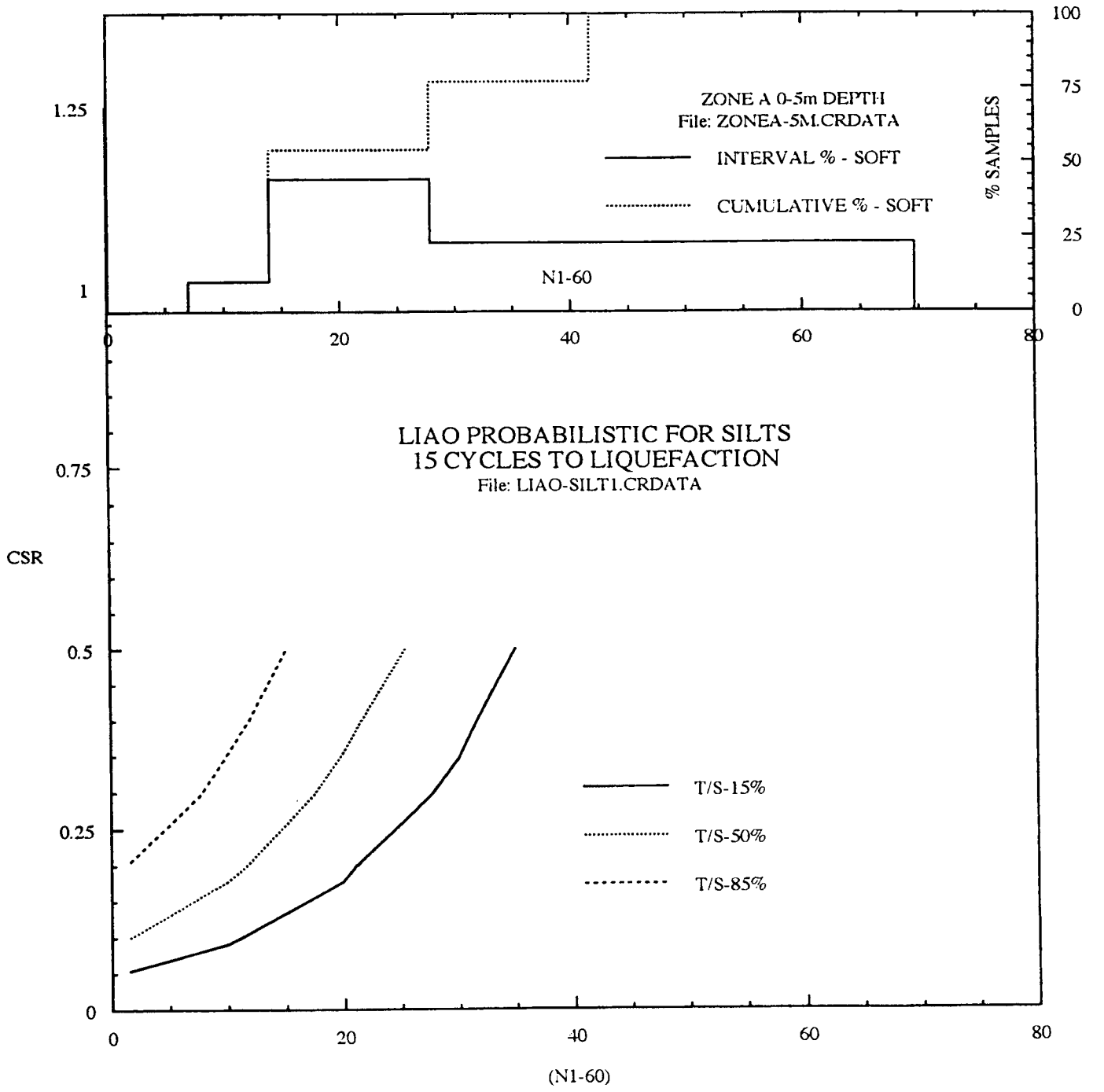

Figure 5.8a. Comparison of $N_{1\text{-}60}$ sample data at soft sites with strength characteristics associated with 15 cycles to liquefaction (0 - 5m depth).

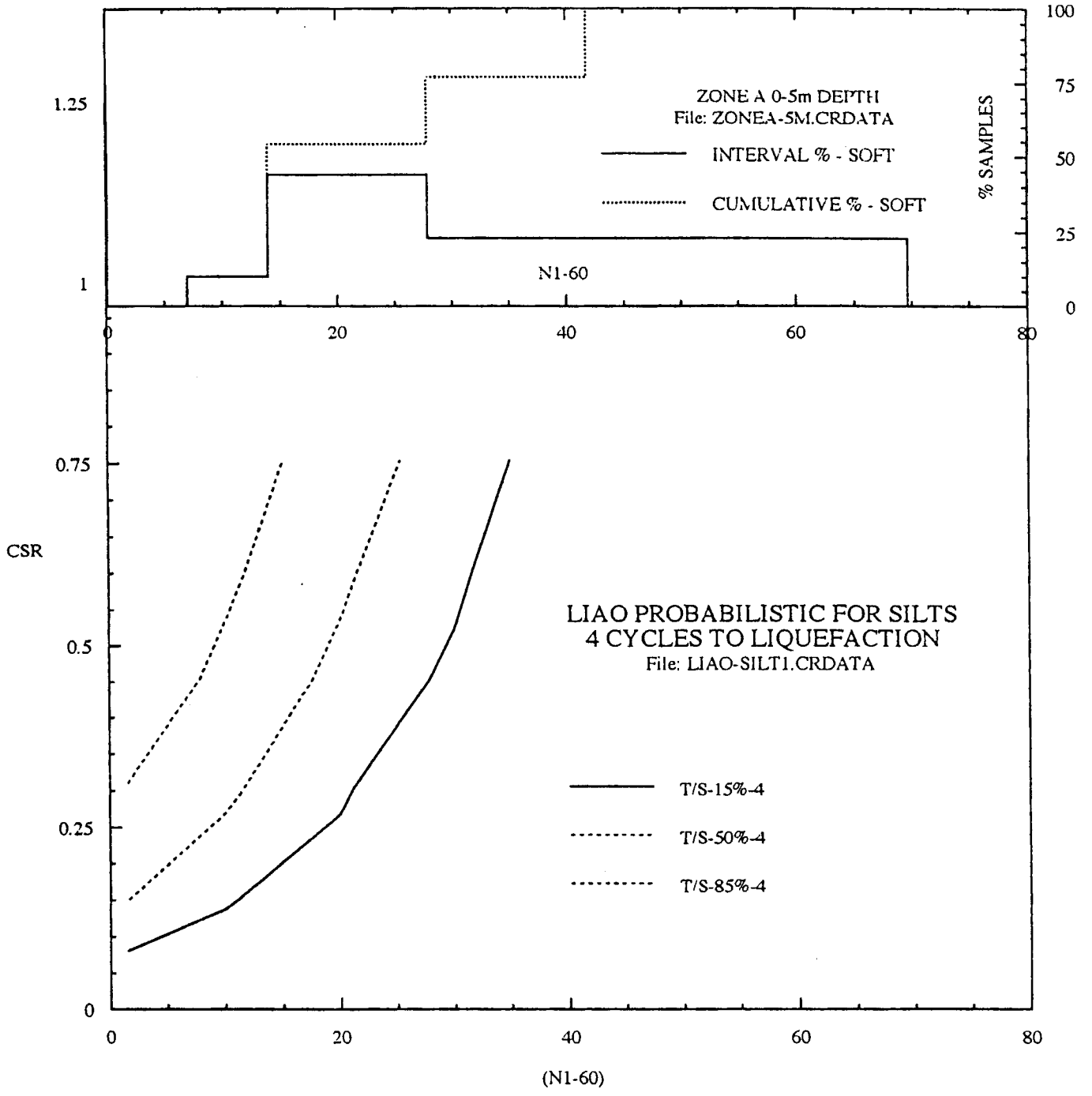

Figure 5.8b. Comparison of $N_{1\text{-}60}$ sample data at soft sites with strength characteristics associated with 4 cycles to liquefaction (0 - 5m depth).

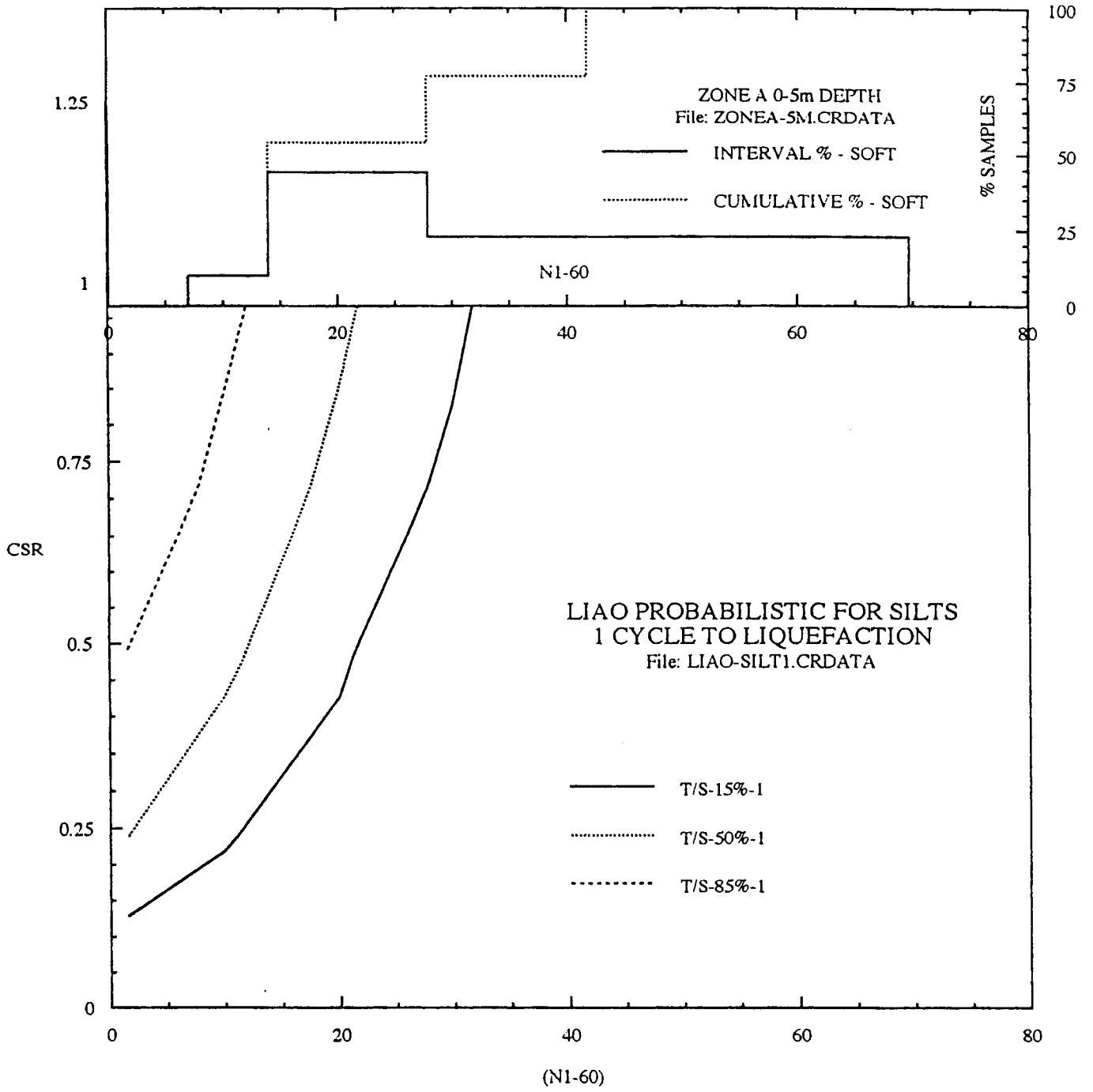

Figure 5.8c. Comparison of $N_{1\text{-}60}$ sample data at soft sites with strength characteristics associated with 1 cycle to liquefaction (0 - 5m depth).

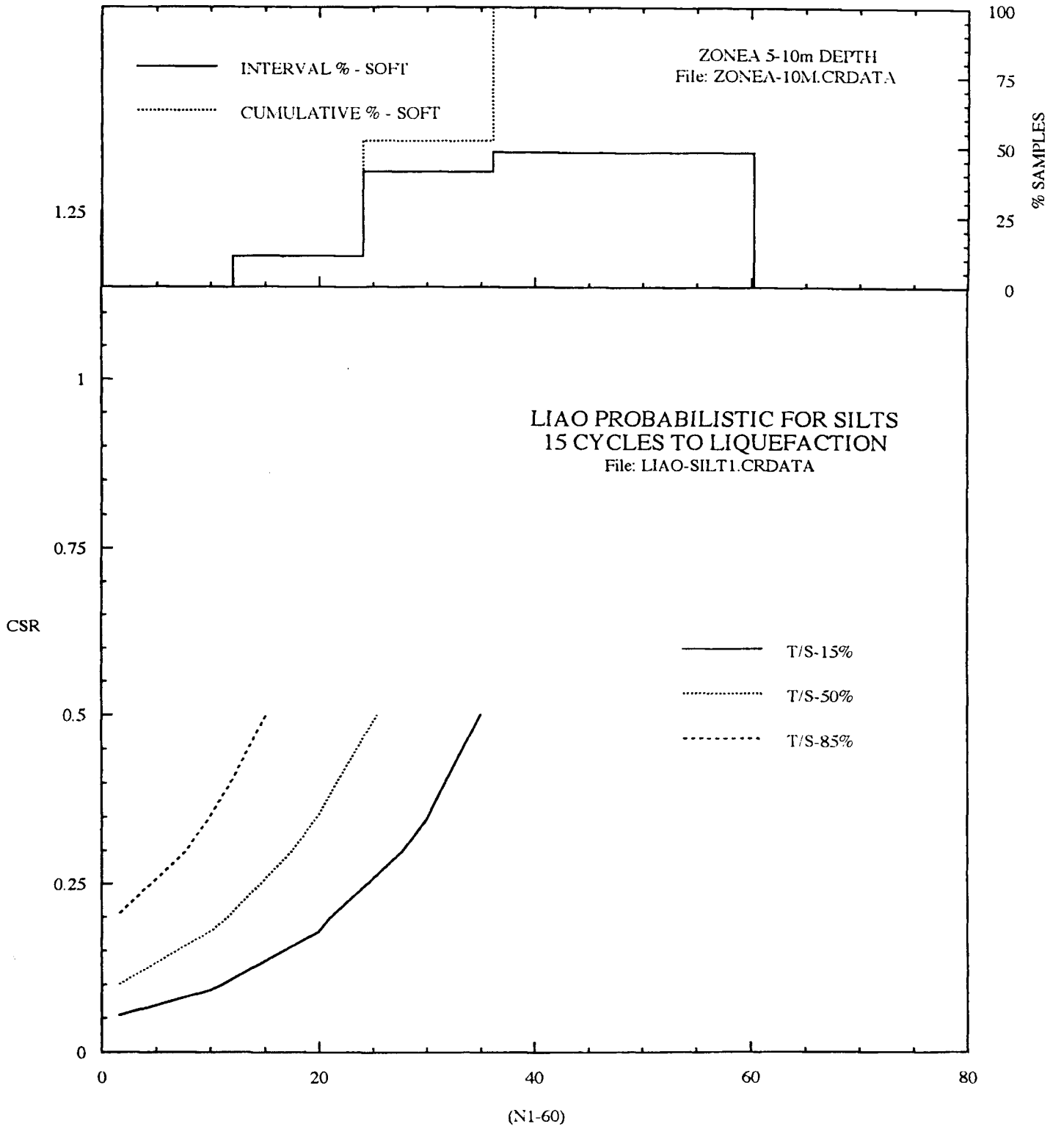

Figure 5.8d. Comparison of $N_{1\text{-}60}$ sample data at soft sites with strength characteristics associated with 15 cycles to liquefaction (5 - 10m depth).

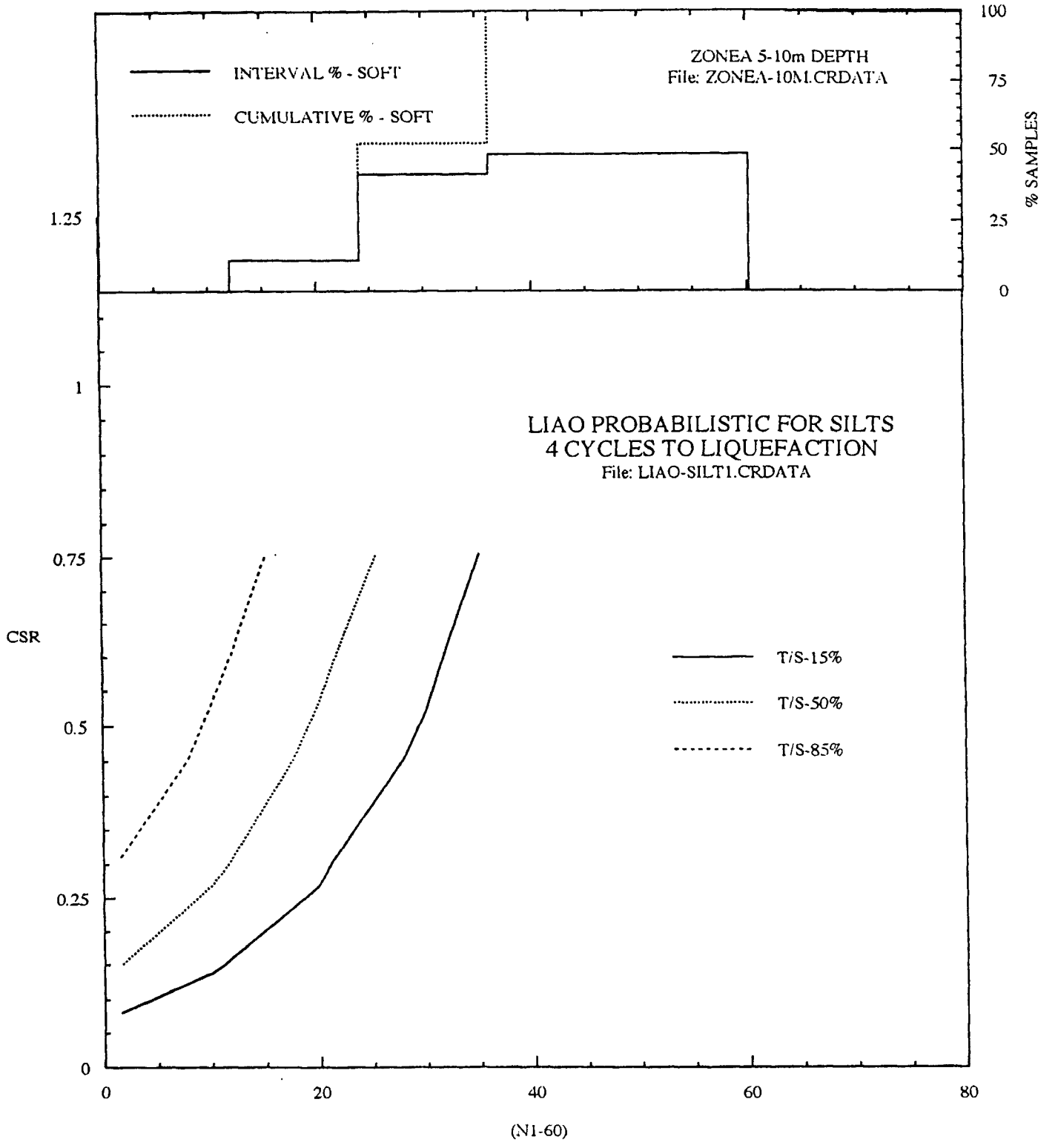

Figure 5.8e. Comparison of $N_{1\text{-}60}$ sample data at soft sites with strength characteristics associated with 4 cycles to liquefaction (5 - 10m depth).

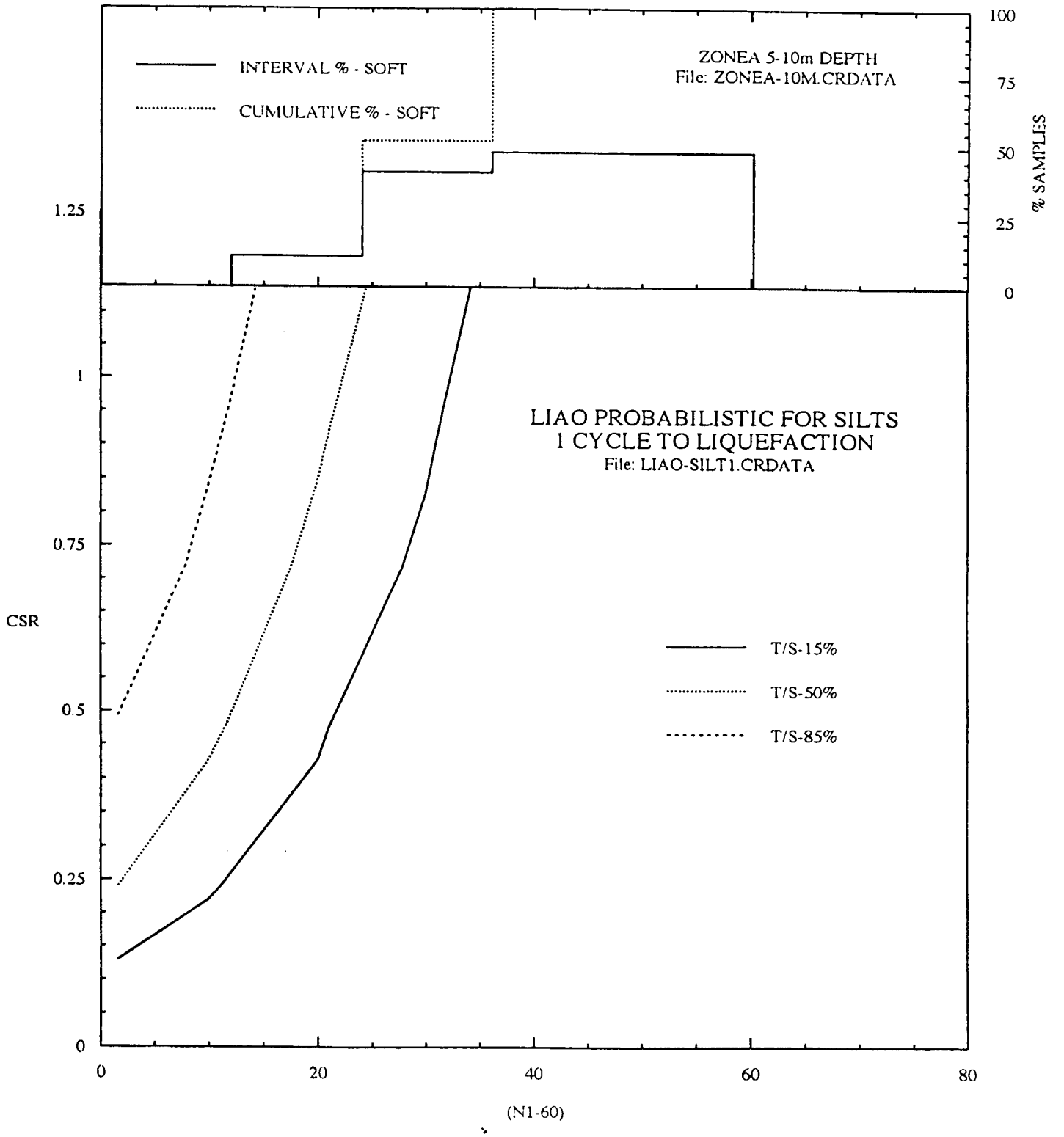

Figure 5.8f. Comparison of $N_{1\text{-}60}$ sample data at soft sites with characteristics associated with 1 cycle to liquefaction (5 - 10m depth).

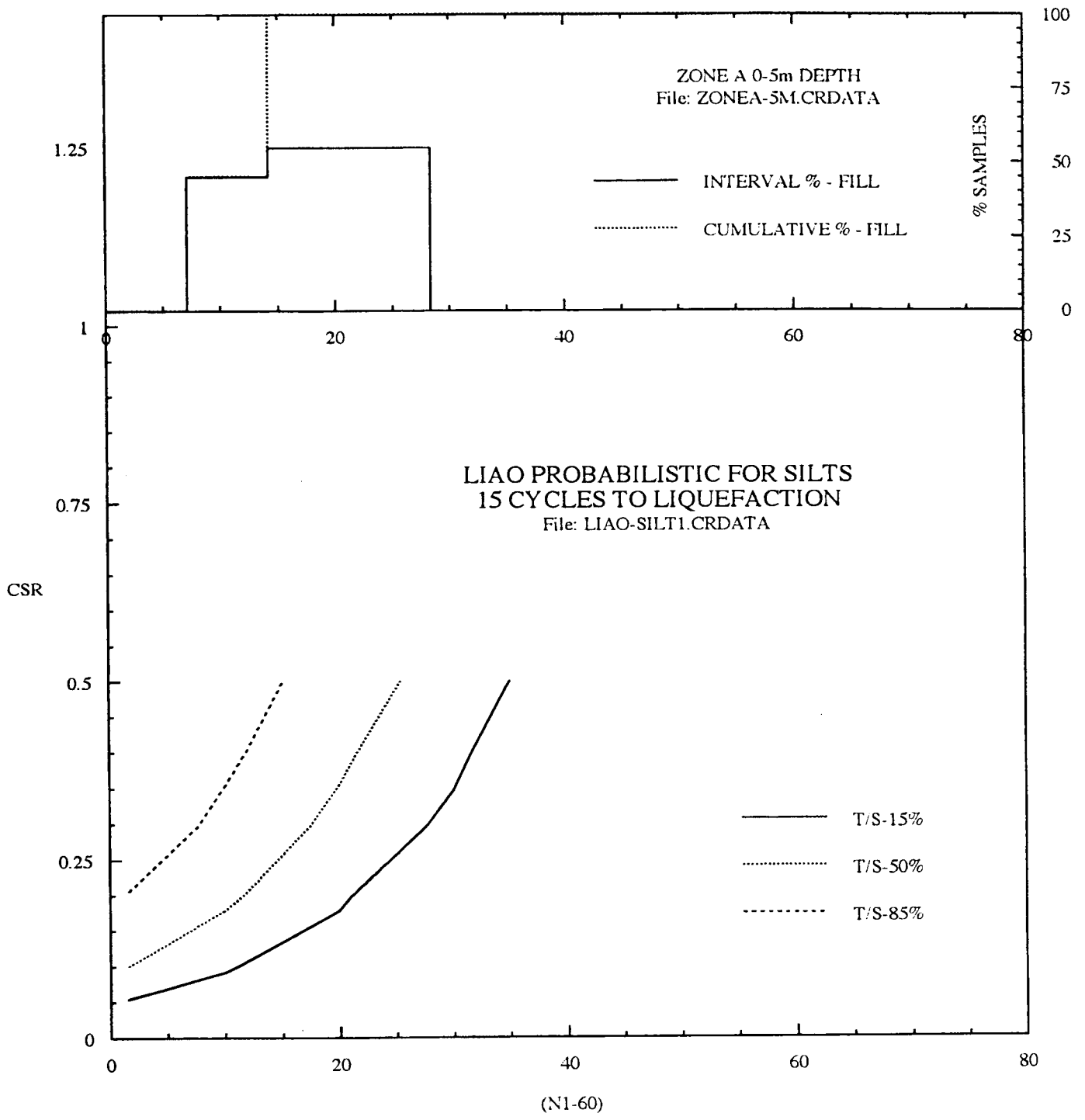

Figure 5.9a. Comparison of $N_{1\text{-}60}$ sample data at fill sites with strength characteristics associated with 15 cycles to liquefaction (0 - 5m depth).

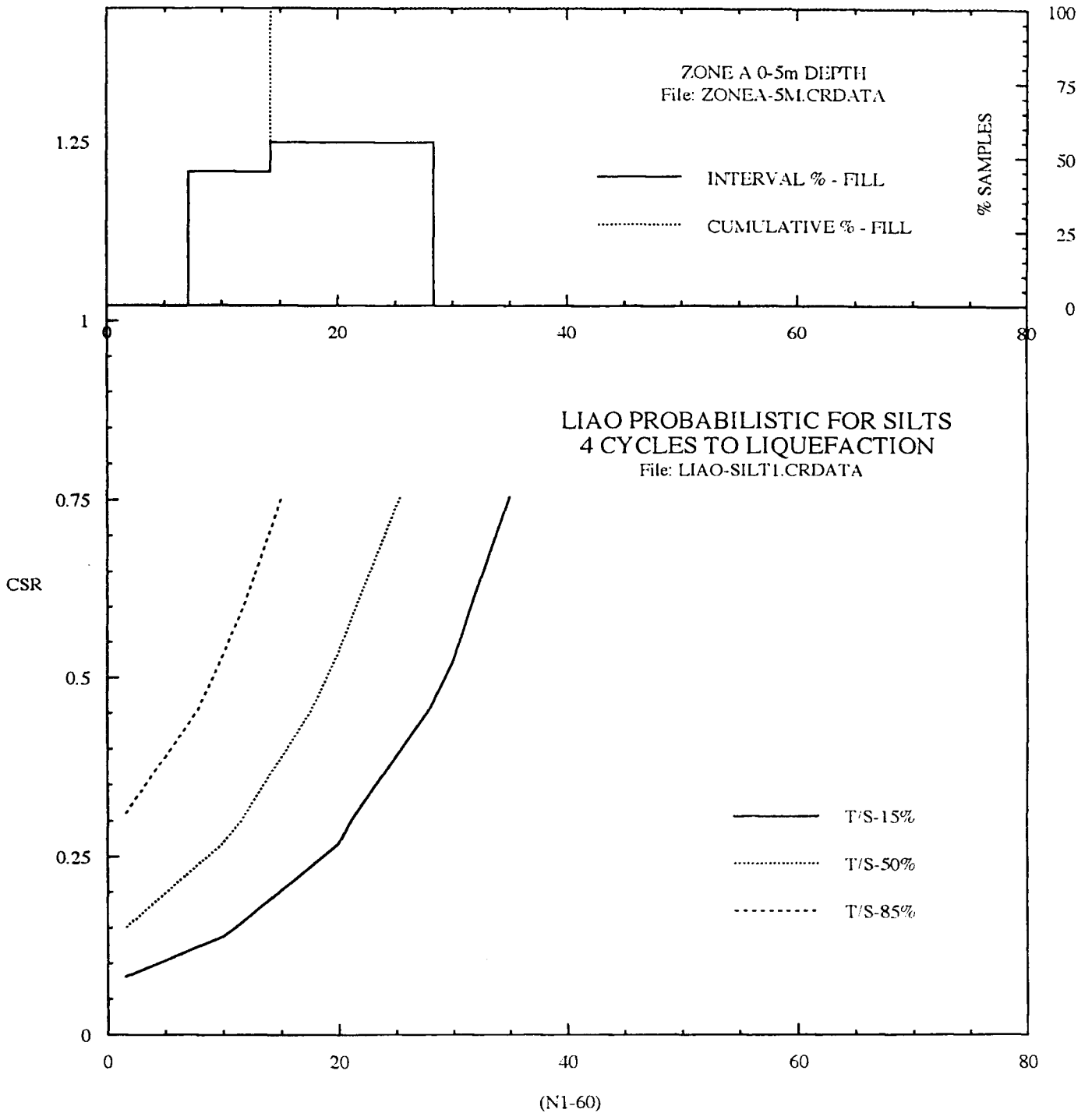

Figure 5.9b. Comparison of $N_{1\text{-}60}$ sample data of fill sites with strength characteristics associated with 4 cycles to liquefaction (0 - 5m depth).

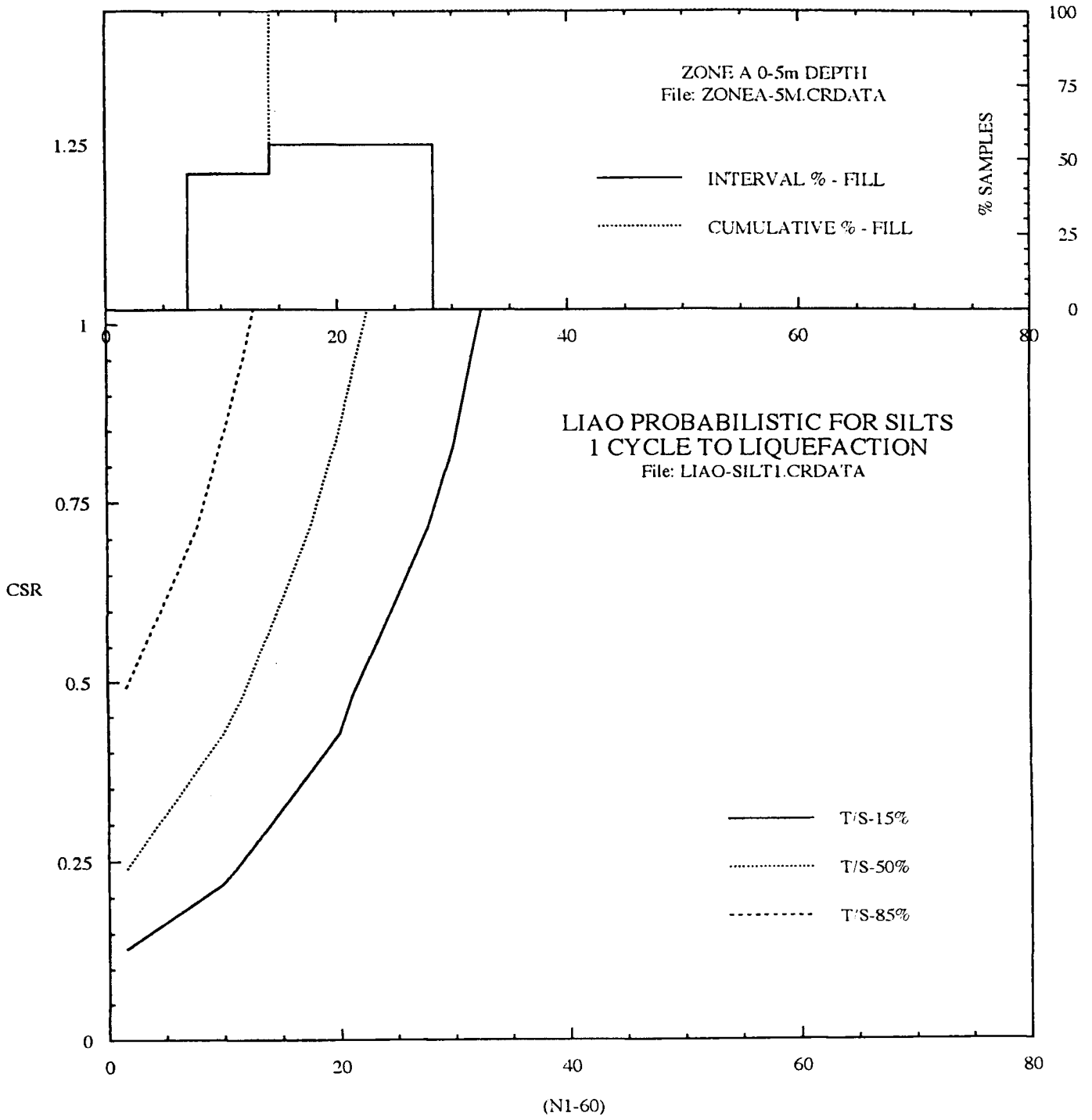

Figure 5.9c. Comparison of $N_{1\text{-}60}$ sample data at fill sites with strength characteristics associated with 1 cycle to liquefaction (0 - 5m depth).

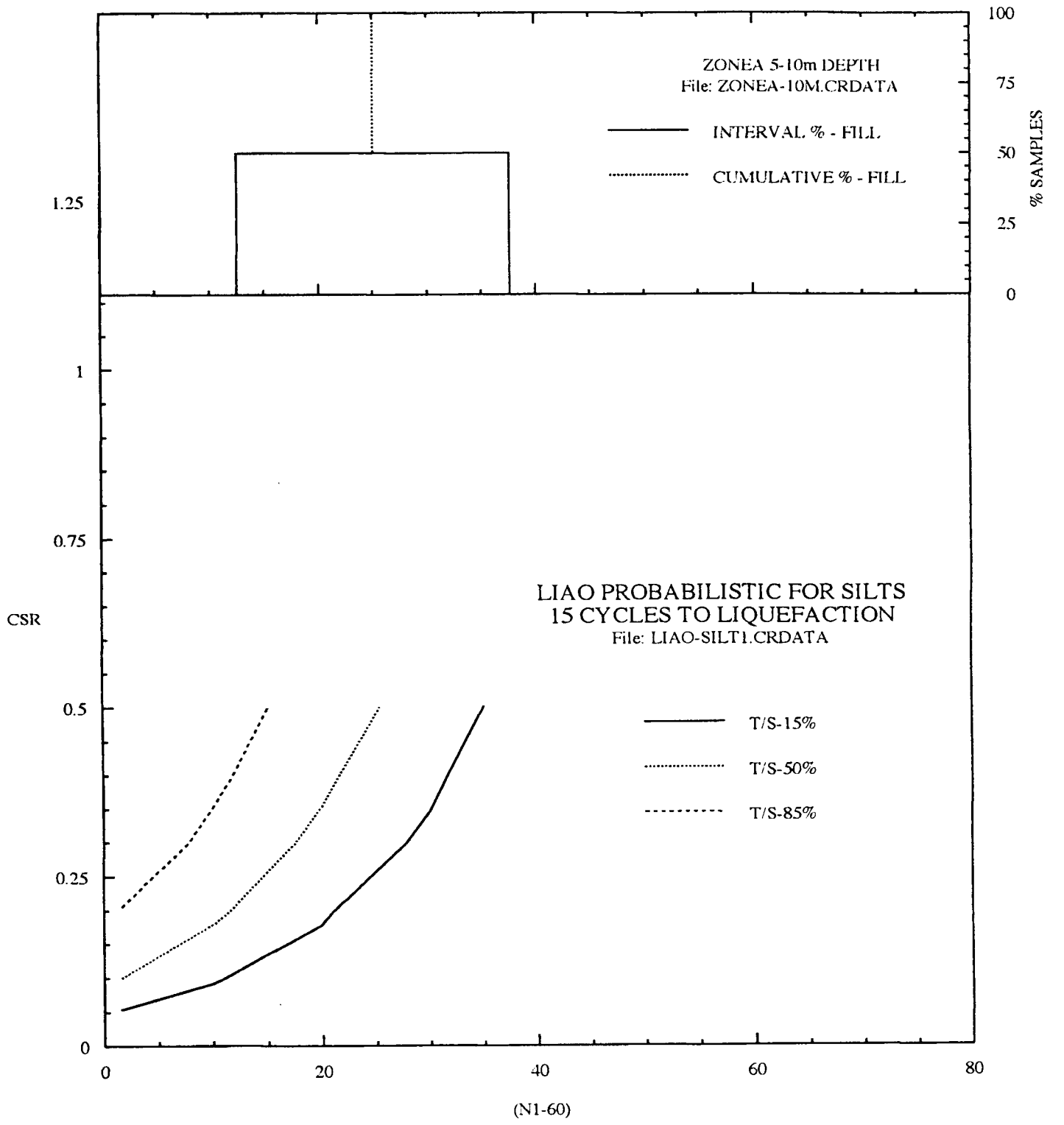

Figure 5.9d. Comparison of $N_{1\text{-}60}$ sample data at fill sites with strength characteristics associated with 15 cycles to liquefaction (5 - 10m depth).

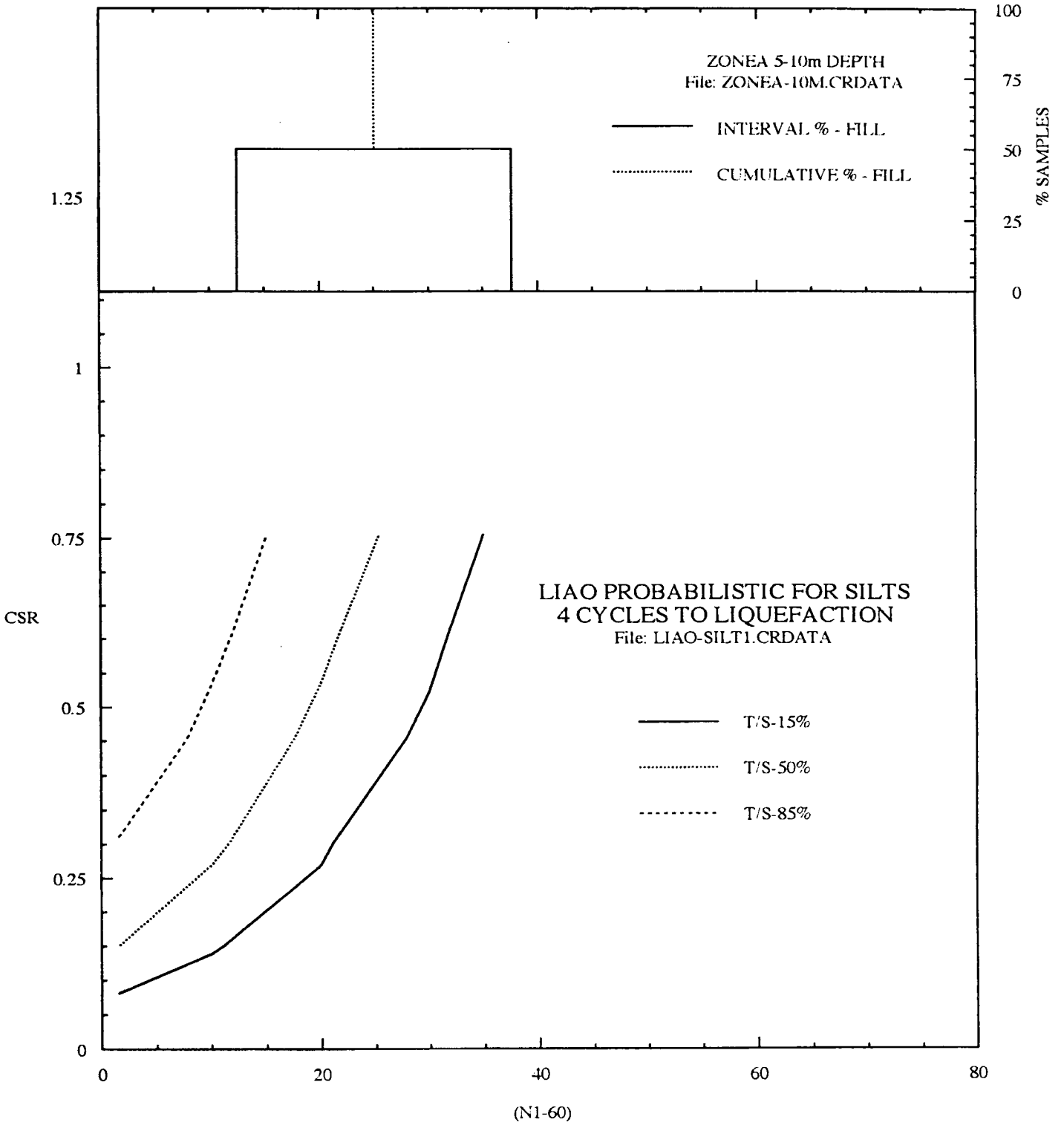

Figure 5.9e. Comparison of $N_{1\text{-}60}$ sample data at fill sites with strength characteristics associated with 4 cycles to liquefaction (5 - 10m depth).

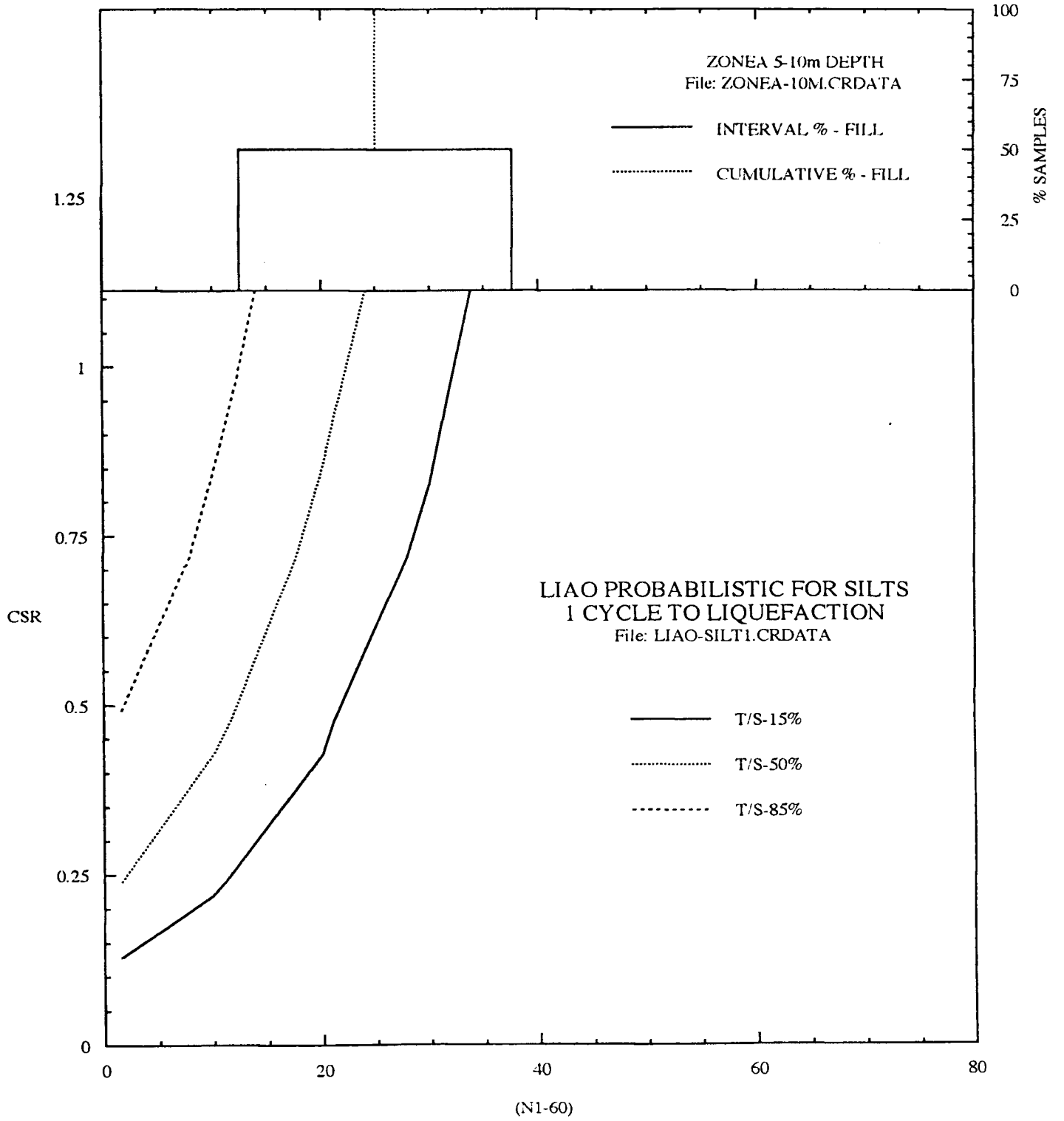

Figure 5.9f. Comparison of $N_{1\text{-}60}$ sample data at fill sites with strength characteristics associated with 1 cycle to liquefaction (5 - 10m depth).

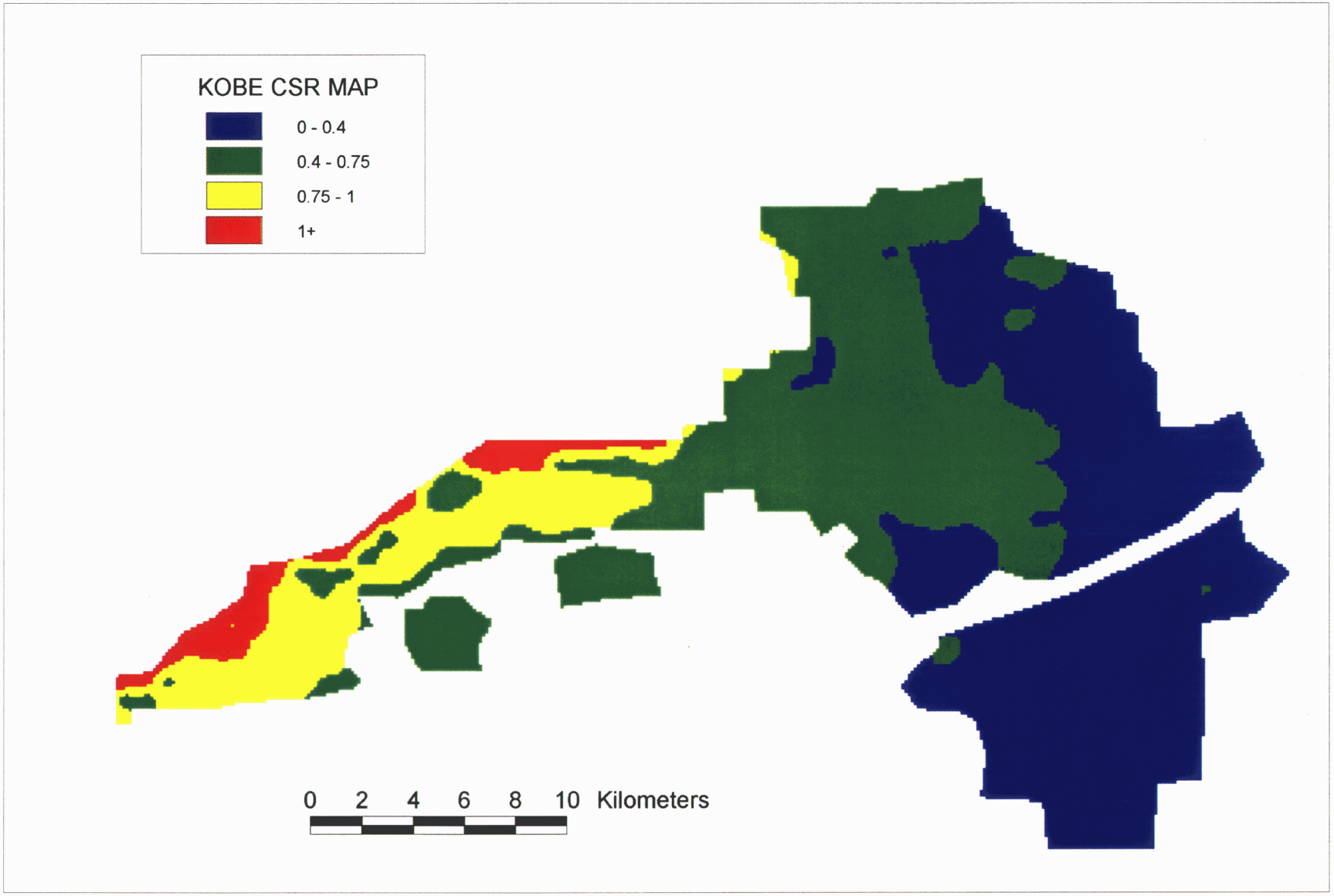

Figure 5.10. Median estimates of cyclic stress ratios for the rock, hard, soft, and fill areas of Kobe, Nishinomiya, and Osaka.

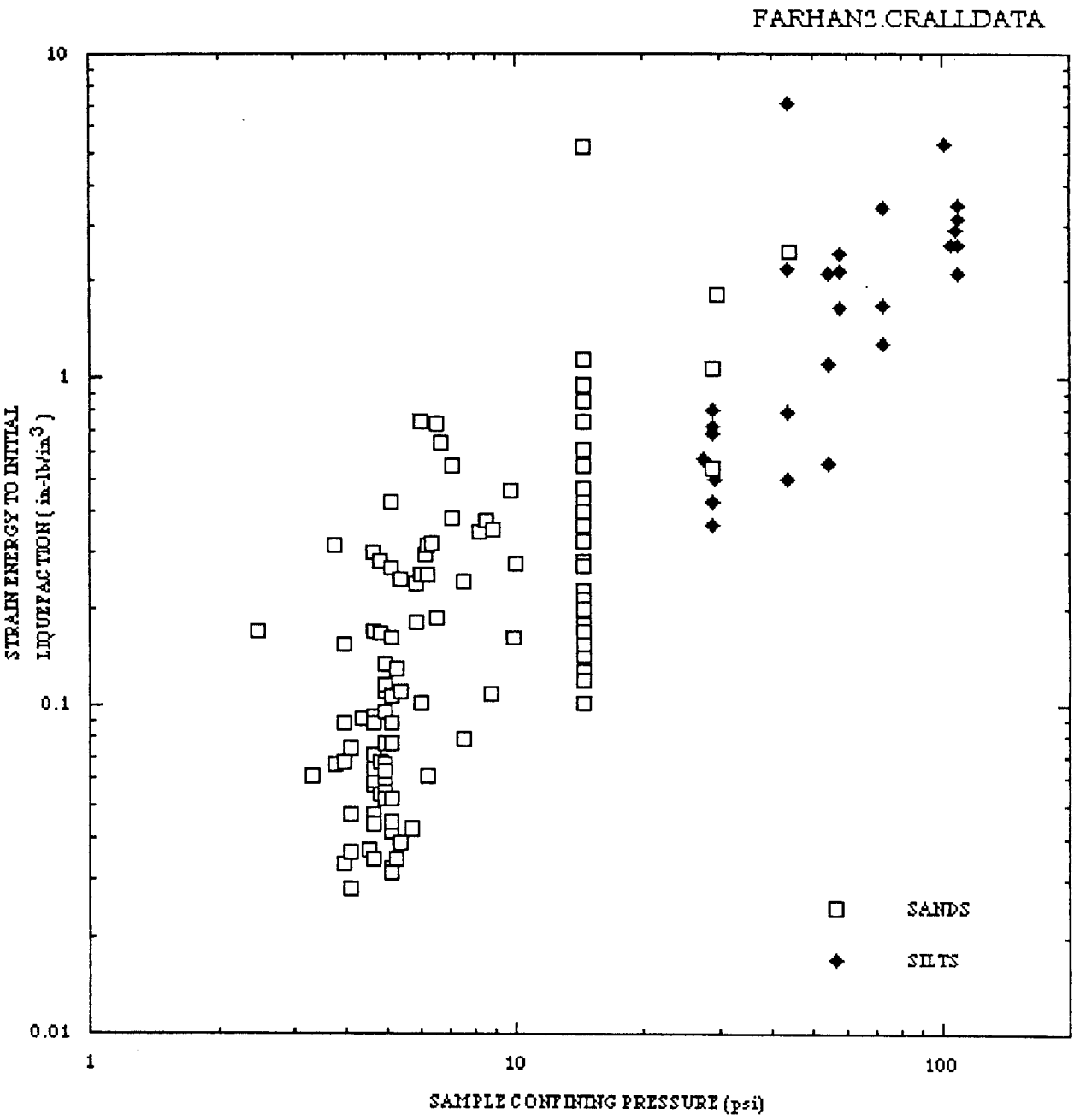

Figure 5.11a. Influence of sample confining pressure on strain energy to liquefaction - all samples.

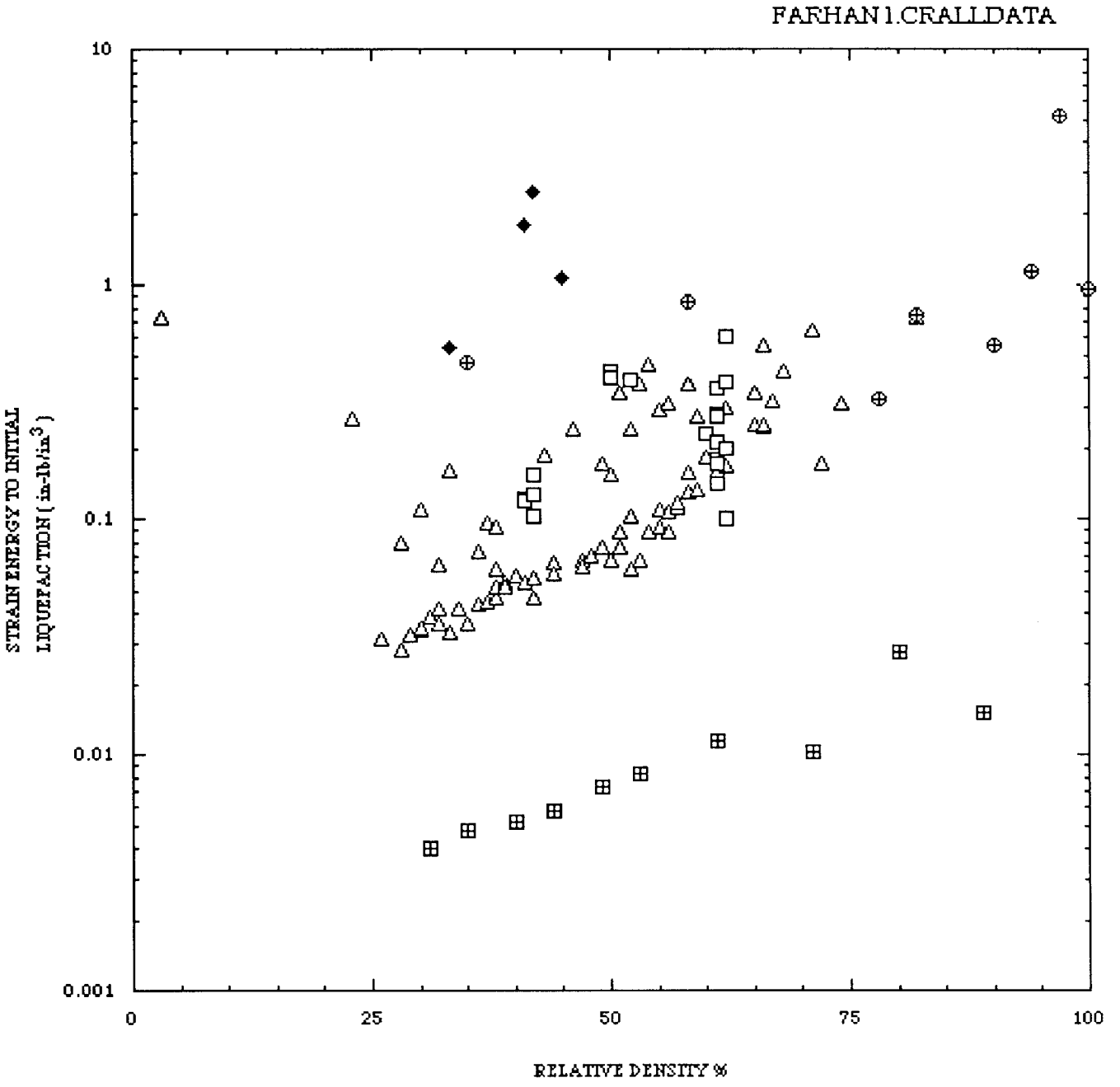

Figure 5.11b. Influence of relative density on strain energy to liquefaction for sand samples.

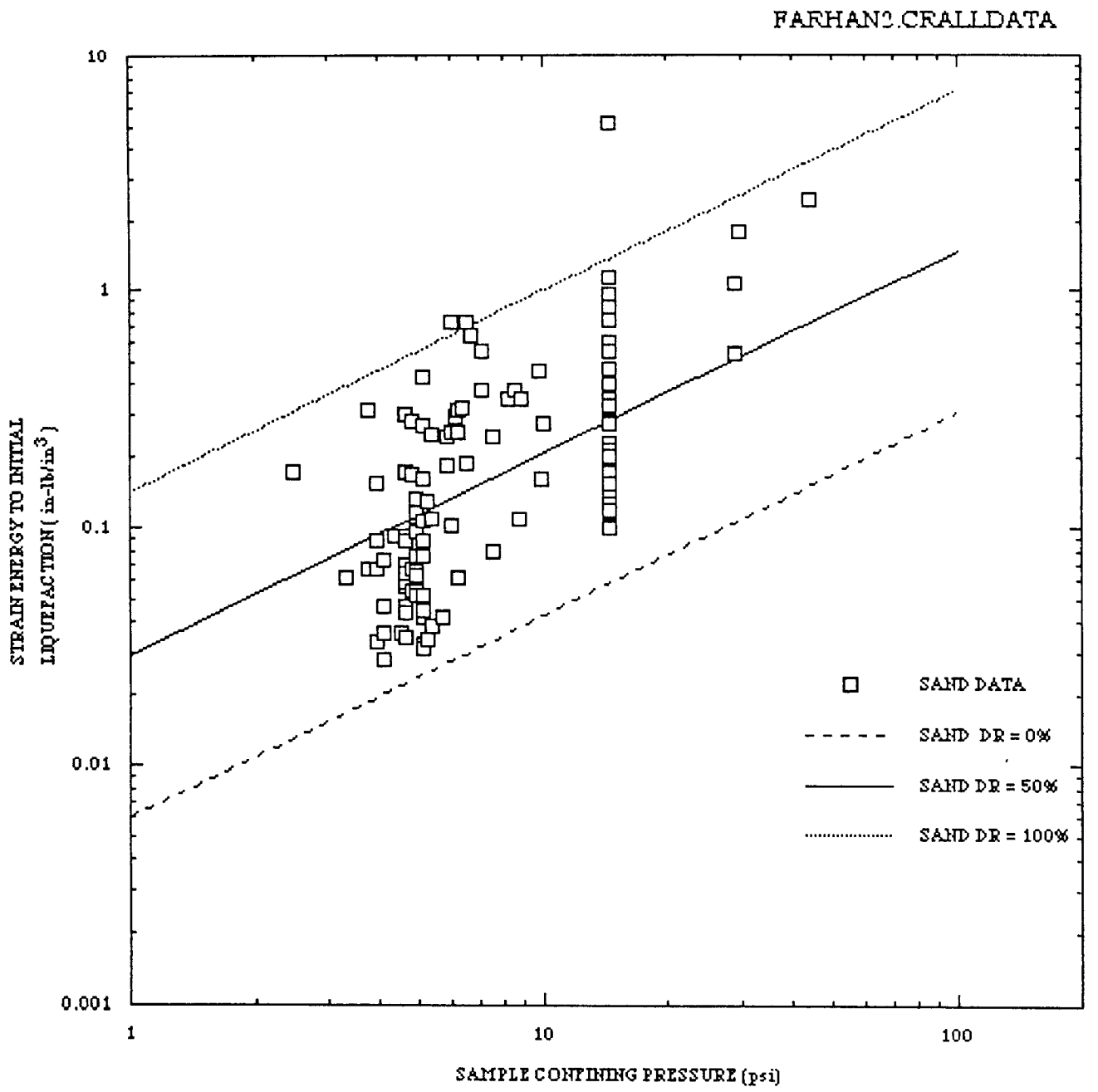

Figure 5.11c. Regression results for sand samples.

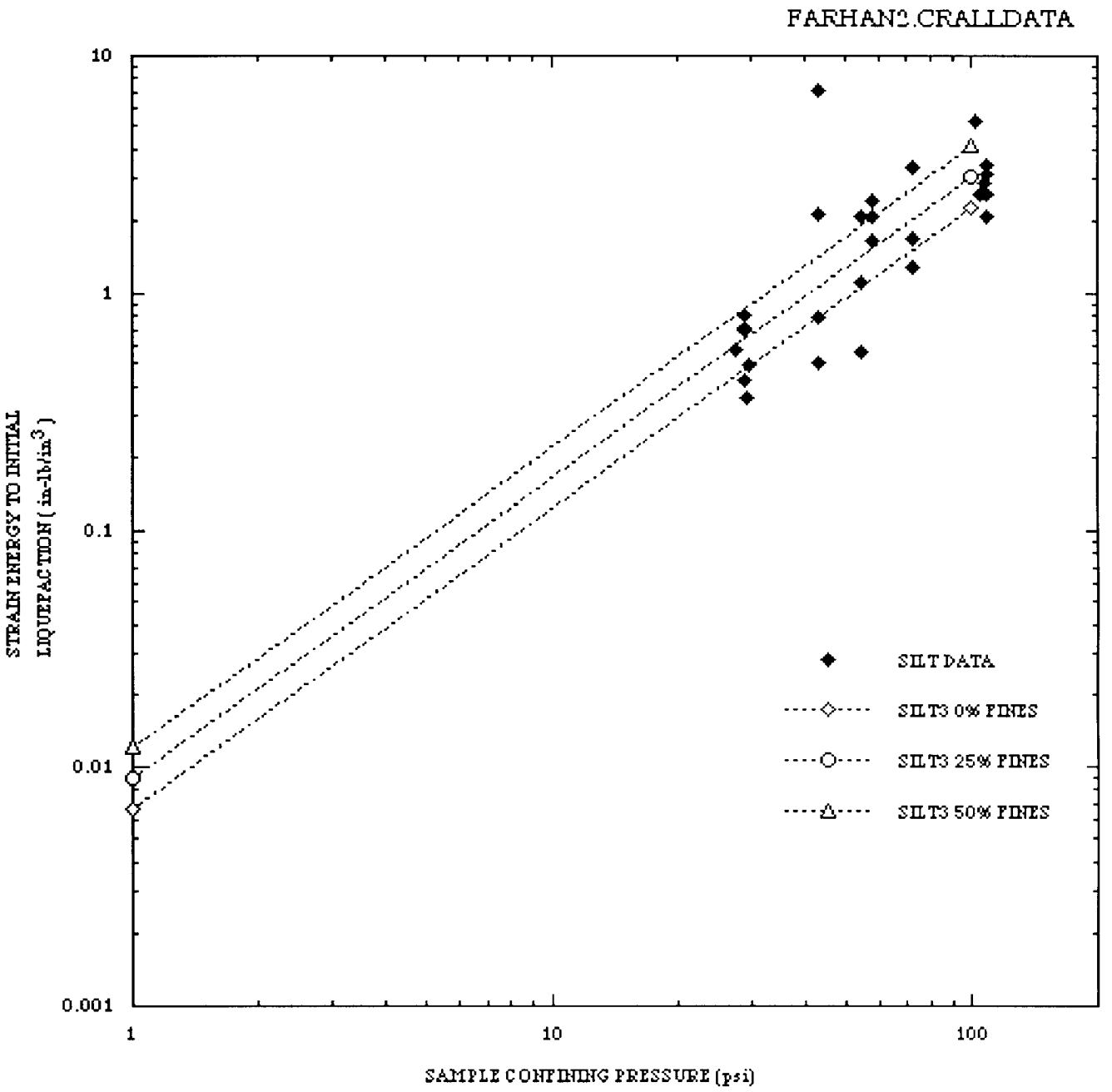

Figure 5.11d. Influence of silt content on strain energy to liquefaction - silt samples.

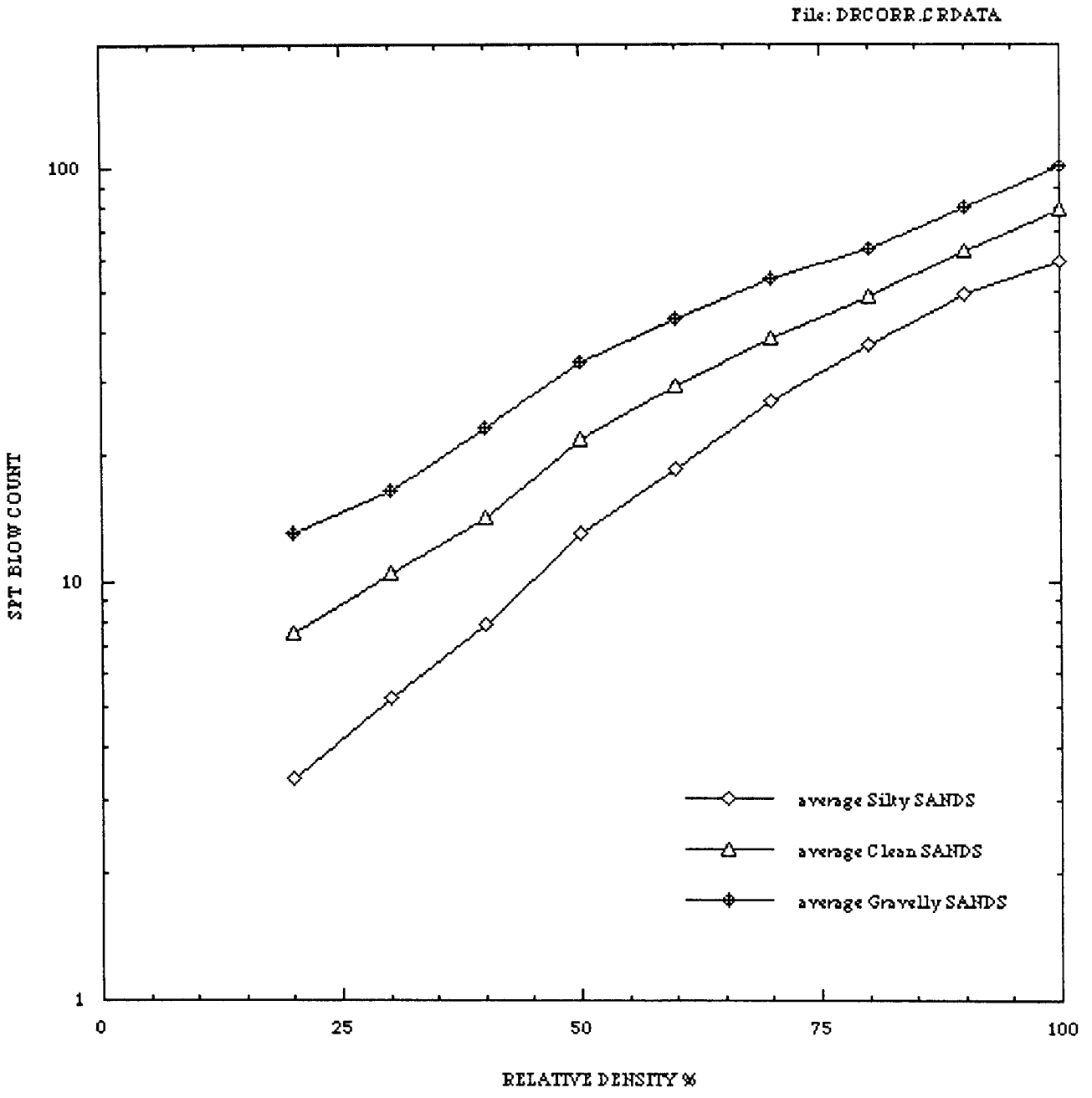

Figure 5.12. Average correlation of SPT blow count with relative density for cohesionless soils.

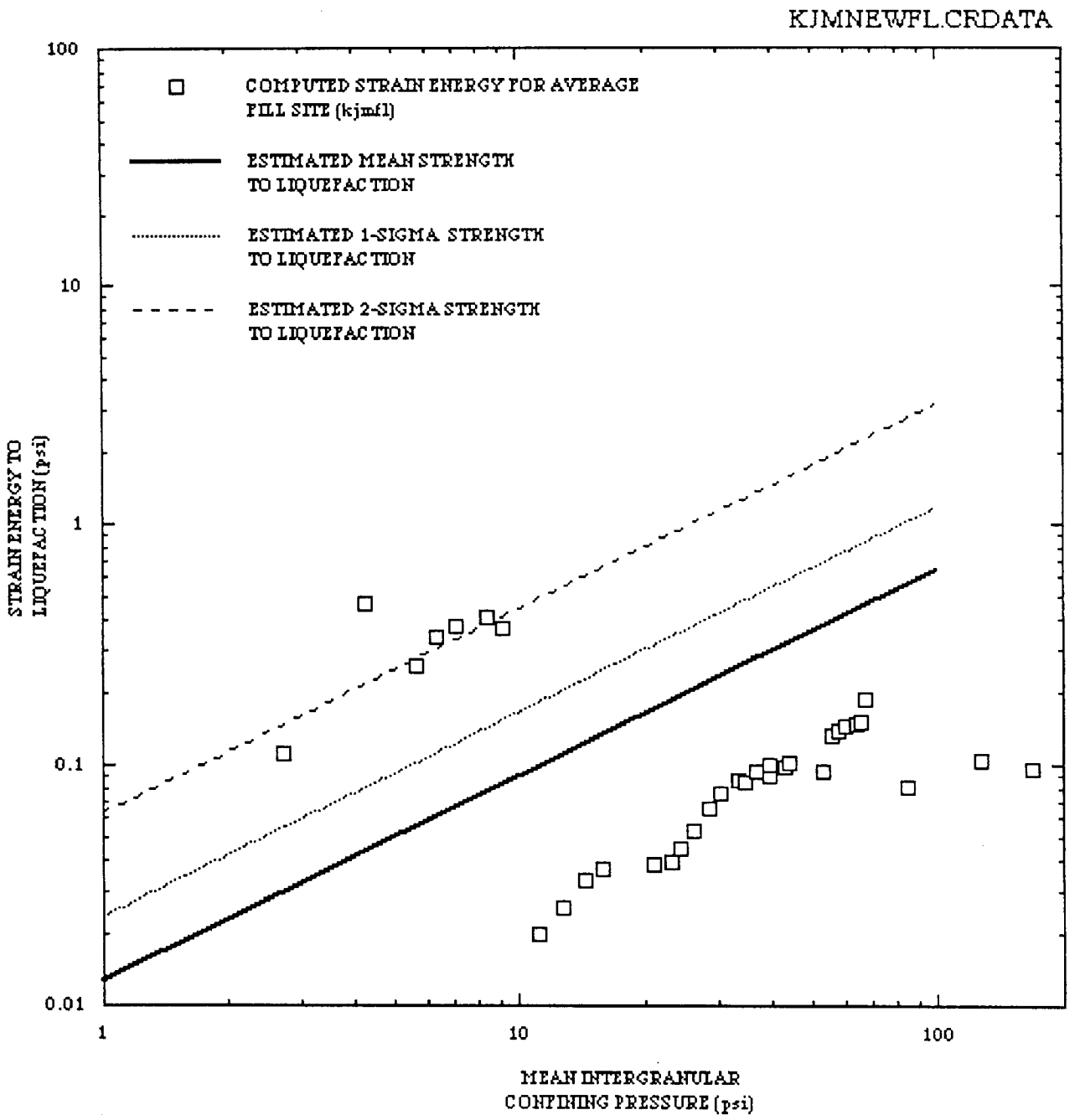

Figure 5.13a. Computed strain energy to onset of liquefaction for average fill site as a function of mean confining pressure (or depth).

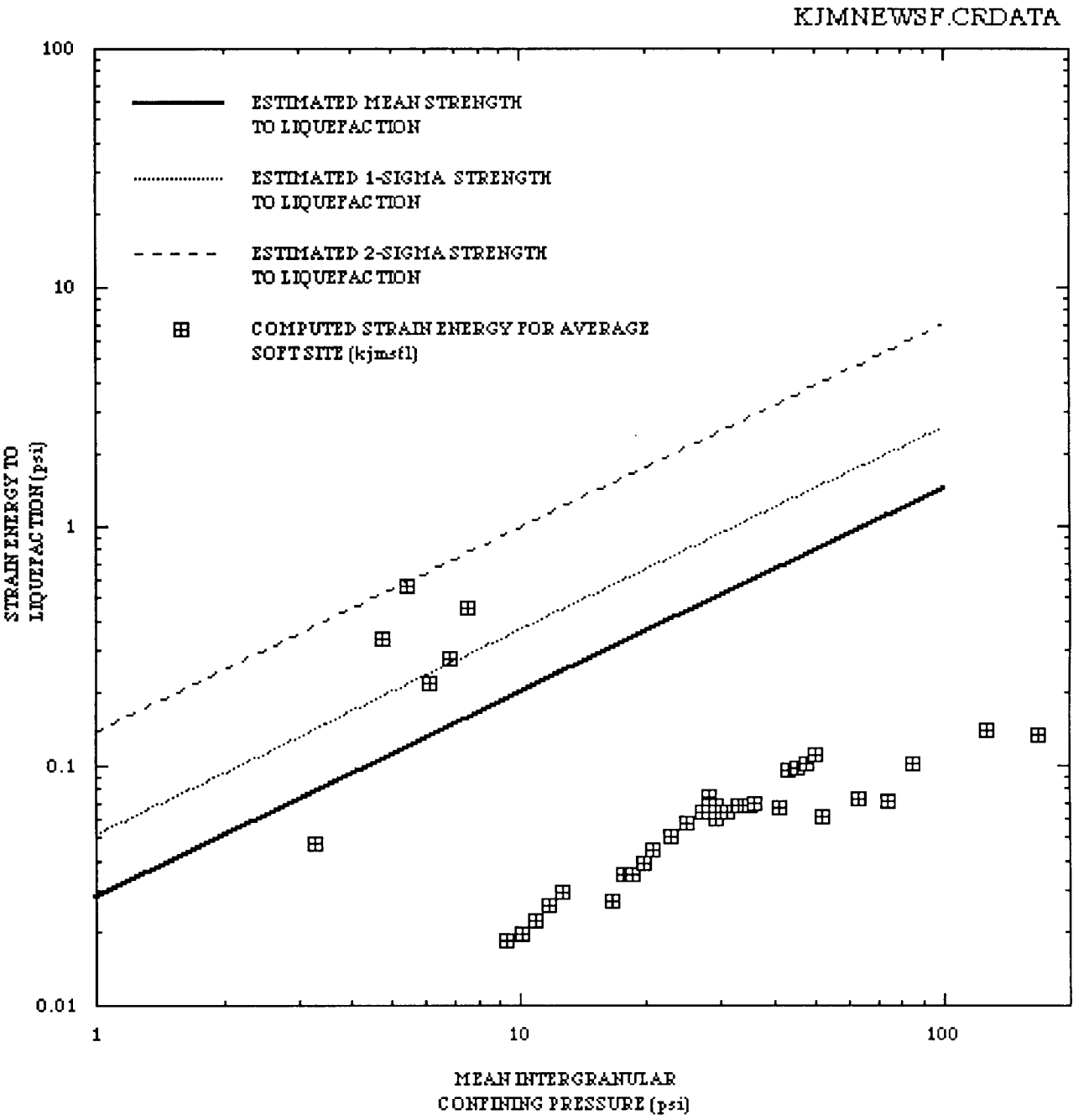

Figure 5.13b. Computed strain energy to onset of liquefaction for average soft site as a function of mean confining pressure (or depth).

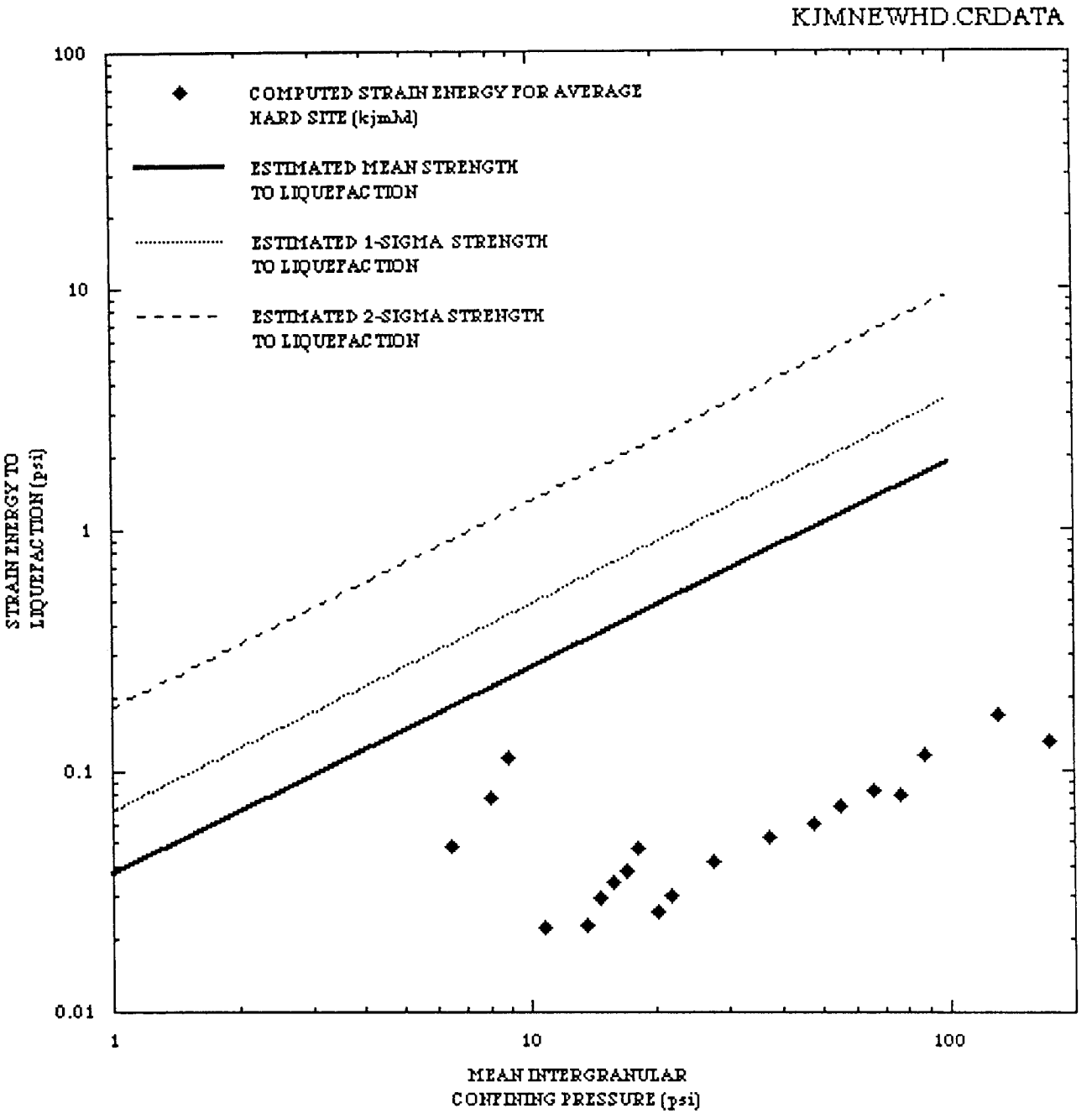

Figure 5.13c. Computed strain energy to onset of liquefaction for average hard site as a function of mean confining pressure (or depth).

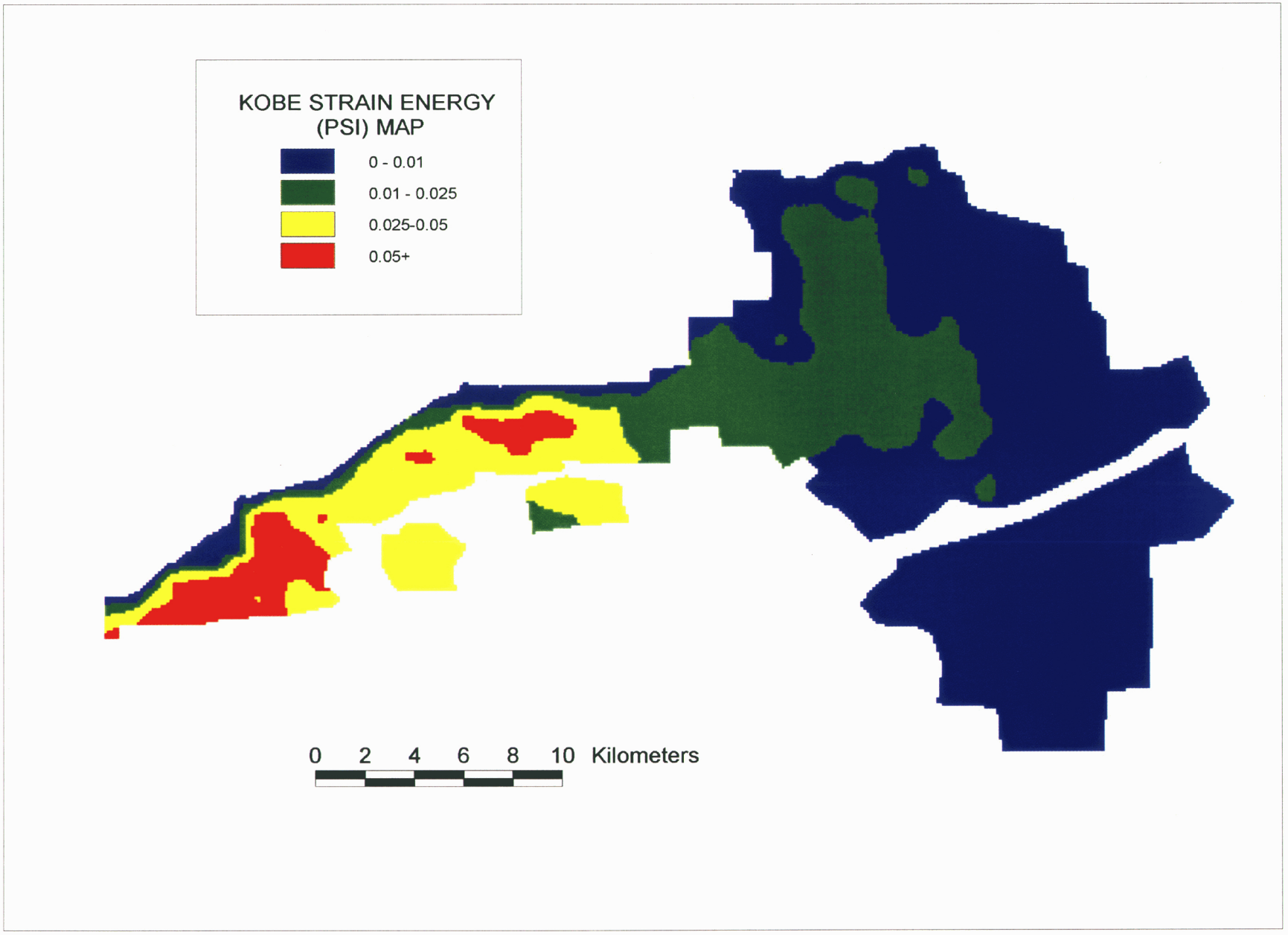

Figure 5.14. Median estimates of strain energy (PSI) for the rock, hard, soft, and fill areas of Kobe, Nishinomiya, and Osaka.

6.0 CONCLUSIONS

The objective of this study has been to investigate the ability of analysis procedures currently in use and incorporated into a stochastic finite-fault ground motion simulation procedure to predict the extent of liquefaction that occurred at Kobe during the 1995 moment magnitude 6.9 earthquake. Extensive zones of liquefaction occurred in the coastal areas of reclaimed lands and more sporadically along a zone of soft soils bordering the fill areas but lying closer to the fault rupture. The procedure followed in this study was to first collect detailed information on soil profiles in an extensive area in the Osaka Bay region, from the close-in Kobe area sites to the more distant locations in the Osaka region. This information consisted of site locations, soil descriptions, and sample SPT blow count data for the various soil layers of the profiles. These data were then combined with information of the deeper bedrock configuration to provide relatively complete descriptions of the soils/rocks in the region. These profiles were then used to model the regional ground motions from source to site, making use of the RVT finite-fault formulation which incorporates equivalent-linear site response analyses for both rock and soil site conditions.

Site specific responses were then generated at 25 sites where recordings of the **M** 6.9 Kobe earthquake are available. Comparisons of the computed responses with the recorded motions indicate that the procedure to model from source to site produces reasonable predictions of surface ground motions defined in terms of both PGA and response spectral shapes. This procedure is similar to that which is often used to generate site responses at critical facilities. In addition to surface motions, the procedure is also used to generate median estimates of effective cyclic stress ratios (CSR) and strain energies which are then used for comparison with generic data, either deterministic or probabilistic, to evaluate the likelyhood of liquefaction.

Using standard evaluation procedures based on the CSR, it is found that the calculated induced stress levels and associated CSR's are so high as to lead to a conclusion that liquefaction would occur over much wider areas than was actually observed. This indicates that the standard methods for prediction of the onset of liquefaction can be very conservative when applied to sites located at close distances to large earthquakes. The primary reason for this behavior is ascribed to the fact that liquefaction in these close-in regions occurred under very few cycles of loading to initiation of high pore pressure ratios. When the increased soil strengths associated with fewer cycles to liquefaction are considered, the method of prediction based upon cyclic stress ratios leads to more reasonable estimates of areas of liquefaction, although still very conservative. Thus, it is concluded that the standard procedure should also incorporate an estimate of the number of cycles that can reasonably be expected to occur for a design event which is also a function of rupture distance to the site. Thus the design or evaluation process should be extended for completeness.

Evaluations based on a strain energy method of analysis indicate that these predictions are significantly closer to the observed extent of liquefaction as compared to the very conservative predictions based on CSR. It should be noted, however, that the calculated strain energy levels within each soil column were found to be very much more sensitive to the particular level of shear modulus and damping ratio used in the calculations than were the calculated CSR's; that is, the variability in the strain energies at each sites due to variations in material properties were found to be significantly higher than for the CSR for the same uncertainty in the parameters controlling site response. This observation suggests that to achieve the same level of uncertainty in the prediction of liquefaction susceptibility between the strain

energy and CSR approaches, lower uncertainty is required in material properties (shear-wave velocity and nonlinear material dependencies) for the strain energy approach. The CSR approach, being fundamentally based on cyclic stresses, appears to be a more robust, although very conservative, estimator of liquefaction potential.

Finally, the following tasks are recommended to better evaluate the use of strain energy as a tool for site liquefaction evaluation. First, additional laboratory data are needed to better define strain energy to the onset of liquefaction, particularly for siltier soils at confining pressures appropriate for shallow soils. Typically such testing is performed for evaluation of critical facilities. Any new cyclic triaxial testing done for such samples should include the computation of strain energy as part of the laboratory output. Secondly, it is strongly recommended that the currently available data base of sites at which liquefaction is known to have occurred be investigated to determine computed strain energy levels for correlation with known surface expressions of liquefaction. This would eliminate the need to use empirical approaches to relate surface expression of liquefaction with laboratory strain energy levels. SPT and soil description data are typically available at such sites and similar correlations with relative density as used herein could be used for the correlations with laboratory data. The evaluations of strain energy at these sites would then allow for direct correlation of computed strain energy levels with liquefaction and at least complement the current evaluation methods based on CSR.

7.0 REFERENCES

Abrahamson, N.A. and Silva, W.J. (1997). "Empirical response spectral attenuation relations for shallow crustal earthquakes." *Seism. Soc. Am.*, 68(1), 94-127.

Arango, I. (1994). "Methodology for Liquefaction Potential Evaluation of Sites East of the Rockies." Report, Bechtel Corporation.

Burmister, D. (1962). "Physical, stress-strain and strength response of granular soils." Symposium on Field Testing of Soils, Spec. Technical Publication No. 322, American Society for Testing Materials.

Comartin, C. D., M. Greene and S. K. Tubbesing, editors (1995). "The Hyogo-Ken Nanbu Earthquake of January 17, 1995, Preliminary Reconnaissance Report." *EERI*, Report 95-04.

DeAlba, P., H. B. Seed and C. K. Chan (1976). "Sand Liquefaction in Large-Scale Simple Shear Tests" Journal of the Geotechnical Engineering Division, *ASCE*, 102(GT9), Proceeding Paper 12403, 909-927.

Dobry, R., R. S. Ladd, F. Y. Yokel, R. M. Chung and D. Powell (1982). "Prediction of Pore Water Pressure Build-Up and Liquefaction of Sands During Earthquakes by th Cyclic Strain Method." NBS Building Science Series 138, National Bureau of Standards.

Ejiri, J., S. Sawada, Y. Goto and K. Toki (1996). "Peak Ground Motion Characteristics During the 1995 Hyogoken-Nambu Earthquake." Special Issue, Soils and Foundations.

Elgamal, A. W., M . Zeghal and E. Parra (1996). "Liquefaction of Reclaimed Island in Kobe, Japan." Japan Journal, Geotechnical Engineering, *ASCE*, 39-49.

Electric Power Research Institute (1993). "Guidelines for determining design basis ground motions." Palo Alto, Calif: Electric Power Research Institute, vol. 1-5, EPRI TR-102293.

vol. 1: Methodology and guidelines for estimating earthquake ground motion in eastern North America.
vol. 2: Appendices for ground motion estimation.
vol. 3: Appendices for field investigations.
vol. 4: Appendices for laboratory investigations.
vol. 5: Quantification of seismic source effects.

Ferritto, J. (1982). "Evaluation of earthquake-induced ground failure." United States Department of the Interior, Geological Survey, Open file Report 82-880.

Fukushima, Y. and K. Irikura (1997). "Attenuation Characteristics of Peak Ground Motions in the 1995 Hyogo-Ken Nanbu Earthquake." *Journal of Physics of the Earth*, vol. 45, 135-146.

Fukushima, Y., J.C. Gariel and R. Tanaka (1995). "Site Dependent Attenuation Relations of Seismic Motion Parameters at Depth Using Borehole Data." *Bull. Seism. Soc. Am.*, 85(6), 1790-1804.

Ghayamghamian, M. and H. Kawakami (1996). "On the Characteristics of Nonlinear Soil Response and Dynamic Soil Properties Using Vertical Array Data in Japan." *Earthquake Eng. and Struct. Dyn.*, vol. 25, 857-870.

Haile, M., K. Seo, K. Kurita, H. Kyuke, H. Yamanaka, K. Yamazaki and A. Nakamaru (1997). "Study of Site Effects in Kobe Area Using Microtremors." *Journal of Physics of the Earth*, vol. 45, 121-133.

Hamada, M., R. Isoyama and K. Wakamatsu (1995). "Liquefaction, Ground Displacement and Soil Condition in Hanshin Area, The 1995 Hyogoken-Nanbu (Kobe) Earthquake." Assoc. for Development of Earthquake Prediction, School of Engineering, Waseda University.

Hatanaka, M., A. Uchida and J. Ohara (1997). "Liquefaction Characteristics of a Gravelly Fill Liquefied During the 1995 Hyogo-ken Nanbu Earthquake." *Japanese Geotechnical Society, Soils and Foundations,* 37(3), 107-115.

Idriss, I. M. (1997) "Evaluation of Liquefaction Potential and Consequences." Presentation Notes, 3rd Short Course on Evaluation and Mitigastion of Earthquake Induced Liquefaction Hazards, San Francisco.

Inoue, T. and T. Miyatake (1997). "3-D simulation of near-field strong ground motion: Basin edge effect derived from rupture directivity." *Geophysical Research Letters,* 24(8), 905-908.

Ishihara, K. (1985). "Stability of natural soil deposits during earthquakes." *11th Inter. Conf. on Soil Mechanics & Foundation Engr.*, vol. 1, pg 321 - 376, 1985, published by A. Balkema, Rotterdam, The Netherlands.

Ito, T. (1995) Dept. of Earth Sciences, Chiba University, Japan, Personal Communications.

Iwasaki, Y., S. Sawada and T. Kagawa (1987) "Microzonation for Predicting Earthquake in the South of Osaka Prefecture."

Japanese Geotechnical Society (1996). "Special Issue on Geotechnical Aspects of the January 17, 1995 Hyogoken-Nambu Earthquake." Soils and Foundations, ISSN 0038-0806.

Kagawa, T., S. Sawada, Y. Iwasaki, and A. Nanjo (1993). "On the modelization of deep sedimentary basin structure beneath the Osaka plain." *Abstr. Seismol. Soc. Jpn.,* 2, 112-117 (in Japanese).

Kamae, K., K. Irikura and A. Pitarka (1998). "A Technique for Simulating Strong Ground Motion Using Hybrid Green's Function." *Bull. Seism. Soc. Am.,* 88(2), 357-367.

Kansai Branch of JSSMFE (1987). "Osaka Soil Foundation Map." edited by Kansai Geologic Surveyors Association.

Kavazanjian, E. and C. L. Ho (1984) "Nonlinear Probabilistic Evaluation of the Number of Equivalent Uniform Cycles for Liquefaction Analyses." *8th World Conference of Earthquake Engineering.*

Kawase, H. (1996). "The cause of the damage belt in Kobe: "The basin-edge effect," constructive interference of the direct S-wave with the basin-induced diffracted/rayleigh waves." *Seism. Research Lett.* 67(5), 25-34.

Kazama, M., A. Yamaguchi and E. Yanagisawa (1998). "Seismic behavior of an underlying alluvial clay on man-made islands during the 1995 Hyogoken-Nambu earthquake." *Special Issue of Soils and Foundations,* 23-32, Japanese Geotechnical Society.

Kimura, M. (1996). "Damage Statistics", Special Issue, Soils and Foundations.

Kokusho, T., K. Sato and M. Matsumoto. (1996) "Nonlinear Dynamic Soil Properties Back-Calculated from Strong Seismic Motions During Hyogoken-Nanbu Earthquake", *11th WCEE*, Mexico.

Kokusho, T., J. Tohma, H. Yajima, Y. Tanaka and M. Kanatani (1992). "Seismic Response of Soil Layer and Its Dynamic Properties." *10th WCEE,* Madrid.

Krinitzsky, E. L., J.P. Koester and R.L. Hall (1995). "Reconnaissance Report." Waterways Experiment Station.

Liao, S., D. Veneziano and R. Whitman (1988). "Regression Models for Evaluating Liquefaction Probability." Journal. Geotechnical Engineering, *ASCE*, 114(4).

Liao, S. (1986). "Statistical Modelling of Earthquake Induced Liquefaction", Ph. D. Dissertation, Dept. of Civil Engineering, MIT.

Loertscher, T. (1994). "Magnitude Scaling Factors for Analysis of Liquefaction Hazard." Ph. D. Dissertation, Dept. of Civil Engineering, Brighasm Young University.

Matsuo, K. (1995). "Lessons from Kobe." Civil Engineering Magazine, *ASCE.*

Mok, C. M., C. Y. Chang and D. E. Legaspi (1989). "Site Response Analysis of Vertical Motion." *Proceedings, Geotechnical Earthquake Engineering and Soil Dynamics III,* pg. 739, Seattle, WA.

Motosaka, M. and M. Nagano (1997). "Analysis of Amplification Characteristics of Ground Motions in the Heavily Damaged Belt Zone During the 1995 Hyogo-ken Nanbu Earthquake." *Earthquake Eng and Structural Dynamics*, vol. 26, 3377-393.

Ostadan, F., N. Deng and I. Arango (1996). "Energy Based Method for Liquefaction Potential Evaluation, Phase I- Feasibility Study." *NIST* Report No. GCR 96-701, Bechtel Corporation for NIST.

Pitarka, A, K. Irikura, T. Iwata and T. Kagawa (1996). "Basin structure effects in the Kobe area inferred from the modeling of ground motions from two aftershocks of the January 17, 1995, Hyogo-ken Nanbu earthquake." *J. Phys. Earth,* 44, 563-576.

Reiter, L. (1990). "*Earthquake Hazard Analysis, Issues and Insights.*" Columbia University Press, New York.

Sadigh, C.-Y. Chang, J.A. Egan, F. Makdisi, and R.R. Youngs (1997). "Attenuation relationships for shallow crustal earthquakes based on California strong motion data." *Seism. Soc. Am.,* 68(1), 180-189.

Satoh, T., T. Sato and H. Kawase (1995). "Nonlinear Behavior of Soil Sediments Identified by Using Borehole Records Observed at the Ashigara Valley, Japan." *Bull. Seism. Soc. Am.,* 85(6), 1821-1834.

Satoh, T., H. Kawase and T. Sato (1995). "Evaluation of Local Site Effects and Their Removal from Borehole Records Observed in the Sendai Region, Japan." *Bull. Seism. Soc. Am.,* 85(6), 1770.

Schnabel, P.B., J. Lysmer and H.B. Seed (1972). *SHAKE: a Computer Program for Earthquake Response Analysis of Horizontally Layered Sites.* Earthq. Engin. Res. Center, Univ. of Calif. at Berkeley, EERC 72-12.

Seed, H. B., K. Tokimatsu, L. F. Harder and R. M. Chung (1984). "The Influence of SPT Procedures in Soil Liquefaction Resistance Evaluation." University of California at Berkeley, Report No. UCB/EERC-84115.

Seed, H. B., R.T. Wong, I.M. Idriss and K. Tokimatsu (1984). "Moduli and dynamic factors for dynamic analyses of cohesionless soils." Earthquake Engin. Res. Center, Univ. of Calif. at Berkeley, EERC-84/14.

Seed, H. B., I. M. Idriss and I. Arango (1983). "Evaluation of Liquefaction Potential Using Field Performance Data." Journal of the Geotechnical Engineering Division, *ASCE*, 109(3), 458-482.

Seed H. B. and I. M. Idriss (1982). "Ground Motions and Soil Liquefaction During Earthquakes Monograph Series," *Earthq. Eng. Res. Inst. Monograph*, Berkeley, California.

Seed, H. B., I. M. Idriss, F. Makdisi and N. Banerjee (1975). "Representation of Irregular Stress Time Histories by Equivalent Uniform Stress Series in Liquefaction Analyses." Report Number EERC 75-29, Earthquake Engineering Research Center, University of California, Berkeley, California.

Seed, H. B. (1979). "Soil Liquefaction and Cyclic Mobility Evaluation for Level Ground During Earthquakes." Journal of the Geotechnical Engineering Division, *ASCE*, 105(2).

Seed, H. B. and I. M. Idriss (1971). "Simplified Procedure for Evaluating Soil Liquefaction Potential." Journal Soil Mechanics and Foundation Division, *ASCE*, 97(9).

Seed, H. B. and I. M. Idriss (1967). "Analysis of Soil Liquefaction; Niigata Earthquake." Journal of the Soil Mechanics and Foundations Division, *ASCE*, 93(SM3), 83-108.

Shibata, T., F. Oka and Y. Ozawa (1996). "Characteristics of Ground Deformation due to Liquefaction." Special Issue, Soils and Foundations.

Silva, W.J. (1997). "Ground motion for new and existing highway facilities." *Proc. Of the FHWA/NCEER Workshop on the Nat'l Representation of Seismic,* I.M. Friedland, M.S Power and R. L. Mayes eds., Technical Report NCEER-97-0010.

Silva, W.J., N. Abrahamson, G. Toro, C. Costantino (1997). "Description and validation of the stochastic ground motion model." Submitted to Brookhaven National Laboratory, Associated Universities, Inc. Upton, New York.

Suetomi, I. and N. Yoshida (1998). "Nonlinear behavior of surface deposit during the 1995 Hyogoken-Nambu earthquake." *Abstr. Special Issue of Soils and Foundations*, Japanese Geotechnical Society.

Tokimatsu, K., H. Mizuno and M. Kakurai (1996). "*Building Damage Associated with Geotechnical Problems.*" Special Issue on Geotechnical Aspects of the January 17, 1995 Hyogoken-Nambu Earthquake, Soils and Foundations, Japanese Geotechnical Society, ISSN 0038-0806.

Tokimatsu, K., H. Arai and Y. Asaka (1989). "Two Dimensional Shear Wave Structure and Ground Motion Characteristics in Kobe Based on Microtremor Measurements." *Proc. Geotechnical Earthquake Engineering and Soil Dynamics III*, pg. 703, Seattle, Washington.

Wald, D.J. (1996). "Slip history of the 1995 Kobe, Japan, earthquake determined from strong motion, teleseismic, and geodetic data." *J. of Physics of the Earth,* 44, 489-504.

Wald, D.J., D.V. Helmberger, and T.R. Heaton (1991). "Rupture model of the 1989 Loma Prieta Earthquake from the inversion of strong motion and broadband teleseismic data." *Bull. Seism. Soc. Amer.*, 81(5), 1540-1572.

APPENDIX A

STOCHASTIC GROUND MOTION MODEL DESCRIPTION

BACKGROUND

In the context of strong ground motion, the term "stochastic" can be a fearful concept to some and may be interpreted to represent a fundamentally incorrect or inappropriate model (albeit the many examples demonstrating that it works well; Boore, 1983, 1986). To allay any initial misgivings, a brief discussion seems prudent to explain the term stochastic in the stochastic ground motion model.

The stochastic point-source model may be termed a spectral model in that it fundamentally describes the Fourier amplitude spectral density at the surface of a half-space (Hanks and McGuire, 1981). The model uses a Brune (1970, 1971) omega-square description of the earthquake source Fourier amplitude spectral density. This model is easily the most widely used and qualitatively validated source description available. Seismic sources ranging from **M** = -6 (hydrofracture) to **M** = 8 have been interpreted in terms of the Brune omega-square model in dozens of papers over the last 30 years. The general conclusion is that it provides a reasonable and consistent representation of crustal sources, particularly for tectonically active regions such as plate margins. A unique phase spectrum can be associated with the Brune source amplitude spectrum to produce a complex spectrum which can be propagated using either exact or approximate (1-2- or 3-D) wave propagation algorithms to produce single or multiple component time histories. In this context the model is not stochastic, it is decidedly deterministic and as exact and rigorous as one chooses. A two-dimensional array of such point-sources may be appropriately located on a fault surface (area) and fired with suitable delays to simulate rupture propagation on an extended rupture plane. As with the single point-source, any degree of rigor may be used in the wave propagation algorithm to produce multiple component or average horizontal component time histories. The result is a kinematic[1] finite-source model which has as its basis a source time history defined as a Brune pulse whose Fourier amplitude spectrum follows an omega-square model. This finite-fault model would be very similar to that used in published inversions for slip models if the 1-D propagation were treated using a reflectivity algorithm (Aki and Richards, 1980). This algorithm is a complete solution to the wave equation from static offsets (near-field terms) to an arbitrarily selected high frequency cutoff (generally 1-2 Hz).

Alternatively, to model the wave propagation more accurately, recordings of small earthquakes at the site of interest and with source locations distributed along the fault of interest may be used as empirical Green functions (Hartzell, 1978). To model the design earthquake, the empirical Green functions are delayed and summed in a manner to simulate rupture propagation (Hartzell, 1978). Provided a sufficient number of small earthquakes are recorded at the site of interest, the source locations adequately cover the expected rupture surface, and sufficient low frequency energy is present in the Green functions, this would

---

[1]Kinematic source model is one whose slip (displacement) is defined (imposed) while in a dynamic source model forces (stress) are defined (see Aki and Richards 1980 for a complete description).

be the most appropriate procedure to use if nonlinear site response is not an issue. With this approach the wave propagation is, in principle, exactly represented from each Green function source to the site. However, nonlinear site response is not treated unless Green function motions are recorded at a nearby rock outcrop with dynamic material properties similar to the rock underlying the soils at the site or recordings are made at depth within the site soil column. These motions may then be used as input to either total or effective stress site response codes to model nonlinear effects. Important issues associated with this approach include the availability of an appropriate nearby (1 to 2 km) rock outcrop and, for the downhole recordings, the necessity to remove all downgoing energy from the at-depth soil recordings. The downgoing energy must be removed from the downhole Green functions (recordings) prior to generating the control motions (summing) as only the upgoing wavefields are used as input to the nonlinear site response analyses. Removal of the downgoing energy from each recording requires multiple site response analyses which introduce uncertainty into the Green functions due to uncertainty in dynamic material properties and the numerical site response model used to separate the upgoing and downgoing wavefields.

To alleviate these difficulties, one can use recordings well distributed in azimuth at close distances to a small earthquake and correct the recordings back to the source by removing wave propagation effects using a simple approximation (say 1/R plus a constant for crustal amplification and radiation pattern), to obtain an empirical source function. This source function can be used to replace the Brune pulse to introduce some natural (although source, path, and site specific) variation into the dislocation time history. If this is coupled to an approximate wave propagation algorithm (asymptotic ray theory) which includes the direct rays and those which have undergone a single reflection, the result is the empirical source function method (EPRI, 1993). Combining the reflectivity propagation (which is generally limited to frequencies $\leq$ 1-2 Hz due to computational demands) with the empirical source function approach (appropriate for frequencies $\geq$ 1 Hz; EPRI, 1993) results in a broad band simulation procedure which is strictly deterministic at low frequencies (where an analytical source function is used) and incorporates some natural variation at high frequencies through the use of an empirical source function (Sommerville et al., 1995).

All of these techniques are fundamentally similar, well founded in seismic source and wave propagation physics, and importantly, they are <u>all</u> approximate. Simply put, all models are wrong (approximations to natural processes) and the single essential element in selecting a model is to incorporate the appropriate degree of rigor, commensurate with uncertainties and variabilities in crustal structure and site effects, through extensive validation exercises. It is generally felt that more complicated models produce more accurate results, however, the implications of more sophisticated models with the increased number of parameters which must be specified is often overlooked. This is not too serious a consequence in modeling past earthquakes since a reasonable range in parameter space can be explored to give the "best" results. However for future predictions, this increased rigor often carries undesirable and overlooked baggage in increased parametric variability (Roblee et al., 1996). The effects of lack of knowledge (epistemic uncertainty; EPRI, 1993) regarding parameter values for future occurrences results in uncertainty or variability in ground motion predictions. It may easily be the case that a very simple model, such as the point-source model can have comparable, or even smaller, total variability (modeling plus parametric) than a much more rigorous model with an increased number of parameters (EPRI, 1993). What is desired in a model is sufficient sophistication such that it captures the dominant and stable features of source, distance, and site dependencies observed in strong ground motions. It is these considerations which led to the development of the stochastic point- and finite-source models and, in part, leads to the

stochastic element of the models.

The stochastic nature of the point- and finite-source RVT models is simply the assumption made about the character of ground motion time histories that permits stable estimates of peak parameters (e.g. acceleration, velocity, strain, stress, oscillator response) to be made without computing detailed time histories (Hanks and McGuire, 1981; Boore, 1983). This process uses random vibration theory to relate a time domain peak value to the time history root-mean-square (RMS) value (Boore, 1983). The assumption of the character of the time history for this process to strictly apply is that it be normally distributed random noise and stationary (its statistics do not change with time) over its duration. A visual examination of any time history quickly reveals that this is clearly not the case: time histories (acceleration, velocity, stress, strain, oscillator) start, build up, and then diminish with time. However poor the assumption of stationary Gaussian noise may appear, the net result is that the assumption is weak enough to permit the approach to work surprisingly well, as numerous comparisons with recorded motions and both qualitative and quantative validations have shown (Hanks and McGuire, 1981; Boore, 1983, 1986; McGuire et al., 1984; Boore and Atkinson, 1987; Silva and Lee, 1987; Toro and McGuire, 1987; Silva et al., 1990; EPRI, 1993; Schneider et al., 1993; Silva and Darragh, 1995; Silva et al., 1997). Corrections to RVT are available to accommodate different distributions as well as non-stationarity and are usually applied to the estimation of peak oscillator response in the calculated response spectra (Boore and Joyner, 1984; Toro, 1985).

Point-source Model

The conventional stochastic ground motion model uses an ω-square source model (Brune, 1970, 1971) with a single corner frequency and a constant stress drop (Boore, 1983; Atkinson, 1984). Random vibration theory is used to relate RMS (root-mean-square) values to peak values of acceleration (Boore, 1983), and oscillator response (Boore and Joyner, 1984; Toro, 1985; Silva and Lee, 1987) computed from the power spectra to expected peak time domain values (Boore, 1983).

The shape of the acceleration spectral density, a(f), is given by

$$a(f) = C \frac{f^2}{1+\left(\frac{f}{f_0}\right)^2} \frac{M_0}{R} P(f)\, A(f)\, e^{-\frac{\pi f R}{\beta_0 Q(f)}} \qquad \text{(A-1)}$$

where

$$C = \left(\frac{1}{\rho_0 \beta_0^{\,3}}\right) \cdot (2) \cdot (0.55) \cdot \left(\frac{1}{\sqrt{2}}\right) \cdot \pi.$$

M_0 = seismic moment,
R = hypocentral distance,
β_0 = shear-wave velocity at the source,
ρ_0 = density at the source
Q(f) = frequency dependent quality factor (crustal damping),
A(f) = crustal amplification,
P(f) = high-frequency truncation filter,
f_0 = source corner frequency.

C is a constant which contains source region density (ρ_0) and shear-wave velocity terms and accounts for the free-surface effect (factor of 2), the source radiation pattern averaged over a sphere (0.55) (Boore, 1986), and the partition of energy into two horizontal components ($1/\sqrt{2}$).

Source scaling is provided by specifying two independent parameters, the seismic moment (M_0) and the high-frequency stress parameter or stress drop ($\Delta\sigma$). The seismic moment is related to magnitude through the definition of moment magnitude **M** by the relation

$$\log M_0 = 1.5\,\mathbf{M} + 16.05 \qquad \text{(Hanks and Kanamori, 1979)} \qquad \text{(A-2).}$$

The stress drop ($\Delta\sigma$) relates the corner frequency f_0 to M_0 through the relation

$$f_0 = \beta_0\,(\Delta\sigma/8.44\,M_0)^{1/3} \qquad \text{(Brune; 1970, 1971)} \qquad \text{(A-3).}$$

The stress drop is sometimes referred to as the high frequency stress parameter (Boore, 1983) (or simply the stress parameter) since it directly scales the Fourier amplitude spectrum for frequencies above the corner frequency (Silva, 1991; Silva and Darragh 1995). High (> 1 Hz) frequency model predictions are then very sensitive to this parameter (Silva, 1991; EPRI, 1993) and the interpretation of it being a stress drop or simply a scaling parameter depends upon how well real earthquake sources (on average) obey the omega-square scaling (Equation A-3) and how well they are fit by the single-corner-frequency model. If earthquakes truly have single-corner-frequency omega-square sources, the stress drop in Equation A-3 is a physical parameter and its values have a physical interpretation of the forces (stresses) accelerating the relative slip across the rupture surface. High stress drop sources are due to a smaller source (fault) area (for the same **M**) than low stress drop sources (Brune, 1970). Otherwise, it simply a high frequency scaling or fitting parameter.

The spectral shape of the single-corner-frequency ω-square source model is then described by the two free parameters M_0 and $\Delta\sigma$. The corner frequency increases with the shear-wave velocity and with increasing stress drop, both of which may be region dependent.

The crustal amplification accounts for the increase in wave amplitude as seismic energy travels through lower- velocity crustal materials from the source to the surface. The amplification depends on

average crustal and near surface shear-wave velocity and density (Boore, 1986).

The P(f) filter is used in an attempt to model the observation that acceleration spectral density appears to fall off rapidly beyond some region- or site-dependent maximum frequency (Hanks, 1982; Silva and Darragh, 1995). This observed phenomenon truncates the high frequency portion of the spectrum and is responsible for the band-limited nature of the stochastic model. The band limits are the source corner frequency at low frequency and the high frequency spectral attenuation. This spectral fall-off at high frequency has been attributed to near-site attenuation (Hanks, 1982; Anderson and Hough, 1984) or to source processes (Papageorgiou and Aki, 1983) or perhaps to both effects. In the Anderson and Hough (1984) attenuation model, adopted here, the form of the P(f) filter is taken as

$$P(f, r) = e^{-\pi \kappa(r) f} \qquad \text{(A-4)}.$$

Kappa (r) ($\kappa(r)$ in Equation A-4) is a site and distance dependent parameter that represents the effect of intrinsic attenuation upon the wavefield as it propagates through the crust from source to receiver. Kappa (r) depends on epicentral distance (r) and on both the shear-wave velocity (β) and quality factor (Q_S) averaged over a depth of H beneath the site (Hough et al., 1988). At zero epicentral distance kappa (κ) is given by

$$\kappa(0) = \frac{H}{\overline{\beta}\ \overline{Q_S}} \qquad \text{(A-5)},$$

and is referred to as κ.

The bar in Equation A-5 represents an average of these quantities over a depth H. The value of kappa at zero epicentral distance is attributed to attenuation in the very shallow crust directly below the site (Hough and Anderson, 1988; Silva and Darragh, 1995). The intrinsic attenuation along this part of the path is not thought to be frequency dependent and is modeled as a frequency independent, but site and crustal region dependent, constant value of kappa (Hough et al., 1988; Rovelli et al., 1988). This zero epicentral distance kappa is the model implemented in this study.

The crustal path attenuation from the source to just below the site is modeled with the frequency-dependent quality factor Q(f). Thus the distance component of the original $\kappa(r)$ (Equation A-4) is accommodated by Q(f) and R in the last term of Equation A-1:

$$\kappa(r) = \frac{H}{\overline{\beta}\ \overline{Q_S}} + \frac{R}{\beta_0\ Q(f)} \qquad \text{(A-6)}.$$

The Fourier amplitude spectrum, a(f), given by Equation A-1 represents the stochastic ground motion model employing a Brune source spectrum that is characterized by a single corner frequency. It

is a point source and models direct shear-waves in a homogeneous half-space (with effects of a velocity gradient captured by the A(f) filter, Equation A-1). For horizontal motions, vertically propagating shear-waves are assumed. Validations using incident inclined SH-waves accompanied with raytracing to find appropriate incidence angles leaving the source showed little reduction in uncertainty compared to results using vertically propagating shear-waves. For vertical motions, P/SV propagators are used coupled with raytracing to model incident inclined plane waves (EPRI, 1993). This approach has been validated with recordings from the 1989 **M** 6.9 Loma Prieta earthquake (EPRI, 1993).

Equation A-1 represents an elegant ground motion model that accommodates source and wave propagation physics as well as propagation path and site effects with an attractive simplicity. The model is appropriate for an engineering characterization of ground motion since it captures the general features of strong ground motion in terms of peak acceleration and spectral composition with a minimum of free parameters (Boore, 1983; McGuire et al., 1984; Boore, 1986; Silva and Green, 1988; Silva et al., 1988; Schneider et al., 1993; Silva and Darragh, 1995). An additional important aspect of the stochastic model employing a simple source description is that the region-dependent parameters may be evaluated by observations of small local or regional earthquakes. Region-specific seismic hazard evaluations can then be made for areas with sparse strong motion data with relatively simple spectral analyses of weak motion (Silva, 1992).

In order to compute peak time-domain values, i.e. peak acceleration and oscillator response, RVT is used to relate RMS computations to peak value estimates. Boore (1983) and Boore and Joyner (1984) present an excellent development of the RVT methodology as applied to the stochastic ground motion model. The procedure involves computing the RMS value by integrating the power spectrum from zero frequency to the Nyquist frequency and applying Parsevall's relation. Extreme value theory is then used to estimate the expected ratio of the peak value to the RMS value of a specified duration of the stochastic time history. The duration is taken as the inverse of the source corner frequency (Boore, 1983).

Factors that affect strong ground motions such as surface topography, finite and propagating seismic sources, laterally varying near-surface velocity and Q gradients, and random inhomogeneities along the propagation path are not included in the model. While some or all of these factors are generally present in any observation of ground motion and may exert controlling influences in some cases, the simple stochastic point-source model appears to be robust in predicting median or average properties of ground motion (Boore 1983, 1986; Schneider et al., 1993; Silva and Stark, 1993). For this reason it represents a powerful predictive and interpretative tool for engineering characterization of strong ground motion.

Finite-source Model Ground Motion Model

In the near-source region of large earthquakes, aspects of a finite-source including rupture propagation, directivity, and source-receiver geometry can be significant and may be incorporated into strong ground motion predictions. To accommodate these effects, a methodology that combines the aspects of finite-earthquake-source modeling techniques (Hartzell, 1978; Irikura 1983) with the stochastic point-source ground motion model has been developed to produce response spectra as well as time histories appropriate for engineering design (Silva et al., 1990; Silva and Stark, 1993; Schneider et al., 1993). The approach is very similar to the empirical Green function methodology introduced by Hartzell (1978) and Irikura (1983). In this case however, the stochastic point-source is substituted for the empirical

Green function and peak amplitudes; PGA, PGV, and response spectra (when time histories are not produced) are estimated using random process theory.

Use of the stochastic point-source as a Green function is motivated by its demonstrated success in modeling ground motions in general and strong ground motions in particular (Boore, 1983, 1986; Silva and Stark, 1993; Schneider et al., 1993; Silva and Darragh, 1995) and the desire to have a model that is truly site- and region-specific. The model can accommodate a region specific Q(f), Green function sources of arbitrary moment or stress drop, and site specific kappa values. The necessity for having available regional and site specific recordings or modifying possibly inappropriate empirical Green functions is eliminated.

For the finite-source characterization, a rectangular fault is discretized into NS subfaults of moment M_0^S. The empirical relationship

$$\log (A) = \mathbf{M} - 4.0, \quad A \text{ in km}^2 \qquad \text{(A-7)}.$$

is used to assign areas to both the target earthquake (if its rupture surface is not fixed) as well as to the subfaults. This relation results from regressing log area on **M** using the data of Wells and Coppersmith (1994). In the regression, the coefficient on **M** is set to unity which implies a constant static stress drop of about 30 bars (Equation A-9). This is consistent with the general observation of a constant static stress drop for earthquakes based on aftershock locations (Wells and Coppersmith 1994). The static stress drop, defined by Equation A-10, is related to the average slip over the rupture surface as well as rupture area. It is theoretically identical to the stress drop in Equation A-3 which defines the omega-square source corner frequency assuming the rupture surface is a circular crack model (Brune, 1970; 1971). The stress drop determined by the source corner frequency (or source duration) is usually estimated through the Fourier amplitude spectral density while the static stress drop uses the moment magnitude and an estimate of the rupture area. The two estimates for the same earthquake seldom yield the same values with the static generally being the smaller. In a recent study (Silva et al., 1997), the average stress drop based on Fourier amplitude spectra determined from an empirical attenuation relation (Abrahamson and Silva, 1997) is about 70 bars while the average static stress drop for the crustal earthquakes studied by Wells and Coppersmith (1994) is about 30 bars. These results reflect a general factor of about 2 on average between the two values. These large differences may simply be the result of using an inappropriate estimate of rupture area as the zone of actual slip is difficult to determine unambiguously. In general however, even for individual earthquakes, the two stress drops scale similarly with high static stress drops (> 30 bars) resulting in large high frequency (> 1 Hz for $\mathbf{M} \geq 5$) ground motions which translates to high corner frequencies (Equation A-3).

The subevent magnitude M_S is generally taken in the range of 5.0-6.5 depending upon the size of the target event. M_S 5.0 is used for crustal earthquakes with **M** in the range of 5.5 to 8.0 and M_S 6.4 is used for large subduction earthquakes with $\mathbf{M} > 7.5$. The value of NS is determined as the ratio of the target event area to the subfault area. To constrain the proper moment, the total number of events summed (N) is given by the ratio of the target event moment to the subevent moment. The subevent and target event rise times (duration of slip at a point) are determined by the equation

$$\log \tau = 0.33 \log M_0 - 8.54 \qquad \text{(A-8)}$$

which results from a fit to the rise times used in the finite-fault modeling exercises, (Silva et al., 1997). Slip on each subfault is assumed to continue for a time τ. The ratio of target-to-subevent rise times is given by

$$\frac{\tau}{\tau^s} = 10^{0.5\,(M\,-\,M^s)} \qquad \text{(A-9)}$$

and determines the number of subevents to sum in each subfault. This approach is generally referred to as the constant-rise-time model and results in variable slip velocity for nonuniform slip distributions. Alternatively, one can assume a constant slip velocity resulting in a variable-rise-time model for heterogenous slip distributions.

Recent modeling of the Landers (Wald and Heaton, 1994), Kobe (Wald, 1996) and Northridge (Hartzell et al. 1996) earthquakes suggests that a mixture of both constant rise time and constant slip velocity may be present. Longer rise times seem to be associated with areas of larger slip with the ratio of slip-to-rise time (slip velocity) being depth dependent. Lower slip velocities (longer rise times) are associated with shallow slip resulting in relatively less short period seismic radiation. This result may explain the general observation that shallow slip is largely aseismic. The significant contributions to strong ground motions appear to originate at depths exceeding about 4 km (Campbell, 1993; Boore et al., 1994) as the fictitious depth term in empirical attenuation relation (Abrahamson and Silva, 1997; Boore et al., 1997). Finite-fault models generally predict unrealistically large strong ground motions for large shallow (near surface) slip using rise times or slip velocities associated with deeper (> 4 km) zones of slip. This is an important and unresolved issue in finite-fault modeling and the general approach is constrain the slip to relatively small values in the top 2 to 4 km. A more thorough analysis is necessary, ideally using several well validated models, before this issue can be satisfactorily resolved.

To introduce heterogeneity of the earthquake source process into the stochastic finite-fault model, the location of the sub-events within each subfault (Hartzell, 1978) are randomized as well as the subevent rise time. The stress drop of the stochastic point-source Green function is taken as 30 bars, consistent with the static value based on the **M** 5.0 subevent area using the equation

$$\Delta\sigma = \frac{7}{16}\left(\frac{M_e}{R_e^3}\right) \qquad \text{(Brune, 1970, 1971)} \qquad \text{(A-10)}$$

where R_e is the equivalent circular radius of the rectangular sub-event.

Different values of slip are assigned to each subfault as relative weights so that asperities or non-uniform slip can be incorporated into the methodology. For validation exercises, slip models are taken from the literature and are based on inversions of strong motion as well as regional or teleseismic recordings. To produce slip distributions for future earthquakes, random slip models are generated based on a statistical asperity model with parameters calibrated to the published slip distributions. This approach has been validated by comparing the modeling uncertainty and bias estimates for the Loma Prieta and Whittier Narrows earthquakes using motion at each site averaged over several (30) random slip models to the bias and uncertainty estimates using the published slip model. The results show nearly identical bias and uncertainty estimates suggesting that averaging the motions over random slip models produces as accurate a prediction at a site as a single motion computed using the "true" slip model which is determined from inverting actual recordings.

The rupture velocity is taken as depth independent at a value of 0.8 times the shear-wave velocity, generally at the depth of the dominant slip. This value is based on a number of studies of source rupture processes which also suggest that rupture velocity is non-uniform. To capture the effects of non-uniform rupture velocity, a random component (20%) is added. The radiation pattern is computed for each subfault, a random component added, and the RMS applied to the motions computed at the site.

The ground-motion time history at the receiver is computed by summing the contributions from each subfault associated with the closest Green function, transforming to the frequency domain, and convolving with the Green function spectrum (Equation A-1). The locations of the Green functions are generally taken at center of each subfault for small subfaults or at a maximum separation of about 5 to 10 km for large subfaults. As a final step, the individual contributions associated with each Green function are summed in the frequency domain, multiplied by the RMS radiation pattern, and the resultant power spectrum at the site is computed. The appropriate duration used in the RVT computations for PGA, PGV, and oscillator response is computed by transforming the summed Fourier spectrum into the time domain and computing the 5 to 75% Arias intensity (Ou and Herrmann, 1990).

As with the point-source model, crustal response effects are accommodated through the amplification factor (A(f)) or by using vertically propagating shear waves through a vertically heterogenous crustal structure. Propagation path damping, through the Q(f) model, is incorporated from each fault element to the site. Near-surface crustal damping is incorporated through the kappa operator (Equation A-1). To model crustal propagation path effects, the raytracing method of Ou and Herrmann (1990) is applied from each subfault to the site.

Time histories may be computed in the process as well by simply adding a phase spectrum appropriate to the subevent earthquake. The phase spectrum can be extracted from a recording made at close distance to an earthquake of a size comparable to that of the subevent (generally **M** 5.0 to 6.5). Interestingly, the phase spectrum need not be from a recording in the region of interest (Silva et al., 1989). A recording in WNA (Western North America) can effectively be used to simulate motions appropriate to ENA (Eastern North America). Transforming the Fourier spectrum computed at the site into the time domain results in a computed time history which then includes all of the aspects of rupture propagation and source finiteness, as well as region specific propagation path and site effects.

For fixed fault size, mechanism, and moment, the specific source parameters for the finite-fault are

slip distribution, location of nucleation point, and site azimuth. The propagation path and site parameters remain identical for both the point- and finite-source models.

Partition and assessment of ground motion variability

An essential requirement of any numerical modeling approach, particularly one which is implemented in the process of defining design ground motions, is a quantative assessment of prediction accuracy. A desirable approach to achieving this goal is in a manner which lends itself to characterizing the variability associated with model predictions. For a ground motion model, prediction variability is comprised of two components: modeling variability and parametric variability. Modeling variability is a measure of how well the model works (how accurately it predicts ground motions) when specific parameter values are known. Modeling variability is measured by misfits of model predictions to recorded motions through validation exercises and is due to unaccounted for components in the source, path, and site models (i.e. a point-source cannot model the effects of directivity and linear site response cannot accommodate nonlinear effects). Results from a viable range of values for model parameters (i.e., slip distribution, soil profile, G/G_{max} and hysteretic damping curves, etc). Parametric variability is the sensitivity of a model to a viable range of values for model parameters. The total variability, modeling plus parametric, represents the variance associated with the ground motion prediction and, because it is a necessary component in estimating fractile levels, may be regarded as important as median predictions.

Both the modeling and parametric variabilities may have components of randomness and uncertainty. Table A.1 summarizes the four components of total variability in the context of ground motion predictions. Uncertainty is that portion of both modeling and parametric variability which, in principle, can be reduced as additional information becomes available, whereas randomness represents the intrinsic or irreducible component of variability for a given model or parameter. Randomness is that component of variability which is intrinsic or irreducible <u>for a given model.</u> The uncertainty component reflects a lack of knowledge and may be reduced as more data are analyzed. For example, in the point-source model, stress drop is generally taken to be independent of source mechanism as well as tectonic region and is found to have a standard error of about 0.7 (natural log) for the CEUS (EPRI, 1993). This variation or uncertainty plus randomness in $\Delta\sigma$ results in a variability in ground motion predictions for future earthquakes. If, for example, it is found that normal faulting earthquakes have generally lower stress drops than strike-slip which are, in turn, lower than reverse mechanism earthquakes, perhaps much of the variability in $\Delta\sigma$ may be reduced. In extensional regimes, where normal faulting earthquakes are most likely to occur, this new information may provide a reduction in variability (uncertainty component) for stress drop, say to 0.3 or 0.4 resulting in less ground motion variation due to a lack of knowledge of the mean or median stress drop. There is, however, a component of this stress drop variability which can <u>never</u> be reduced in the context of the Brune model. This is simply due to the heterogeneity of the earthquake dynamics which is not accounted for in the model and results in the randomness component of parametric variability in stress drop. A more sophisticated model may be able to accommodate or model more accurately source dynamics but, perhaps, at the expense of a larger number of parameters and increased parametric uncertainty (i.e. the finite-fault with slip model and nucleation point as unknown parameters for future earthquakes). That is, more complex models typically seek to reduce modeling randomness by more closely modeling physical phenomena. However, such models often require more comprehensive sets of observed data to constrain additional model parameters, which generally leads to increased parametric variability. If the increased parametric variability is primarily in the form of uncertainty, it is

possible to reduce total variability, but only at the additional expense of constraining the additional parameters. Therefore, existing knowledge and/or available resources may limit the ability of more complex models to reduce total variability.

The distinction of randomness and uncertainty is model driven and somewhat arbitrary. The allocation is only important in the context of probabilistic seismic hazard analyses as uncertainty is treated as alternative hypotheses in logic trees while randomness is integrated over in the hazard calculation (Cornell, 1968). For example, the uncertainty component in stress drop may be treated by using an N-point approximation to the stress drop distribution and assigning a branch in a logic tree for each stress drop and associated weight. A reasonable three point approximation to a normal distribution is given by weights of 0.2, 0.6, 0.2 for expected 5%, mean, and 95% values of stress drop respectively. If the distribution of uncertainty in stress drop was such that the 5%, mean, and 95% values were 50, 100, and 200 bars respectively, the stress drop branch on a logic tree would have 50, and 200 bars with weights of 0.2 and 100 bars with a weight of 0.6. The randomness component in stress drop variability would then be formally integrated over in the hazard calculation.

Assessment of Modeling Variability

Modeling variability (uncertainty plus randomness) is usually evaluated by comparing response spectra computed from recordings to predicted spectra and is a direct assessment of model accuracy. The modeling variability is defined as the standard error of the residuals of the log of the average horizontal component (or vertical component) response spectra. The residual is defined as the difference of the logarithms of the observed average 5% damped acceleration response spectra and the predicted response spectra. At each period, the residuals are squared, and summed over the total number of sites for one or all earthquakes modeled. Dividing the resultant sum by the number of sites results in an estimate of the model variance. Any model bias (average offset) that exists may be estimated in the process (Abrahamson et al., 1990; EPRI, 1993) and used to correct (lower) the variance (and to adjust the median as well). In this approach, the modeling variability can be separated into randomness and uncertainty where the bias corrected variability represents randomness and the total variability represents randomness plus uncertainty. The uncertainty is captured in the model bias as this may be reduced in the future by refining the model. The remaining variability (randomness) remains irreducible for this model. In computing the variance and bias estimates only the frequency range between processing filters at each site (minimum of the 2 components) should be used.

Assessment of Parametric Variability

Parametric variability, or the variation in ground motion predictions due to uncertainty and randomness in model parameters is difficult to assess. Formally, it is straight-forward in that a Monte Carlo approach may be used with each parameter randomly sampled about its mean (median) value either individually for sensitivity analyses (Silva, 1992; Roblee et al., 1996) or in combination to estimate the total parametric variability (Silva, 1992; EPRI, 1993). In reality, however, there are two complicating factors.

The first factor involves the specific parameters kept fixed with all earthquakes, paths, and sites when computing the modeling variability. These parameters are then implicitly included in modeling variability provided the data sample a sufficiently wide range in source, path, and site conditions. The

parameters which are varied during the assessment of modeling variation should have a degree of uncertainty and randomness associated with them for the next earthquake. Any ground motion prediction should then have a variation reflecting this lack of knowledge and randomness in the free parameters.

An important adjunct to fixed and free parameters is the issue of parameters which may vary but by fixed rules. For example, source rise time (Equation A-8) is magnitude dependent and in the stochastic finite-source model is specified by an empirical relation. In evaluating the modeling variability with different magnitude earthquakes, rise time is varied, but because it follows a strict rule, any variability associated with rise time variation is counted in modeling variability. This is strictly true only if the sample of earthquakes has adequately spanned the space of magnitude, source mechanism, and other factors which may affect rise time. Also, the earthquake to be modeled must be within that validation space. As a result, the validation or assessment of model variation should be done on as large a number of earthquakes of varying sizes and mechanisms as possible.

The second, more obvious factor in assessing parametric variability is a knowledge of the appropriate distributions for the parameters (assuming correct values for median or mean estimates are known). In general, for the stochastic models, median parameter values and uncertainties are based, to the extent possible, on evaluating the parameters derived from previous earthquakes (Silva, 1992; EPRI, 1993).

The parametric variability is site, path, and source dependent and must be evaluated for each modeling application (Roblee et al., 1996). For example, at large source-to-site distances, crustal path damping may control short-period motions. At close distances to a large fault, both the site and finite-source (asperity location and nucleation point) may dominate, and, depending upon site characteristics, the source or site may control different frequency ranges (Silva, 1992; Roblee et al., 1996). Additionally, level of control motion may affect the relative importance of G/G_{max} and hysteretic damping curves.

In combining modeling and parametric variations, independence is assumed (covariance is zero) and the variances are simply added to give the total variability.

$$_{ln}\sigma^2_T = {}_{ln}\sigma^2_M + {}_{ln}\sigma^2_P{}^2 \qquad \text{(A-11)},$$

where

$_{ln}\sigma^2_M$ = modeling variation,

$_{ln}\sigma^2_P$ = parametric variation.

---

[2]Strong ground motions are generally considered to be log normally distributed.

Validation Of The Point- and Finite-Source Models

In a recent Department of Energy sponsored project (Silva et al., 1997), both the point- and finite-source stochastic models were validated in a systematic and comprehensive manner. In this project, 16 well recorded earthquakes were modeled at about 500 sites. Magnitudes ranged from **M** 5.3 to **M** 7.4 with fault distances from about 1 km out to 218 km for WUS earthquakes and 460 km for CEUS earthquakes. This range in magnitude and distance as well as number of earthquakes and sites results in the most comprehensively validated model currently available to simulate strong ground motions.

A unique aspect of this validation is that rock and soil sites were modeled using generic rock and soil profiles and equivalent-linear site response. Validations done with other simulation procedures typically neglect site conditions as well as nonlinearity resulting in ambiguity in interpretation of the simulated motions.

Point-Source Model

Final model bias and variability estimates for the point-source model are shown in Figure A1. Over all the sites (Figure A1) the bias is slightly positive for frequencies greater than about 10 Hz and is near zero from about 10 Hz to 1 Hz. Below 1 Hz, a stable point-source overprediction is reflected in the negative bias. The analyses are considered reliable down to about 0.3 Hz (3.3 sec) where the point-source shows about a 40% overprediction.

The model variability is low, about 0.5 above about 3 to 4 Hz and increases with decreasing frequency to near 1 at 0.3 Hz. Above 1 Hz, there is little difference between the total variability (uncertainty plus randomness) and randomness (bias corrected variability) reflecting the near zero bias estimates. Below 1 Hz there is considerable uncertainty contributing to the total variability suggesting that the model can be measurably improved as its predictions tend to be consistently high at very low frequencies ($\leq$ 1 Hz). This stable misfit may be interpreted as the presence of a second corner frequency for WNA sources (Atkinson and Silva, 1997).

Finite-Source Model

For the finite-fault, Figure A2 shows the corresponding bias and variability estimates. For all the sites, the finite-source model provides slightly smaller bias estimates and, surprisingly, slightly higher variability for frequencies exceeding about 5 Hz. The low frequency ($\leq$ 1 Hz) point-source overprediction is not present in the finite-source results, indicating that it is giving more accurate predictions than the point-source model over a broad frequency range, from about 0.3 Hz (the lowest frequency of reliable analyses) to the highest frequency of the analyses.

In general, for frequencies of about 1 Hz and above the point-source and finite-source give comparable results: the bias estimates are small (near zero) and the variabilities range from about 0.5 to 0.6. These estimates are low considering the analyses are based on a data set comprised of earthquakes with **M** less than **M** 6.5 (288 of 513 sites) and high frequency ground motion variance decreases with increasing magnitude, particularly above **M** 6.5 (Youngs et al., 1995) Additionally, for the vast majority

of sites, generic site conditions were used (inversion kappa values were used for only the Saguenay and Nahanni earthquake analyses, 25 rock sites). As a result, the model variability (mean = 0) contains the total uncertainty and randomness contribution for the site. The parametric variability due to uncertainty and randomness in site parameters: shear-wave velocity, profile depth, G/G_{max} and hysteretic damping curves need not be added to the model variability estimates. It is useful to perform parametric variations to assess site parameter sensitivities on the ground motions, but only source and path damping Q(f) parametric variabilities require assessment on a site specific basis and added to the model variability. The source uncertainty and randomness components include point-source stress drop and finite-source slip model and nucleation point variations (Silva, 1992).

Empirical Attenuation Model

As an additional assessment of the stochastic models, bias and variability estimates were made over the same earthquakes (except Saguenay since it was not used in the regressions) and sites using a recently develop empirical attenuation relation (Abrahamson and Silva, 1997). For all the sites, the estimates are shown in Figure A3. Interestingly, the point-source overprediction below about 1 Hz is present in the empirical relation perhaps suggesting that this suite of earthquakes possess lower than expected motions in this frequency range as the empirical model does not show this bias over all earthquakes (50) used in its development. Comparing these results to the point- and finite-source results (Figures A1 and A2) show comparable bias and variability estimates. For future predictions, source and path damping parametric variability must be added to the numerical simulations which will contribute a σ_{ln} of about 0.2 to 0.4, depending upon frequency, source and path conditions, and site location. This will raise the modeling variability from about 0.50 to the range of 0.54 to 0.64, about 10 to 30%. These values are still comparable to the variability of the empirical relation indicating that the point- and finite-source numerical models perform about as well as a recently developed empirical attenuation relation for the validation earthquakes and sites.

These results are very encouraging and provide an additional qualitative validation of the point- and finite-source models. Paranthetically this approach provides a rational basis for evaluating empirical attenuation models.

Table A.1

CONTRIBUTIONS TO TOTAL VARIABILITY
IN GROUND MOTION MODELS

	Modeling Variability	Parametric Variability
Uncertainty *(also Epistemic Uncertainty)*	Modeling Uncertainty: Variability in predicted motions resulting from particular model assumptions, simplifications and/or fixed parameter values. *Can be reduced by adjusting or "calibrating" model to better fit observed earthquake response.*	Parametric Uncertainty: Variability in predicted motions resulting from incomplete data needed to characterize parameters. *Can be reduced by collection of additional information which better constrains parameters*
Randomness *(also Aleatory Uncertainty)*	Modeling Randomness: Variability in predicted motions resulting from discrepancies between model and actual complex physical processes. *Cannot be reduced for a given model form.*	Parametric Randomness: Variability in predicted motions resulting from inherent randomness of parameter values. *Cannot be reduced a priori*[***] *by collection of additional information.*

[***]Some parameters (e.g. source characteristics) may be well defined after an earthquakes.

REFERENCES

Abrahamson, N.A. and W.J. Silva (1997). "Empirical response spectral attenuation relations for shallow crustal earthquakes." *Seismological Research Let.,* 68(1), 94-127.

Abrahamson, N.A., P.G. Somerville, and C.A. Cornell (1990). "Uncertainty in numerical strong motion predictions" *Proc. Fourth U.S. Nat. Conf. Earth. Engin.*, Palm Springs, CA., 1, 407-416.

Aki, K. and P.G. Richards. (1980). *"Quantitative siesmology."* W. H. Freeman and Co., San Francisco, California.

Atkinson, G.M and W.J. Silva (1997). "An empirical study of earthquake source spectra for California earthquakes." *Bull. Seism. Soc. Am.* 87(1), 97-113.

Anderson, J.G. and S.E. Hough (1984). "A Model for the Shape of the Fourier Amplitude Spectrum of Acceleration at High Frequencies." *Bulletin of the Seismological Society of America,* 74(5), 1969-1993.

Atkinson, G.M. (1984). "Attenuation of strong ground motion in Canada from a random vibrations approach." *Bull. Seism. Soc. Am.*, 74(5), 2629-2653.

Boore, D.M., W.B. Joyner, and T.E. Fumal (1997). "Equations for estimating horizontal response spectra and peak acceleration from Western North American earthquakes: A summary of recent work." *Seism. Res. Lett.* 68(1), 128-153.

Boore, D.M., W.B. Joyner, and T.E. Fumal (1994). "Estimation of response spectra and peak accelerations from western North American earthquakes: and interim report. Part 2. *U.S. Geological Survey Open-File Rept.* 94-127.

Boore, D.M., and G.M. Atkinson (1987). "Stochastic prediction of ground motion and spectral response parameters at hard-rock sites in eastern North America." *Bull. Seism. Soc. Am.*, 77(2), 440-467.

Boore, D.M. (1986). "Short-period P- and S-wave radiation from large earthquakes: implications for spectral scaling relations." *Bull. Seism. Soc. Am.*, 76(1) 43-64.

Boore, D.M. and W.B. Joyner (1984). "A note on the use of random vibration theory to predict peak amplitudes of transient signals." *Bull. Seism. Soc. Am.*, 74, 2035-2039.

Boore, D.M. (1983). "Stochastic simulation of high-frequency ground motions based on seismological models of the radiated spectra." *Bull. Seism. Soc. Am.*, 73(6), 1865-1894.

Brune, J.N. (1971). "Correction." *J. Geophys. Res.* 76, 5002.

Brune, J.N. (1970). "Tectonic stress and the spectra of seismic shear waves from earthquakes." *J. Geophys. Res.* 75, 4997-5009.

Campbell, K.W. (1993) "Empirical prediction of near-source ground motion from large earthquakes." in V.K. Gaur, ed., *Proceedings, Intern'l Workshop on Earthquake Hazard and Large Dams in the Himalya.* INTACH, New Delhi, p. 93-103.

Cornell, C.A. (1968). "Engineering seismic risk analysis." *Bull. Seism. Soc. Am.*, 58, 1583-1606.

Electric Power Research Institute (1993). "Guidelines for determining design basis ground motions." Palo Alto, Calif: Electric Power Research Institute, vol. 1-5, EPRI TR-102293.
vol. 1: Methodology and guidelines for estimating earthquake ground motion in eastern North America.
vol. 2: Appendices for ground motion estimation.
vol. 3: Appendices for field investigations.
vol. 4: Appendices for laboratory investigations.
vol. 5: Quantification of seismic source effects.

Hanks, T.C. (1982). "f_{max}." *Bull. Seism. Soc. Am.*, 72, 1867-1879.

Hanks, T.C. and R.K. McGuire (1981). "The character of high-frequency strong ground motion." *Bull. Seism. Soc. Am.*, 71(6), 2071-2095.

Hanks, T.C. and H. Kanamori (1979). "A moment magnitude scale." *J. Geophys. Res.*, 84, 2348-2350.

Hartzell, S., A. Leeds, A. Frankel, and J. Michael (1996). "Site response for urban Los Angeles using aftershocks of the Northridge earthquake." *Bull. Seism. Soc. Am.*, 86(1B), S168-S192.

Hartzell, S.H. (1978). "Earthquake aftershocks as Green's functions." *Geophys. Res. Letters*, 5, 1-4.

Hough, S.E., J.G. Anderson, J. Brune, F. Vernon III, J. Berger, J. Fletcher, L. Haar, T. Hanks, and L. Baker (1988). "Attenuation near Anza, California." *Bull. Seism. Soc. Am.*, 78(2), 672-691.

Hough, S.E. and J.G. Anderson (1988). "High-Frequency Spectra Observed at Anza, California: Implications for Q Structure." *Bull. Seism. Soc. Am.*, 78(2), 692-707.

Irikura, K. (1983). "Semi-empirical estimation of strong ground motions during large earthquakes." *Bull. Disaster Prevention Res. Inst.*, Kyoto Univ., 33, 63-104.

McGuire, R. K., A.M. Becker, and N.C. Donovan (1984). "Spectral Estimates of Seismic Shear Waves." *Bull. Seism. Soc. Am.*, 74(4), 1427-1440.

Ou, G.B. and R.B. Herrmann (1990). "Estimation theory for strong ground motion." *Seism. Res. Letters.* 61.

Papageorgiou, A.S. and K. Aki (1983). "A specific barrier model for the quantitative description of inhomogeneous faulting and the prediction of strong ground motion, part I, Description of the model." *Bull. Seism. Soc. Am.*, 73(4), 693-722.

Roblee, C.J., W.J. Silva, G.R. Toro and N. Abrahamson (1996). "Variability in site-specific seismic ground-motion design predictions." in press.

Rovelli, A., O. Bonamassa, M. Cocco, M. Di Bona, and S. Mazza (1988). "Scaling laws and spectral parameters of the ground motion in active extensional areas in Italy." *Bull. Seism. Soc. Am.*, 78(2), 530-560.

Schneider, J.F., W.J. Silva, and C.L. Stark (1993). "Ground motion model for the 1989 **M** 6.9 Loma Prieta earthquake including effects of source, path and site." *Earthquake Spectra*, 9(2), 251-287.

Silva, W.J., N. Abrahamson, G. Toro, and C. Costantino (1997). "Description and validation of the stochastic ground motion model." Submitted to Brookhaven National Laboratory, Associated Universities, Inc. Upton, New York.

Silva, W.J. and R. Darragh (1995). "Engineering characterization of earthquake strong ground motion recorded at rock sites." Palo Alto, Calif:Electric Power Research Institute, TR-102261.

Silva, W.J. and C.L. Stark (1993) "Source, path, and site ground motion model for the 1989 **M** 6.9 Loma Prieta earthquake." CDMG draft final report.

Silva, W.J. (1992). "Factors controlling strong ground motions and their associated uncertainties." *Dynamic Analysis and Design Considerations for High Level Nuclear Waste Repositories, ASCE* 132-161.

Silva, W.J. (1991). "Global characteristics and site geometry." Chapter 6 in *Proceedings: NSF/EPRI Workshop on Dynamic Soil Properties and Site Characterization.* Palo Alto, Calif.: Electric Power Research Institute, NP-7337.

Silva, W. J., R. Darragh, C. Stark, I. Wong, J. C. Stepp, J. Schneider, and S-J. Chiou (1990). "A Methodology to Estimate Design Response Spectra in the Near-Source Region of Large Earthquakes Using the Band-Limited-White-Noise Ground Motion Model". *Procee. of the Fourth U.S. Conf. on Earthquake Engineering,* Palm Springs, California. 1, 487-494.

Silva, W.J., R.B. Darragh, R.K. Green and F.T. Turcotte (1989). *Estimated Ground Motions for a new madrid Event.* U.S. Army Engineer Waterways Experiment Station, Wash., DC, Misc. Paper GL-89-17.

Silva, W. J. and R. K. Green (1988). "Magnitude and Distance Scaling of Response Spectral Shapes for Rock Sites with Applications to North American Environments." In *Proceedings: Workshop on Estimation of Ground Motion in the Eastern United States*, EPRI NP-5875, Electric Power Research Institute.

Silva, W. J., T. Turcotte, and Y. Moriwaki (1988). "Soil Response to Earthquake Ground Motion," Electric Power Research Institute, Walnut Creek, California, Report No. NP-5747.

Silva, W.J. and K. Lee (1987). "*WES RASCAL code for synthesizing earthquake ground motions.*" State-of-the-Art for Assessing Earthquake Hazards in the United States, Report 24, U.S. Army Engineers Waterways Experiment Station, Miscellaneous Paper S-73-1.

Somerville, P.G., R. Graves and C. Saikia (1995). "TECHNICAL REPORT: Characterization of ground motions during the Northridge earthquake of January 17, 1994." *Structural Engineers Association of California (SEAOC).* Report No. SAC-95-03.

Toro, G. R. and R. K. McGuire (1987). "An Investigation into Earthquake Ground Motion Characteristics in Eastern North America." *Bull. Seism. Soc. Am.*, 77(2), 468-489.

Toro, G. R. (1985). "Stochastic Model Estimates of Strong Ground Motion." In *Seismic Hazard Methodology for Nuclear Facilities in the Eastern United States*, Appendix B, R. K. McGuire, ed., Electric Power Research Institute, Project P101-29.

Wald, D.J. (1996). "Slip history of the 1995 Kobe, Japan, earthquake determined from strong motion, teleseismic, and geodetic data." *J. of Physics of the Earth,* in press.

Wald, D.J. and T.H. Heaton (1994). "Spatial and temporal distribution of slip for the 1992 Landers, California, earthquake." *Bull. Seism. Soc. Amer.*, 84(3), 668-691.

Wells, D.L. and K.J. Coppersmith (1994). "New empirical relationships among magnitude, rupture length, rupture width, rupture area, and surface displacement." *Bull. Seism. Soc. Am.* 84(4), 974-1002.

Youngs, R.R., N.A. Abrahamson, F. Makdisi, and K. Sadigh (1995). "Magnitude dependent dispersion in peak ground acceleration." *Bull. Seism. Soc. Amer.*, 85(1), 161-1, 176.

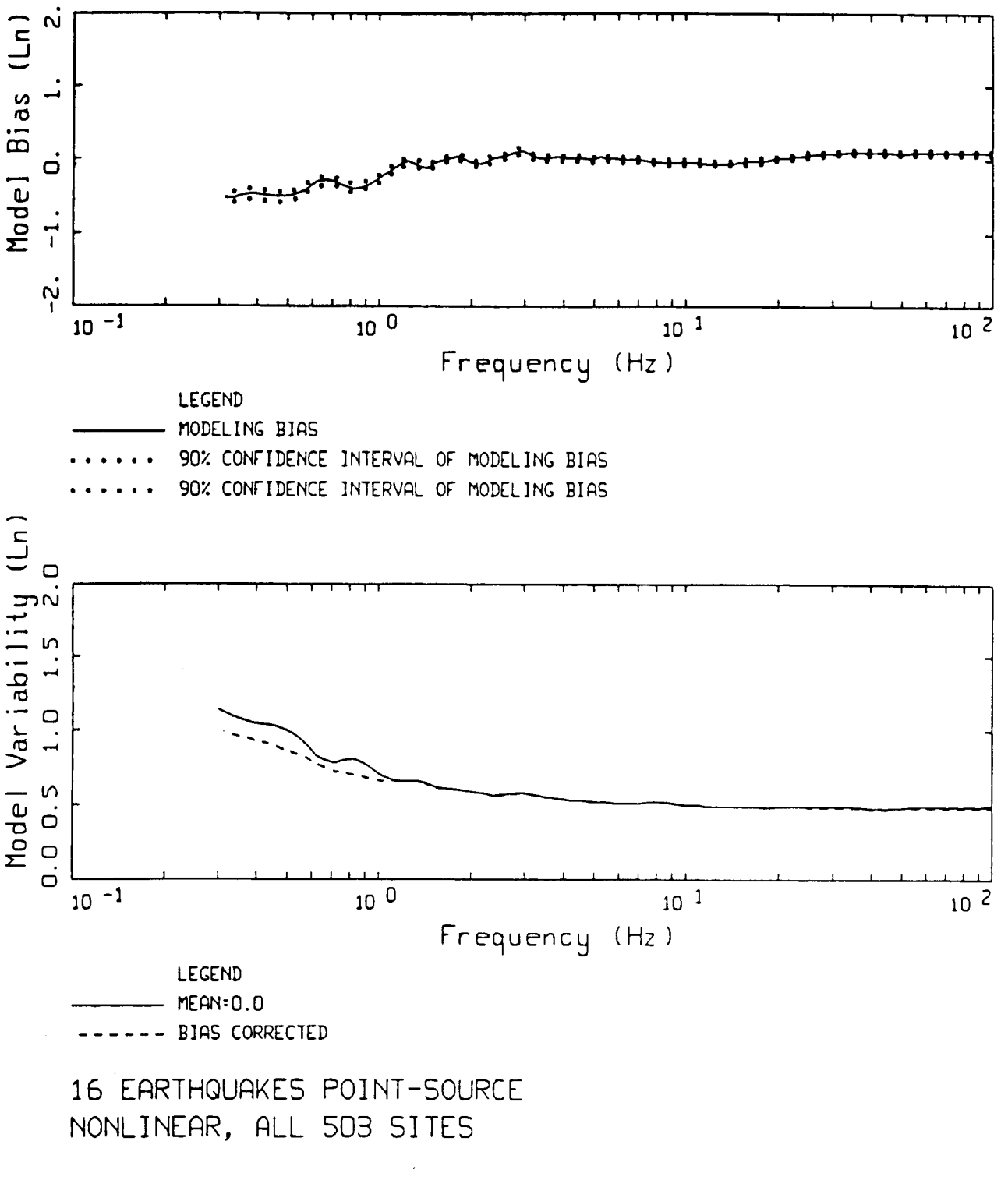

Figure A1. Model bias and variability estimates for all earthquakes computed over all 503 sites for the point-source model.

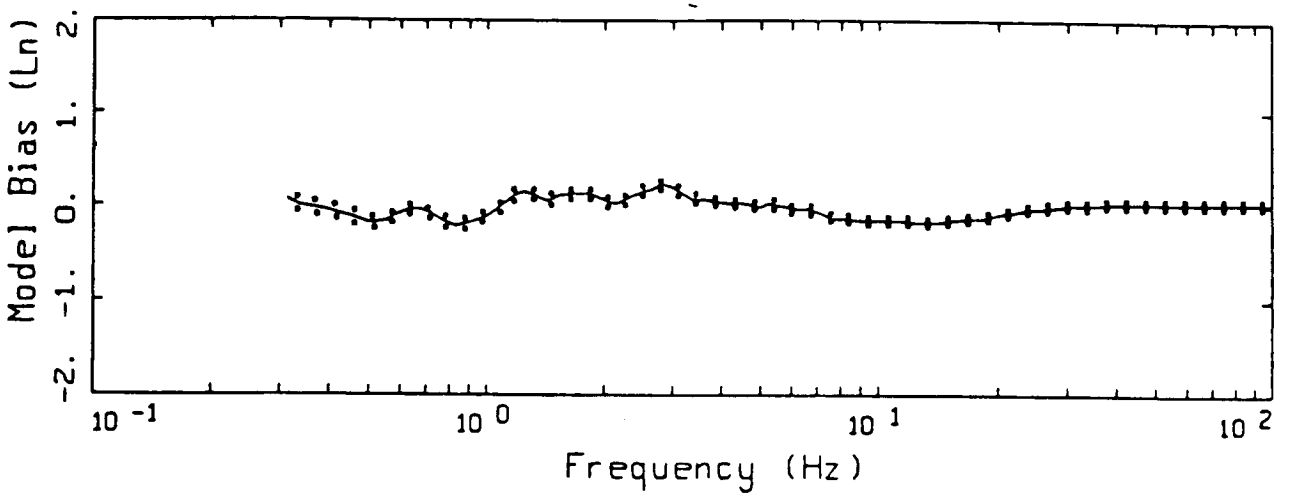

LEGEND
——— MODELING BIAS
• • • • • • 90% CONFIDENCE INTERVAL OF MODELING BIAS
• • • • • • 90% CONFIDENCE INTERVAL OF MODELING BIAS

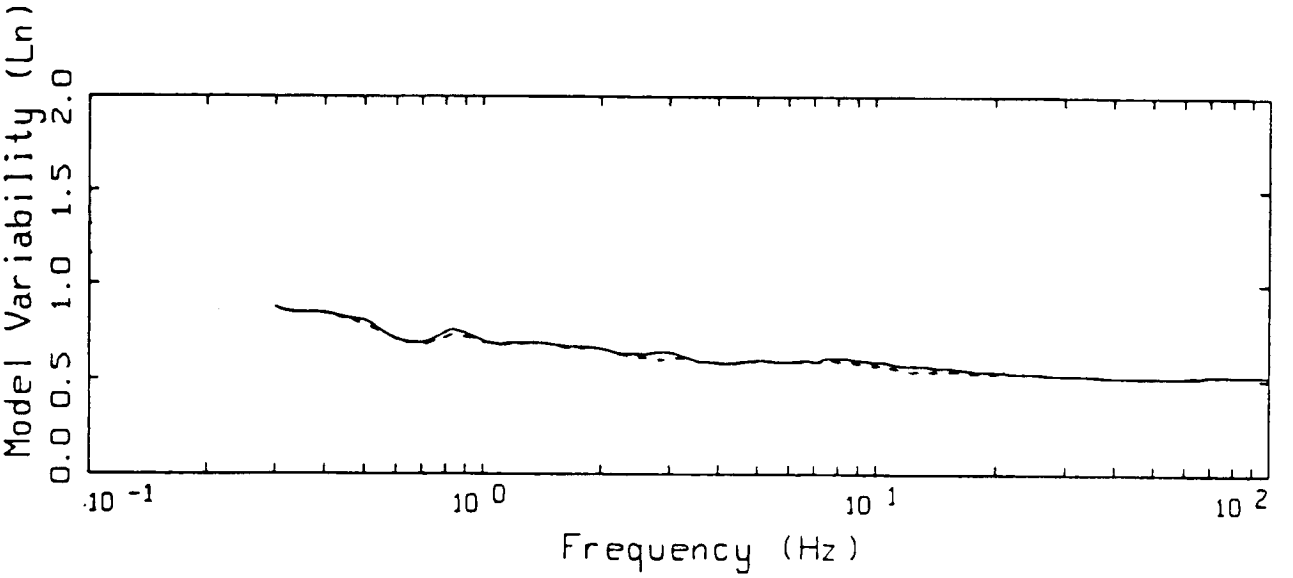

LEGEND
——— MEAN=0.0
- - - - - - BIAS CORRECTED

15 EARTHQUAKES FINITE-SOURCE
NONLINEAR, ALL 487 SITES

Figure A2. Model bias and variability estimates for all earthquakes computed over all 487 sites for the finite-source model.

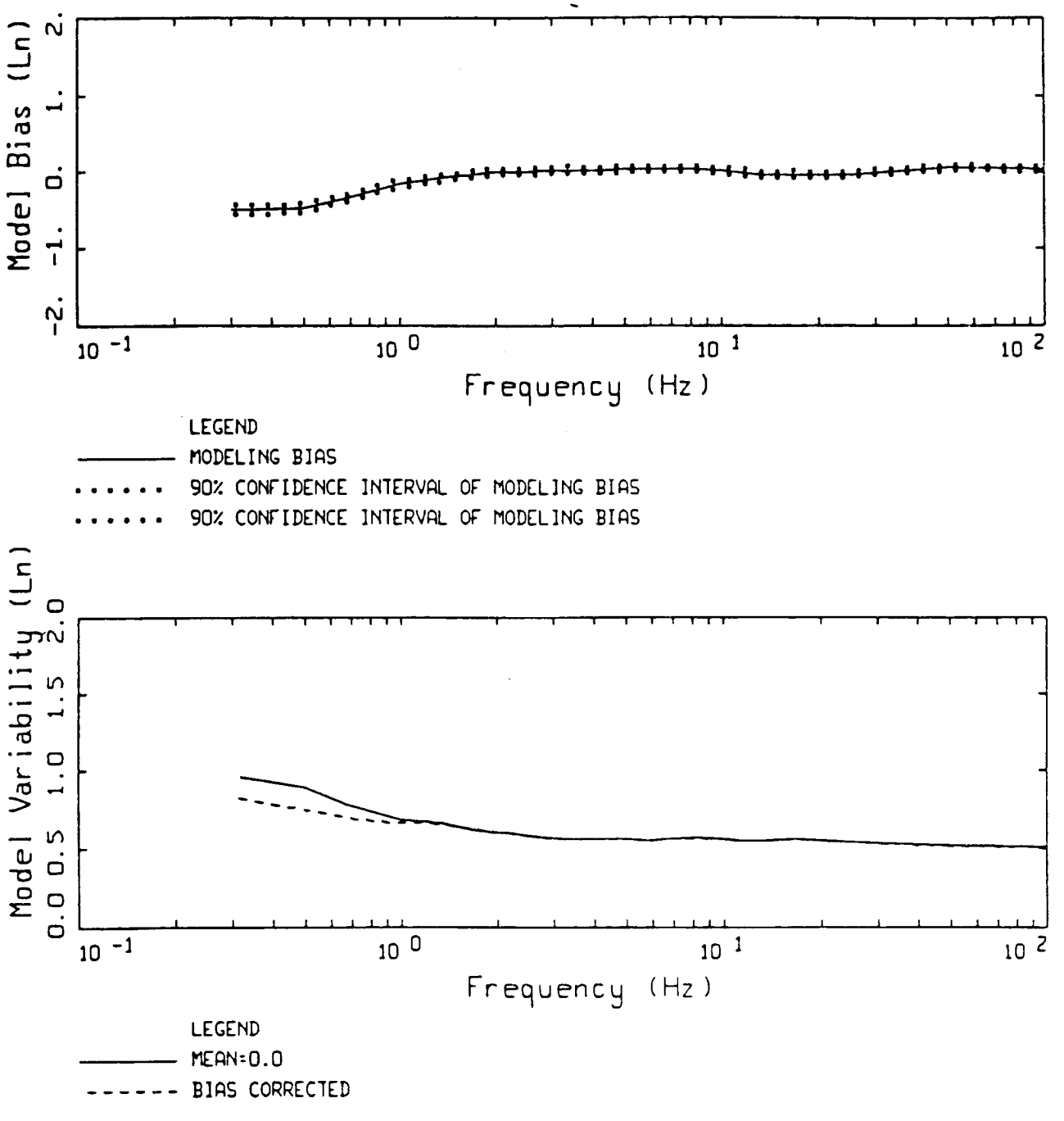

Figure A3. Model bias and variability estimates for all earthquakes computed over all 481 sites for the empirical model.

APPENDIX B

RVT SITE RESPONSE ANALYSIS METHOD

Equivalent-Linear Computational Scheme

The computational scheme which has been most widely employed to evaluate one-dimensional site response assumes vertically-propagating plane shear-waves. Departures of soil response from a linear constitutive relation are treated in an approximate manner through the use of the equivalent-linear approach.

The equivalent-linear approach, in its present form, was introduced by Seed and Idriss (1970). This scheme is a particular application of the general equivalent-linear theory developed by Iwan (1967). Basically, the approach is to approximate a second order nonlinear equation, over a limited range of its variables, by a linear equation. Formally this is done in such a way that the average of the difference between the two systems is minimized. This was done in an ad-hoc manner for ground response modeling by defining an effective strain which is assumed to exist for the duration of the excitation. This value is usually taken as 65% of the peak time-domain strain calculated at the midpoint of each layer, using a linear analysis. Modulus reduction and hysteretic damping curves are then used to define new parameters for each layer based on the effective strain computations. The linear response calculation is repeated, new effective strains evaluated, and iterations performed until the changes in parameters are below some tolerance level. Generally a few iterations are sufficient to achieve a strain-compatible linear solution.

This stepwise analysis procedure was formalized into a one-dimensional, vertically propagating shear-wave code called SHAKE (Schnabel et al., 1972). Subsequently, this code has easily become the most widely used analysis package for one-dimensional site response calculations.

The advantages of the equivalent-linear approach are that parameterization of complex nonlinear soil models is avoided and the mathematical simplicity of a linear analysis is preserved. A truly nonlinear approach requires the specification of the shapes of hysteresis curves and their cyclic dependencies through an increased number of material parameters. In the equivalent-linear methodology the soil data are utilized directly and, because at each iteration the problem is linear and the material properties are frequency independent, the damping is rate independent and hysteresis loops close.

Careful validation exercises between equivalent-linear and fully nonlinear formulations using recorded motions from 0.05 to 0.50g showed little difference in results (EPRI, 1993). Both formulations compared very favorably to recorded motions suggesting both the adequacy of the vertically propagating shear-wave model and the approximate equivalent-linear formulation. While the assumptions of vertically propagating shear-waves and equivalent-linear soil response certainly represent approximations to actual conditions, their combination has achieved demonstrated success in modeling observations of site effects and represent a stable, mature, and reliable means of estimating the effects of site conditions on strong ground motions (Schnabel et al., 1972; Silva et al., 1988; Schneider et al., 1993; EPRI, 1993).

To accommodate both uncertainty and randomness in dynamic material properties, analyses are typically done for the best estimate shear-wave velocity profile as well as upper- and lower-range profiles. The upper- and lower-ranges are usually specified as twice and one-half the best estimate shear-wave moduli. Depending upon the nature of the structure, the final design spectrum is then based upon an envelope or average of the three spectra.

For vertical motions, the SHAKE code is also used with compression-wave velocities and damping substituted for the shear-wave values. To accommodate possible nonlinear response on the vertical component, since modulus reduction and hysteretic damping curves are not generally available for the constrained modulus, the low-strain Poisson's ratio is usually fixed and strain compatible compression-wave velocities calculated using the strain compatible shear moduli from the horizontal component analyses combined with the low-strain Poisson's ratios. In a similar manner, strain compatible compression-wave damping values are estimated by combining the strain compatible shear-wave damping values with the low-strain damping in bulk or pure volume change. This process assumes the loss in bulk (volume change) is constant or strain independent. Alternatively, zero loss in bulk is assumed and the equation relating shear- and compression-wave damping (η_S and η_P) and velocities (V_S and V_P)

$$\eta_P \approx \frac{4}{3} \frac{V_S}{V_P} \eta_S \,, \tag{B-1}$$

is used.

RVT Based Computational Scheme

The computational scheme employed to compute the site response for this project uses an alternative approach employing random vibration theory (RVT). In this approach the control motion power spectrum is propagated through the one-dimensional soil profile using the plane-wave propagators of Silva (1976). In this formulation only SH waves are considered. Arbitrary angles of incidence may be specified but normal incidence is used throughout the present analyses.

In order to treat possible material nonlinearities, an RVT based equivalent-linear formulation is employed. Random process theory is used to predict peak time domain values of shear-strain based upon the shear-strain power spectrum. In this sense the procedure is analogous to the program SHAKE except that peak shear-strains in SHAKE are measured in the time domain. The purely frequency domain approach obviates a time domain control motion and, perhaps just as significant, eliminates the need for a suite of analyses based on different input motions. This arises because each time domain analysis may be viewed as one realization of a random process. Different control motion time histories reflecting different time domain characteristics but with nearly identical response spectra can result in different nonlinear and equivalent-linear response.

In this case, several realizations of the random process must be sampled to have a statistically stable estimate of site response. The realizations are usually performed by employing different control motions with approximately the same level of peak accelerations and response spectra.

In the case of the frequency domain approach, the estimates of peak shear-strain as well as oscillator response are, as a result of the random process theory, fundamentally probabilistic in nature. For fixed material properties, stable estimates of site response can then be obtained with a single run.

In the context of the RVT equivalent-linear approach, a more robust method of incorporating uncertainty and randomness of dynamic material properties into the computed response has been developed. Because analyses with multiple time histories are not required, parametric variability can be accurately assessed through a Monte Carlo approach by randomly varying dynamic material properties. This results in median as well as other fractile levels (e.g. 16^{th}, mean, 84^{th}) of smooth response spectra at the surface of the site. The availability of fractile levels reflecting randomness and uncertainty in dynamic material properties then permits a more rational basis for selecting levels of risk.

In order to randomly vary the shear-wave velocity profile, a profile randomization scheme has been developed which varies both layer velocity and thickness. The randomization is based on a correlation model developed from an analysis of variance on about 500 measured shear-wave velocity profiles (EPRI, 1993; Silva et al., 1997). Profile depth (depth to competent material) is also varied on a site specific basis using a uniform distribution. The depth range is generally selected to reflect expected variability over the structural foundation as well as uncertainty in the estimation of depth to competent material.

To model parametric variability for compression-waves, the base-case Poisson's ratio is generally fixed. Suites of compatible random compression- and shear-wave velocities are then generated based on the random shear-wave velocities profiles.

To accommodate variability in modulus reduction and hysteretic damping curves on a generic basis, the curves are independently randomized about the base case values. A log normal distribution is assumed with a σ_{ln} of 0.35 at a cyclic shear strain of $3 \times 10^{-2}\%$. These values are based on an analysis of variance on a suite of laboratory test results. An upper and lower bound truncation of 2σ is used to prevent modulus reduction or damping models that are not physically possible. The random curves are generated by sampling the transformed normal distribution with a σ_{ln} of 0.35, computing the change in normalized modulus reduction or percent damping at $3 \times 10^{-2}\%$ shear strain, and applying this factor at all strains. The random perturbation factor is reduced or tapered near the ends of the strain range to preserve the general shape of the median curves (Silva, 1992).

To model vertical motions, incident inclined compression- and shear (SV)-waves and assumed. Raytracing is done from the source location to the site to obtain appropriate angles of incidence. In the P-SV site response analyses, linear response is assumed in both compression and shear with the low-strain shear-wave damping used for the compression-wave damping (Johnson and Silva, 1981). The vertical and horizontal motions are treated independently in separate analyses. Validation exercises with a fully 3-D soil model using recorded motions up to 0.50%g showed these approximations to be validate (EPRI, 1993).

In addition, the site response model for the vertical motions has been validated at over 100 rock and soil sites for three large earthquakes: 1989 **M** 6.9 Loma Prieta, 1992 **M** 7.2 Landers, and the 1994 Northridge earthquakes. In general, the model performs well and captures the site and distance dependency of vertical motions over the frequency range of about 0.3 to 50.0 Hz and the fault distance range of about 1 to 100 km.

REFERENCES

Electric Power Research Institute (1993). "Guidelines for determining design basis ground motions." Palo Alto, Calif: Electric Power Research Institute, vol. 1-5, EPRI TR-102293.

vol. 1: Methodology and guidelines for estimating earthquake ground motion in eastern North America.

vol. 2: Appendices for ground motion estimation.

vol. 3: Appendices for field investigations.

vol. 4: Appendices for laboratory investigations.

vol. 5: Quantification of seismic source effects.

Iwan, W.D. (1967). "On a class of models for the yielding behavior of continuous and composite systems." *J. Appl. Mech.,* 34, 612-617.

Johnson, L.R. and W.J. Silva (1981). "The effects of unconsolidated sediments upon the ground motion during local earthquakes." *Bull. Seism. Soc. Am.*, 71, 127-142.

Schnabel, P.B., J. Lysmer, and H.B. Seed (1972). *SHAKE: a Computer Program for Earthquake Response Analysis of Horizontally Layered Sites.* Earthq. Engin. Res. Center, Univ. of Calif. at Berkeley, EERC 72-12.

Schneider, J.F., W.J. Silva, and C.L. Stark (1993). Ground motion model for the 1989 **M** 6.9 Loma Prieta earthquake including effects of source, path and site. *Earthquake Spectra,* 9(2), 251-287.

Seed, H.B. and I.M. Idriss (1970). "*Soil Moduli and Damping Factors for Dynamic ResponseAnalyses,*" Earthq. Eng. Res. Center, Univ. of Calif. at Berkeley, Report No. UCB/EERC-70/10.

Silva, W.J., N. Abrahamson, G. Toro, and C. Costantino (1997). "Description and validation of the stochastic ground motion model." Submitted to Brookhaven National Laboratory, Associated Universities, Inc. Upton, New York.

Silva, W.J. (1992). "Factors controlling strong ground motions and their associated uncertainties." *Dynamic Analysis and Design Considerations for High Level Nuclear Waste Repositories, ASCE* 132-161.

Silva, W. J., T. Turcotte, and Y. Moriwaki, (1988). "Soil Response to Earthquake Ground Motion," Electric Power Research Institute, Walnut Creek, California, Report No. NP-5747.

Silva, W.J. (1976). "Body Waves in a Layered Anelastic soilid." *Bull. Seis. Soc. Am.*, vol.66(5), 1539-1554.